TREATMENT OF INDUSTRIAL EFFLUENT USING SPECIALIZED, MAGNETIZED COAGULANTS

Submitted in fulfillment of the requirements for the degree of:
Master of Engineering in the Department of Chemical Engineering,

Faculty of Engineering and the Built Environment

at Durban University of Technology

By

Nomthandazo Precious Sibiya (21327638)

Date: January 2023

Supervisor: Prof S. Rathilal

PREFACE

The study was conducted under the supervision of Prof. Sudesh Rathilal at Durban University of Technology (DUT), Department of Chemical Engineering in collaboration with eThekwini municipality, FFS Refiners (Pty) Ltd and Umgeni Water-Amanzi as part of a project financed by the Water Research Commission (WRC) of South Africa, with the identitfaction WRC Project: C2019/2020-00212. Wastewaters were sampled in the sites of collaborators. The testing and analysis of data took place in the Department of Chemical Engineering.

DECLARATION

I, **Nomthandazo Precious Sibiya (21327638),** the undersigned student, declare that

(i) The research reported in this dissertation, except where otherwise indicated, is my original work.

(ii) This dissertation has not been submitted for any degree or examination at any other university.

(iii) This dissertation does not contain other persons' data, pictures, graphs, or other information, unless specifically acknowledged as being sourced from other persons.

(iv) This dissertation does not contain other persons' writing, unless specifically acknowledged as being sourced from other researchers. Where other written sources have been quoted, then:

(a) their words have been re-written but the general information attributed to them has been referenced;

(b) where their exact words have been used, their writing has been placed inside quotation marks, and referenced.

(v) Where I have reproduced a publication of which I am an author, co-author or editor, I have indicated in detail which part of the publication was actually written by myself alone and have fully referenced such publications.

(vi) This dissertation does not contain text, graphics or tables copied and pasted from the Internet, unless specifically acknowledged, and the source being detailed in the dissertation and in the **References** sections.

Signature: Date: 31 July 2022

Supervisor: Prof S Rathilal

Signature:…….. Date:18 May 2023……..

ACKNOWLEDGEMENT

First and foremost, God provided me the strength and sanity to accomplish this degree. Also, I want to thank my mother, Mrs R.H Ndlovu, for her prayers. Second, I'd like appreciate the supervisor, Prof. S Rathilal, for the advice, support, encouragement, and care during my Master's project (March 2020 to July 2022), for which I sincerely appreciate and will be eternally grateful.

Dr E.K. Tetteh deserves special recognition for mentoring and grooming me, as well as encouraging and inspiring me to produce the best. God bless you abundantly. Also, a particular appreciation goes to Miss Gloria Amo-Duodu for being the sister and friend I never had, for emotional support, and for being there when I was at my weakest point. This holds a special place in my heart. To the members of the Green Engineering research group, particularly Mr E.O Ezugbe, Dr M. Chollom, Mr D. Kukwa, and the whole Chemical Engineering department, for establishing a welcoming atmosphere to do my study.

Also, thank you to the Faculty of Engineering and The Built Environment for holding research clinics on topics such as Ethics, Accessing Literature & Endnote, The Structure of a Thesis, Writing a Research Proposal, and so on. In addition,special gratitude goes to National Research Foundation (NRF) for their funding (reference **MND190618448553** and **MND210421596570**). It also brings me great pleasure to convey my appreciation to Durban University of Technology (DUT) and the University of Valladolid (UVa) for the 5 months (10 February 2021 to 10 July 2021) ERASMUS scholarship. This chance enabled my desire to become a reality and realizing my aspirations, of which I will be eternally grateful to Almighty God.

I would like to thank the love of my life, Mr Khanyisani Dlomo, for loving me flawlessly without fail, for not being selfish, and for supporting my scholastic path. You're not any closer to perfection, yet you make it easier for me to adore you. Finally, I would want to thank my siblings, Mr Siphesihle Ndlovu and Mr Thamsanqa Ndlovu for their encouraging words. Furthermore, I thank everyone, even those whose names are not mentioned, for your kind effort and support.

DEDICATION

The dissertation is written in honor of my late father, Mr B Ntombela. I wish you were still alive father, to witness how your baby girl has grown into a strong, committed, and responsible woman. **Qhubeka ulale ngokuthula MAHLOBO, MPANGAZITHA, DLUKULA, lokhu ngikubhalele wena**.

Finally, I would like to dedicate this work to my daughter, Miss Ongeziwe Zethembiso Dlomo and my unborn generations.

ABSTRACT

The rapid degradation of water quality caused by industrial effluent presents a significant threat to public health and the ecosystem. This necessitates ecologically sustainable solutions through the coagulation treatment method. Coagulation with chemical coagulants (e.g. alum) is cost-effective, but comes with non-recoverability, health and environmental risks. As a result, this study proposes a magnetic-coagulation separation technique as an alternative. Against this brief, the goal of this research was to produce specialized magnetic coagulants for the treatment of industrial wastewater. Three magnetized coagulants (MCs) viz. chitosan magnetite (CF), eggshell magnetite (EF), and rice starch magnetite (RF) were synthesized via the co-precipitation technique by using chitosan, eggshell, or rice starch with Fe_3O_4 nanoparticles (F) in three distinct ratios (1:2, 1:1, and 2:1).

The analytical results via the Fourier-transform infrared (FTIR) spectroscopy, Brunauer–Emmett–Teller (BET) analyzer, X-ray diffraction (XRD) analyzer, and scanning electron microscopy (SEM) combined with energy-dispersive X-ray (EDX) spectroscopy respectively affirmed the success of MCs functional and molecular properties, surface area, crystal structure, surface morphology, and elemental compositions. Following that, a series of investigations were carried out utilizing coagulation and dissolved air flotation (DAF) methods to investigate the application and treatability performance of the MCs. Amongst the MCs, the RF(1:1) was found to be the most successful, removing over 75% of the turbidity, total suspended solids (TSS), and over 50% of the chemical oxygen demand (COD) from a local industrial effluent. Furthermore, response surface methodology (RSM) based on a Box–Behnken design (BBD) was used to optimize and compare the coagulation and DAF methods.

With coagulant dose (2 – 4 g), settling/flotation time (10 – 60 min) and mixing rate (50 – 150 rpm), the optimum coagulation conditions of 4 g dose, 30 minutes of settling time, and a mixing rate of 50 rpm, achieved a desirability of 87.20%. A 15-min flotation time, with a mixing rate of 50 rpm, and a coagulant dose of 4 g resulted in 77.4% desirability in the DAF method. The DAF method was considered to be more favorable with a shorter settling/flotation time and a desirability of 75% with 95% confidence. Notably, the RSM-BBD models demonstrated a strong correlation ($0.9 < R^2 < 1$) with predicted results that were consistent with the experimental data. The recent findings indicate that the prospects of MCs are possible for wastewater treatment, and hence magnetic separation technology should be given consideration in water and wastewater treatment settings.

RESEARCH OUTPUTS

JOURNAL ARTICLES:

I. **Sibiya, N. P.,** Rathilal, S. and Kweinor Tetteh, E. 2021. Coagulation treatment of wastewater: kinetics and natural coagulant evaluation. Molecules, 26 (3): 698. Available: https://doi.org/10.3390/molecules26030698

II. **Sibiya, N. P.**, Amo-Duodu, G., Tetteh, E. K. and Rathilal, S. 2022. Response surface optimisation of a magnetic coagulation process for wastewater treatment via Box-Behnken. *Materials Today: Proceedings*, 42 (Suppliment 1): S122-S126. Available: https://www.sciencedirect.com/science/article/pii/S221478532200671X

III. **Sibiya, N. P**., Amo-Duodu, G., Tetteh, E. K. and Rathilal, S. 2022. Modelling magnetic coagulation process using response surface methodology (RSM) and artificial neural network (ANN). Scientific Africa, 17: e01282. Avalaibale: https://www.sciencedirect.com/science/article/pii/S2468227622001892

IV. **Sibiya, N. P**., Amo-Duodu, G., Rathilal, S. and Tetteh, E. K. 2022. Effect of Magnetized Coagulants on Wastewater Treatment: Rice Starch and Chitosan Ratios Evaluation. Polymers, 14 (20): 4342. Available : https://www.mdpi.com/2073-4360/14/20/4342

V. **Sibiya, N. P**., Amo-Duodu, G., Tetteh, E. K. and Rathilal, S. 2022. Evaluation of the effect of recycled- magnetized coagulants on wastewater treatment. Journal of Pharmaceutical Negative Results, 13(09): 3466-3472. Available: https://www.pnrjournal.com/index.php/home/article/view/4117

VI. **Sibiya, N. P**., Amo-Duodu, G., Rathilal, S. and Tetteh, E. K. 2022. Magnetic field effect on coagulation treatment of wastewater using different coagulant types. Polymers, 15(1): 10. Available: https://www.mdpi.com/2073-4360/15/1/10

CONFERENCE/(S):

I. **Sibiya, N. P.,** Rathilal, S. and Tetteh, E. K. 2020. Coagulation treatment of wastewater: kinetics and evaluation of coagulants. 5th Interdisciplinary Research and Innovation Conference 2020. 15 - 17 September 2020. Virtual, DUT, South Africa.

II. **Sibiya, N. P.,** Rathilal, S., Govender, P. and Tetteh, E K. 2020. Application of natural coagulants as an alternative to alum for wastewater treatment. 18th Johannesburg Int'l Conference on Science, Engineering, Technology & Waste Management (SETWM-20). 16 - 17 November 2020. Boksburg (SA). DOI: 10.17758/EARES10.EAP1120255.

III. **Sibiya, N. P.,** Amo-Duodu, G., Tetteh, E. K. and Rathilal, S. 2021. Effect of magnetized-chitosan and rice starch on coagulation wastewater treatment: A comparative study. Sustainable Development on the Africa Continent Conference 2021, 7 - 9 December 2021. Virtual, Durban, South Africa.

IV. **Sibiya, N. P.,** Amo-Duodu, G., Tetteh, E. K. and Rathilal, S. 2021. Response surface of a magnetic coagulation process for wastewater treatment via Box-Behnken. 2021 International Symposium on Nanostructured and Advanced Materials. 24 - 26 November, 2021.University of Johannesburg, South Africa.

V. **Sibiya, N. P**., Amo-Duodu, G., Tetteh, E. K. and Rathilal, S. 2022. Evaluation of the effect of recycled- magnetized coagulants on wastewater treatment. 33rd Johannesburg International Conference on Chemical, Biological and Environmental Engineering (JCBEE-22), 17 - 18 March, 2022. Virtual, Johannesburg, South Africa.

TABLE OF CONTENT

LIST OF FIGURES

LIST OF TABLES

NOMENCLATURE

Alum	Aluminium Sulfate
ANOVA	Analysis of variance
BBD	Box-Behnken design
BOD	Biological oxygen demand
CD	Charge density
COD	Chemical oxygen demand
CS	Chitosan
DAF	Dissolved air flotation
DOE	Design of experiment
ES	Eggshell
Fe_3O_4	Magnetite
MCs	Magnetized coagulants
MF	Magnetic field
NPs	Magnetic nanoparticles
NTU	Nephelometric turbidity units
OFAT	One factor at a time
RM	Reverse microemulsion
rpm	Revolution per minute
RS	Rice starch
RSM	Response surface methodology
TSS	Total suspended solids
WWTP	Wastewater treatment plant

CHAPTER 1-INTRODUCTION

1.1 Background

Clean water has been the crucial naturally occurring resource required by all lifeforms, including humans, who drink, bathe, wash, and use latrines (Ali 2014; Ugya *et al.* 2016; Kumar *et al.* 2017b; Kurniawan *et al.* 2020; Nath *et al.* 2020; Chaudhary *et al.* 2021). Humans may survive for many weeks without food but may not survive for several days without water, since it is continually necessary for the proper functioning of the body's cells, tissues, and organs (Iloms 2018). Aside from human use, water is crucial in a variety of industries, including agriculture, cattle ranching, horticulture, fish stocks, energy production, industrial activities, as well as other sorts of innovation (Tyagi *et al.* 2013; Beyene *et al.* 2016). Agriculture and industrialization are reported to consume more water than home users across the world (Teh 2014). Water reservoirs, such as rivers, lakes, and the ocean, are part of the hydrological cycle and help to maintain an ecological balance (Ambashta *et al.* 2010; Tyagi *et al.* 2013; Nath *et al.* 2020). However, alongside the rise in human population, industrialization, and urbanization, clean water sources are depleting daily and is associated with wastewater pollution generation (Ernest *et al.* 2017; Tetteh *et al.* 2019; Khouni *et al.* 2020; Nath *et al.* 2020; Zhang *et al.* 2021b). When this effluent is released into the ecosystem without adequate treatment, it poses a severe ecological concern with significant environmental consequences (Tetteh *et al.* 2019; Gautam *et al.* 2020; Noor *et al.* 2021). Apart from the effects upon abiotic components such as soil and water, this has a significant impact on the health of living creatures (Teh 2014; Gautam *et al.* 2020).

Also, agricultural operations are severely affected since farms end up not having access to enough water supplies for year-round irrigation and animal farming (Ezugbe *et al.* 2020). In developing countries, most people drink untreated polluted water, resulting in water-borne illnesses like diarrhoea, hepatitis, and others (World Health Organization 2011; Nath *et al.* 2020) and cause mortality, paticularly among youngsters, the elderly, and individuals suffering from chronic illnesses (Bodlund 2013b; Khettaf *et al.* 2021). As a result, many countries' economies are jeopardized in terms of water, food, and energy security (Tetteh 2018a). Wastewater treatment plants (WWTPs) are a significant source of pollutants discharged into bodies of water (Tetteh *et al.* 2017; Chollom *et al.* 2020; Tetteh *et al.* 2020b) because they do not meet the Environmental Protection Agency's stringent criteria for controlling effluent plant quality (Zahrim *et al.* 2013; Sibiya *et al.* 2021). Most industrial effluents are treated differently, which depends on the industry. Wastewater could include the range of contaminants like lactose, oils and greases, proteins, nitrogen and phosphorus-rich compounds, sediments, other organic materials, and

detergents (Nharingo *et al.* 2015; Gautam *et al.* 2020; Nath *et al.* 2020; Nimesha *et al.* 2021; Sibiya *et al.* 2021). However, not all recovered effluents fulfil necessary disposal or reuse standards (Tetteh *et al.* 2019). Heavy metals, viruses, bacteria, nitrates, and viruses are some of the pollutants present in wastewater that can be hazardous to the ecosystem and human health (Beyene *et al.* 2016; Iloms 2018; Ahmed *et al.* 2020b; Chollom *et al.* 2020; Chaudhary *et al.* 2021). Major producers of industrial effluents include palm oil mills (Saifuddin *et al.* 2011; Jagaba *et al.* 2020; Noor *et al.* 2021), slaughterhouses (Chollom *et al.* 2019), dairy industries (Devi *et al.* 2012; Muniz *et al.* 2020), paper and pulp industries (Pokhrel *et al.* 2004; Ahn *et al.* 2009; Hubbe *et al.* 2016), breweries and wineries (Muhammad 2014), cosmetic industries, tannery industries, paint industries, etc. (Sahu *et al.* 2013; Gautam *et al.* 2020). In essence, industrial effluent compositions make them needed to be treated for de-oiling, desalination, reduction of suspended particles, soluble organics, dissolved gases, natural organic matters (NOM) and to remove excess water hardness (Ødegaard *et al.* 2010; Igunnu 2014).

Figure 1-1 shows a conventional waste treatment process that has been explored to enhance the quality of water to meet the water demand (Hong *et al.* 2016; Kurniawan *et al.* 2020; Ullah *et al.* 2020; Nimesha *et al.* 2021) at a low- cost (Siddique *et al.* 2016). These technologies are classified into three groups; (1) physical (settling, filtration and membrane technology), (2) chemical (coagulation, ion exchange, disinfection, oxidation, catalytic reduction and softening processes) and (3) biological (microbial biodegradation, bioreactor processes, etc.) treatment techniques (Mahmoud 2009; Momba *et al.* 2009; Sher *et al.* 2013; Karhu *et al.* 2014; Hong *et al.* 2016; Crini *et al.* 2018; Nizamuddin *et al.* 2019; Nimesha *et al.* 2021).

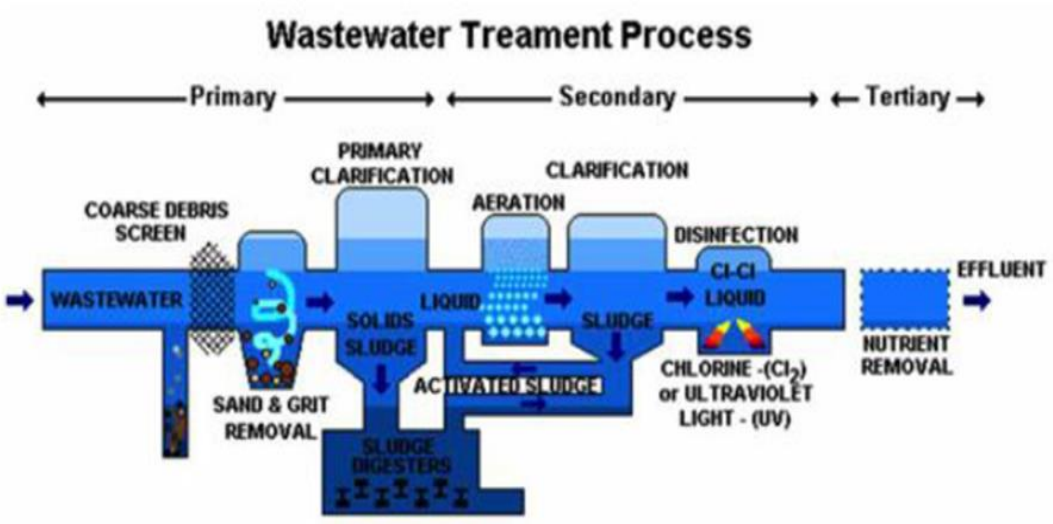

Figure 1-1 Conventional waste treatment process, adapted from Hong *et al.* (2016)

Coagulation is a frequently used primary technique in water and wastewater treatment (Amran *et al.* 2018; Gautam *et al.* 2020) to effectively minimize the organic burden prior to further remedial methods (Saifuddin *et al.* 2011; Hossain *et al.* 2019; Ahmed *et al.* 2020b; Muniza *et al.* 2020; Nimesha *et al.* 2021). It aggregates tiny particles to bigger aggregates (flocs), then dissolved organic matters are attracted to particle aggregates, allowing these contaminants to be removed in subsequent separation techniques (Jagaba *et al.* 2016; Cui *et al.* 2020; Gautam *et al.* 2020; Nath *et al.* 2020; Nimesha *et al.* 2021). Furthermore, it has sparked widespread attention in the industrial sector because of its ease of use, high efficiency and low cost (Jagaba *et al.* 2020; Zhang *et al.* 2021b). Coagulation involves a sequence of stages, beginning with the electrostatic interaction of cationic ions to negatively charged suspended contaminants and ending with particle destabilization (Kumar *et al.* 2016; Cui *et al.* 2020; Nath *et al.* 2020). This is accomplished through three distinct pathways: (1) charge neutralization (particle destabilization at low coagulant dosage), (2) sweep (the addition of coagulant at sufficiently high concentrations to produce anhydrous, amorphous precipitates enmeshing colloidal particles in these precipitates), and (3) bridge formation (Fearing 2004; Amran *et al.* 2018; Muniza *et al.* 2020; Nath *et al.* 2020; Sibiya *et al.* 2021). The parameters of the raw wastewater affect the efficacy of the coagulation process (Kumar *et al.* 2004; Carmona *et al.* 2006; Nath *et al.* 2020), the pH and temperature of the solution, the type and dose of coagulants, and the intensity and time of mixing (Jagaba *et al.* 2016; Ernest *et al.* 2017; Tetteh 2018a; Mosaddeghi *et al.* 2020). Coagulants or flocculants can alter the physical state of wastewater, causing charged particles to become unstable and promoting agglomeration (Freitas *et al.* 2017; Tetteh *et al.* 2019; Cui *et al.* 2020; Noor *et al.* 2021).

They can be divided into inorganic coagulants (aluminum sulfate: alum, ferric chloride), inorganic polymeric coagulants (poly aluminum chloride [PAC] and polysilicate aluminum chloride [PASiC]), organic synthetic polymeric flocculants (polyacrylamide [PAM] and its derivatives), natural polymeric flocculants (starch, chitosan, cellulose, okra leaves, banana or orange or cassava peels, neem leaves and other polysaccharide materials), and microbial flocculants (Anju *et al.* 2016; Rezaeiana *et al.* 2016; Kurniawan *et al.* 2020; Nimesha *et al.* 2021; Zhang *et al.* 2021b). Nonetheless, alum and ferric chlorides are coagulants that are normally utilized in the coagulation method (Jagaba *et al.* 2020; Kurniawan *et al.* 2020; Noor *et al.* 2021; Sibiya *et al.* 2021). However, previous researchers have indicated that aluminium-based coagulants can be harmful to aquatic life by generating hazardous sludge with costs, and may cause Alzheimer's disease (Yang *et al.* 2010; dos Santos *et al.* 2018a; Mateus *et al.* 2018b; Chollom *et al.* 2019; Hossain *et al.* 2019; Oke *et al.* 2019; Mosaddeghi *et al.* 2020; Muniza *et al.* 2020). The disadvantages of synthetic coagulants have prompted in the quest for environmentally firendly and renewable coagulants in their use.

Several possible electrochemical technology-based systems have been proposed (Ni'am 2006) and the progress of nanotechnology has substantially contributed to the creation of innovative ways of tackling several human health and environmental concerns whilst using less power (Ambashta *et al.* 2010; Rossi *et al.* 2013; Santos *et al.* 2016; Tetteh *et al.* 2020; Sibiya *et al.* 2021). Previous studies have demonstrated great efficiency in the reduction of heavy metals and hazardous chemicals from wastewater (Singh *et al.* 2011; Akbarzadeh *et al.* 2012; dos Santos *et al.* 2018b; Mateus *et al.* 2018b; Chua *et al.* 2021b) using iron oxide nanoparticles like maghemite (y-Fe_2O_3), magnetite (Fe_3O_4), and Hematite ($\propto$-Fe_2O_3) (Singh *et al.* 2011; Akbarzadeh *et al.* 2012; dos Santos *et al.* 2018b; Mateus *et al.* 2018b; Chua *et al.* 2021b). Furthermore, they have recently emerged as better adsorbents than metallic nanoparticles for the removal of different contaminants in water due to their exceptional sorption capabilities and the ability to attain equilibrium in short periods of time (Dung *et al.* 2009; Akbarzadeh *et al.* 2012). There are many methods that have been employed to synthesize these materials which includes co-precipitation, thermal decomposition, chemical vapor deposition, electrochemical, electron-spinning, hydrothermal, reverse micelle, gamma irradiation, and sol-gel processes (Starowicz *et al.* 2011; Hasany *et al.* 2013; Ealias *et al.* 2017; Saratale *et al.* 2018; Yadollahpour 2020; Zhao *et al.* 2021c). Other techniques include sonolysis, hydrolytic and non-hydrolytic wet chemical processes, liquid phase, laser evaporation, and micro-emulsion (Willard *et al.* 2004; Hasany *et al.* 2013; Rossi *et al.* 2013; Yao *et al.* 2015; Abdelsalam *et al.* 2017). Due to large capital investment, operational expenses, and safety concerns, only a handful them have been commercialized for industrial-scale production. The following are some of the most important aspects of nanoparticle synthesis: particle size uniformity, size control, crystal structure, shape control, and device alignment (Hasany *et al.* 2013).

The synthesis of distict magnetic nanoparticles having diameters from 2 to 20 nm is critical due to their usage in multi-terabit magnetic storage systems (Mu *et al.* 2011; Hasany *et al.* 2013; Peeters *et al.* 2016; Nizamuddin *et al.* 2019; Li *et al.* 2020). Magnetic nanoparticles (NPs) are used to coat a variety of surfactants to prevent aggregation induced by magnetic dipole - dipole attractions between particles (Dung *et al.* 2009; Akbarzadeh *et al.* 2012). They offer unique and advantageous properties in terms of application, such as low cost and health effects, magnetism, longevity and bio-compatibility and ease of separation from aqueous solution (Wang *et al.* 2008; Dung *et al.* 2009; dos Santos *et al.* 2018a). Owing their powerful magnetic characteristics, they can be safely utilized in both medical and biological disciplines such as medication administration, biosensors, systems for purifying water, and bio molecular separation (Singh *et al.* 2011; Akbarzadeh *et al.* 2012). Their stiny size and large surface area have unique physical

and chemical properties when combined with natural polymers (Karapinar 2003; Dung *et al.* 2009; Akbarzadeh *et al.* 2012; Ealias *et al.* 2017; Cartwright *et al.* 2020; Tetteh *et al.* 2020; Khan *et al.* 2021b).

Natural coagulants like eggshells (ES), moringa oleifera (Mo) seeds, chitosan (CS), starch, etc. have also received a lot of attention as an efficient heavy metal adsorbent because of nitrogen and sulfur atoms' great capacity and affinity to interact with metal ions (Morsi *et al.* 2018; Chaudhary *et al.* 2021; Sibiya *et al.* 2021). The super paramagnetic characteristics indicates that they respond to a magnet, making sampling and collecting easier and faster (Ni'am 2006; Wang *et al.* 2008; Saifuddin *et al.* 2011). However, their magnetization fades if the external magnetic field (MF) is removed. MF improves sedimentation capabilities, lowering the concentration of suspended solids and activated sludge and increasing wastewater treatment efficiency (Haritwal *et al.* 2015). Its speculation has an impact on water treatment technical processes and is classified as: crystallization during magnetic water processing and contaminant coagulation in wastewater treatment (Ni'am 2006). After magnetic separation, the NPs can be reused by eliminating the adsorbed hazardous pollutants (Chang *et al.* 2006; Shen *et al.* 2009).

1.2 Problem statement

Water resources are at risk as a result of over-exploitation, poor management, and environmental pollution (Aboelfetoh *et al.* 2021; Ahmed *et al.* 2021c). The statistics show that about 2.3 billion people lack access to clean water in their household and over four billion people face acute water shortages at minimum once a year (Pavon 2019; Ang *et al.* 2020b). Approximately 80% of diseases in underdeveloped nations are directly tied to dirty drinking water countries directly related to polluted drinking water (World Health Organization 2011). The use of coagulation and flocculation techniques to pre-treat industrial wastewater is very critical in order to successfully lower the organic pollutants before subsequent treatment operations (Prosper *et al.* 2021; Sibiya *et al.* 2021). However, the coagulation/flocculation technique employs synthetic chemicals, which are problematic because of their semi nature, incapacity to dissolve, and the health hazards associated with persistent residues (Muniz *et al.* 2020; Tetteh *et al.* 2020). Furthermore, the problem of disposing of large amounts of sludge and metals in effluents, like the utilization of hydroxide precipitation, necessitates the development of technology to extract precious or dangerous metals from sludge (Nnaji *et al.* 2014; Oke *et al.* 2019; Tetteh *et al.* 2019).

As a result, there has been a search for environmentally benign and viable natural coagulants in usage and synthesis. Nanotechnology appears to solve the high coagulant reliance, pH correction,

and high sludge production with complexions in the event of coagulation (Naghizadeh *et al.* 2017; Tetteh *et al.* 2020). Therefore, this study aimed to develop and identify eco-friendly coagulants that address the water scarcity issues.

1.3 Aims and objectives

This study aims to develop and test magnetic coagulants as a replacement for alum in the pre-treatment of industrial effluents. The specific objectives are:

1. To synthesize and characterize an iron oxide nanoparticle (Ferro-magnetite) and functionalize it with natural coagulants viz. chitosan, egg shell, and rice starch in different ratios (1:1; 1:2 and 2:1).
2. To apply and evaluate the synthesized coagulants treatability efficiency using coagulation with settling and dissolved air flotation (DAF) techniques.
3. To apply the best-synthesized coagulant and optimize the coagulation with settling and DAF process using response surface methodology (RSM). The input variables considered were settling/flotation time, mixing rate and coagulant dosage as a function of COD, turbidity and TSS.
4. To compare and validate the coagulation and DAF treatability efficiency under the optimum conditions.

1.4 Approach

The availability of potable water is vital for supporting human well-being as well as enhancing people's ecological integrity and livelihoods across the world. Proper water treatment methods not only assist end users or customers, but they may also increase production in the water sector. Furthermore, they contribute to environmental conservation and the general improvement of the waterways. Local governments are in charge of treating and delivering excessive water supplies to all users. As a result, the study utilized approaches from the literature to satisfy SDG 2030 number 6: Clean water & Sanitation. The wastewaters used in the study were acquired after chlorination from local wastewater treatment facilities in Umbilo, Pietermaritzburg, and Pinetown, in the KwaZulu-Natal province, South Africa. The Fe_3O_4 nanoparticles were created using the co-precipitation process with a molar ratio of 1:2 for Fe (II): Fe (III). The first set of experiments examined different coagulants for wastewater treatment and these were performed in triplicate. The best performing coagulant was utilized to optimize the overall treatment process with 14 runs for coagulation and DAF using the Box Behnken Design of response surface

methodology (RSM) and synthetic wastewater. Finally, at the acquired optimal conditions, three confirmation runs for coagulation and the DAF techniques were performed.

1.5 Structure of the thesis

This dissertation is divided into five chapters, which are briefly summarized below;

Chapter 1: The first chapter introduces and contextualizes the whole investigation, emphasizing the purpose for the study and the intended conclusion.

Chapter 2: The second chapter provides a review of the literature, focusing on the existing and traditional wastewater treatment methods. It also presents coagulant types, their mechanisms and inadequacies, and the need for improvement in connection with industrial wastewater characteristics, as well as the fundamental water management that is handled. Furthermore, the discusions about various types of nanoparticles and synthesis processes, the design of experiment (DoE) knowledge, which is a tool for process optimization is clearly displayed.

Chapter 3: The third chapter describes the research approach for synthesizing magnetic coagulants, including materials, procedures, and equipment descriptions. In addition, the processes for the characterization of industrial effluents are described in depth. It also outlines the two setups (coagulation and DAF) employed in this investigation, as well as their operating circumstances. Finally, it explains the process optimization, analytical and data simulation approaches.

Chapter 4: The findings and discussions from the characterization of magnetized coagulants (MCs) and their applications are presented in this chapter. The findings and discussions are provided and discussed as follows: the comparison of magnetized coagulants on contaminant removals, the impacts of settling time on contaminant removals, the influence of the magnetic field (MF), coagulation kinetics, and comparative studies between the performance of coagulation and DAF are presented. Finally, the results of RSM optimization are provided.

Chapter 5: The conclusion and recommendations are presented in this chapter. This chapter summarizes the major results of the study and draws recommendations for future works.

CHAPTER 2- LITERATURE REVIEW

2.1. Introduction

Chapter two entails a depth background on coagulation and dissolved air flotation (DAF) mechanisms for wastewater treatment using magnetized coagulants. As a focus, an exhaustive survey was employed to evaluate some conventional wastewater treatment techniques such as coagulation-sedimentation, coagulation-flotation, their mechanism, operational conditions, and limitations. Also, the novelty of using magnetized coagulants and the techniques of synthesising are explored. Response surface methodology is highlighted as an experimental design, modeling, and optimization tool. A summary of the literature survey was provided with a knowledge gap underpinning the use of coagulation and DAF techniques identified.

2.2. Wastewater treatment

Rapid industrial expansion, along with a rapid population increase, has exacerbated difficulties dealing with water scarcity as the global desire for freshwater grows (Nharingo *et al.* 2015; Goli *et al.* 2018; Tetteh 2018a; Gautam *et al.* 2020; Gumbi 2020; Zhang *et al.* 2021b). Increasing water shortage is amongst urgent concerns across the world. Herein, the upsurging water pollution from industrial operations in the petroleum, agricultural, mining, pharmaceutical, and other manufacturing industries poses a great threat to available freshwater resources (Diya'uddeen *et al.* 2011; Muhammad 2014; Tee *et al.* 2016). Globally, wastewater treatment remains a complex process associated with many challenges such as sludge disposal, health-hazardous chemicals, and dissolved organic materials discharged into rivers (Hubbe *et al.* 2016; de Souza Fermino *et al.* 2017). In addition to the environmental consequences, sludge disposal and chemical usage also come with a cost (Gautam *et al.* 2020). Meanwhile, industries continue to emit a variety of pollutants that have hazardous chemicals viz high organic matter like biological oxygen demand (BOD) and COD, nitrates and nitrites, and abundant nutrients like phosphate and ammonia (Gautam *et al.* 2020; Adeogun *et al.* 2021). Volatile organic compounds (VOCs), polyaromatic compounds (PAHs), pharmaceuticals and personal care products (PPCPs), industrial by-products, food additives, and engineered nanomaterials are among the other pollutants (El-Gohary *et al.* 2010; Abdallh *et al.* 2016; Ali *et al.* 2017; Gutierrez *et al.* 2017; Al-Khalid *et al.* 2018). It becomes critical to remove these pollutants using appropriate wastewater treatment techniques (Mecha *et al.* 2016; Kurniawan *et al.* 2020; Ullah *et al.* 2020) towards clean water usability and a sustainable environment (Sahu *et al.* 2013; Tetteh *et al.* 2019).

In addressing this, a robust wastewater treatment process is warranted to reprocess wastewater for reuse while meeting all stringent bylaws of the state (van Wilgen *et al.* 2016). Some bylaws and policies used in regulating South African water treatment are highlighted in Section 2.2.1. In essence, selection of treatment technologies are usually based on the wastewater chemistry and avaliability, the objective of the end user and disharge limits (Gupta *et al.* 2012; Hubbe *et al.* 2016; Ernest *et al.* 2017; Crini *et al.* 2018; Tetteh 2018a; Gumbi 2020). In general, wastewater treatment is accomplished by combining a series of processes to obtain the required effluent quality (Tetteh *et al.* 2017). Some of these conventional techniques include filtration, anaerobic digestion, coagulation, sedimentation, DAF, disinfection or chlorination, and flocculation (Ewerts *et al.* 2014; Tetteh *et al.* 2019; Ezugbe *et al.* 2020). Of recent, advanced oxidation processes (AOPs), membrane and adsorption technologies are gaining attention (Qu *et al.* 2013; Palansooriya *et al.* 2020). Section 2.3 of this dissertation contains a comprehensive description of the water treatment techniques applicable to this study.

2.2.1. South Africa's regulations that protect the environment

2.2.1.1. Act 36 of 1919: Public Health Act

This legislation was made applicable in South Africa to prevent and control infectious illnesses, venereal diseases, and epidemics through sewage disposal (Ngwena 2003). This is also used in regulating sanitation, food, and public water supply. The Chief Officer of the Public Health Department in charge of this policy must guarantee that the best solutions are available to reduce pollution caused by sewage disposal. Furthermore, avoid liquid effluents from sewage treatment from being released directly into aquatic bodies without adequate treatment.

2.2.1.2. Act 54 of 1956: Water Act

It has been renamed Act 36 of 1998. Its goal is to regulate the use, treatment, and disposal of industrial liquid effluents (Tempelhoff 2017). It guarantees that adequately treated water is returned to bodies of water such as reservoirs, the sea, and so on to avoid depletion. It also intends to reduce pollution since there is too much natural organic mattersin wastewater.

2.2.1.3. Act 36 of 1998: National Water Act

This act ensures that the nation and its resources are safeguarded, advanced, confined, utilized, maintained, and conserved through the following factors while fostering equitable access to water (King *et al.* 2011).

- Encouraging basic needs for current and future generations,
- Promoting dam safety,
- Promoting beneficial, sustainable, and well-organized use of water in the public interest,
- Facilitating social and economic expansion,
- Redressing the consequences of the previous gender and racial discrimination,
- Meeting international obligations,
- Prevent and minimize water supply pollution,
- Provide for accumulating demand for water usage, and
- Manage floods and droughts.

2.2.1.4. Act 39 of 2004: Air Quality Act

This Act is aimed to safeguard the environment and improve air quality. It also prohibits air pollution and environmental degradation in SA by prohibiting activities or emissions that could have an adverse effect on the environment (Tshehla *et al.* 2019).

2.3. Current and conventional water treatment technologies

Conventional wastewater often involves the integration of physical, chemical, and/ or biological procedures and operations to eliminate solids from effluents such as colloids, organic matter, nutrients, and soluble pollutants (metals, organics, and so on). Furthermore, they are intended to generate high-quality effluent prior releazing it into the environment (Tiwari *et al.* 2017). They had great success in removing organics and other pollutants from wastewater (Tetteh *et al.* 2018b). Figure 2-1 shows a wide range of techniques classified as conventional methods, established recovery processes, and developing removal methods that are available for wastewater.

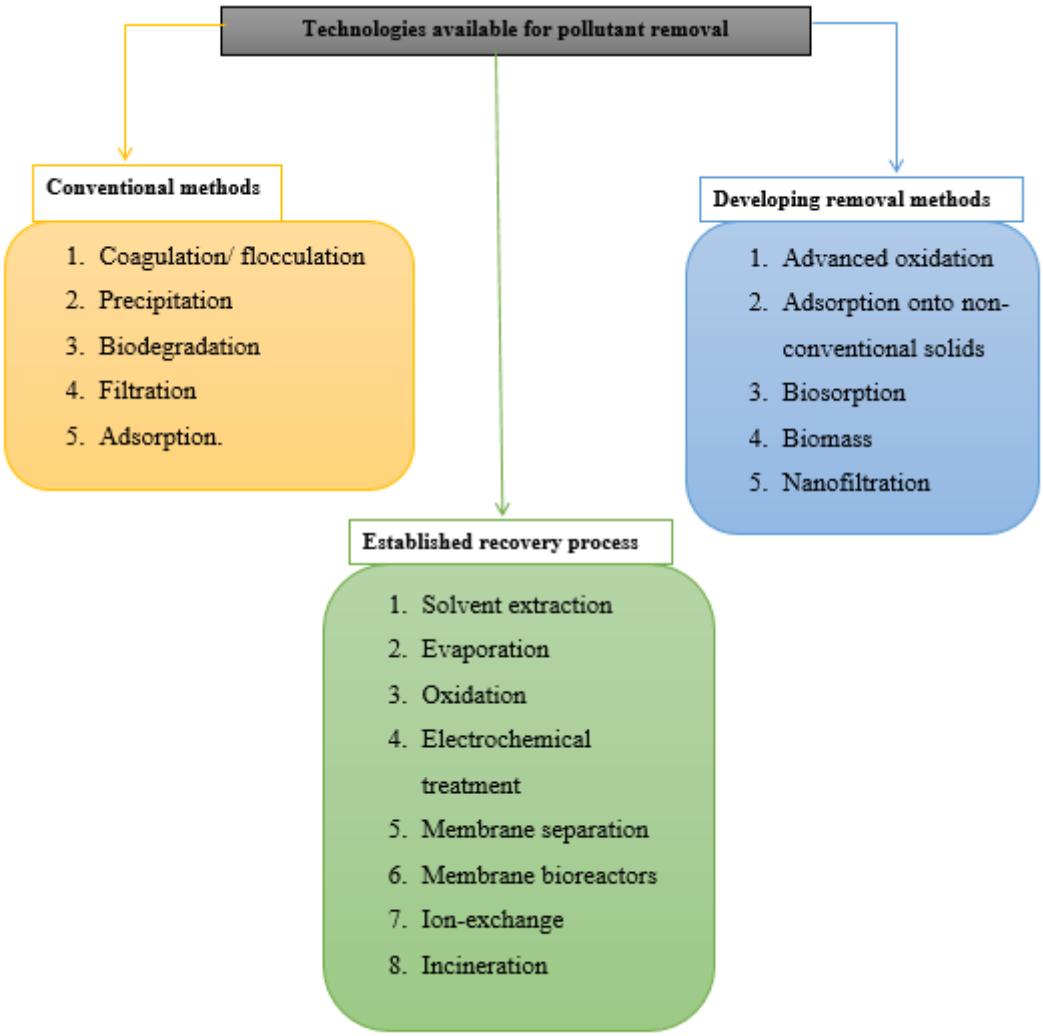

Figure 2-1 Classification of various pollution removal methods, as well as examples of approaches, adapted from (Crini *et al.* 2018; Ince *et al.* 2019)

2.3.1. Screening, filtration and centrifugal separations

Screening is usually the first stage in a wastewater treatment process. Its primary goal is to eliminate solid waste from the effluent, and eliminate fabric scraps, paper, wood, cork, hair, fiber, kitchen trash, fecal solids, and other materials from wastewater (Gupta *et al.* 2012; Asthana *et al.* 2017; Ince *et al.* 2019). Efficient removal of these components will safeguard the downstream systems from potential damage, needless wear and tear, pipe obstructions, and the accumulation of undesirable material that may interfere with the essential wastewater treatment procedures. Screening is classied into two categories: coarse and fine screening. Coarse screening will remove big particles, rags, and debris from wastewater and often have apertures of 6 mm (0.25 in.), whereas small screens normally have openings ranging from 1.5 to 6 mm (0.06 to 0.25 in.) and

very fine screens with openings of 0.2 – 1.5 mm (0.01 – 0.06 in.) are used to remove suspended particles to levels similar to those attained by primary clarity (Asthana *et al.* 2017). Filtration is a physical process of removing turbidity and suspended solids from the wastewater (Shanmuganathan *et al.* 2017). The filtration process involves the use of filter media with holes varying from 0.1 to 0.5 mm to remove particles with a particle size less than 100 mg/L. (Gupta *et al.* 2012; Ince *et al.* 2019). In an emblematic filtration process, wastewater runs down through the filter bed, forming a layer of algae, plankton, and other tiny plant life on top (Gumbi 2020). Particles in suspension are eliminated through straining through the seive pores of the filtration medium (Zahrim *et al.* 2013). Sand filters are effective at retaining suspended materials such as algae, organic matter, fine sand, silt, micro-plastics, pesticides, and nitrates (Hoslett *et al.* 2018; Gumbi 2020; Wolff *et al.* 2021).

Ideally, after a month or two, filter beds should undergo a backwashing or cleaning process or the top 2 cm of the sand media should be replenished with new sand media (Zanacic *et al.* 2016). Sand filters are classified based on the driving force as either a slow or rapid filtration process (Gumbi 2020). Slow sand filters have largely been replaced by fast gravity sand filters, that are preferable for coagulant-treated water (Deshmukh *et al.* 2016). In the centrifugal separation process, different kinds of centrifugal machines that are employed to extract suspended non-colloidal particles sized up to 1 µm (Gupta *et al.* 2012; Ince *et al.* 2019). When separating solid materials by centrifugation, the density of suspended particles is the most essential characteristic (Ince *et al.* 2019).

2.3.2. Sedimentation-Flotation

The suspended particles, grits, and silts are removed in the sedimentation process by allowing water to remain undisturbed or semi-disturbed over a period of time in various types of tanks (Ince *et al.* 2019; Gumbi 2020). The suspended solid materials fall to tanks's bottom due to gravity. This mechanism occurrence usually varies based on the size and density of the suspended solid material (Ince *et al.* 2019). The settling time is determined by the size and density of the solids, as well as the velocity of the water in motion (Gupta *et al.* 2012). However, without the usage of coagulation, it is reported that about 60% suspended solids can be removed by sedimentation or gravity settling (Khiadani *et al.* 2014; Ince *et al.* 2019). On other hand, flotation works directly oppposite to sedimentation. Herein, the suspended solids are aggregated on top of the clear water at the bottom for easy removal. Its advantage is that it separates extremely tiny particles like lipids, oils, and lubricants, which can be eliminated more effectively using a scrubber (El-Gohary *et al.* 2010; Gupta *et al.* 2012; Tetteh 2018a; Gumbi 2020; Santos *et al.*

2021). Flotation processes are commonly used for the treatment of wastewater from the paper and refining industries (Gupta *et al.* 2012; Ince *et al.* 2019). This technique was utilized to reduce suspended contaminants like oil and lubricants, which were easily removed with a 75 to 99% efficiency (Gupta *et al.* 2012; Tetteh 2018a; Ince *et al.* 2019; Khouni *et al.* 2020; Zhang 2020). Flotation may be accomplished through a variety of techniques such as electrolytic, DAF and dispersed-air flotation (Edzwald 2010; Tetteh 2018a; Tetteh *et al.* 2020a). For instance, the DAF process uses air bubbles as the driving force to transport the particles in the liquid phase to the top surface (Tetteh 2018a; Gumbi 2020; Khouni *et al.* 2020), as shown in Figure 2-2. Changes in the separation phase are caused by four mechanisms: (1) air bubble creation due to coagulant addition, (2) interaction between air bubbles with particles, attachment of gas bubbles to particulates, and (4) surging up of an air bubble-particulate mixture (Meyer *et al.* 2005; Hanafy *et al.* 2007; Tetteh *et al.* 2019; Azadi *et al.* 2020).

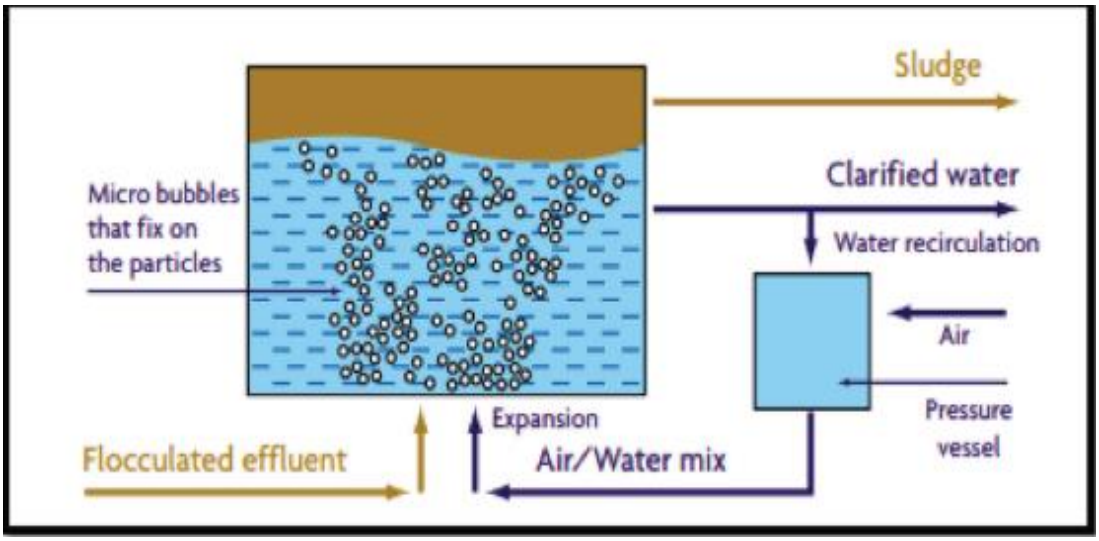

Figure 2-2 Schematic of coagulation coupled with dissolved flotation process, adapted from Tetteh *et al.* (2019)

2.3.2.1. Dissolved air flotation (DAF)

The design and integration of DAF into wastewater treatment systems is recently gaining much attention (Tetteh 2018a; Basso *et al.* 2019). Aside from the wastewater treatment settings, DAF has numerous applications namely the mineral sector, sludge thickening, biological algae separation, and the petrochemical and oil refinery industries (Edzwald 2010; Fonseca *et al.* 2017; eSilva *et al.* 2018; Sanchez *et al.* 2018; Jelodar *et al.* 2021; Soares *et al.* 2021). Furthermore, DAF has proven to be the best method for treating ultra-fine material containing brittle flocs as it

necessitates less denser flocs (Amaral Filho *et al.* 2016; Dlangamandla *et al.* 2018; Tetteh 2018a; Tetteh *et al.* 2019). The DAF process was found to be much favorable for the treatment of large volumes of wastewater at rates of 100 to 20,000 m^3/h to achieve the necessary footprint (Mokonyama *et al.* 2017). In a typical DAF system, the dissolved air bubbles are produced through the saturation of the water with an air saturator at a pressure between 3 and 6 atm (Karhu *et al.* 2014; Tetteh *et al.* 2020a; Santos *et al.* 2021). The saturated water discharge via needle valves or orifices produces micro-bubbles with diameters ranging from 10 to 100 µm (Santana *et al.* 2012; Karhu *et al.* 2014; Santos *et al.* 2021).

2.3.2.2. DAF operating parameters

The DAF is a multidimensional system. Its treatability efficiency is commonly affected by the operating parameters. Some of these parameters similar to that of the coagulation process include the percentage of air-water recycling, contact zone up flow rate and residency time, cross-flow, and hydraulic loading speed (Wang *et al.* 2007; Khannous *et al.* 2011; Oliveira *et al.* 2014; Tetteh 2018a; Tetteh *et al.* 2018a).

a) Residence time

The optimal retention period for the air-water combination is calculated in DAF when the pressurized saturator air-water is released into the floating zone (Tian *et al.* 2018). The flotation machine is visible at this phase because the air bubbles are attached to or enclosed by the flocs. This activity causes the flocs to become more buoyant, allowing flocs toreach the sludge zone; thus, a lengthy period of time is required. Flotation normally takes 10 to 15 min, but in practice, the period normally ranges from 10 to 40 min (Tetteh 2018a).

b) Bubble generation

The bubble is created by injecting pressurized air into the flotation tank then dissolve air under pressure. The air supplied for flotation is stated as a percentage of the air-water flow rate ranging from 5 to 12% (Khuntia *et al.* 2012; Sobieszuk *et al.* 2021). The air bubbles are produced to entrap the agglomerated flocs causing them to be buoyant to float and be collected by a skimmer (Tetteh 2018a). However, when particle-bubble contact time increases, tiny bubbles rise to the top more slowly, but bigger bubbles disturb or cause turbulence of the float layer (Dlangamandla *et al.* 2018; Epoyan *et al.* 2020; Qrenawi *et al.* 2021; Souza *et al.* 2021). The nature of air bubble size enhances the agglomerated pollutant particle-bubble adhesion before flotation. As a result, the

upward movement of water and bubbles in the interface region does not affect specific minimum particle sizes, resulting in low flotation efficiency. The particle density becomes the determining element for floatability in this case. Theoretically, particle sizes ranging from 10 to 50 µm proved to be appropriate for the use of DAF in treating wastewater (Edzwald 2010). DAF can efficiently treat particles with diameters much larger than 50 µm (Tian *et al.* 2018; Epoyan *et al.* 2020; Kyzas *et al.* 2021).

c) Rising velocity

The rate of ascent is determined by a pace at which waters in the floating zone rises. It is a critical part of determining the DAF's effectiveness. This is also known as the surface loading or the overflowing speed, therefore, is defined as the flow rate per unit surface area of the clarification tank. The quicker the floating period, the earlier the flocs will start to collapse, which the process typically claimed to take around 10 and 30 minutes (Edzwald 2010; Khuntia *et al.* 2012; Karhu *et al.* 2014; eSilva *et al.* 2018; Soares *et al.* 2021).

d) Air: Water recycle ratio

In a pressurized vessel, water is saturated with air. Water fills up to 80% of the overall volume, which is then sealed closed (Tetteh 2018a; Tian *et al.* 2018; Satpathy *et al.* 2020). Thereafter, the pressurized air is released into the contact region through the nozzle at the desired saturator operating pressure. The vapour ratio refers to the quantity of air introduced into the DAF to help the suspended solids float. Regrettably, no set-theoretical estimations of air to solid ratio exist since it is dependent on the kind of materials and the DAF setup (dos Santos Pereira *et al.* 2018; Fuad *et al.* 2021; Mukandi *et al.* 2021; Nikfar *et al.* 2021). About 6 to 22% of water is recycled back (Edzwald 2010).

e) Hydraulic loading

Hydraulic loading rate (HLR) is a significant component of DAF units, with a rate of 5 to 40 m/h contrasted to sedimentation flow rate of 0.5 to 5 m/h. However, this is generally determined by the flow velocity and quality of the water, as well as the temperature and shape of the flotation tank (Tetteh 2018a). HLR (Equation 2.1) is the maximum amount of input that may have been applied per DAF surface area over time. The inflow for the effective separation area equates the sum of feed solution flow velocity and plus the recycled air-water flow velocity. Nevertheless, when HLR is managed, does not produce turbulence into the working fluid (Dassey *et al.* 2012; dos Santos Pereira *et al.* 2018; Nikfar *et al.* 2021).

$$\text{Hydraulic load rate (HLR)} = \frac{\text{Effluent flow rate } \left(\text{m}^3/\text{h}\right)}{\text{Total clarifier footprint } (\text{m}^2)} \qquad \text{Equation 2.1}$$

2.3.2.3. Types of DAF systems

There are three prominent DAF designs based on the manner of producing air pressure, (1) vacuum flotation (VF), (2) micro-flotation (SF), and (3) pressure flotation (PT) (Al-Shamrani *et al.* 2002; Younker *et al.* 2014; Wu 2017; Choi *et al.* 2018; Yang *et al.* 2019; Al-Abri *et al.* 2020; Hollanda *et al.* 2021). Aside from potable water, the DAF idea offers a diverse set of uses in wastewater treatment, including the mineral sector, sludge thickening, biological algae separation, and the petrochemical and oil refinery industries (Edzwald 2010; Fonseca *et al.* 2017; eSilva *et al.* 2018; Sanchez *et al.* 2018; Jelodar *et al.* 2021; Soares *et al.* 2021). Furthermore, DAF has proven to be the most suited approach for treating an ultra-fine material with brittle flocs as because it necessitates a less thick floc (Amaral Filho *et al.* 2016; Dlangamandla *et al.* 2018; Tetteh 2018a; Tetteh *et al.* 2019). The DAF process has been observed to be more favorable for treating large amounts of wastewater at rates of 100 to 20,000 m^3/h to achieve the necessary footprint (Mokonyama *et al.* 2017). However, VT, SF, and PT are determined process of creating air pressure (Younker *et al.* 2014; Choi *et al.* 2018; Yang *et al.* 2019; Al-Abri *et al.* 2020; Hollanda *et al.* 2021). All these processes necessitate a supply of air bubbles in order to promote liquid-solid separation.

a) Vacuum flotation (VT)

In this technique, wastewater is saturated with air at atmospheric pressure (Tetteh 2018a). The flotation tank is then vacuumed to generate a moderately super - saturated solution, leading in the discharge of air in the form of little bubbles. The vacuum's practicality on the amount of air available for floating restricts the usage of this technique (Al-Shamrani *et al.* 2002; Kamaruddin *et al.* 2017; Song *et al.* 2017; Tetteh *et al.* 2018a; Zhao *et al.* 2020).

b) Micro-flotation (SF)

In this technique, the quantity of water in the saturator vessel must be pressured first to enhance the bubbles. As a result, the water is aerated in the down flow segment, and the quantity of water with dissolved air will increase as the hydrostatic pressure (HP) rises. HP reduces when water increases in the upstream flow phase, as a result of which air bubbles are released. To facilitate successful led to improvements or bubble formation, water must be pushed up and down a 10-

meter-deep shaft, where the amount of air given impacts the quantity of air accessible (Tian *et al.* 2018; Ortiz-Oliveros *et al.* 2019; Satpathy *et al.* 2020).

c) Pressure flotation (PT)

Pressure flotation is based on the fluctuation of air solubility in water with system pressure (Santos *et al.* 2021) that may be utilized in modes namely full-flow, split-flow, and recycled-flow pressurization (Edzwald 2010; Morozova *et al.* 2017; Shi *et al.* 2017; Tetteh 2018a; Tetteh *et al.* 2018c). In full-flow, entire wastewater is compressed and aerated inside the flotation tank to generate bubbles. Furthermore, it is widely utilized in businesses with influent streams containing particulates including more than 800 mg/L (Tetteh 2018a). While in split-flow, about 30-50% is pressurized and the rest travels directly to the flotation tank (Edzwald 2010). Spit-flow is typically used when the concentration of suspended materials is low or where micro bubbles are required to improve separation. The split flow pressure configuration system is far more costly compared to the full flow pressure configuration system because the saturator and piping system just manage a portion of the total flow sample. Furthermore, divided circulation offers very little air but yet demands significant pressure to give that very same volume of air (Yu *et al.* 2013; Dlangamandla *et al.* 2018; Sánchez Ortega 2019; Souza *et al.* 2021). In the recycle flow, a portion of the treated effluent, ranging from 15 to 50%, can be compressed and returned back to the flotation tank. This is done through a pressure discharge mechanism with air bubble sizes ranging from 20 to 100 μm (Tian *et al.* 2018). In wastewater treatments, the recycle-flow pressurization phase is preferred because the other phases may interfere with the coagulation process (Edzwald 2010; El-Gohary *et al.* 2010; Karhu *et al.* 2014; Crini *et al.* 2018).

2.3.3. Coagulation/ Flocculation

Coagulation is the act of using chemicals or coagulants to destabilize suspended particles in order to ignite the commencement point for them to combine. When the destabilized suspended particles get together, form agglomerates, flocculation begins (Usefi *et al.* 2019; Cui *et al.* 2020; Gautam *et al.* 2020; Muniz *et al.* 2020; Khettaf *et al.* 2021; Noor *et al.* 2021; Sibiya *et al.* 2021). The agglomerated flocs can then be eliminated by either sedimentation or direct filtration or flotation process (Jagaba *et al.* 2016; Ugya *et al.* 2016; Gumbi 2020; Tetteh *et al.* 2020). Since water contains negatively charged suspended particulates owing to the same sort of surface charge, it causes repulsion and prevents aggregation and settling (Bodlund 2013a; Jagaba *et al.* 2016). This becomes very critical in decontamination of turbidity, color, COD, and TSS of wastewater (Varjani *et al.* 2017; Varjani *et al.* 2020). A successful coagulation results in the

elimination of approximately 90% of the suspended materials (Matilainen *et al.* 2010; Zahrim *et al.* 2017; Momeni *et al.* 2018; Tetteh *et al.* 2019; Jagaba *et al.* 2020; Sibiya *et al.* 2021).

2.3.3.1. Mechanisms of coagulation/flocculation

Coagulation changes the colloidal particles in water such that they may approach and cling to one another to produce bigger flocs as shown in figures 2-3 (Ernest *et al.* 2017). This phenenomon can occur in three distinct mechanisms (1) charge neutralization (particle destabilization at low coagulant dosage), (2) sweep (the addition of coagulant at sufficiently high concentrations to cause anhydrous, amorphous precipitate enmeshing colloidal particles into precipitates), and (3) bridge formation (Amran *et al.* 2018; Cui *et al.* 2020; Sibiya *et al.* 2021). However, the majority of coagulants and flocculants used in potable water and wastewater treatment contain divalent positively charged chemical compounds (Balls 2014). The negatively charged polymers have large molecular weight flocculant (Kurniawan *et al.* 2020). According to Sahu *et al.* (2013), the charge density of the coagulants can contribute to the agglomerated floc size of diameters between 10^{-7} to 10^{-14} cm. In essence, agglomeration of the suspended particles usually depends on the source, content, and ionic strength of the coagulant. Also, operation factors such as temperature, pH, effluent quality, dose, and coagulant type can affect the coagulation mechanism (Xiao *et al.* 2009; Yang *et al.* 2010; Ernest *et al.* 2017; Tetteh *et al.* 2018a; Ince *et al.* 2019; Tetteh *et al.* 2019; Gumbi 2020; Mosaddeghi *et al.* 2020; Khettaf *et al.* 2021). The type of interactions between chemical coagulants and colloidal particles determine the coagulation process (Sahu *et al.* 2013).

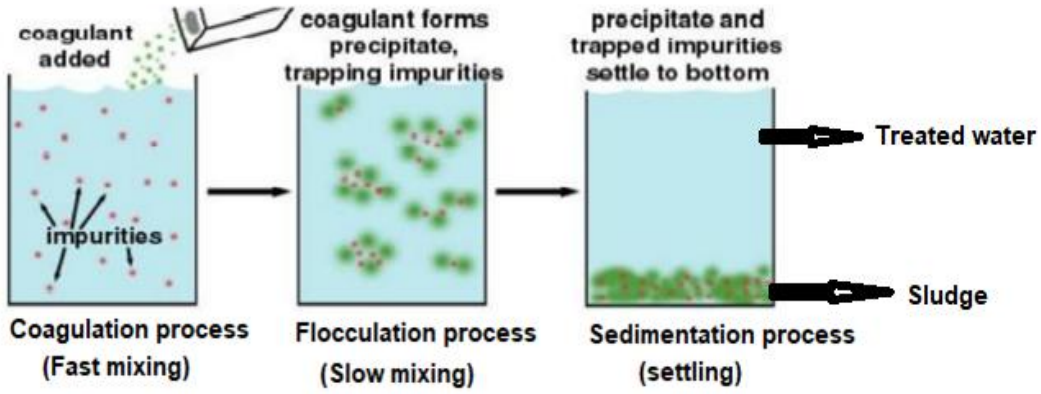

Figure 2-3 Modified schematic diagram of a coagulation process, adapted from (Gumbi 2020)

Adsorption and bridging, double-layer compression, charge neutralization, and sweep coagulation can all cause colloidal particle instability. Each of these mechanisms is discussed in detail below.

Double-Layer compression

This mechanism involves decreasing of the double layer around the colloidal particle due to a change in ionic strength caused by adding new coagulants that can lead to colloid instability (Freitas *et al.* 2017; Ghorpade *et al.* 2018; Wahaab *et al.* 2019; Xia *et al.* 2020). The suspended particles in the solution are negatively charged, attracting counter-ions (Teh *et al.* 2016; Vepsäläinen *et al.* 2020; Bhamidipati *et al.* 2021). Surface attraction is caused by opposing ion charges moving towards the surface of an electrolytic solution, whereas repulsion is caused by ions with the same charge moving away from the surface. Stern layer is formed because of electrostatic and Van der Waals forces (Pokhrel *et al.* 2004; Teh *et al.* 2016; Vepsäläinen *et al.* 2020). A diffuse layer forms surrounding the Stern Layer by attracting co-ions of the primary colloid onto the counter-ions size (Tripathy *et al.* 2006; Amran *et al.* 2018; Bhamidipati *et al.* 2021). Figure 2-4 shows a representation of an electrical double layer formed by charge separation on the top of a colloidal particle (Pokhrel *et al.* 2004; Tripathy *et al.* 2006).

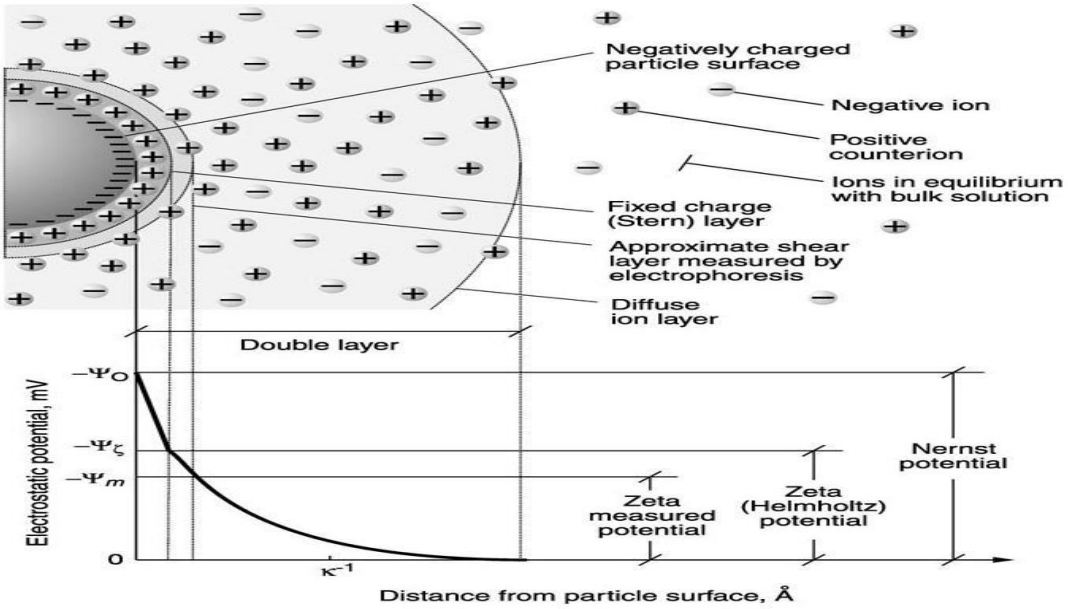

Figure 2-4 Representation of electrical double layer adapted from (Pokhrel *et al.* 2004; Vepsäläinen *et al.* 2020)

Electric double layer is a diffused layer that consist of anions and cations (Tripathy *et al.* 2006; Teh *et al.* 2016; Tetteh 2018a). Colloidal particles are difficult to approach one other under steady circumstances with low counter-ion concentrations due to their thick double electrical barrier (Teh *et al.* 2016; Freitas *et al.* 2017). However, when the quantity of counter-ions increases as a result of salt (counter-ion) addition, the diffuse layer thins and particles can interact more intimately

prior experiencing repulsion (Bhamidipati *et al.* 2021). Shearing transports just a portion of the diffuse layer with the colloid, and the potential at the shear surface is referred to as the zeta potential (Bhamidipati *et al.* 2021). Compression of the electrical double layer, is the major coagulation mechanism for divalent ions, namely Ca^{2+} and Mg^{2+}, in the usual pH range of water treatment (Duan *et al.* 2009; Freitas *et al.* 2017). The interface of a charged surface can be explained by the Helmholtz, Gouy, and Chapman models (Doblhoff-Dier *et al.* 2021). Stern used the aforementioned models to create an electrical double layer model (Vepsäläinen *et al.* 2020). The electrical double layer is divided into two regions as the Stern/Helmholtz layer (inner plane) and the Gouy-Chapman layer (outer plane), where ions are strongly attached to the surface and ions move about due to diffusion (Tripathy *et al.* 2006; Vepsäläinen *et al.* 2020). A capabilty of an inner area affects colloidal particle stability. Furthermore, the ionic strength and valence of the ions have a significant influence on the thickness of the double layer (1/k) shown in equation 2.2 (Vepsäläinen *et al.* 2020). The thickness of the double layer diminishes as the ionic strength increases, and maximal destabilization occurs when the colloidal surface's zeta potential approaches 0 mV (Duan *et al.* 2009; Freitas *et al.* 2017; Vepsäläinen *et al.* 2020).

$$\frac{1}{k} = 10^{10}\left[\frac{2000e^2 N_A I}{\varepsilon_0 KT}\right]^{-0.5} \qquad \text{Equation 2.2}$$

Where;

$\frac{1}{k}$ Debye-Hückel length (m)

K Boltzmann's constant (J/ K)

T Temperature (K)

N_A Avogadro's number (6.02214076×10^{23})

I Ionic strength (mol/m^3)

ε_0 Permittivity in vacuum (8.854×10^{-12} Farad /m)

a) Adsorption and bridging

This mechanism is only conceivable with plant-based coagulants and proceeds by polymer adsorption, in which long chain polymers or electrolytes attach themselves to the surface of the colloidal particle (Tripathy *et al.* 2006; Freitas *et al.* 2017; Amran *et al.* 2018). A crucial prerequisite for bridging is that the particles provide enough empty surface area for the adsorption of polymer chain segments trapped on other particles (Freitas *et al.* 2017; Bhamidipati *et al.* 2021). Figure 2-5 shows stages of this mechanism.

Adsorption must occur uniformly throughout the solution for successful coagulation, hence polyelectrolytes must be disseminated at fast mixing for a brief amount of time (Bhamidipati *et al.* 2021). Thereafter, polymer chains are linked to the particle at various adsorption sites, minimizing dangling ends (Tetteh 2018a; Vepsäläinen *et al.* 2020) as shown in figure 2-5a. Molecular mass of the natural coagulant is critical in particle bridging. Natural coagulants with a larger molecular weight can create strong bridges with particles, resulting in the production of strong flocs and improved settling (Ang *et al.* 2020b; Nimesha *et al.* 2021).

Adsorption consists of three types namely electrostatic interaction, hydrogen bonding and ionic bonding (Amran *et al.* 2018; Bhamidipati *et al.* 2021). Only a few polymer segments are connected to the particle, with the remainder forming loops and tails (Tripathy *et al.* 2006; Vepsäläinen *et al.* 2020; Bhamidipati *et al.* 2021; Nimesha *et al.* 2021). Colloidal particles connect to these tails and loops, resulting in the creation of huge flocs, which is at the heart of polymer bridging as shown in figure 2-5b.

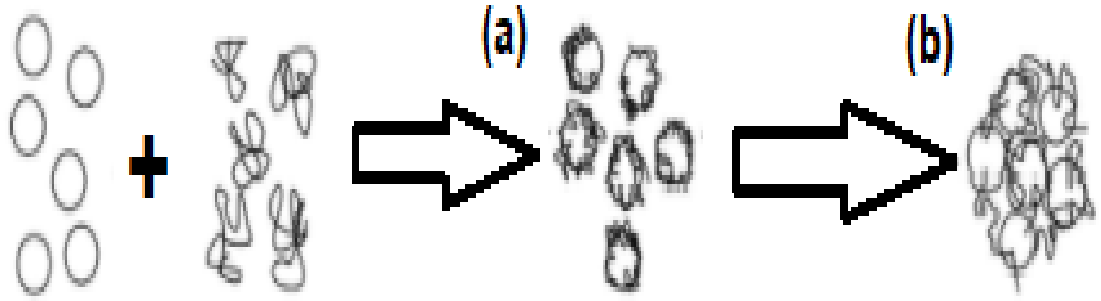

Figure 2-5 Systematic presentation of mechanism (a) adsorption (b), bridging adapted from Bhamidipati *et al.* (2021)

The availability of adsorption sites on the particles near polyelectrolytes is a critical criterion for bridging. This is determined by the concentration of polyelectrolyte used; if the dose is too high, full adsorption occurs, and no sites for inter-particle bridging are available (Tripathy *et al.* 2006; Sher *et al.* 2013; Bhamidipati *et al.* 2021). When it is low, it results in poor adsorption and bridging. As a result, there is an ideal polymer dose based on the number of adsorption sites accessible and hence on particle concentration (Choy *et al.* 2015; Freitas *et al.* 2017; Tetteh 2018a; Kristanda *et al.* 2021).

b) Charge neutralization

The ability to add cationic metals or polymeric materials to particles to balance their negative charges whilst reducing double layer repulsion is known as charge neutralization (Sahu *et al.* 2013; Freitas *et al.* 2017; Amran *et al.* 2018; Tetteh 2018a; Ang *et al.* 2020b; Nath *et al.* 2020; Bhamidipati *et al.* 2021; Nimesha *et al.* 2021) as shown in figure 2-6. An ionizable polymer (polyelectrolytes) is utilized as a coagulant because it keeps negatively charged colloidal particles stable (Nimesha *et al.* 2021). To stabilize the particles, polycation is used, resulting in a zeta potential near to zero (Amran *et al.* 2018). The optimal polyelectrolyte dose will be determined by the charge distribution of the polyelectrolyte. Electrostatic interactions cause substantial adsorption in these systems, as well as particle surface neutralization and even charge reversal (Zouboulis *et al.* 2000; Teh 2014; Choy *et al.* 2015; Vepsäläinen *et al.* 2020).

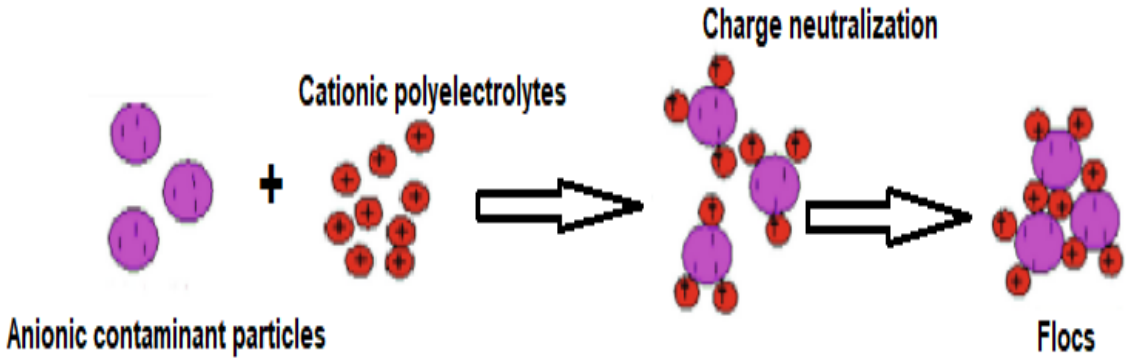

Figure 2-6 Charge neutralization mechanism, adapted from (Nath *et al.* 2020)

c) Sweep Coagulation

This mechanism occurs when suspended particles get entwined in metal hydroxide precipitates or are washed out of the water by an irregular hydroxide precipitation (Duan *et al.* 2003b; Tetteh

2018a; Vepsäläinen *et al.* 2020; Bhamidipati *et al.* 2021). In general, this provides far greater particle elimination as opposed to soley charge neutralization (Duan *et al.* 2003b; Freitas *et al.* 2017). However, the flocs created are weaker than those formed in the bridging mechanism (Bhamidipati *et al.* 2021).

2.3.4. Types of coagulants

A coagulant is added to industrial and surface wastewater to speed up the process by converting suspended particles into flocs, which allow them to bridge together while improving strength, settling time, and reaching ideal weight (Abdelaal 2004; Beyene *et al.* 2016; Ang *et al.* 2020b; Kurniawan *et al.* 2020). An enhanced efficiency coagulation method facilitates the microbial quality of the end product and increases the longevity of filter media, lowering the overall cost of treated water (Kumar *et al.* 2016; Kamaruddin *et al.* 2017; Kumar *et al.* 2017b; Nimesha *et al.* 2021). Coagulants are used in treating wastewater rely on the composition of the wastewater (Tetteh 2018a; Tetteh *et al.* 2019; Nath *et al.* 2020). Additionally, it is important to explore the selection of suitable coagulants (Figure 2-7) based on long-term treatment plant performance, chemical usage reduction, and production of high-quality water (Sahu *et al.* 2013; Tetteh 2018a).

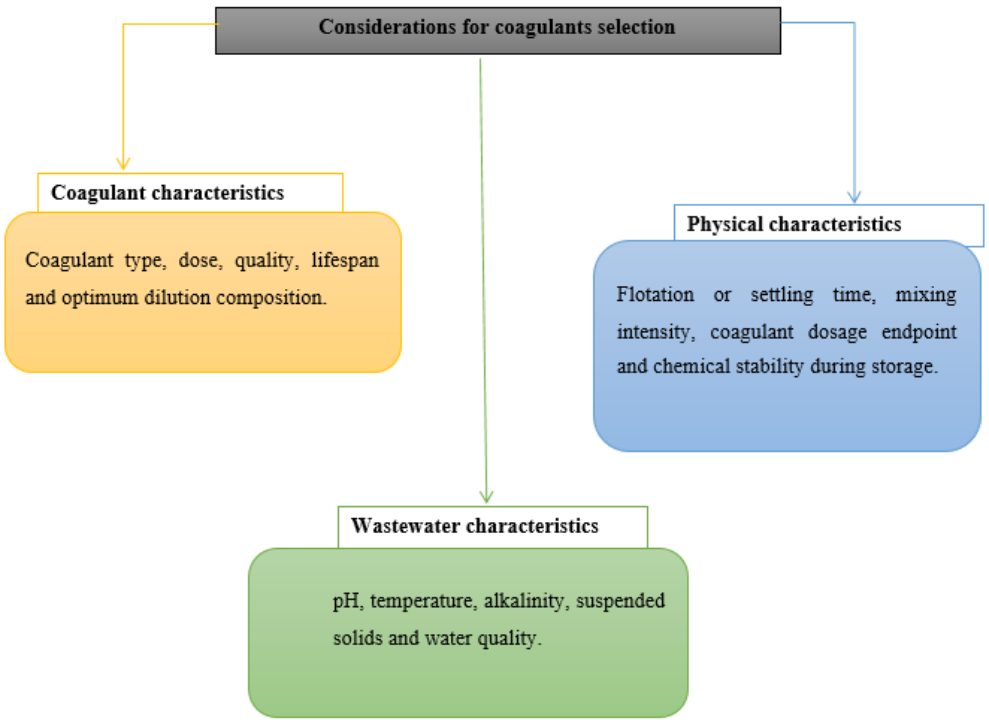

Figure 2-7 Factors to consider when choosing coagulants, adapted from (Abdelaal 2004; Kumar *et al.* 2017b; Saxena *et al.* 2018; Tetteh 2018a; Gautam *et al.* 2020; Nimesha *et al.* 2021)

2.3.4.1. Natural coagulants

Coagulants come in a variety of forms, including inorganic and polymeric organic coagulants. (Abdelaal 2004). Organic and inorganic coagulants have been used over decades due to their easy access and low cost (Jagaba *et al.* 2020; Muniza *et al.* 2020; Noor *et al.* 2021). Furthermore, they do not exhibit toxic properties in an aquatic environment (Gautam *et al.* 2020; Muniz *et al.* 2020; Nimesha *et al.* 2021). The natural polymers can be categorized into three groups such as animal-based, plant-based, and microorganism-based as shown in figure 2-8. Natural coagulants are supplied locally, are abundant, create less sludge, and produce biodegradable sludge (which may be reused) and may be waste-based resources such as fruit wastes, eggshells, cassava peel, okra leaves, etc. (Choy *et al.* 2014; Anju *et al.* 2016; Amran *et al.* 2018; Ang *et al.* 2020b; Gautam *et al.* 2020; Asharuddin *et al.* 2021). This research focuses on three natural coagulants: chitosan, eggshells, and rice starch, which are discussed more below.

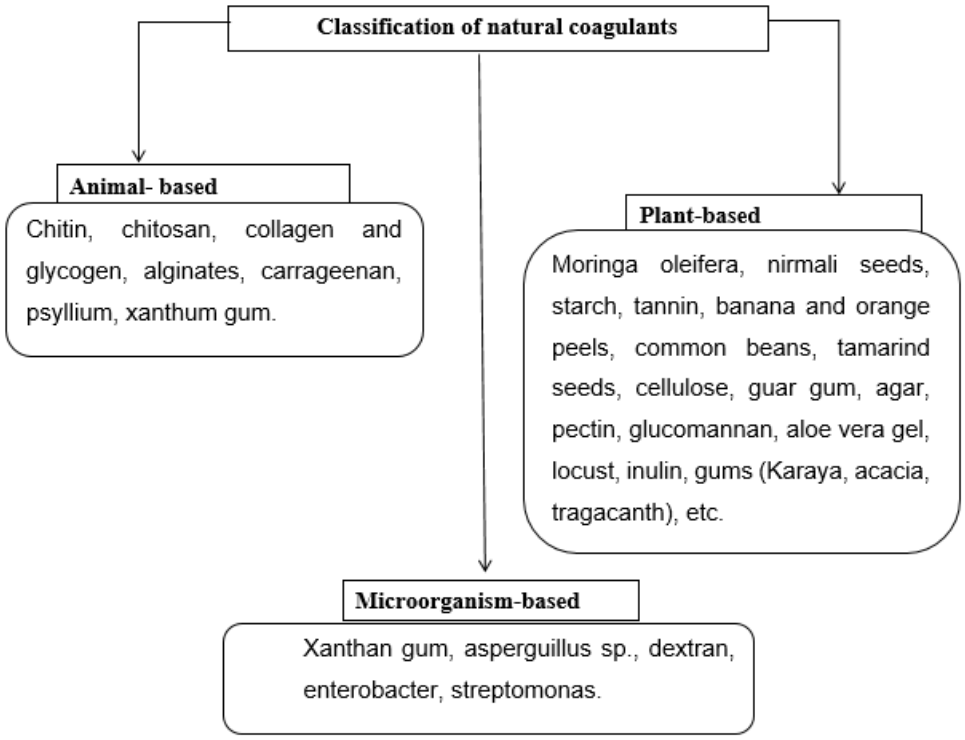

Figure 2-8 Categories of natural coagulants

a) Chitosan

Chitosan (CS) is known as poly[*β*-(1→4)-2-amino-2-deoxy-*D*-glucopyranose] (Dung *et al.* 2009; Zaidi *et al.* 2014; Morsi *et al.* 2018; Vidal *et al.* 2018; Kocabas *et al.* 2019; Prasetiyo *et al.* 2021),

and is a high-molecular-weight biopolymer derived from the deacetylation of chitin (Vishakha *et al.* 2012; Lozano-Navarro *et al.* 2018; Nimesha *et al.* 2021). Chitin or poly(b-1-4)-2-acetamido-2-deoxy-D-glucopyranose is the second most prevalent natural polymer following cellulose derived from crustacean shells such as snails, crabs, bugs, and prawns (Vishakha *et al.* 2012; Vidal *et al.* 2018; Jo *et al.* 2019; Ang *et al.* 2020a; Prasetiyo *et al.* 2021). It is present in mollusks, annelids, and arthropods, as well as in the mycelia and spores of numerous fungi (Vishakha *et al.* 2012; Jana *et al.* 2019; Fufaeva *et al.* 2020).

Chitin is a cellulose derivative in which the hydroxyl groups are on the second carbon of each glucose unit. Chitin deacetylation s associated with the formation of amine groups (NH_2) from acetamide groups ($NHCOCH_3$) in many ways, the most frequent are reactions with alkaline aqueous medium at high temperatures, which can take up to three hours depending on the reaction conditions (Vishakha *et al.* 2012; Lozano-Navarro *et al.* 2018; Vidal *et al.* 2018; Jo *et al.* 2019; Ang *et al.* 2020a). The degree of acetylation (DA) is a metric that describes the average concentration of N-acetyl-d-glucosamine units in chitin, which generates a range of chitosan with changing physical and chemical parameters like solubility, relative molecular mass, pKa, and viscosity (Frick *et al.* 2018; Lozano-Navarro *et al.* 2018; Vidal *et al.* 2018; Prasetiyo *et al.* 2021). Depending on the deacetylation process utilized, the degree of deacetylation (DD) reflects the average value of d-glucosamine units on the chain content of 50 to 95 percent (Figure 2-9).

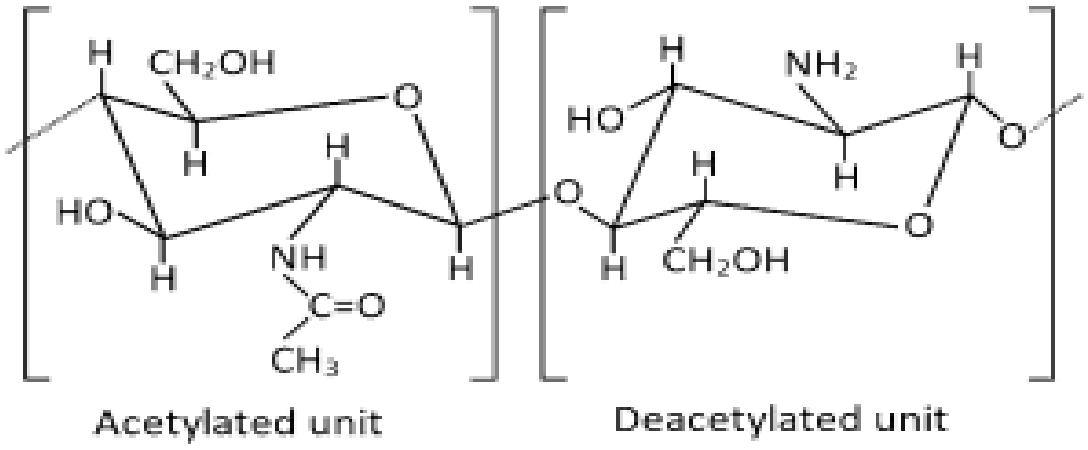

Figure 2-9 Structure of chitosan with acetylated and deacetylated units, adapted from (Vidal *et al.* 2018)

The relationship between these factors is given by Zhang *et al.* (2021c) as follows: DA (%) =100 - DD (%). CS has a good catalytic activity and recyclability for its free main $–NH_2$ and -OH groups (Wang *et al.* 2008; Hoang Tran *et al.* 2009; Kumar *et al.* 2017b; Ang *et al.* 2020a). In

solution, CS shows to be positively charged (Saifuddin *et al.* 2011; Vidal *et al.* 2018; Zhang *et al.* 2021c). Furthermore, CS may be dissolved in an acidic solution via interaction between H^+ and the amine group due to inter-molecular and intra-molecular hydrogen bonding (Wang *et al.* 2009; Mansoori *et al.* 2020; Prasetiyo *et al.* 2021). At $pH < 6$, Acidic liquids promote the degradation of chitosan and render it insoluble, lowering its efficacy (Frick *et al.* 2018; Vidal *et al.* 2018; Vainshtein *et al.* 2020). When the pH rises over 6, the chitosan amine groups start to denature, and the polymer precipitates. Since pKa value is greatly reliant on DA, chitosan solubility is determined by the degree and manner of deacetylation utilized, the distribution of the acetyl groups on its structure, and its molar mass (Vidal *et al.* 2018; Mansoori *et al.* 2020). Thus, the more protonated groups there are, the higher the electrostatic opposition between the chains, as a result, he greater the molecular effects on the overall in an aqueous solution (Kumar *et al.* 2017b).

Due to their inherent biological features and biodegradability, chitosan-based materials have the potential to be environmentally benign coagulants and flocculants in the harvesting process (Vidal *et al.* 2018; Gautam *et al.* 2020). Furthermore, its recyclability, effectiveness and ability to chelate arsenic, molybdenum, cadmium, chromium, lead, and cobalt ions makes it an appealing choice for treating industrial effluents (Ummalyma *et al.* 2016; Ang *et al.* 2020b).

There are several techniques for physically or chemically modifying raw chitosan flakes to improve their adsorption behavior for different kinds of contaminants (Bhatnagar *et al.* 2009; Frick *et al.* 2018; Vidal *et al.* 2018; Mansoori *et al.* 2020; Prasetiyo *et al.* 2021; Zhang *et al.* 2021c). All of the alterations reveal that there could be only one improvement between two parameters, either molecular weight or water solubility, and not both (Wang *et al.* 2009). Even though crosslinking reduces adsorption capacity, it increases the resistance of chitosan against acid, alkali, and other chemicals (Ngah *et al.* 2002; Babakhani *et al.* 2020; Okpaegbe *et al.* 2021). Furthermore, cross-linking alters the crystalline structure of CS, stabilizing and preserving its strength in both acidic and basic conditions (Zeng *et al.* 1998; Jana *et al.* 2019; Fufaeva *et al.* 2020; Kildeeva *et al.* 2020; Mansoori *et al.* 2020).

b) Rice starch

In the last 5000 years, rice (known as Oryza sativa L.) has been a significant cereal grain and a basic food supply for more than 50% of the worldwide people (Wani *et al.* 2012; Chua *et al.* 2019). During the rice milling process, around 20 to 30% of milled rice ends up as broken rice (Teh *et al.* 2014a; Chua *et al.* 2021a; Nimesha *et al.* 2021). Rice starch (RS) are the tiniest found in cereal grains, with sizes ranging from 2 to 7 μm (Wani *et al.* 2012). As a result, the usage or

valorization of this by-product is extremely advantageous. RS has a distinct flavor, a milky, chewy texture, and a smooth finish. These properties include hypoallergenicity, digestibility, consumer acceptability, bland flavor, tiny granules, white color, enhanced paste freeze-thaw stability, better acid resistance, and a wide spectrum of amylose: amylopectin ratios (Wani *et al.* 2012).

Starch is the most essential element of rice, contributing for more over 80% of the overall content (Chua *et al.* 2019). It occurs in nature as distinct particles known as granules. Starch, also known as amylum, is a carbohydrate composed of a high number of glucose units linked together by glycosidic bonds (Vishakha *et al.* 2012). All green plants synthesize this polysaccharide as an energy storage (Singh *et al.* 2012; Amran *et al.* 2018). It seems to be the most prevalent kind of carbohydrate reserve in green plants, and it is especially abundant in seeds and subterranean organs (Hamidi *et al.* 2021).

Starch, is one of the world's most prevalent natural polymers,is made up of two polymers of anhydroglucose units, amylose, and amylopectin, in its unrefined form (Wani *et al.* 2012; Teh 2014; Irinislimane *et al.* 2017; Amran *et al.* 2018; Chua *et al.* 2021a; Kumar *et al.* 2021b). Amylose is a non-branching helical polymer made up of -1,4 connected D-glucose monomers, whereas amylopectin is a highly branched polymer made up of both -1,4 and -1,6 linked D-glucose monomers as shown in figure 2-10 (Damager *et al.* 2010; Singh *et al.* 2012; Vishakha *et al.* 2012; Amran *et al.* 2018; Chua *et al.* 2021a; Hamidi *et al.* 2021). Amylose is the most important component controlling rice starch's physicochemical qualities. Starch expands irreversibly and its crystalline structure collapses when heated in aqueous solutions, a condition known as gelatinization.

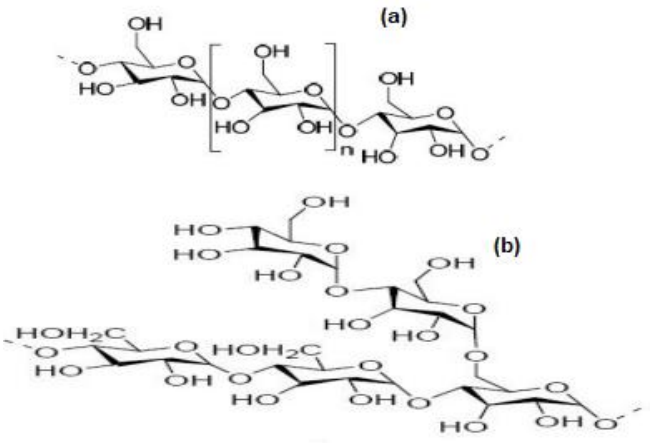

Figure 2-10 Structure of a) Amylose b) Amylopectin, adapted from Vishakha *et al.* (2012)

Amylopectin can expand starch, but amylose has been shown to inhibit it (Goel *et al.* 2020; Hong *et al.* 2021; Mosisa *et al.* 2021). Gelatinization is the process by which starch is transformed into tangible form that is beneficial in in several food production (Wani *et al.* 2012). Starch gels, on the other hand, are thermodynamically unstable and undergo changes that affect their technical applicability (Lupi *et al.* 2020). When starch molecules cool, they re-associate in a complex crystal growth process known as retrogradation, and is typically related with gel water separation (Wani *et al.* 2012). These modifications may cause textural and optical gel degradation (Fredriksson *et al.* 2000; Chelliah *et al.* 2019).

Starch has attracted commercial attention as a coagulant because of its its recyclability, biocompatible, and inexpensive (Pal *et al.* 2005; Teh 2014; Choy *et al.* 2016; Usefi *et al.* 2019; Chua *et al.* 2021a; Hamidi *et al.* 2021). The majority of existing research has focused on starch modification to boost the efficacy of the coagulant in effluent treatment, which has several downsides such as formaldehyde, extremely corrosive caustic soda, and a high volume of solvent (Choy *et al.* 2016; Chua *et al.* 2019; Hamidi *et al.* 2021; Kumar *et al.* 2021b). These modifications are accomplished by graft copolymerization, in which synthetic polymers like acrylamide are mixed with starch to increase the total molecular weight of the polymer (Whistler 2009; Choy *et al.* 2016). Unmodified starches might be used in conjunction with chemical coagulants to reduce the negative effects of these proprietary coagulants (Teh 2014; Hamidi *et al.* 2021). A study by Teh *et al.* (2014b) achieved 84.1% TSS removal solely by utilization of RS as a coagulant. RS, on the other hand, has more advantages than other starches (corn, cereal, wheat, oat, potatoes, barley, etc.) because of its great stability, as well as acid resistance.(Chua *et al.* 2019).

c) Eggshells

The disposal of egg shells causes severe land contamination, bad odors as a result of microbiological action, and costly disposal expenses (Kulpa *et al.* 2018). However, the method of employing eggshells has a fantastic upsurge of excellent ideals (Guru *et al.* 2014; Naghizadeh *et al.* 2017). Eggshells have between 7000 and 17000 pores and are an excellent alternative biosorbent, particularly for the elimination of dyes and dangerous inorganic ions (Kocabas *et al.* 2019) as well as the capacity to remove heavy metals from water (Jayan *et al.* 2015). These pores exchange materials between the exterior and interior of eggshells while being strong enough to avoid cracking from impact.

When compared to the microstructure of sea turtle eggshells (Kitimasak *et al.* 2003), chicken eggshells are more compact, suggesting that the porosity structure of eggshells is influenced by the damp environment. These eggshells are a highly organized structure with five structurally

distinct layers (Moreno-Azanza *et al.* 2016). hese are the shell membranes (inner and outer), mammillary layer, palisade layer, vertical crystal layer, and cuticle, from the inside out as shown in figure 2-11.

Crystal arrangement and size vary over various strata (Teyssier *et al.* 2015). The mammillary layer is the first mineralized layer formed by the inner membranes and is considered to include randomly oriented calcite ($CaCO_3$) crystals (Guru *et al.* 2014; Jayan *et al.* 2015; Naghizadeh *et al.* 2017; Kulpa *et al.* 2018). A variety of experiments, including powder line broadening research, have shown that the calcite crystals are enormous, with dimensions more than 1 mm (Guru *et al.* 2014). The palisade layer comprises of majority of the calcified component of the shell; here, calcite crystals form with a long aspect perpendicular to the surface (Guru *et al.* 2014). The palisade layer is continuing as the vertical crystal layer, which is a thin layer just beneath the cuticle.

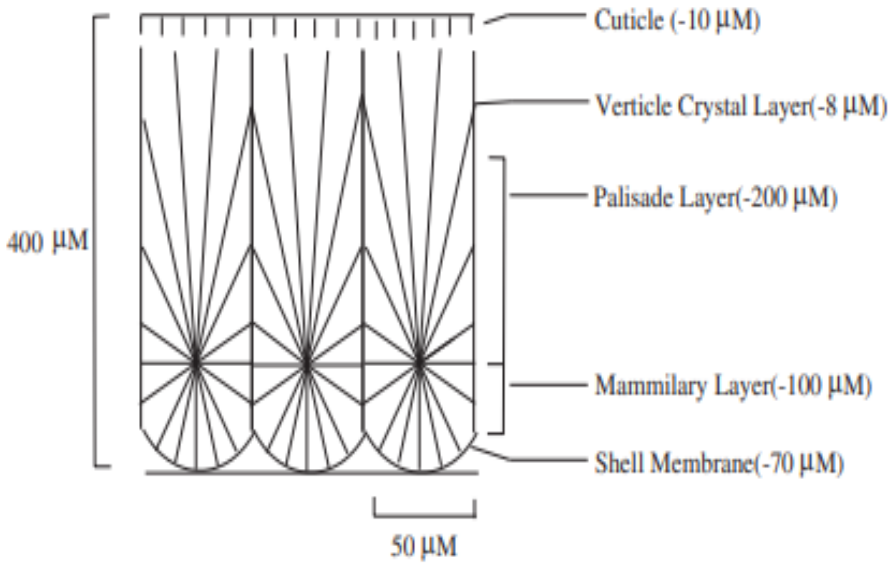

Figure 2-11 The five structurally distinct layers within the eggshell are depicted schematically, adapted from Guru *et al.* (2014).

Eggshells (ES) are a low-cost, readily accessible biomaterial, and their waste is frequently employed as a bone replacement, for catalysis, scaffolding, and useful bio-templates due to their high catalytic activity, ease of handling, reusability, and benign nature (Yang *et al.* 2002; Valtchev *et al.* 2008; Viriya-empikul *et al.* 2010; Kocabas *et al.* 2019). They have several surface functional groups, including as amines, amides, and carboxylic groups (Jayan *et al.* 2015). Precisely

eggshells contain calcium carbonate (94%), magnesium carbonate (1%), calcium phosphate (1%) and organic matter (4%) (Cai *et al.* 2007; Guru *et al.* 2014; Naghizadeh *et al.* 2017).

In biological systems, organic components are hypothesized to impact nucleation, govern crystal development and form, and have a role in defining the mechanical characteristics of the final composite (Gautron *et al.* 2021). Proteins are the primary elements of eggshell and shell membrane organic matter, with minor quantities of carbohydrates and lipids (Zeidler 2002; Mine 2007; Pundir *et al.* 2009; Okubo *et al.* 2018; Guha *et al.* 2019; Kalifah 2019).

Concentrations of "organic matrix cores" and matrix material at the ends of the shell mammillae aid in the diffusion of a physiological decalcifying agent developed during the chick's embryonic development into the mammillary "*mineral cores*". Furthermore, the shell matrix contains an acid mucopolysaccharide that acts as a calcium chelator during shell formation (Guru *et al.* 2014). Proteins, proteoglycans, and fibronectin in the matrix may thus contribute to the mechanical properties of ES (a) indirectly by affecting the shell calcite fabric and (b) directly by influencing the elasticity of the shell when these biomolecules get incorporated into the shell (Kaur 2010; Johnson 2015; Teyssier *et al.* 2015; Nys *et al.* 2018).

2.3.4.2. Chemical-based coagulants

This type is classified into three types of chemical coagulants: hydrolyzing metallic salts (alum, ferric chloride, ferric sulfate, magnesium chloride), pre-hydrolyzing metallic salts (polyaluminium chloride, polyferic chloride, polyferrous sulfate, polyaluminium ferric chloride), and synthetic cationic polymers (polyamine, polyethylenimine, polyalkylene, aminomethyl polyacrylamide) (Abdelaal 2004; Freitas *et al.* 2017; Tetteh 2018a; Cui *et al.* 2020; Asharuddin *et al.* 2021; Nimesha *et al.* 2021). Iron (ferric sulfate, ferrous sulfate and ferric chloride) and aluminum (aluminium chloride, aluminium sulfate as alum and sodium aluminate) metal salts are two of the most often utilized inorganic coagulants (Ugya *et al.* 2016; Freitas *et al.* 2017; Cui *et al.* 2020; Gautam *et al.* 2020; Nimesha *et al.* 2021) because of their inexpensive cost, simplicity of use, handling, storage, and mixing capabilities (Sher *et al.* 2013; Jagaba *et al.* 2016; Freitas *et al.* 2017). Also hydrated lime and magnesium carbonate are commonly used chemicals as coagulants (Kumar *et al.* 2017b; Nath *et al.* 2020).

Chemical coagulants are divalent or trivalent metal ions that have been used to neutralize the charge on the surface of anionic particles and aggregate them into bigger flocs (Teh *et al.* 2016; Ernest *et al.* 2017). Both the aluminum and iron-based salts interact with the hydroxyl ions (OH^-), producing monomeric and polynuclear species that react with the negatively charged

particles (Freitas *et al.* 2017; Tetteh 2018a; Nath *et al.* 2020). This causes the salts to dissociate into their trivalent ions (i.e., Al^{3+}, Fe^{3+}), which hydrate to to form multiple water molecules and securely attach onto an anionic particles (Teh *et al.* 2016; Freitas *et al.* 2017; Cui *et al.* 2020). The benefits and drawbacks of the most commonly utilized coagulants are shown in Table 2-1.

Table 2-1 Effectiveness and disadvantages of chemical coagulants, adapted from (Kumar *et al.* 2017b; Tetteh 2018a; Nath *et al.* 2020)

Common name	**Chemical formula**	**Effectiveness**	**Disadvantages**
Lime	$Ca(OH)_2$	It is widely utilized; it is extremely effective; and it does not add salts to effluent. It improves the removal of heavy metals (manganese) and softens the water.	pH dependant; generates a substantial amount of sludge; overdosage can result in poor effluent quality.
Alum	$Al_2(SO_4)_3.18H_2O$	Simple to use and apply; generates less sludge than lime; best effective between pH 5.5 and 7.7.	Adds dissolved particles (salts) to water; its toxicity may lead to neurological conditions.
Sodium aluminate	$Na_2Al_2O_4$	Effective in hard water; and generally, a minimum quantity is required.	Frequently used in conjunction with alum; expensive; and it is ineffective in soft waters.
Polyaluminium Chloride (PAC)	$Al_{13}(OH)_{20}(SO)_4.Cl_{15}$	Floc produced is denser and settles faster than alum in various applications.	Not widely utilized; little full-scale data as compared to other aluminum derivatives.
Ferric Sulfate	$Fe_2(SO_4)_3$	It is effective between pH 4-6 and 8.8-9.2. It can remove color at a low dose.	Adds dissolved solids (salts) to water; and generally, it requires alkalinity.
Ferric Chloride	$FeCl_3.6H_2O$	It is effective between pH 4 and 11.	Adds dissolved particles (salts) to water; uses twice as much alkalinity as alum. It is very corrosive to almost all metals.
Ferrous Sulfate (Copperas)	$FeSO_4.7H_2O$	Not as sensitive to pH as lime. It effectively controls odour by avoiding the development of hydrogen sulphide.	Adds dissolved solids (salts) to water; and generally, it requires alkalinity.

2.3.5. Factors affecting coagulation

There are various operational elements that affect the parallel and consecutive processes that take place whenever a coagulant is added to wastewater. There are a number of transportation processes that occur to enhance interparticle bridging and floc formation, including Brownian diffusion and fluid motion (Tetteh *et al.* 2019). All of these factors (2.3.5.1. to 2.3.5.6.) have an impact on the efficiency and efficacy of the wastewater coagulation process.

2.3.5.1. Coagulant dosage

Coagulant dose is an important component in determining how coagulants interact with organic material in wastewater to increase clarity (Tetteh *et al.* 2019). In general, the insufficient or excessive dose would result in poor flocculation performance (Daud *et al.* 2015; Teh *et al.* 2016; Ernest *et al.* 2017; Tetteh 2018a; Asharuddin *et al.* 2021). Charge neutralization is often the dominant mechanism at low coagulant dosages (Sahu *et al.* 2013; Saxena *et al.* 2018). A further increase in dose may result in a return to normal. Coagulation develops as the dosage is increased further. Controlling the correct dose for charge neutralization becomes critical since an excess dose might result in destabilization (Saxena *et al.* 2018; Tetteh 2018a). The amount and form of the NOM have been shown to regulate coagulant dosages for the high color source water (Othman *et al.* 2008; Qiu *et al.* 2019; Gonzalez-Perez *et al.* 2021).

2.3.5.2. Temperature

Temperature is a crucial factor impacting coagulants in water treatment (Xiao *et al.* 2009). This affects both the coalescence and the properties of the polymer, like fluidity, mobility, interaction and solubility, density, and the ascending or descending velocity of the flocs (Othman *et al.* 2008; Tetteh *et al.* 2019). Temperature influences the solubility of the metal hydroxide precipitate as well as the rate of production of metal hydrolysis products (Sahu *et al.* 2013; Moruzzi *et al.* 2018; Sun *et al.* 2019; Gautam *et al.* 2020; Nimesha *et al.* 2021). At lower temperatures, larger flocs are broken down hence, the flocculation effectiveness is diminished (Xiao *et al.* 2009; Tetteh *et al.* 2019; Gautam *et al.* 2020). Warmer temperatures are hence favored for improved flocculation due to an increase in wastewater viscosity (Fitzpatrick *et al.* 2004; Othman *et al.* 2008). However, warm water tends to raise the concentration of algae and other organic materials in raw water (Sahu *et al.* 2013; Asharuddin *et al.* 2021). At low temperatures, alum flocs are particularly susceptible to breaking apart because of fluid shear, also the weak ferric floc became harder than

the strongest alum agglomerates, which has a major impact on sedimentation. (Fitzpatrick *et al.* 2004; Tetteh 2018b; Nimesha *et al.* 2021). Nonetheless, multiple studies on natural coagulants have revealed that they work best at room temperature (Teh 2014; Asharuddin *et al.* 2021; Kumar *et al.* 2021b).

2.3.5.3. pH/Alkalinity adjustment

The pH has a considerable impact on the pre-treatment stage , such as the efficacy of the charge adsorption-neutralization mechanism (Bratby 2016; Gautam *et al.* 2020; Asharuddin *et al.* 2021). The pH of the wastewater regulates the efficiency of coagulants in wastewater treatmen (Yang *et al.* 2010; Tetteh 2018a; Tetteh *et al.* 2019; Gautam *et al.* 2020). The pH must be adjusted before coagulation in order to improve the series of reactions that will take place (Yang *et al.* 2010; Beyene *et al.* 2016). The pH between 4 and 8 influences the solubility of metal hydroxide species (Wei *et al.* 2018). The residual conductivity increased at pH greater than 5, indicating a larger presence of the OH^- ions in the treated water supernatant (Othman *et al.* 2008). Therefore, recommended range for effectiveness coagulation is between 6.0 and 8.5. When the pH is too low, the coagulation process may be ineffective, whereas excessive pH can disperse coagulated particles (Ernest *et al.* 2017; Asharuddin *et al.* 2021). The efficient metal-based ions, can impact floc generation through double –layer compression (Tetteh *et al.* 2019; Yaseen *et al.* 2019). As the pH rises, those species become electrified, causing a shift in behavior. For example, pH will affect oxidation reaction if the colloidal particles are hydrophilic, like acids.

2.3.5.4. Mixing conditions

The mixing time and speed are critical in pre-treatment stage (Nimesha *et al.* 2021). Destabilization and agglomeration of coagulated flocs occur sequentially via two stirrig mechanisms, namely rapid and slow stirring (Sahu *et al.* 2013; Tetteh *et al.* 2019). Rapid mixing occurs once the coagulants are added, which necessitates turbulent mixing to generate a homogenous solution (Gupta *et al.* 2012). A lack of fast mixing may result in poor coagulant performance owing to underdosing or overdosing (Sahu *et al.* 2013). Slow mixing, on the other hand, occurs shortly after vigorous stirring and is meant to improve particle trapping as well as floc development (Kurniawan *et al.* 2020; Nimesha *et al.* 2021). Furthermore, persistent slow mixing enhances floc aggregation and particle entrapment in suspension to improve separation. Slow mixing produces a motion differential for particles of identical size, that can be larger 1 μm in size (Tetteh *et al.* 2019). As a result, the relationship between aggregation of a particular size

and polymer molecular weight may boost the bridging or breaking forces of the flocs to either settle or float (Akratos 2016; Kyzas *et al.* 2021).

2.3.5.5. Ionic strength

The ionic strength that induces floc formation has a substantial impact on polyelectrolyte alignment in solution. When a metal-based coagulant is introduced to a solution, metal ions inhibit hydrolysis activity (Akratos 2016; Tetteh *et al.* 2019). When there is reciprocal repulsion, like-charges in a polymer chain tend to extend. As ionic strength decreases, the viscosity of a polyelectrolyte solution increases. Furthermore, a rise in ionic strength covers the polymer's charged region, influencing its hydrodynamic volume expansion by reducing solution viscosity (Lee *et al.* 2014; Liu *et al.* 2017; Sun *et al.* 2019; Zhao *et al.* 2021a).

2.3.5.6. Molecular weight (MW) and charge density (CD)

MW and CD of a polymer influence the inter-particle bridging and electrostatic force mechanism, both that may aid in coagulation efficiency (Verma 2017; Gautam *et al.* 2020; Ramesh *et al.* 2021), such that increasing molecular weight increases agglomeration and floc development. Despite the fact that negative charge on the polymer might prevent adsorption onto an undesired surface, it strengthens the polymers by equal charge repulsion between polymeric chains. (Lee *et al.* 2014; Tetteh *et al.* 2019). Organic polymer concentration is based on ionic strength rather than molecular weight. As illustrated in equation 2.3 to 2.5, CD is stated according to length (q_L), area (q_A), and volume (q_V) in relation to the quantity of ionic charge (q_Q) in coulomb (C) per length (L in meter (m)), area (A in square meter), or volume (V in cubic meter).

$$q_L\left(C/m\right) = \frac{d_Q}{L} \qquad \text{Equation 2.3}$$

$$q_A\left(C/m^2\right) = \frac{d_Q}{A} \qquad \text{Equation 2.4}$$

$$q_V\left(C/m^3\right) = \frac{d_Q}{V} \qquad \text{Equation 2.5}$$

2.4. Natural-based coagulant economic obstacles

The majority of natural compounds have demonstrated coagulation characteristice in eliminating COD, BOD, TSS, turbidity, and other contaminants; however, few have been approved and commercialized (Choy *et al.* 2017; Freitas *et al.* 2017; Nath *et al.* 2020; Nimesha *et al.* 2021). Four factors are impeding natural coagulant commercialization namely financial competence, regulatory permission, market awareness, and research development which are summarized in table 2-2 (Choy *et al.* 2014; Freitas *et al.* 2017; Nimesha *et al.* 2021).

Table 2-2 Summarized commercialization challenges for natural coagulants

Environmental and technical restrictions	**Economic and social restrictions**	**References**
Complicated extraction procedure	Inadequate funds and time to engage in research and development.	(Choy et al. 2014; Kurniawan et al. 2020)
Lack of mass planting for bulk processing	Failure to reach the bare minimum of quality. Inability to maintain a consistent supply of raw resources.	(Freitas et al. 2017; Nimesha et al. 2021)
COD levels may rise as a result of the organic characteristics of natural coagulants.	Plant-based coagulants do not have regulatory authorization.	(Oladoja 2015; Freitas *et al.* 2017; Saleem *et al.* 2019)
A lack of toxicity investigations on pure coagulants.	A lack of market awareness and enthusiasm.	(Freitas et al. 2017)
Seasonal fluctuations in a few plant sources (Cactus grow in hot weather).	Market is well-established and competitive.	(Choy *et al.* 2017; Kurniawan *et al.* 2020)
A lack of study on actual usage and challenges that arise during plant operations.	Expensive early start-up costs.	(Oladoja 2015; Nimesha et al. 2021)
A lack of suitable storage procedures for natural coagulants in stock.	Industrial acceptability.	(Kurniawan et al. 2020)
Insufficient estimate of the qualitative features of the treated water	A lack of understanding about how to enhance one's health.	(Choy et al. 2014; Oladoja 2016; Nimesha et al. 2021)

2.5. Nanotechnology

Current nanotechnology research provides the prospect of generating technically and economically feasible alternatives to traditional techniques (Ambashta *et al.* 2010; Anju *et al.*

2016; dos Santos *et al.* 2018a; Patil-Sen *et al.* 2018; Boskovic *et al.* 2021; Galluzzia *et al.* 2021). It is at minimal cost and a reliable way of boosting the volume and consistency of water (Nadejde *et al.* 2015; Khan *et al.* 2021b). In this realm of technology, the amount of manufacturing applications for cutting production overall energy consumption, as well as enhancing quality and environmental controls, is expected to expand (Lakshmanan *et al.* 2013; Samanta *et al.* 2016; Abdulhameed *et al.* 2019; Mohammad *et al.* 2019). This technique is based on the application of materials on the nanometre scale (1-100 nm), allowing novel structures, components and materials to be manufactured at the atomic level (Akbarzadeh *et al.* 2012; Rossi *et al.* 2013; Samanta *et al.* 2016; Ealias *et al.* 2017; Khan *et al.* 2021b; Samrot *et al.* 2021). These materials are composed of carbon (fullerene, graphene, carbon black & carbon nanofiber), metals (Fe, Zn, Au, Pb, Cu, Co, Ag, Al, etc.), metal oxides (cerium oxide, zinc oxide, cobalt oxide, iron oxide, magnesium oxide, manganese oxide, silicon dioxide, aluminium oxide, etc.) and organic matter such as dendrimers, micelles, liposomes and ferritin (Okoli *et al.* 2011; Rossi *et al.* 2013; Hasan 2015; Vaiano *et al.* 2016; Zhang *et al.* 2016; Ealias *et al.* 2017; Mateus *et al.* 2018b; Saratale *et al.* 2018; Madhura *et al.* 2019; Abdelwahab *et al.* 2020; Li *et al.* 2020; Chaudhary *et al.* 2021).

Silver oxides, titanium dioxides, aluminum oxide, and zinc oxides, on the other hand, are nanoparticle catalysts with enhanced efficacy for eliminating microbiological and hazardous element pollutants from water and they are recyclable (Nizamuddin *et al.* 2019; Shamshad *et al.* 2019; Ahmed *et al.* 2021a). While highly magnetic elements like cobalt and nickel are prone to oxidation and are poisonous, they are of less enthusiasm (Akbarzadeh *et al.* 2012; Kanwal *et al.* 2019; Sule *et al.* 2020; Sargazi *et al.* 2021). Pollutants become much more volatile and quicker to break down as a result of nanoparticle catalysts. Toxic components such as lead as well as other organic and inorganic contaminants, and a wide range of deadly microbes, have been effectively eliminated utilizing various nanomaterials (Samanta *et al.* 2016; Mohammad *et al.* 2019; Sekoai *et al.* 2019; Ahmed *et al.* 2020a). NPs have the potential to revolutionize several industries, including health, energy, materials, consumer goods, and manufacturing (Hasany *et al.* 2013; Jiao *et al.* 2021).

NPs have distinct chemical and structural properties that have pushed research into the knowledge-based economy (Khan *et al.* 2021b). Apart from their substance, nanoparticles vary in dimensions, shapes, and sizes (Nadejde *et al.* 2015; Cartwright *et al.* 2020; Burns *et al.* 2021). It might have a shape of a sphere, circle, tube, cone, hollowed core, spiral, flat, or irregular in shape. The surface might be smooth or heterogeneous. Some nanomaterials are crystal or unstructured, with single and multi solids that are scattered or aggregated (Hasany *et al.* 2013;

Machado *et al.* 2017; Martins *et al.* 2017; Chang *et al.* 2019; Nizamuddin *et al.* 2019; Al Kindi *et al.* 2021; Conde-Cid *et al.* 2021).

A nanoparticle can indeed be zero-dimensional, with length, width, and height fixed at a single position, as in nanodots, one-dimensional only with one parameter, as in graphene, two-dimensional, with length and breadth, as in carbon- nanotubes, or three-dimensional, with all parameters, as in gold nanomaterials (Ealias *et al.* 2017; Ramadan *et al.* 2020). Iron-based nanomaterials stand out as one of the most efficient nanomaterials due to their widespread availability, adsorption capacity, and cheaper manufacturing costs when compared to other nanoparticles (Sahu *et al.* 2013; dos Santos *et al.* 2018b; Nizamuddin *et al.* 2019; Hassan *et al.* 2020; Serrani *et al.* 2021). Numerous research by scientists, engineers, chemists, and physicians have discovered that iron oxide nanoparticles are beneficial because of their distinguishing qualities such as low size-specific surface energy, reactivity, and transferrable atomicity, as well as their unusual traits such as their vast surface area (Akbarzadeh *et al.* 2012; Nadejde *et al.* 2015; Khan *et al.* 2018; Nizamuddin *et al.* 2019; Ain *et al.* 2020; Chaudhary *et al.* 2021; Ganea *et al.* 2021; Khan *et al.* 2021c).

2.5.1. Iron-based NPs

Iron-based nanomaterials have recently demonstrated exceptional adsorption ability for removing heavy metals, pigments, and inorganic and organic chemicals (Akbarzadeh *et al.* 2012; Rossi *et al.* 2013; Madhura *et al.* 2019; Nizamuddin *et al.* 2019; Zhou *et al.* 2019; Tan *et al.* 2020a; Chaudhary *et al.* 2021; Zhao *et al.* 2021d). Over the last two decades, the remarkable performance and benefits of employing iron oxide nanoparticles have opened doors and led to a new stride in the field of nanotechnology (Xiao *et al.* 2012; Reed *et al.* 2014; Nizamuddin *et al.* 2019; Zhao *et al.* 2019; Frattini *et al.* 2021). The diameter of the particle controls the magnetic behavior of single nanomaterials, resulting in unique phenomena such as superparamagnetic, high electric field irreversibility, high saturation field, extra anisotropy contributions, or altered loops post field cooling (Huang *et al.* 2018; Blanco-Gutiérrez *et al.* 2019; Escoda-Torroella *et al.* 2020; Foltynowicz *et al.* 2020; Das *et al.* 2021). A ferromagnetic particle with a size smaller than a threshold particle size (< 15 nm) would have a single magnetic domain (Rossi *et al.* 2013; Liu *et al.* 2018; Satheeshkumar *et al.* 2020; Wei *et al.* 2020; Chen *et al.* 2021). Domains are areas in which all of the atomic moments point in the same direction, causing the magnetization to be saturated and reach its maximum value inside each domain (Owens *et al.* 2008). Above the blocking temperature, the magnetic behavior of these particles is identical to that of atomic paramagnets (superparamagnetism) according to Rossi *et al.* (2013).

At barrier temperature, particle latent heat is larger than the energy of particle-particle interaction with the magnetization, causing the magnetic moments of the particles towards the direction of the magnetization and the chances of being disorganized (Moerland *et al.* 2019; Polichetti *et al.* 2020; Galluzzia *et al.* 2021; Yang 2021). Nanoscale zero-valent metals (NZVMs) represent the cutting edge of technology and are regarded to be prospective materials for environmental clean-up and antibacterial impact because of their excellent reduction and adsorption abilities. NZVMs have been important in research since the 1980s as a class of effective reducers for eliminating pollutants from water (Bhateria *et al.* 2019; Li *et al.* 2021c). Due to its redox potential of -0.44 V, iron is an efficient outcome when it is combined with oxidized pollutants in water (Xue *et al.* 2017; Zeng *et al.* 2020). Its core-shell structure, as depicted in figure 2-12, make heavy metal removal and conversion easier. The metallic core serves as an electron source and reducer, whilst the oxide shell can absorb pollutants by electrostatic interactions and surface complexation, and the competent electron can travel from the metallic core to the surface (Liu *et al.* 2014; Cheng *et al.* 2021; Sepúlveda *et al.* 2021). The core is mostly made up of zero-valent iron and provides lowering the power required for interactions with contaminants in the ecosystem. As a result of the oxidation of zero-valent iron, the shell is made up of iron oxides or hydroxides. The shell serves as a platform for the development of chemical complexes such as chemisorption (Li *et al.* 2006; Vilardi *et al.* 2018; Bhateria *et al.* 2019).

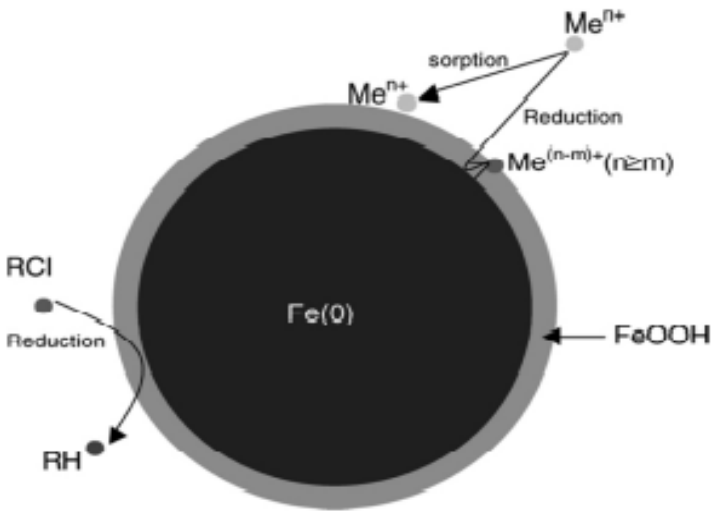

Figure 2-12 Core-shell model of zero-valent iron NPs, adapted from Li *et al.* (2006)

The exterior iron oxide and inner core of Fe were found to have thicknesses of 10 and 20 nm, consecutively (Tanboonchuy *et al.* 2011; Bhateria *et al.* 2019; Filip *et al.* 2019; Handojo *et al.* 2019). The shell is mostly magnetite with some maghemite and lepidocrocite (y-FeOOH) thrown in for good measure. When nano iron comes into contact with air, it becomes extremely reactive

(Ali *et al.* 2016; Phenrat *et al.* 2019b), lowering its surface reactivity. Iron NPs have both zero-valent iron (reduction) and iron hydroxide properties (complex formation) (Bhateria *et al.* 2019; Phenrat *et al.* 2019a).

2.5.1.1. Iron oxide NPs

Iron oxide may be found in nature in a variety of forms, including goethite, lepidocrocite, akaganeite, schwertmannite, feroxyhyte, ferrihydrite, bernalite, green rusts, wustite, maghemite, magnetite, hematite, and others (Ramimoghadam *et al.* 2014; Xiao *et al.* 2018; Setyawan *et al.* 2019; Braga de Oliveira *et al.* 2020; Svobodova *et al.* 2020; Cai *et al.* 2021; Samrot *et al.* 2021). However, maghemite, magnetite, and non-magnetic hematite shown in figure 2-13a, are frequently utilized as nano-adsorbents because they have been discovered competent and most accepted prospects because of polymorphism, which includes temperature-induced phase lag. (Hasany *et al.* 2013; Madhura *et al.* 2019; Nizamuddin *et al.* 2019; Li *et al.* 2020; Svobodova *et al.* 2020; Cai *et al.* 2021; Namgung *et al.* 2021).

These iron oxides exhibit specific biochemical, magnetic, catalytic, and other characteristics, making them promising for technical and biological uses (Ramimoghadam *et al.* 2014; Bhateria *et al.* 2019). The physical and chemical characteristics of iron oxide magnetic nanoparticles differ from those of their atoms and bulk counterparts (Shamaila *et al.* 2017; Patil-Sen *et al.* 2018; Li *et al.* 2020; Sultan *et al.* 2020; Ali Dheyab *et al.* 2021; Chaudhary *et al.* 2021; Mohammadi *et al.* 2021). Therefore, section 2.5.3 of this study focuses on different kinds of iron oxide synthesis processes.

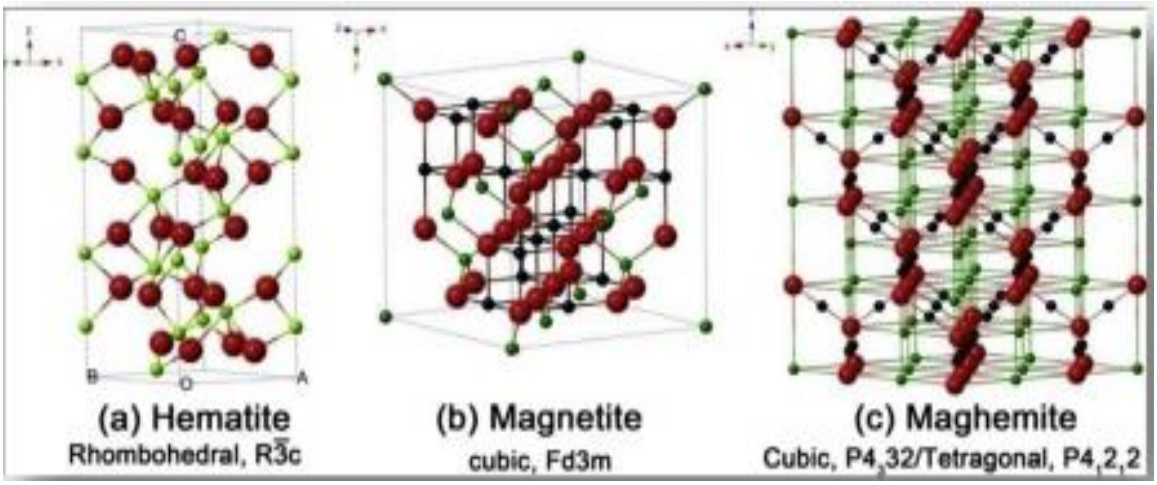

Figure 2-13 Hematite, magnetite, and maghemite crystal structures and crystallographic data (the black ball is Fe^{2+}, the green ball is Fe^{3+}, and the red ball is O^{2-}), adapted from Bhateria *et al.* (2019)

a) Hematite

Iron oxide in the form of hematite is the most stable (Bhateria *et al.* 2019). Maghemite may be converted into hematite, a very weak ferromagnet (Starowicz *et al.* 2011). It's environmentally friendly, non-toxic, biocompatible, cost-effective, and corrosion-resistant. It has n-type semiconducting characteristics and is frozen in the space group of the rhombohedral system R-3c (2.1 eV band gap) (Wu *et al.* 2015; Bhateria *et al.* 2019). In bulk hematite, the Neel temperature (T_N) is at approximately 960 K, while the Morin transition temperature (T_M) occurs at approximately 263 K (Samrot *et al.* 2021). Above T_M, the material is weakly ferromagnetic; below T_M, the material is anti-ferromagnetic. T_M decreases as particle size decreases and disappears for particles that are 10 nm or less in size (Tadic *et al.* 2009; Arasu *et al.* 2019; Roy *et al.* 2021). To encapsulate and produce hematite nanoparticles with octyl ether and oleic acid, a simple chemical method was adopted in a study by Kausar (2020). They discovered that the existence or absence of morin transition is controlled by changes in magnetic properties caused by tiny particle size, i.e. 7–25 nm.

b) Magnetite

Magnetite is distinct from several other iron oxides in that it contains either divalent and trivalent iron. At room temperature, magnetite is ferrimagnetic. Magnetite is ferrimagnetic at ambient temperature and has a Curie temperature of 850 K (Samrot *et al.* 2021). It has a cubic inverse spinel structure with a cubic close-packed arrangement of oxide ions, with Fe^{2+} ions occupying half of the octahedral sites and Fe^{3+} ions distributed consistently throughout the remaining octahedral and tetrahedral sites (Bhateria *et al.* 2019). Magnetite has a solitary domain 5–20 nm in diameter (Mu *et al.* 2011; Hasany *et al.* 2013; Teh 2014; Peeters *et al.* 2016; Gutierrez *et al.* 2017; Nizamuddin *et al.* 2019; Li *et al.* 2020; Sibiya *et al.* 2021).

At room temperature, magnetite particles that are less than 6 nm are superparamagnetic, albeit their magnetic characteristics are heavily dependent on the procedures employed in their synthesis (Starowicz *et al.* 2011). Magnetite with diameter varying from 10 - 15 nm were produced and employed in ultrasonic aided adsorption in a study by Ghaedi *et al.* (2015). Both, with maghemite, have great oxidative stability and are currently the only nontoxic magnetic materials that are recognized for medical purposes (Starowicz *et al.* 2011; Nanda *et al.* 2020; Boskovic *et al.* 2021; Kumar *et al.* 2021a). Magnetic fluid hyperthermia may have medicinal benefits, such as bringing about beneficial results in alternative cancer therapy (Neuberger *et al.* 2005), magnetic field-directed medication delivery (Voltairas *et al.* 2002) as well as its use as a contrasting agent in nuclear magnetic resonance (Cheng *et al.* 2005).

c) Maghemite

Maghemite is ferrimagnetic at ambient temperature, weak at high temperatures and reduces resilience (Starowicz *et al.* 2011; Roostaee *et al.* 2020; Samrot *et al.* 2021). Its effective activity as a photocatalyst on organic pollutant degradation processes and metallic pollutant reduction, as well as on virus inactivation in aquatic media, demonstrate the material's potential for application in residual water purification (Ambashta *et al.* 2010; Gadkari *et al.* 2018; Yarima *et al.* 2020). Maghemite has a cubic structure with 32 O^{2-} ions, 21⅓ Fe^{3+} ions, and 2⅓ vacancies. The oxygen anions are arranged in a cubic close-packed pattern, whilst the ferric ions are distributed on tetrahedral (eight Fe ions per unit cell) and octahedral sites (the remaining Fe ions and vacancies). As a result, maghemite may be considered as a totally oxidized magnetite with n-type semiconductor properties and a band gap of 2.0 eV (Wu *et al.* 2015; Ahmed *et al.* 2021b; Jung *et al.* 2021).

2.5.2. Magnetized coagulants

Natural coagulants are a kind of polymers that are frequently employed in conjunction with artificial coagulants since they have limited turbidity reduction when used alone (Choy *et al.* 2014). NPs functionalized with natural coagulants ,e.g. eggshells, chitosan, rice starch, banana peels, moringa oleifera seeds, seashells, cashew nuts, okra peels, neem leaf powder, cassava peels, and others are attracting interest in wastewater treatment settings (Freitas *et al.* 2017; Saratale *et al.* 2018; Xu *et al.* 2019; Ang *et al.* 2020a; Mosaddeghi *et al.* 2020; Tetteh *et al.* 2020; Sibiya *et al.* 2021; Sibiya *et al.* 2022b). This technique is considered particularly appealing because of large efficacy, ability to minimize the quantity of sludge, rapid sedimentation, and low cost (Akbarzadeh *et al.* 2012; Lakshmanan *et al.* 2013; Nnaji *et al.* 2014). Furthermore, it improves the biocompatibility and biodegradability of organic materials, facilitating the usage and re-use of nanoparticles (Okoli *et al.* 2012; Santos *et al.* 2016; Inozemtseva *et al.* 2018; Mateus *et al.* 2018b; Kristianto *et al.* 2020). Nevertheless, it has been observed that its application is very limited in wastewater treatment. When evaluating the performance of several coagulants discovered in the literature, polymers functionalized with ferromagnetite show a tremendous promise for potential large-scale uses in industrial effluent treatment, as displayed in table 2-3.

Table 2-3 Comparative study on various nanocomposites used in wastewater treatment

Nanocomposite/(s)	Effluent or contaminants	Operating condition(s)	Contaminant removal efficiency	Reference
Fe_2O_3-MO	Surface raw water	400 mg/L dosage	94.4% turbidity, 87.5% color	(dos Santos *et al.* 2018b)
		30 min sedimentation		
	Food industry wastewater	pH = 3	68.33% color	(Mateus *et al.* 2018a)
		10 min magnetic exposure		
	Textile wastewater	10 min magnetic exposure	92.37% color	(dos Santos *et al.* 2018a)
			91.43% turbidity	
	Superficial raw water	400 mg/L dosage	96.8% turbidity 97.10% color	Mateus *et al.* (2018b)
		10 min sedimentation		
	Sanitation wastewater	30 min magnetic exposure	90% turbidity	(Santos *et al.* 2016)
			85% color	
	Congo red synthetic wastewater	pH = 3	80% turbidity	(Kristianto *et al.* 2020)
		30 min sedimentation	90% color	
	Synthetic textile wastewater	20 min sedimentation	93.7% color	(Miyashiro *et al.* 2021)
Fe_3O_4-Eggshell	Synthetic wastewater	20 mg/L dosage	94.86% TSS	(Sibiya *et al.* 2021)
		30 min sedimentation	92.56% turbidity	
			96.24% color	
Fe_3O_4-Alum			99.75% TSS	
			99.50% turbidity	
			99.66% color	
Fe_3O_4-Alum	Textile wastewater	45 mg/L dosage, pH = 4	85% turbidity	(Tetteh *et al.* 2020)
			82% color	
		50 min magnetic exposure		
Fe_3O_4-CS	Palm oil mill effluent (POME)	pH = 6	97.7% TSS	(Saifuddin *et al.* 2011)
		370 mg/L dosage	91.70% COD	
			42.70% turbidity	
$\alpha - Fe_2O_3 - Mo$	Textile wastewater	400 mg/L dosage	92.37% color	dos Santos *et al.* (2018a)
		10 min sedimentation	91.43% Turbidity	

2.5.3. Synthesizing methods

This section reveals different techniques to synthesize magnetite. So far, these approaches have been established to achieve enough control over particle diameter, morphology, orientation, crystalline nature, and magnetic properties of magnetic iron oxide. There are three main synthesis methods namely physical (powder ball milling, laser-induced pyrolysis, gas-phase deposition, aerosol, electron beam lithography and pulse laser ablation), chemical (Figure 2-14), and biological (bacteria mediated, Fungi mediated and protein-mediated) (Aziz *et al.* 2013; Hasany *et al.* 2013; Calvino-Casilda *et al.* 2019; Roostaee *et al.* 2020). Chemical approaches are the most extensively utilized because of their simplicity and ease of control over the size, content, and even form of the nanoparticles. Furthermore, they are more viable, and reproducible than physical and biological techniques.

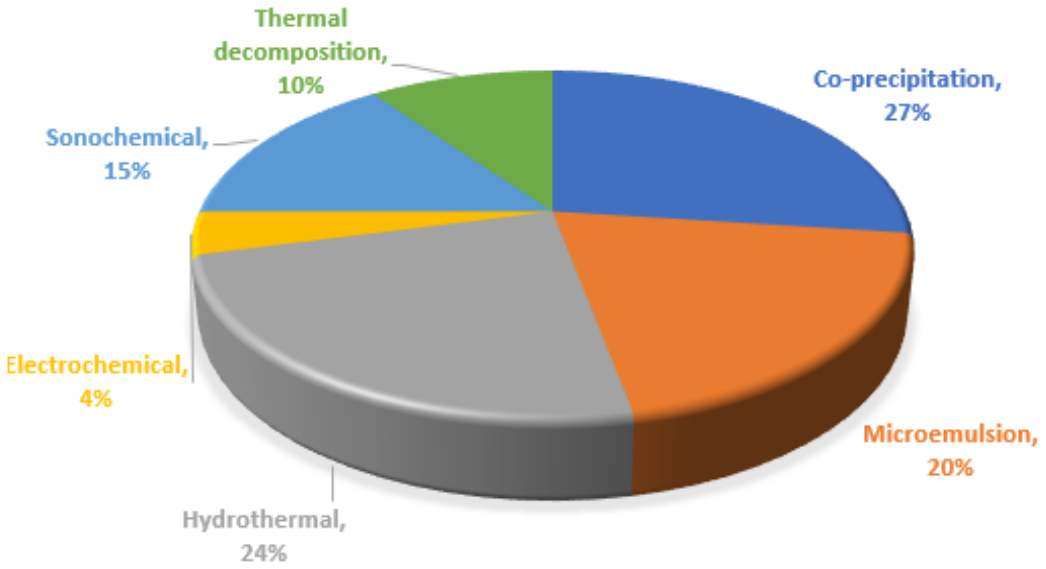

Figure 2-14 Statistical analysis of previous studies employing various chemical synthesis methods, adapted from Hasany *et al.* (2013)

2.5.3.1. Chemical co-precipitation

Co-precipitation from aqueous solutions of ferric and ferrous salts has been the most employed technique (Majewski *et al.* 2007; Dung *et al.* 2009; Jiang *et al.* 2010; Mateus *et al.* 2018b; Morsi *et al.* 2018). Iron precursors are converted to iron oxides in this procedure by utilizing a moderate reductant like NaOH, NH_3, and so on (Ramimoghadam *et al.* 2014; Samrot *et al.* 2021) in addition to adequate aging. According to Hribernik *et al.* (2012), their diameter, form and composition are

associated to the type of salts (chlorides, nitrates, sulfates, acetates) used. The interaction of a Fe (III) salt, a base, and a moderate oxidant in aqueous solutions can produce spherical magnetite particles (<20 nm) (El Ghandoor *et al.* 2012; Hasany *et al.* 2013; Aziz *et al.* 2020; Biswas *et al.* 2020; Elhambakhsh *et al.* 2020; Islama *et al.* 2020; Sibiya *et al.* 2021). Fe_3O_4 can be synthesized via the chemical reaction described in equation 2.6 and its precipitation is likely to occur at a pH of 8 to 14 (Ramimoghadam *et al.* 2014; Bhateria *et al.* 2019; Samrot *et al.* 2021). Magnetite, prone to oxidation and transformation into maghemite (y-Fe_2O_3) when exposed to air as shown in equation 2.7.

$$Fe^{2+} + 2Fe^{3+} + 8OH^- \rightarrow Fe_3O_4 + 4H_2O \qquad \text{Equation 2.6}$$

$$Fe_3O_4 + 2H^+ \rightarrow y - Fe_2O_3 + Fe^{2+} + H_2O \qquad \text{Equation 2.7}$$

Magnetite is not the only chemical that oxidizes when exposed to air; changes in the pH of the solution can allow for the transmission of various electrons or ions. As shown in equation 2.7, iron ions are desorbed from the surface of magnetite, resulting in cationic vacancies and the formation of maghemite to maintain the structure's charge balance. As a result, beneath basic circumstances, magnetite oxidation is the oxidation-reduction of the magnetite's surface. Magnetite is distinct from maghemite in terms of the distribution of Fe ions in the spinel structure's octahedral and tetrahedral sites. Maghemite, unlike magnetite, has cationic vacancies in the octahedral site (Ramimoghadam *et al.* 2014). The vacancy ordering approach is associated with the synthesizing method and results in symmetric reductions and maybe superstructures. The vacancies might be partial or total random or clearly arranged. According to the results by Morales *et al.* (1999) of FTIR spectroscopy and X-ray diffraction, only particles larger than 5 nm are subject to vacancy ordering.

The co-precipitation technique takes advantage of the large number of nanoparticles that can be produced. However, because crystal growth is solely controlled by kinetic factors, particle size distribution is difficult to control. The mechanism is divided into two phases (Cornell *et al.* 2003). The first brief nucleation occurs as the reactant concentration reaches critical supersaturation, and the second is the steady development of the nuclei caused by solute diffusion to the crystal's surface (Ramimoghadam *et al.* 2014). To obtain monodisperse iron oxide nanoparticles, the above-mentioned two processes must be differentiated; it is preferred that no nucleation occur while crystal formation is being conducted (Tartaj *et al.* 2005; Katz 2019; Varshney *et al.* 2021).

Furthermore, because the ultimate particle number is decided by the end of the nucleation and does not vary throughout the growth stage, size management of monodispersed particles is

normally conducted during the first step. Many different factors may be changed during the process of synthesizing the iron oxide nanoparticles to influence their size, magnetic characteristics, and surface qualities. The particle state and diameter is determined by the concentration of cations, the presence of counter ions, and the pH of the suspension (Chastellain *et al.* 2004; Maneeprakorn *et al.* 2017; Oliveira *et al.* 2018; Aziz *et al.* 2020; Nelson *et al.* 2020; Zahoor *et al.* 2021). The mean particle diameter may be maintained at 2-15 nm by changing the pH and ionic strength (Tartaj *et al.* 2005; Hribernik *et al.* 2012; Hasany *et al.* 2013; Ali *et al.* 2018; Gulbagca *et al.* 2020; Muro Cruces 2020; Satheeshkumar *et al.* 2020; Villacorta *et al.* 2020; Chen *et al.* 2021; Li *et al.* 2021b; Materón *et al.* 2021; Plachy *et al.* 2021). Nanoparticles are more inclined to combine to minimize their surface energy because of irregular surface area to volume ratio (Hasany *et al.* 2013; Ali *et al.* 2016; Samrot *et al.* 2021). The use of anionic surfactants as dispersion agents results in the stabilization of the nanoparticle suspension (Kim *et al.* 2003; Lin *et al.* 2005; Amatya *et al.* 2021; Asri *et al.* 2021; Hajalilou *et al.* 2021; Khan *et al.* 2021a; Kurnia *et al.* 2021).

Adsorption of substances such as proteins, starches, non-ionic detergent, and polyelectrolytes stabilizes the particles at electrolyte concentrations that would otherwise cause coagulation (Cornell *et al.* 2003; Kim *et al.* 2003; Hasany *et al.* 2013; Alabresm 2020; Cai *et al.* 2021; de Oliveira *et al.* 2021). Massart *et al.* (1987) were the first to use alkaline precipitation of $FeCl_3$ and $FeCl_2$ to prepare the superparamagnetic iron oxide particles with a diameter size of 8 nm.

2.5.3.2. Micro-emulsion

Water-in-oil micro-emulsions are stable solutions since their drops are exceedingly active and the density fluctuation in the continuous liquid phase induces Brownian motion (Hasany *et al.* 2013; Ramimoghadam *et al.* 2014; Samrot *et al.* 2021). Furthermore, microemulsion droplets undergo coalescence and decalescence with other droplets. This causes an interchange of the water pool's contents, and a reaction may occur if such contents are reactive. Such dynamic motion guarantees that any solubilized reactant in the water pools is distributed uniformly. This method was proven quite effective in producing a broad variety of metal oxides with large surface areas (Bumajdad *et al.* 2009; Calvache-Muñoz *et al.* 2017; Pujar *et al.* 2020; Cam *et al.* 2021). The presence of surfactants reduces the surface tension between the continuous and immiscible phases, allowing the droplets to remain stable (Ramimoghadam *et al.* 2014). In other words, they are in charge of micellization, which allows the produced iron oxide nanoparticles to spread.

Surfactants have a large impact on iron reductions, resulting in distinct polymorphs of iron oxides (Salazar Alvarez 2004; Hasany *et al.* 2013; Ahmed *et al.* 2018; Stojanovic *et al.* 2018; Liu *et al.* 2020). If anionic surfactants are employed, it will result in α-Fe with a body centered cubic crystal structure (Kombaya-Touckia-Linin *et al.* 2019). However, if a non-ionic surfactant is used, a face-centered cubic crystal structure emerges (Kalita *et al.* 2017; Fantechi *et al.* 2020; Basina *et al.* 2021; Duran-García *et al.* 2021). Tuttolomondo *et al.* (2013) researched the production of monodispersed magnetic silica nanoparticles in the absence of co-surfactants utilizing a unique water-in-oil reverse microemulsion method. It revealed many advantages like obtaining saturation magnetization of 10 emu/g, particle homogeneity, etc. over microemulsion approach.

Zhu *et al.* (2013) investigated a comparison of basic and surfactant-modified reverse microemulsion (RM) procedures for the manufacturing of iron oxide or silica core-shell colloidal particles. Their findings revealed that short-chain alcohols were utilized as a co-surfactant in the alcohol- RM technique. The particle size increased to about 100 nm, with a weak core-shell structure in the basic RM whilst the particle size increased to over 200 nm in the emulsifiers pair modified RM approach, and a restricted growth window was shown to be advantageous for improving the stability and stiffness of the surfactant's layers.

The fundamental benefit of RM technology is the variety of nanoparticles that may be produced by modifying the kind and quantity surfactant and co-surfactant, the oil phase, or the reacting conditions. Due to the oil and water phases frequently including many dissolved components, the surfactant (and cosurfactant) of choice is determined by the physicochemical properties of the system. Surfactants of various sorts, such as cationic, anionic, or non-ionic, can be utilized. Research by Kekalo *et al.* (2012) synthesized iron oxide nanoparticles using a microemulsion process with three distinct surfactants: octane, and n-butanol, yielding nanoparticles with a core size of 8 – 16 nm and shell size of 2 to 3 nm. The primary disadvantages of the microemulsion technology are the difficulty in scaling-up operations and the negative impact of residual surfactants on particle characteristics (Hasany *et al.* 2013).

2.5.3.3. Hydrothermal reaction methods

According to Sierra-Pallares *et al.* (2016), hydrothermal synthesis is a classic example of bottom-up synthesis. Furthermore, it is a simple technique that was previously known to make metal oxide crystals such as (AlOOH, Fe_3O_4, NiO, $CoFe_2O_4$, ZrO_2, CeO_2, VO_2, and TiO_2) in the reactor/ autoclave from a metal salt aqueous stream combined with a superheated water stream (Hasany *et al.* 2013; Dunne *et al.* 2015; Tran *et al.* 2021). Nanocrystalline products with mean diameter <

10 nm and tny particle size distributions can be produced using a continuous flow reactor (Becker *et al.* 2008). According to Aoki *et al.* (2016), the benefits of the hydrothermal process over other conventional processes include enhanced nucleation rate, higher dispersion, faster response rate, and improved shape control.

Supercritical conditions (374 ℃ and 22.1 MPa) are useful in the pilot-scale production of nanoparticles because the spectacular properties of supercritical water are advantageous for the synthesis of crystalline and surface-modified luminescent nanoparticles (Hasany *et al.* 2013; Aoki *et al.* 2016). These nanoparticles are capped with long alkyl chains of organic modifiers on the particles' surfaces to make them dispersible in nonpolar solvents (Singh *et al.* 2014). Furthermore, this approach is inexpensive, sustainable, and provides highly scalable pathways (Dunne *et al.* 2015). It displays some of the favorable qualities of nanoparticles generated in continuous methods, such as low viscosity and high diffusivity (Aoki *et al.* 2016). However, it is dependent on the capacity of water to separate and dry out metal salts at increased temperatures (>374 ℃) (Hasany *et al.* 2013; Bhateria *et al.* 2019; Park *et al.* 2021). According to Sierra-Pallares *et al.* (2016), when superheated water reaches a critical temperature (374 °C) and pressure (22.1 MPa), It undergoes a transformation from a polarized liquid to a liquid with a small dielectric value and ionic product, which is necessary for some applications (Adschiri *et al.* 2001) but not all materials (Aoki *et al.* 2016). Many researchers have proven their synthesis using batch type reactors since they are simple to run and suitable for lab-scale output (Singh *et al.* 2013; Singh *et al.* 2014) because large-scale piloting can be hard; due to low process dependability, repeatability, and control (Lester *et al.* 2006). As a result, rapid mixing is critical to achieving a regulated reaction state, and a quick temperature increase is necessary to obtain a high degree of supersaturation with the creation of tiny and homogenous nanoparticles. For high throughput and repeatability of nanoparticles, the mixing process must be closely regulated (Lim *et al.* 2014).

The size and form of the nanoparticles may be adjusted using the hydrothermal process by altering the reaction time, temperature, reactant concentration and ratio, type of solvent, complexing strength, and precursors (Ramimoghadam *et al.* 2014). A study by Hasany *et al.* (2013) investigated how precursor concentration, temperature, and residence time affected the diameter and shape of the particle and shape. They observed an increase in particle size and dispersion as the concentration increased. Nonetheless, as compared to precursor concentration, residence time had a significantly greater influence on average particle size. The shape and size of the particles rely on the stirring process occurring inside the reactor due to its subsequent influence on the nucleation rate (Ramimoghadam *et al.* 2014; Sierra-Pallares *et al.* 2016). As a result, while

constructing a reactor for supercritical synthesis of nanoparticles, it is important to first address the mixing device to get particles on a nano-scale (Lester *et al.* 2006).

2.5.3.4. Sonochemical

Acoustic cavitation is the physical phenomenon that causes the sonochemical process. Sonochemistry is the study of molecules that undergo chemical reactions as a result of the use of strong ultrasonic radiation ranging from 20 kHz – 10 MHz (Gedanken 2004; Xu *et al.* 2013; Lauterborn *et al.* 2015). In a normal liquid, sound velocity speed varies from 1000 to 1500 m/s, and ultrasonic wavelengths range from around 10 cm down to 100 µm (Lauterborn *et al.* 2015). In sonochemistry, acoustic cavitation or the development, growth, and implosive collapse of a bubble in an irradiated liquid , creates a transitory localized hot spot as shown in figure 2-15 with an effective temperature of 5000 K and a nanosecond lifespan (Pokhrel *et al.* 2016; Majumdar 2019; Kolasinski 2021), pressures greater than 1000 atmospheres, and heating and cooling speeds more than 10^{10} K/ s (Xu *et al.* 2013). The above-mentioned conditions (temperature and pressure) are dissimilar from those seen in other common synthetic processes such as photochemistry, wet chemistry, hydrothermal synthesis, or flame pyrolysis (Bang *et al.* 2010; Lim *et al.* 2021; Santiago *et al.* 2022).

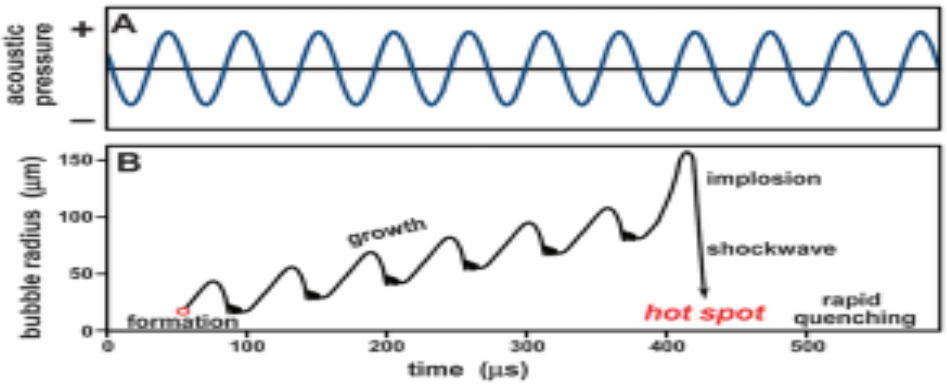

Figure 2-15 A schematic representation of the acoustic cavitation process: the development, growth, and implosive collapse of bubbles in a liquid treated with high intensity ultrasound, adapted from Xu *et al.* (2013)

Light (200 to 800 nm) is produced by acoustic bubbles containing highly energetic particles for a limited time (about 100 ps), when they shrink (Pokhrel *et al.* 2016; Vukovic *et al.* 2021; Yasui 2021). This is referred as sonoluminescence, should be utilized to examine the condition of the acoustic bubble (Suslick *et al.* 2008; Suslick *et al.* 2011; Ghorbani *et al.* 2018). The implosive

collapse process is essentially adiabatic in its later phases and is responsible for the sonochemical severe circumstances (Xu *et al.* 2013). The hotspot, or core area, is characterized by high energetic particle collisions that create energy as high as 13 eV (Flannigan *et al.* 2005; Pokhrel *et al.* 2016). Though controversial, nuclear fusion during cavitation exemplifies the influence of ultrasound and provides a simple, feasible technique for studying nuclear processes (Taleyarkhan *et al.* 2002). Such circumstances can cause anomalous physical and chemical changes, as well as enhance the most fundamental interaction between atoms and molecules, resulting in an exceptional class of materials (Vabbina *et al.* 2014) and they also enable tabletop syntheses in a room-temperature liquid that would usually necessitate high temperatures, high pressures, or extended interaction periods (Xu *et al.* 2013).

Microjets and shock waves are the most essential physical phenomena for preparing or modifying nanomaterials. According to Blake *et al.* (1987), bubbles produce microjets when they collide at an extended surface (surfaces that are several times bigger than the bubble radius). A laser-induced collapsing bubble can produce a shock wave. In water, this shock wave may achieve pressure about 6000 MPa and a speed of 4 km/s (Xu *et al.* 2013). The benefit of sonochemistry, on the other hand, stems from the fact that the ions and radicals within the bubble are derived from the chemical solution; thus, selecting acceptable chemicals based on their vapor pressure may assist and adapt the whole process (Pokhrel *et al.* 2016). When a liquid is exposed to high-intensity ultrasound, high-energy chemical reactions occur. Sonochemistry is used to synthesize compounds from volatile or non-volatile precursors, although often by distinct methods, as seen in figure 2-16. Primary sonochemistry involves the sonolysis of weak metal–carbon bonds from fragile organometallic within the collapsing bubble, which then diffuses into the bulk liquid to form functional nanomaterials. Secondary sonication products can be produced by chemically active species (for example, chemical radicals from vapour sonolysis) that form inside the bubble but then infiltrate into the liquid phase and react with solution precursors to produce a variety of nanomaterials.The physical phenomena occur as a result of either implosion caused by ambient pressure or explosion caused by a barrier. Bubbles that reach the border blow outwards, producing microjets with unique applications (Bang *et al.* 2010; Dheyab *et al.* 2020; Zhao *et al.* 2021e). Similarly, exploding bubbles create shocks that accelerate particles of non - soluble solute to 700 m/s (Pokhrel *et al.* 2016; Tan *et al.* 2020b). Collision at 700 m/s causes substantial structural alteration and can be employed for a variety of applications.

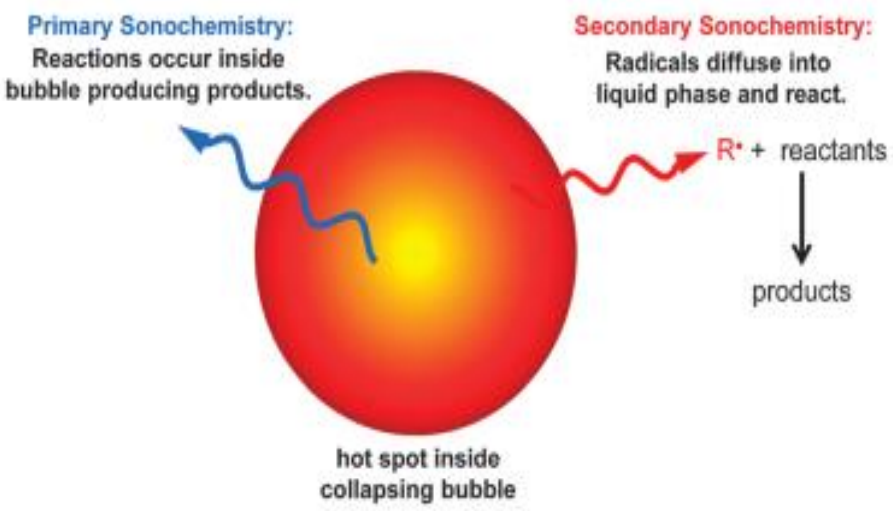

Figure 2-16 Primary and secondary sonochemistry utilized to prepare nanomaterials, adapted from (Xu *et al.* 2013; Pokhrel *et al.* 2016)

Ductile materials decompose into pieces to generate small particles, a process known as sonofragmentation and has been shown to be more effective and less harmful than milling or comparable techniques (Pokhrel *et al.* 2016). Shock waves can also directly affect particles and cause fragmentation without the necessity for collision (Zeiger *et al.* 2011; Pokhrel *et al.* 2016). Aside from fragmentation, the physical effect is often used in graphite, boron nitride, molybdenum disulphide, and others to form 2D equivalents (Viculis *et al.* 2003; Xu *et al.* 2011; Wang *et al.* 2013; McKenzie *et al.* 2019; Pradeep *et al.* 2021; Raksha *et al.* 2021). The influence of sonochemistry on the surrounding environment is largely benign since the dispersal of particles and the effects of vibration that follow a bubble death barely cover a small region. Sonochemistry's associated, facilitating impacts that enable the production of delicate and uncommon substances like proteins, liquid microspheres, hollow nanospheres, graphene, fibers, etc, and the usage of substrates such as paper, cotton, nylon, and so on (Zhang *et al.* 2010; Gottesman *et al.* 2011; Li *et al.* 2019; Pugazhendhi *et al.* 2021; Zhao *et al.* 2021b).

2.5.3.5. Thermal decomposition

Another method for creating monodisperse iron oxide nanoparticles is thermal degradation of iron organic precursors under extreme temperature, often known as thermolysis. hermal decomposition of iron organic precursors at high temperatures is another approach for producing monodisperse iron oxide nanoparticles and it is also known as thermolysis (Ramimoghadam *et al.* 2014). This seems to be an endothermic because the links between molecules must be destroyed using heat. Iron precursors such as iron pentacarbonyl and iron (III) acetylacetonate are

used in this process, along with organic solvents and surfactants (Starowicz *et al.* 2011). Iron oxide nanoparticles of good quality and size approximately 15 nm may be produced using this process (Gonzales-Weimuller *et al.* 2009; Batlle *et al.* 2021).

A study on the thermal degradation of iron oxide nanoparticles using $Fe(CO)_5$ in the existence of oleic acid produced extremely crystalline and monodisperse particles with diameters varying from 4 to 16 nm (Zhang *et al.* 2005). Iron oxide nanoparticles can be produced by heating precursor molecules, such as organometallic precursors until they break down into iron oxide molecules (Wu *et al.* 2008; Samrot *et al.* 2021).

Hyeon *et al.* (2001) successfully synthesized monodispersed maghemite from iron pentacarbonyl and oleic acid by thermally decomposing them at 100 °C and oxidizing the resulting iron oleic acid metal complex to yield maghemite particles. When iron chloride is utilized in the existence of sodium oleate surfactant at 317 °C to acquire iron oxide nanocrystals (Xu *et al.* 2010), iron (III) acetylacetonate is phenyl ether in the existence of alcohol, oleic acid, and oleyl amine at 265 °C (Sun *et al.* 2002) , iron carboxylate salts (William *et al.* 2004) , $Fe(CO)_5$ (Woo *et al.* 2004)], iron pentacarbonyl (Park *et al.* 2005) and the synthesise of iron oxides in the existence of sodium oleate at 320 °C (Hufschmid *et al.* 2015).

Nanocrystalline magnetite was produced utilizing thermal decomposition and iron choline citrate ($C_{11}H_{24}FeNO_{11}$) in the study by Fu *et al.* (2012). Also, the fabrication of superparamagnetic nanoparticles via a thermal decomposition technique with no solvent has been reported (Karami *et al.* 2020; Keçili *et al.* 2021). Solvothermal energy has been employed by several researchers using ethylene diamine as a solvent to manufacture magnetic platelets lowering agent/solvent (Morales *et al.* 1999; Tartaj *et al.* 2005; Katz 2019; Varshney *et al.* 2021).

2.5.3.6. Electrochemical

Only a few applications have been identified for electrochemical ways of producing metal nanoparticles in an electrolyte. This technique is utilized to generate maghemite and magnetite nanoparticles (Jahangirian *et al.* 2020). An electrochemical synthesis is essentially defined as the passage of an electric current between two or more electrodes, known as the anode and cathode, which are placed in an electrolyte, as illustrated in figure 2-17. In this approach, the anode may be oxidized to metal ion species in the electrolyte, and the metal ion is then reduced to metal by the cathode with the help of stabilizers. Generally, synthesis occurs at the electrode-electrolyte

contact. The electrochemical synthesis technique transpires near the electrode in the electric double layer, which has a strong potential gradient of 105 V/cm (Ramimoghadam *et al.* 2014).

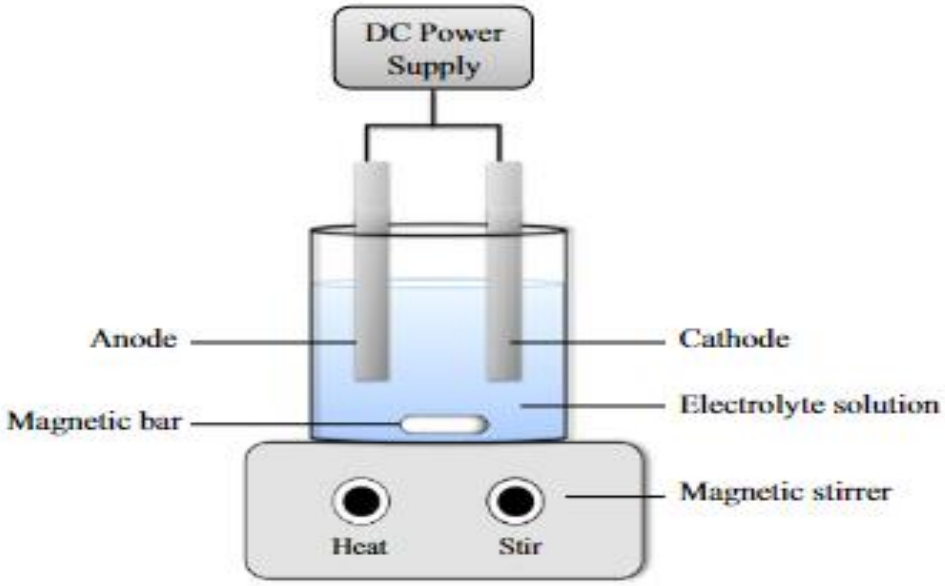

Figure 2-17 The standard electrochemical cell, adapted from Ramimoghadam *et al.* (2014)

According to these parameters, electrochemical reactions typically produce compounds that cannot be obtained by chemical synthesis. Normally, the product is placed on the electrode in the form of a coating or a thin layer. Furthermore, a solid–liquid interface promotes the formation of coatings on substrates with varying morphology. As a result, when a suitably designed counter electrode is used, homogeneous polarization is obtained. This approach does not necessitate high temperatures and should not surpass the boiling point of the electrolyte.

Kinetic control is achieved by varying the current flowing through the cell, whereas thermodynamic control is achieved by varying the cell potential. Due to the fact that electrochemical synthesis is based on an oxidation/ reduction process, so by varying and modifying the cell voltage, the oxidizing and/ or reducing power may be continually varied and correctly selected, which is not possible with other techniques of chemical synthesis. The film structure can be manipulated by altering the bath composition, and the tests are simple to carry out and the tools are inexpensive and readily available. Due to the reactions that are carried out at ambient temperature, the electro synthesis approach frequently creates poorly ordered products, making detailed structural characterisation difficult (Fu *et al.* 2012; Fantechi *et al.* 2020).

A study by Starowicz *et al.* (2011) proposed a simple electrochemical process for the manufacture of magnetic nanoparticles, primarily in the maghemite phase. The reaction was carried out in a LiCl solution containing ethanol and water. The spherical form nanoparticles with an average size of 5 to 40 nm were produced when the water-to-ethanol ratio was adjusted.

According to Gopi *et al.* (2016), the electrochemical production of super paramagnetic cubic magnetite nanoparticles via electro-oxidizing iron in an aqueous solution containing 0.1 M Fe $(ClO_4)_2$ at 50 mA/ cm^2. Therefore, homogenous particles with a size of 15 ± 6 nm were produced. These findings indicate the possibility of a surface plasmon resonance effect in iron oxide nanoparticles when no micelles, stabilizing agents, or surfactants were used to prevent cluster formation (Ramimoghadam *et al.* 2014).

Pascal *et al.* (1999) did research on the electrochemical production of y-Fe_2O_3 nanoparticles in an organic solution. The particle size was promptly monitored by the used current density. Furthermore, the introduction of cationic surfactants improved the stability of the colloidal suspension, and average particles ranging in size from 3 to 8 nm formed a narrow particle size distribution.

Franger *et al.* (2004) reported the electrochemical production of pure, homogenous, and ultrafine magnetite particles at ambient temperatures using an Fe electrode immersed in an alkaline solution containing complexing chemicals. Their findings reveal that at 300 K, pure magnetite exhibits a magneto resistance of around 3% when subjected to a magnetic field (MF) of 1 Tesla (T). The agents of complexity can be utilized in the improvement of charge transfer kinetics to asisst in reducing the diameter of produced particles to the nano-scale (Franger *et al.* 2004; Thenuwara *et al.* 2019; Li *et al.* 2021a).

2.5.4. Magnetic properties of iron oxide phases

Magnetic separation technique impacts particle aggregation by numerous external factors such as magnetic gravity, van der Waals forces, an electric double layer, gravity, Brownian motion, and fluid motion to produce separation (Cui *et al.* 2020). It has been proven to be more efficient in mineral processing industries (Karapinar 2003) to anti-scale treatment of pipe lines to seeding magnetic flocculent (Ambashta *et al.* 2010). Hence, it has been recommended for wastewater treatment because when wastewater passes through a MF, it consequently alters some of its physicochemical properties (Ni'am 2006; Zaidi *et al.* 2014). In addition, due to various their action on water molecules located surrounding colloids, MF causes asymmetry in hydrated shells,

which leads to increased electro-kinetic activity among the colloids. The application of this technique is simple, cost-effective, shows ecological purity, and safety and can operate at a high flow rate to remove non-magnetic water pollutants (Karapinar 2003).

2.5.4.1. Magnetic properties

Iron-based nanoparticles have gained a significant deal of interest recently due to their unusual features and possible technological uses (Akbarzadeh *et al.* 2012; Rossi *et al.* 2013; dos Santos *et al.* 2018a; Kristianto *et al.* 2020; Boskovic *et al.* 2021). These types of materials are susceptible to an external MF (Figure 2-18a) and behaves similarly to a paramagnetic material, however removing the applied MF instantaneously returns the total net magnetic moment to zero (Ni'am 2006; Shuang *et al.* 2012; Al Kindi *et al.* 2021) as shown in figure 2-18b. As a result, super paramagnetic NPs have no "magnetic memory", and they may be retrieved and redistributed instantly after the MF are terminated by introducing distant MF as shown in figure 2-18. By removing the adsorbed toxic contaminants by a magnet, NPs can be reused after magnetic separation (Shen *et al.* 2009; Okoli *et al.* 2011; Singh *et al.* 2011; Lombi *et al.* 2012; Kango *et al.* 2013; Sirivisoot *et al.* 2015; Zaidi *et al.* 2018; Omara *et al.* 2019). Equation 2.8 show important characteristics such as magnetization of a material (J) after exposure to magnetic field (M) and magnetic susceptibility (k) of the electrons in molecules owing to magnetization., that are used to characterize particle magnetic properties. Magnetic susceptibility can be expressed in terms of volume (v) in , or mass (x), m^3/kg (Ramimoghadam et al. 2014; Zaidi et al. 2014).

$$J\left(^{\text{Amperes}}/_{\text{meter}}\right) = k \times M \text{ (Telsa)} \qquad \text{Equation 2.8}$$

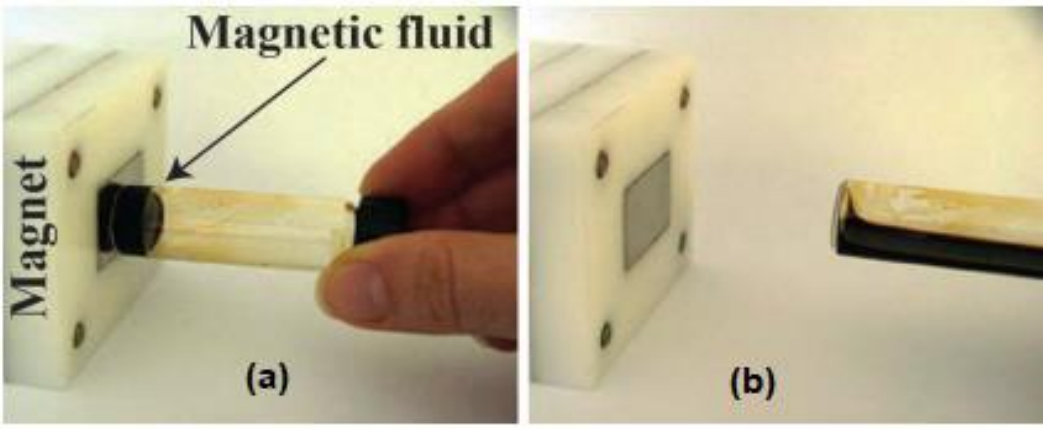

Figure 2-18 Magnetic characteristics of Fe_3O_4 NPs in both the existence (a) and exclusion (b) of a MF applied, adapted from Rossi *et al.* (2013)

2.5.4.2. Types of magnetism

Diamagnetism is an inherent a property of all chemicals that produces a little repulsion by MF. As a result, a diamagnetic substance's magnetic susceptibility is expected to be tiny, negative, and temperature-independent (Makarova 2005; Mukherjee 2011; Ramimoghadam *et al.* 2014; Chen *et al.* 2019). Extra forms of magnetism can be found in iron oxides.

Paramagnetic compounds are drawn in the direction of MF. These compounds have unpaired electrons that are arbitrarily positioned on various atoms. Each atom (ion or molecule) of a paramagnetic material can be seen as a tiny magnet with its intrinsic magnetic moment. Using MF causes these magnets to be (partially) oriented parallel to the field (Bozhinova 2004; Ni'am 2006). The magnetic susceptibility (X_m), a positive characteristics of paramagnetic materials and modest < 0.01 (Ramimoghadam *et al.* 2014). It is temperature-dependent, and its behavior may be represented by the Curie–Weiss law, as shown in equation 2.9.

$$X_m = \frac{C_m}{T - T_c} \qquad \text{Equation 2.9}$$

where T is an absolute tempereature,T_C is Curie temperature,both in Kelvin and C_m is a material-specific Curie constant in Kelvin. The temperature dependency is the outcome of two conflicting tendencies; the greater alignment of the magnetization in the material is resisted by stronger thermal vibrations as the temperature goes up, resulting in a fall in value. Compounds undergo a magnetically ordered state transition below a particular temperature (Neel or Curie) depending on the kind of oxide and becomes ferromagnetic, ferrimagnetic, antiferromagnetic, and/ or speromagnetic (Machala *et al.* 2007; Šesták *et al.* 2011; Muscas *et al.* 2018; McCloy 2019). The transition temperature for ferromagnetic and ferrimagnetic materials is T_C, while for antiferromagnetic materials, is T_N (Ramimoghadam *et al.* 2014; Počuča-Nešić *et al.* 2019; Guillou *et al.* 2020; Das 2021).

Ferro- and ferrimagnetic materials are strongly drawn to MF. They include unpaired electrons with moments caused by interactions between nearby spins that are at least partially aligned even when no MF are present. The spin coupling has positive energy. Electron spins in a ferromagnetic material are parallel aligned. Such materials exhibit a significant important magnetization potential, with a quite great susceptibility of 0.01 to $l0^6$ (Ramimoghadam *et al.* 2014; Pathak 2020; Paudel 2021), and a high magnetic permeability. When the temperature rises, the ordered alignment of the spins decreases concerning thermal fluctuations of the individual magnetic moments, and the susceptibility decreases dramatically. The Curie–Weiss law does not apply to

the temperature-dependent behavior of susceptibility. The electron spins in an anti-ferromagnetic substance have an equal magnetic moment and are organized in an anti-parallel configuration (Ramimoghadam *et al.* 2014; Cook 2016).

These materials have a zero overall magnetic moment, a tiny positive susceptibility of 0 to 0.1, and a positive permeability. Temperature increases frequently which increases sensitivity because the anti-parallel ordering is disrupted. Ferrimagnetic materials, like anti-ferromagnetic materials, are made up of at least two interpenetrating sub lattices with anti-parallel spin alignment. Different spins in a ferrimagnetic material, on the other hand, have uneven moments; hence, a ferrimagnetic substance has a net magnetic moment.

Ferromagnetic, ferrimagnetic, and anti-ferromagnetic materials all have a domain structure; however, only particles with sizes ranging from 50 to 500 nm are made up of a single domain spin (Filippou 2019). The spin inside a domain can be either anti-parallel or parallel, but the spin alignment varies between domains. Domains must be removed in a ferro- or anti-ferromagnetic material, by employing sufficient and strong MF; when the used MF are increased, the alignment of the spins in the domains increases (Shai 2012; Paudel 2021). At sufficiently large MF, saturation magnetization occurs, i.e., all domain spin orientations become parallel.

2.5.4.3. Magnetic behavior of iron oxides

The most important kind of magnetic contact amongst Fe ions on contiguous sites in a solid material is electrostatic exchange interaction, which causes spins to align in parallel or anti-parallel alignment. Because the Fe (III) ions in iron oxides are surrounded by O^{2-} orOH^{-} ions, the exchange interactions begin via the intervening ligand. This is referred to as super-exchange. Unpaired electrons in the e- orbitals of the Fe (III) ions engage magnetically with electrons in the p- orbitals of the O^{2-} ions, resulting in a chain coupling effect that percolates through the crystal if the cation and ligand are near enough to allow electron coupling (Shai 2012; Ramimoghadam *et al.* 2014). The observed exchange constants for these processes were discovered to be bond length and are angle-dependent. When the Fe (III) bond angles are within 120 to 180°, exchange contacts are robust, but they become significantly weaker when the angle is 90° (Aparnadevi *et al.* 2016). Super exchange interactions in Fe (II) oxides have a similar reliance on a bond angle. As a result of the existence of both Fe (II) and Fe (III) in magnetite, electron delocalization can occur between iron ions on a neighboring site (Wright *et al.* 2002; Tang *et al.* 2003; He *et al.* 2005; Ramimoghadam *et al.* 2014).

2.6. Process optimization

An optimization is a method of achieving optimal operating circumstances for a production process in order to maximize and create the optimum response. An unsatisfactory approach, on the other hand, may result in major environmental issues, excessive energy consumption, high maintenance costs, and high chemical usage (Tetteh 2018a).

2.6.1. Application of Response surface methodology (RSM)

One of the most difficult issues in utilization of various physicochemical processes for treating effluents is the right selection of experimental circumstances, which may be accomplished through a larger concept known as design of experiments (DoE) (Karimifard *et al.* 2018). Design Expert software (Version .11.1.0.1, Stat-Ease Inc., Minneapolis, MA, USA) was used to create the experimental design. Herein, optimization and modelling studies have been explored successfully utilizing the Response Surface Methodology (RSM) statistical approach. RSM incorporates both the independent variables and the experimental data input before producing a prediction model as the output or response (Tetteh *et al.* 2017). This statistical design of experiment is a significant tool for optimizing various chemical and biological processes (Chinenye Adaobi Igwegbea *et al.* 2019; Louhichi *et al.* 2019; Bell *et al.* 2021; Khettaf *et al.* 2021; Rodriguez-Granrose *et al.* 2021). RSM is commonly used because of its speed and less necessary experimental runs, well-designed regression analysis, assessment and selection of the most significant input variables that can impact the process, and supporting the investigator in focusing on discovering and managing the process (Khannous *et al.* 2011; Yusri *et al.* 2018). Meanwhile the conventional way of DoE via one factor at a time (OFAT) has some limitations, including (a) a lack of interactive effects among the input variables on the response; (b) requiring a significant amount of time and resources to complete an investigation for the influence of input on the output ; and (c) requiring a large number of experimental runs, which increases experimental costs in terms of chemical usage and analyses (Tetteh 2018a; Khettaf *et al.* 2021).

In addressing this, RSM is gaining attention over the conventional OFAT method due to the major advantages it offers in statistical analysis and cost savings of the experiment at work (Pambi *et al.* 2016; Tetteh *et al.* 2017). RSM is capable of eliminating bias in an experiment, effectively isolating noise within the experiment from its improvements (Li *et al.* 2016). Again, using RSM, the interaction between operational factors may be explored, with the option of simultaneously altering these variables (Iqbal *et al.* 2016; Chaves *et al.* 2021; Sarkar *et al.* 2021). Another significant benefit of RSM is the ability to optimize important process parameters, which is

difficult to do using OFAT (Elumalai 2018; Fath *et al.* 2020). To ensure statistical significance and accurate portrayal of DoE data, analysis of variance (ANOVA), half-normal plots, and a variety of other model-defining techniques are used. Analysis of variance (ANOVA), half-normal plots, and a batch of other model-defining techniques are used to ensure statistical significance and accurate portrayal of DoE data. Contour plots and response surface plots give excellent visual effects that aid researchers in understanding the changes in process factors and their responses (Jiang 2015; Chinenye Adaobi Igwegbea *et al.* 2019; Mohd-Salleh *et al.* 2019; Bell *et al.* 2021; Rodriguez-Granrose *et al.* 2021).

2.6.2. The Box-Behnken Design (BBD)

There seem to be a number of experimental designs featuring focus points for interdisciplinary design optimization. There are three kinds of Response surface methods: the first-order, the second-order, and three- level fractional factorial. The most well-known second-order models are central composite design (CCD), Doehlert design (DD), and Box–Behnken design (BBD) (Li *et al.* 2016; Li *et al.* 2017; Tetteh 2018a). When these three are compared, DD is found to be the most efficient design system followed by the BBD. Additionally, DD provides the capability of sequentiality. However, DD uniform shell designs have not been widely used since their design variables are treated unequally. Hence, BBD was chosen for optimization. Using three levels of incomplete factorial designs, these are rotatable or nearly rotatable second-order designs (Ferreira *et al.* 2007; Alwan *et al.* 2020; Alhajabdalla *et al.* 2021).

The number of experimental runs that should be performed are adjusted by using BBD in such in such a way that it analyzes the probable interactions between the investigated variables and their potential effect on the process's response. The BBD contains three levels for each variable: -1, 0 and +1, which correspond to three positions,namely, low, center, and maximum, respectively (Iqbal *et al.* 2016; Tetteh *et al.* 2017; Louhichi *et al.* 2019; Blandin *et al.* 2021).

2.7. Summary

From the literature survey, the growing fresh water needs and industrial activities has exacerbated the lack of available clean water. Furthermore, fresh water supplies are being depleted as a result of anthropogenic activities. Coagulation has been utilized extensively among the different procedures and technologies (physical, chemical and biological treatment) used to improve water quality. Conventional coagulants (iron and aluminium salts) are mostly used in most of the WWTPs. However, the bottlenecks associated with these conventaional coagualants include the

inefficiency for the treatment of eliminating emerging pollutants (EPs) as well as producing secondary pollutants. They include the need for expensive machinery and monitoring systems, high reagent and energy costs, and/or the production of hazardous sludge or other waste products that need to be disposed. This poses a significant risk to both public health and aquatic species. Hence, researchers and water sector stakeholders are looking for frinendly and cost-effective coagulants.

Against this background of working towards zero-waste and sustainable environment the use of natural materials and magnetized nanocomposite were found to have great potential to be explored as coagulants. Egg shells are found to be a cheap and readily accessible biomaterial. Hence, using them as coagulants will be advantageous, due to their high catalytic activity, simplicity of handling, reusability, and benign nature. The production of rice generates waste, so converting unwanted rice into coagulants comes in handy. It is a common and affordable natural polymer that offers more benefits than other starch because of its excellent stability and acid resistance. Also, chitosan was found to possess positively charged functional groups, which have a greater potential for interacting with hydroxyl groups (OH-) in wastewater. Furthermore, it has a high density, is biodegradable, simple to handle, non-toxic, leaves no residual metal in treated water, and eliminates secondary contamination issues. Due to the benefits indicated above, chitosan, rice starch, and eggshells were chosen for this study. Furthermore, they are available locally, generate less sludge, and produce biodegradable sludge (which may be reused).

Some of the methods of synthesizing the nanocomposites were explored, whereby co-precipitation was found to be the most suitable for engineering magnetized nanocomposites. Furtheremore, RSM via Design Expert was found as a potential tool for experimental design, process optimization, statistical data analysis and modelling. Therefore, employing the RSM for optimizing the operating conditions of the coagulation and DAF process comes in handy.

CHAPTER 3-MATERIALS AND METHODS

3.1. Introduction

The section describes the experimental strategy utilized to meet the objectives of the study. It discusses the synthesis of magnetic coagulants, the chemicals utilized, wastewater sampling, and characterization together with the analytical equipment and protocols employed. The experimental setup such as the coagulation and DAF descriptions and operating procedures are outlined. The DAF tester experimental setup includes installation, troubleshooting, and commissioning. A primary study on coagulation and the DAF process was carried out using the OFAT approach. The experimental design, process optimization, and modeling using the Box-Behnken design (BBD) of response surface methodology (RSM) adapted from the design expert (DOE) software (Stat-Ease Inc, Minneapolis, USA) are highlighted.

3.2. Chemicals and materials

All of the chemicals and reagents utilized in the research were of analytical quality and did not require additional purification except for the stated ones. In the solution preparation, deionized water (ELGA PURELAB Option-Q water deionizer, UK) was utilized. Sigma Aldrich supplied ferric chloride hexahydrate ($FeCl_3.6H_2O$), iron sulfate ($FeSO_4.7H_2O$), chitosan, oleic acid, sodium hydroxide pellets (NaOH), ethanol (95%), chitosan (with a deacetylation level of 75–85%) as well as the other chemicals used to prepare synthetic wastewater. The raw eggs and rice starch were acquired from a local South African market in Durban, KwaZulu Natal Province, and were thoroughly rinsed with distilled water. The technique developed by Anju *et al.* (2016) was adapted to prepare the eggshell and rice starch powders.

3.3. Wastewater samples and analytical instruments

The wastewaters used in the study were acquired after chlorination from local wastewater treatment facilities in Umbilo, Pietermaritzburg, and Pinetown, KwaZulu-Natal province, South Africa. Immediately upon collection, the effluents were characterized as per APHA (2012) for turbidity ,TSS and COD. A Hach 2100N turbidimeter (Hach Company, Loveland, CO, USA) was used to measure turbidity, whilst a spectrophotometer (HACH DR3900: Hach Company, Loveland, CO, USA) was used to measure COD and TSS. However, 0.2 mL of each wastewater sample was measured and put into the COD vials using the COD high range vials from Hach. After that, it was digested for 2 hours at 150 °C and let to cool to at 23 ± 2 °C. By selecting the

specifid COD range, the spectrophotometer (DR3900) was used to measure the COD. Also for the primary study, a synthetic wastewater was simulated at room temperature by dissolving peptone (4 g), glucose (2.75 g), $NaHCO_3$ (27.5 g), urea (0.75 g), meat extract (6.25 g), $MgSO_4 \cdot 7H_2O$ (0.05 g), K_2HPO_4 (0.7 g), $CuCl_2.2H_2O$ (0.00125 g), NaCl (0.22 g) and $CaCl_2$ (0.10 g) (Figure A-6), in 20 L of wastewater and 5 L of distilled water (Sibiya *et al.* 2021). Then it was characterized for different scenarios as reported in table 3-1. The use of synthetic wastewater provides for improved control over the process, standardization of test conditions, and process replicability (Bi *et al.* 2007; Muniz *et al.* 2020).

Table 3-1 Feed composition of each objective

Wastewater parameters	**Objective 2: Coagulation**	**Objective 2: DAF**	**Objective 3: Coagulation RSM**	**Objective 3: DAF-RSM**
COD (mg/L)	315 ±0.781	351.80 ±0.718	293.20 ±0.471	493.20 ± 0.538
TSS (mg/L)	68.20 ± 0.748	43.20 ± 0.216	91.80 ± 0.816	41.80 ± 0.519
Turbidity (NTU)	45.60 ± 0.290	39.20 ± 0.419	83.10 ± 0.519	46.92 ± 0.470

3.4. Synthesis of magnetized coagulants

Firstly, 1 L stock solution for each chemical was computed using their mass (g) and molecular weights as shown in Table 3-2. In fact, the 0.4 M Fe^{3+}, 0.2 Fe^{2+}, and 3 M NaOH stock solutions were prepared with respective weights of 108.12 g, 55.61 g, and 199.99 g dissolved in 1 L distilled water (Amo-Duodu *et al.* 2021). These were estimated based on a known concentration and volume with Sigma Aldrich mass molarity calculator.

Table 3-2 Stock solution composition

Chemicals	**Concentration (M)**	**Molar mass (g/mol)**	**Mass (g)**
$FeCl_3.6H_2O$	0.4	270.29	108.21
$FeSO_4.7H_2O$	0.2	287.55	55.61
NaOH	3	39.997	199.99

3.4.1. Co-precipitation

Fe_3O_4 NPs were produced via co-precipitation as stipulated by equation 3.1 (El Ghandoor *et al.* 2012; Mascolo *et al.* 2013; Amo-Duodu *et al.* 2021; Samrot *et al.* 2021; Sibiya *et al.* 2022b) . The Fe_3O_4 was then produced in a volume ratio of 1:1 by utilizing 0.5 L of each of the Fe^{3+} and Fe^{2+} stock solutions. To achieve homogeneity, the solution was constantly agitated at 50 rpm while adding 2 mL oleic acid as a surfactant. The addition of the surfactant was to enhance the compatibility between iron oxides surface and the organic molecules such as the natural coagulants. Surfactants also play a role in providing the entropic repulsion needed to overcome the short-range van der Waals attraction, which would otherwise result in irreversible particle aggregation (Maity and Agrawal 2007; Zhang et al. 2006; Zhu et al. 2011).

$$FeCl_2 \cdot 4H_2O + 2FeCl_3 + 8NaOH \rightarrow Fe_3O_4 + 8NaCl + 20H_2O \qquad \text{Equation 3.1}$$

Subsequently, the pH of the solution was regulated between 11 and 12 by dropwisely adding 0.25 L of 3 M NaOH until a black precipitate is formed. After that, the thick black precipitate heated (aged for 2 hours) at 70 ± 5 °C, was allowed to cool at ambient temperature (Amo-Duodu *et al.* 2021). To remove any undesirable particles, the supernatant was decanted, and the precipitate was washed three times with distilled water and ethanol. The precipitate was then oven dried for 12 hours at 80 ± 5 °C. Table 3-3 indicates the quantity of natural coagulants/polymers functionalized with magnetite to form magnetized coagulants (MCs), which were then calcined for 1 hour at 550 °C. Following that, the MCs were packed for characterization.

Table 3-3 Amounts measured for polymer and magnetite to make 10g of magnetized coagulants

MC ratio/(s)	**CF**		**EF**		**RF**	
	CS (g)	**Fe_3O_4 (g)**	**ES (g)**	**Fe_3O_4 (g)**	**RS (g)**	**Fe_3O_4 (g)**
1:1	5	5	5	5	5	5
2:1	6.667	3.333	6.667	3.333	6.667	3.333
1:2	3.333	6.667	3.333	6.667	3.333	6.667

*CF-magnetized chitosan, EF-magnetized eggshells, RF-magnetize rice starch

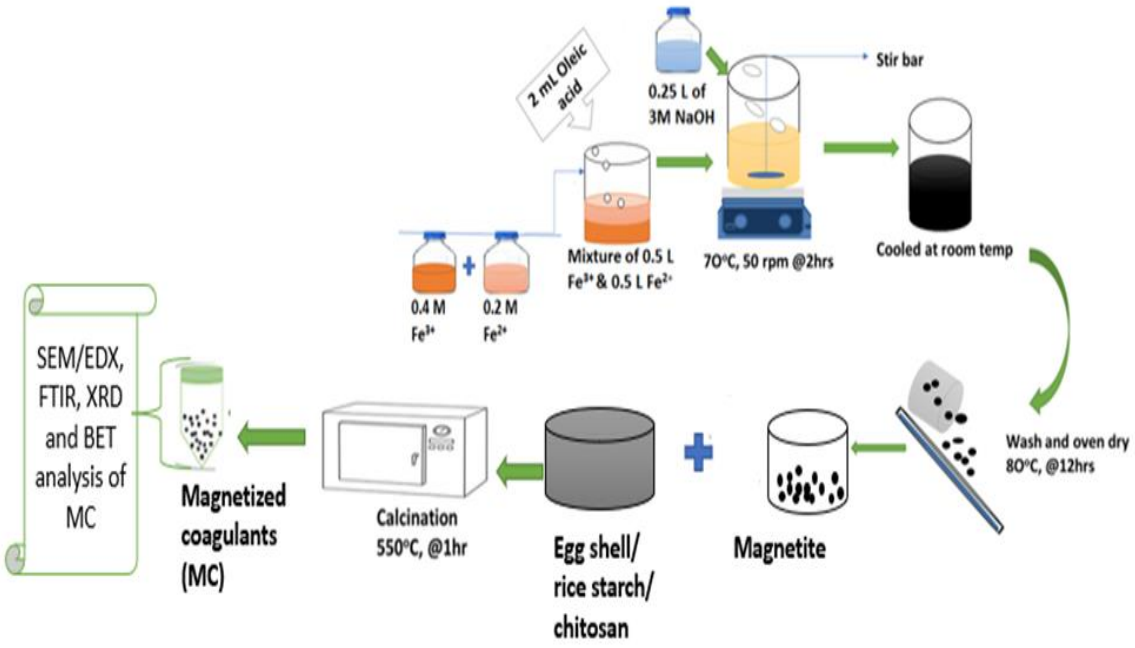

Figure 3-1 Flow diagram for the co-precipitation synthesis of magnetic coagulants

3.4.2. Characterization

3.4.2.1. Morphological and elemental examination

The morphology and elemental analysis of the resulting MCs and magnetite were detected using scanning electron microscopy and energy dispersive X-ray (SEM/EDX) at the University of Cape Town, South Africa (Nova NanoSEM coupled with EDT and TLD detector). This was done using a 5 kV acceleration voltage and a magnification of 10–50 kx.

3.4.2.2. Crystal structure examination

The crystal structures of the produced MCs were examined using an X-ray diffractometer (Bruker AXS, D8 Advance) linked with PANalytical software (Empyrean, PRO MPD, Netherlands) at 40 kV and a target current of 40 mA (Figure A-2). The samples were packed tightly in a rectangular glass cell and scanned using a J-J scan in conjunction with the copper anode (Cu-K$\propto$ radiation: λ=1.5406 Å) and Bragg-Brentano setup. After the sample was put in the center of the sample holder on a glass slide and leveled up to the desired height, the materials to be studied were finely ground, homogenized, and the average bulk composition was calculated. The measurements were performed within a range of 15 to 80 (2θ) with an average step size rate of 0.0340 °/min. Lyn-Eye, a feature attributes monitor, was utilized to capture diffraction data at a typical speed of 0.5

sec/step, which was comparable to an effective time of 92 sec/step for a dazzling counter. The diameters of the MCs were determined from the XRD data using the Debye-Scherrer equation 3.2, which gives a link between particle size and peak enlargement.

$$d = \frac{0.98\,\delta}{\beta \cos\theta} \qquad \text{Equation 3.2}$$

Where d is the particle size of the crystal, δ is the wavelength of X-ray radiation (CuKα = 0.15406 nm), 0.98 is the Sherrer constant, β is the line broadening in radians obtained from the full width at half maximum height (FWHM) of the peak (determined using Origin software), and θ is the Bragg diffracting angle of the XRD diffraction patterns.

3.4.2.3. Functional and molecular examination

A Fourier Transform Infrared spectrometer (Shimadzu FTIR 8400) was used to record the organic, polymeric, and inorganic molecular structures and functional groups of the NPs spanning the 400 – 1200 cm^{-1} range at a resolution of 7 cm^{-1}.

3.4.2.4. Surface area examination

The Brunauer–Emmett–Teller (BET) analysis was carried out using Micromeritics TriStar II Plus equipment (Durban, South Africa) and Tristar Plus software version 3.01. Helium and nitrogen were employed as the carrier gases. Samples were weighed and put into a sample holder on the analyzer and degassed separately for 24 hours at 400 °C. They were then allowed to cool before being stored under nitrogen gas at a pressure of 5 mmHg for 24 hours.

3.5. Experimental configurations

3.5.1. Coagulation configuration process

The jar test is the most often used method for performing the water treatment test (Gregory 2009; Ng *et al.* 2021). The basic premise of the jar test is to add coagulant to untreated or polluted water. Figure 3-2 depicts the jar test equipment (JTL6) made by Velp Scientifica (Velp Inc, USA) and outfitted with six 1 L beakers used to assess the coagulant settling time (10-60 min). A 500 mL homogenized wastewater sample was placed into each beaker, leaving a 500 mL headspace. Then swiftly stirred (at 150 rpm – quick coagulation) for 2 min at a constant pH (7.2) using Hannah pH-meter (HI98130, Hanna Instruments, Woonsocket RI, USA, shown in figure A-4 and a dose of 3 g, accompanied by 15 minutes of gentle stirring (at 30 rpm – slow coagulation). The

supernatant sample was collected with a syringe at 2 cm under the surface after the settling time had passed (10-60 min) without disturbing the settled floc particles. Equation 3.3 was used to calculate the treatability efficiencies.

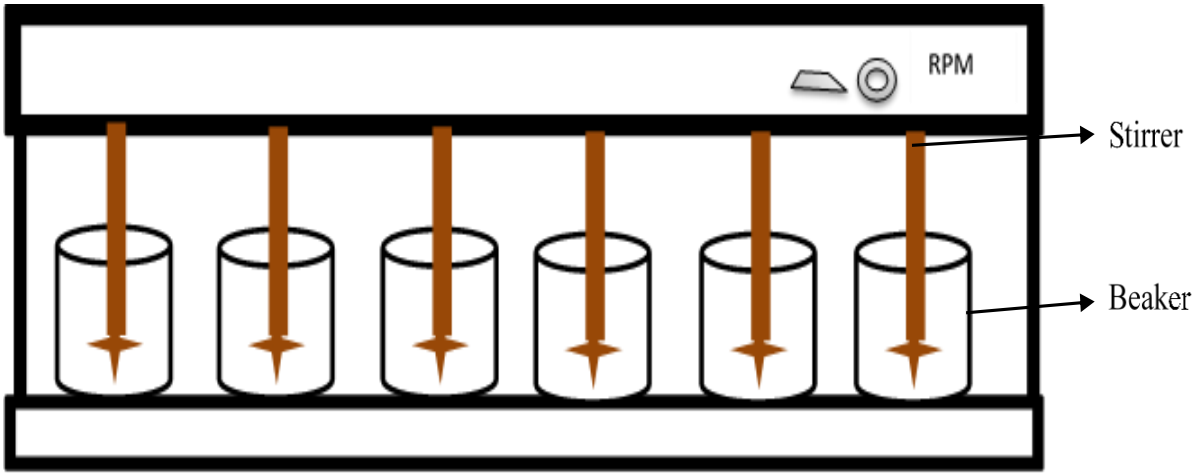

Figure 3-2 Schematic diagram of jar test (JTL6)

$$R_{removal}(\%) = \frac{Z_A - Z_B}{Z_A} \times 100 \qquad \text{Equation 3.3}$$

Where Z_A and Z_B represent the initial and final values of each pollutant (TSS or turbidity or COD), and R is the % removal.

3.5.1.1. The Kinetics modelling

Brownian motion of suspended particles directs coagulation in the early stages (Kumar *et al.* 2016; Sibiya *et al.* 2021). When colloidal particles collapse and agglomerate to a diameter larger than 1 µm, Brownian motion becomes feeble (Sun *et al.* 2019; Ghernaout 2020). The rate of turbidity reduction is described by the kinetics of the coagulation process, which is described by the rate equation (Nnaji *et al.* 2014; Kumar *et al.* 2016; Zahrim *et al.* 2017; Sibiya *et al.* 2021). Furthermore, the kinetics govern the pace of floc production and help to shorten the crucial period before flocs collapse. Kinetics research is critical because the rate of pollutant removal from effluent is determined by kinetic parameters (n and k). An independent variable (t), a dependent variable (C), and kinetic parameters are all included in the rate equation 3.4.

$$\frac{dC}{dt} = -kC^n \qquad \text{Equation 3.4}$$

where C denotes particle concentration, t the coagulation time, k the nth order coagulation rate constant, and n is the coagulation process order. The collision efficiency is used to calculate the rate constant (Nnaji *et al.* 2014; Oke *et al.* 2019). However, particle concentration is related to time in an indirect manner denoted by a negative sign (Oke *et al.* 2019; Fard *et al.* 2021a). The quantity contaminant concentration absorbed by the coagulant used can be directly related to the rate of contaminant reduction (Nnaji *et al.* 2014; Sibiya *et al.* 2021). The rate constant (k) in equation 3.5 is the product of collision efficiency (E) and the Smoluchowski rate constant (K_{RC}) for a rapid coagulation process (Daud *et al.* 2015; Oke *et al.* 2019; Fard *et al.* 2021a).

$$k = E \times K_{RC} \qquad \text{Equation 3.5}$$

Where equation 3.6 shows the formular for K_{RC}

$$K_{RC} = \frac{4K_B \times T}{3\mu} \qquad \text{Equation 3.6}$$

Where μ denotes the viscosity of a fluid. Also, equation 3.7 give the Brownian diffusion coefficient (D_B).

$$D_B = \frac{K_B \times T}{\beta} \qquad \text{Equation 3.7}$$

$$\beta = 2k \qquad \text{Equation 3.8}$$

T denotes absolute temperature in Kelvin, and D_B denotes particle diffusivity. In practical, 'n' theoretically is $1 \leq n \leq 2$ for perikinetic aggregation of particles in coagulation/flocculation systems (Oke *et al.* 2019). Equation 3.4 is integrated for the first order reaction (n = 1), to produce Equation 3.9:

$$\ln\left(\frac{C}{C_0}\right) = k_1 \times t \qquad \text{Equation 3.9}$$

where C_0 and C are the initial and ultimate concentrations (mg/L) of an effluent at time t and k_1 is the first order rate constant in 1/min. Using equation 3.9, a plot of $\ln(C/C_0)$ against t will provide a straight line passing through the origin with a slope of k_1 (Othman *et al.* 2008; Nnaji *et al.* 2014; Singh *et al.* 2020b; Fard *et al.* 2021a). However, if the line does not intersect the origin but instead passes through another y-intercept, it follows the second order process (Nnaji *et al.* 2014; Kumar *et al.* 2016; Oke *et al.* 2019; Singh *et al.* 2020b; Fard *et al.* 2021b). Hence, equation 3.10 expresses

the kinetic equation for the second-order (n = 2) coagulation process. Equation 3.11 shows the linearized version of the differential equation after it has been solved and simplified.

$$\frac{dC}{dt} = -kC^2 \qquad \text{Equation 3.10}$$

$$\frac{1}{C} = \frac{1}{C_0} + K_2 \qquad \text{Equation 3.11}$$

Equation 3.11 is a straight line with a slope of k_2 or second-order rate constant (L/mg.min) and ln $(1/C_0)$ is the intercept produced by the line along the y-axis.

3.5.2. DAF configuration process

In this study, Jar equipment (JTL6, Velp Inc, USA) was utilized for the coagulation process together with Platypus DAF Tester Accessories (Assembly part number, 4GSAT) as shown in figure 3-3. The following are included in the Platypus DAF Jar Tester Accessories kit;

- Air compressor
- 2 L Saturator with level sight tube, air pressure regulator, air diffuser and static air bleed facility.
- DAF assembly for 2 L jars, including dispersers and subnatant sample taps.
- 4 port distribution manifold tubing with push-in connections and easy disconnect (air in or saturator out).

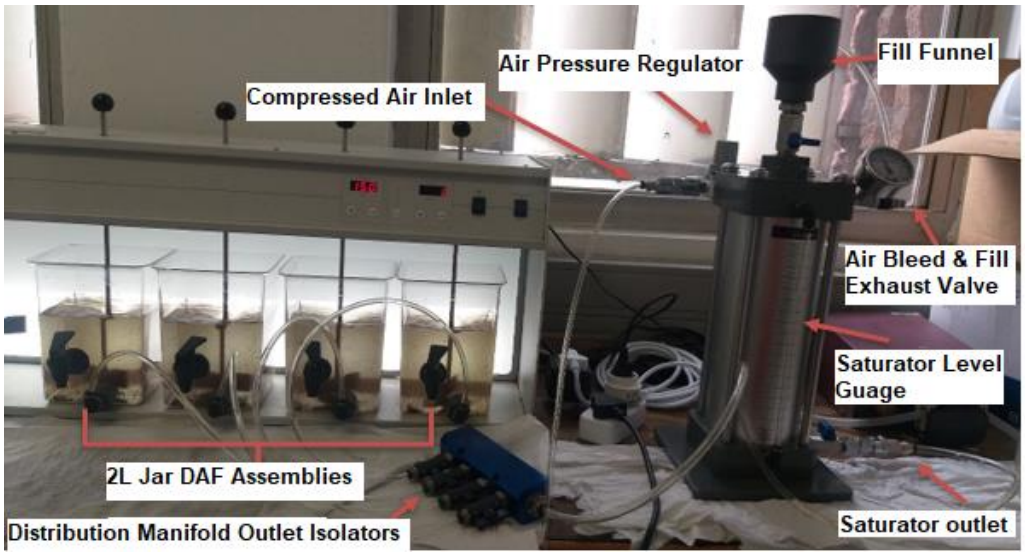

Figure 3-3 Components used for DAF experiments

3.5.2.1. Operational procedure

The operating steps mentioned in the handbook are detailed in Appendix B. The air saturator vessel was filled with deionized water to around 80% (1600 mL) of its entire volume, sealed shut, and properly attached to the compressor. To pressurize the water, the valve connecting the air compressor and the air saturator vessel was opened, and the compressor was turned on. Compressed air was pumped into the system until the pressure reaches 400 ± 50 kPa. The compressor was subsequently disengaged, and the valve was closed. For about 30 seconds, the saturator was shaken intermittently, which aided in the full mixing and dissolving of the air into the water. Each DAF jar testing beaker was filled with a measured 1500 mL wastewater sample. Following that, test trials were carried out under constant working circumstances of a high stirring rate of 150 rpm for 2 min, accompanaied with genttle stirring rate of 30 rpm for 15 min. Following the completion of the mixing, the distribution manifold outlet isolators and saturator outlet were fully opened, and a retention time of 30 seconds was employed to introduce air/water mix into the wastewater samples. The jar test unit was left undisturbed for 10-60 min to allow the sludge to float to the surface. After 10 min of floating time, a marked sample A bottle was located beneath every outlet port to obtain 50 ml samples for analysis. Equation 3.3 was used to calculate the treatability efficiency for TSS, COD, and turbidity.

3.6. Design of experiments and optimization using Box Behnken Design (BBD)

Design expert software (Design Expert software V.11.1.0.1, Stat-Ease Inc., Minneapolis, MA, USA) was used for the systematic layout of the experiment in this study to obtain enough information to optimize the process with the fewest amount of tests possible. The purpose was to determine the best range of operating parameters and the most important aspects for controlling, improving, and optimizing the percent removal efficiency in coagulation and DAF technique. Also, to collect data that can be used to fit and create modelling techniques for each response (COD, TSS, and turbidity), to establish a comprehensive knowledge showing the interactions and relationships between the input factors and turbidity/TSS/COD. BBD generated 14 runs with three replications, three input factors, three levels, and five center points for each process (Table 3-4). The three distinct standardized middle levels were encoded as 1, 0, +1, correlating to the elements' low, median, and maximum. To eliminate bias, these experimental runs were randomized. The best conditions have been used for confirmation runs, which comprised of three separate runs under identical conditions.

Table 3-4 BBD-adapted from RSM experimental design conditions and factor values

Process	Input variables	Coded level		
		-1	**0**	**1**
Coagulation	X1: Mixing rate (rpm)	50	100	150
	X2: Settling time (min)	15	22.5	30
	X3: Coagulant dosage (g)	2	3	4
DAF	X1: Mixing rate (rpm)	50	100	150
	X2: Settling time (min)	15	22.5	30
	X3: Coagulant dosage (g)	2	3	4

CHAPTER 4- RESULTS AND DISCUSSIONS

4.1. Introduction

The section discusses the outcomes of the synthesizing and characterizating MCs as alternative coagulants to alum. Also, the engineered coagulants applicability was evaluated using the conventional Jar tester and the DAF tester. Results obtained in terms of treatability performance and decontamination efficiency were compared and discussed. Furthermore, highlights of the experimental data evaluation via kinetic modeling and the process optimization using RSM are presented. Additional information related to this study is presented in the candidate's published papers (I-VI). These also highlighted the kinetics, optimization, and economic viability of using magnetized coagulants for the treatment of different wastewater streams.

4.2. Characteristics of the MCs

4.2.1. Scanning electron Micrography (SEM)/Energy Disperse X-ray (EDX)

This section describes the shape and size of the magnetized coagulants produced from natural coagulants utilized in this study. Figure 4-1 (a-d) shows the SEM results of chitosan (CS), eggshell (ES), rice starch (RS), and magnetite (Fe_3O_4) which were obtained at width distances (WD) of 5.30, 5.33, 5.6, and 6.0 mm, respectively, ranging from low to large porosity. It was found that the Fe_3O_4, ES, CS (Figure 4-1a-c), and all different ratios of MCs (Figure 4-3 and 4-5) were acquired at a microscale of 1 µm, with a magnification of 50 Kx, view field of 4.5 µm, and accelerating voltage of 5 kV. Whereas, the RS (Figure 4-1d) was obtained at a microscale of 10 µm, with a magnification of 10 kx, horizontal view width of 29.8 µm, and a landing energy capacity of 20 keV. The difference in their appearance and view width may be due to the high calcination temperature of 550 °C, which increased the liquid-solid adsorption capacity (Amo-Duodu *et al.* 2021; Sibiya *et al.* 2021). Figure 4-1a shows that Fe_3O_4 has a regular cellular appearance with a slightly agglomerated structure (Petcharoen *et al.* 2012; Nechita 2017; Tetteh *et al.* 2022), showing that the iron crystals were partially obscured by carbon particles, possibly as a result of the sample's calcination process and carbon coating prior to the analysis (Rao *et al.* 2003; Deravi 2009; Amo-Duodu *et al.* 2021). Figure 4-1b shows morphology of ES, were textural and irregular structures of eggshell particles may be observed (Tsai *et al.* 2006b; Zaman *et al.* 2018). Furthermore, the presence of particles of varying sizes was also observed. Figure 4-1c-depicts the aggregation of CS particles on the surface, which was heterogeneous and produced a smooth surface (Mohanasrinivasan *et al.* 2013; Taspika *et al.* 2020). Figure 4-1d depicts the SEM

of RS, which had a polygonal irregular shape with a smooth surface, as seen in the images observed by (Xu *et al.* 2012; Teh 2014; Kumar *et al.* 2017a; Han *et al.* 2020). In this study, RS was calcined far above the temperature (62 to 78 ℃) at which crystals shred their deformability, commonly referred to as the gelatinization temperature (Teh 2014; Castanha *et al.* 2018; Karp *et al.* 2021). RS granules swelled, and the crystallites melted as a result of the continuous heating (1 hr calcination), as a consequence of which amylose and amylopectin have been completely separated from the starch (Ratnayake *et al.* 2006; Xing *et al.* 2018; Gerçekaslan 2020; Azanza *et al.* 2021).

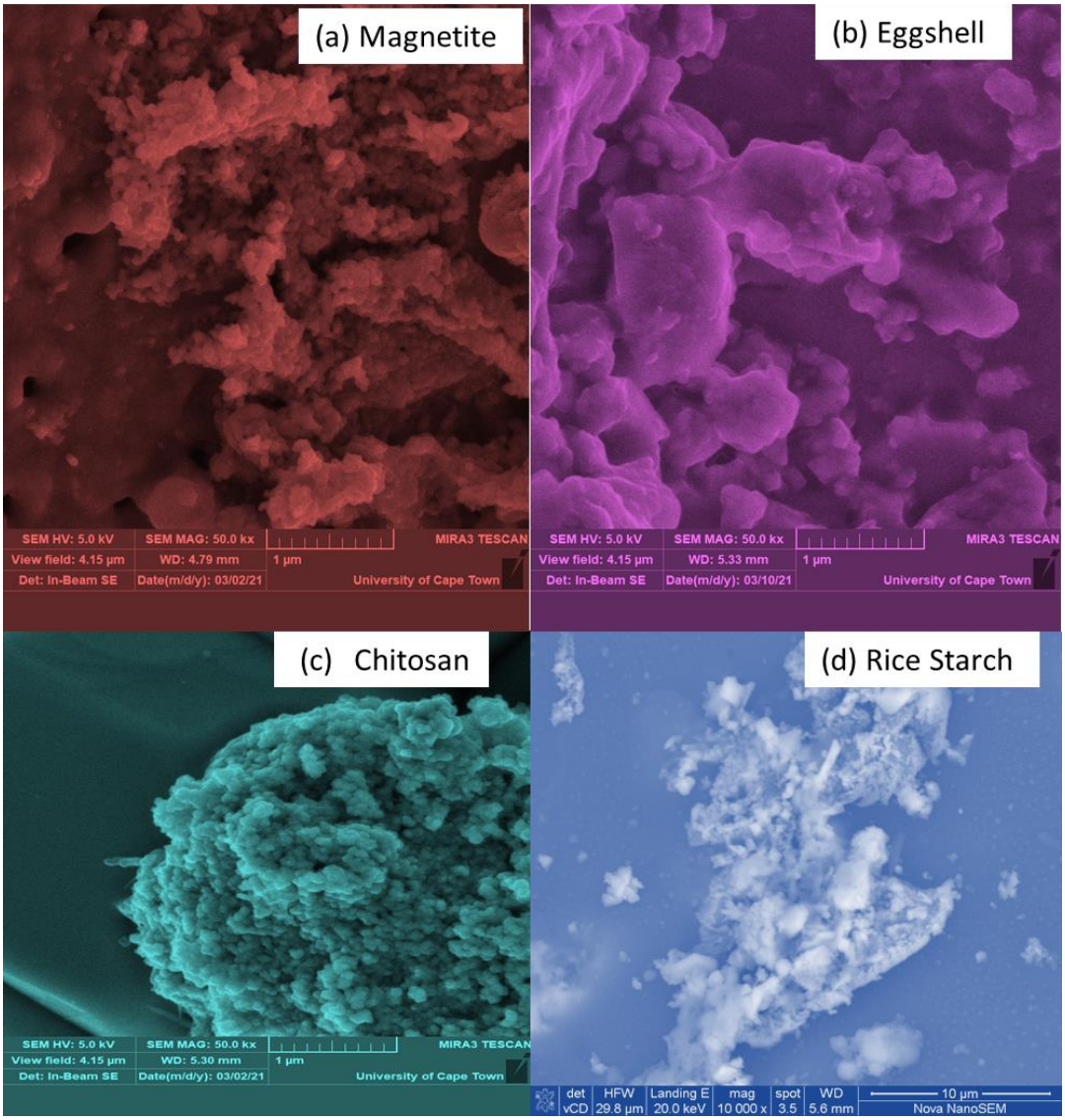

Figure 4-1 SEM images (a-d) of natural coagulants and Fe_3O_4

Figure 4-2a–d depicts the EDX analyses of Fe_3O_4, ES, CS, and RS, together with their respective elemental distributions. Fe_3O_4 spectrum (Figure 4-2a) revealed the composition Fe (39.13%) > O (38.43%) > C (10.36%) > S (9.72%) > Cl (2.37%) (Sibiya *et al.* 2021). The presence of carbon (C) in figure 4-2a was apparently due to the samples being coated with carbon gases (Amo-Duodu *et al.* 2021). The CS spectrum (Figure 4-2b) showed the composition C (92.89%) > O (6.86%) > Na (0.25%); whereas ES (Figure 4-2c) revealed the composition O (50.15%) > Ca (31.93%) > C (17.92%); and the composition C (84.55%) > O (14.62%) > P (0.43%) > K (0.40%) was found for RS (Figure 4-2d).

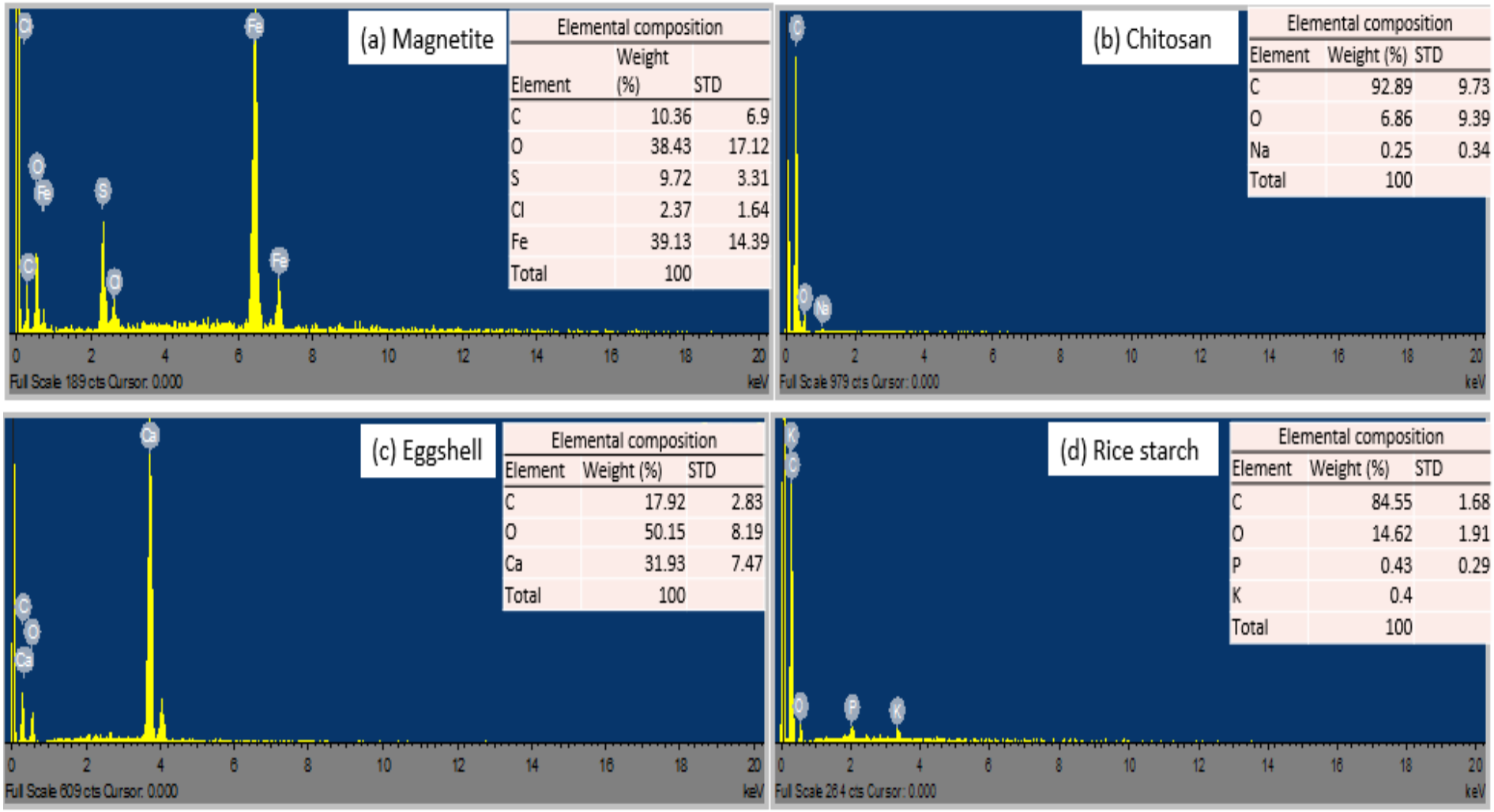

Figure 4-2 EDX images (a-d) of natural coagulants and Fe_3O_4

Figure 4-3 a-c shows the SEM micrographs of an uneven, non-homogeneous, and rough surface of the magnetized coagulants in CF ratios. The formation of a wide pore size distribution (CF (1:1) > CF (1:2) > CF (2:1), as 7.69 > 7.44 > 6.19 mm, respectively). Figure 4-3d appears to be distinct from the other RF ratios (Figure 4-3e-f); it contains smaller and more heterogeneous granules. Furthermore, it had the greatest porosity (8.18 mm), followed by figure 4-3f (6.02 mm) and figure 4-3e (5.98 mm). Figure 4-3e indicates that morphology was more compact, suggesting the production of bigger, firmer, and extremely easy flocs. These flocs with huge particle diameters settle more quickly (Sibiya *et al.* 2022b). The porous aspect of ES is seen in Figure 4-4g with an angular pattern of fracture in the organization – of eggshell granules (Tsai *et al.* 2006b). In general, the micro porous eggshell powder's high porosity provides a broad contact surface for initiating the process (Mosaddegh *et al.* 2013). Figure 4-4h-i clearly shows that these two samples have surfaces that are porous and not homogeneous compared to Figure 4-4g (Asgari *et al.* 2019).

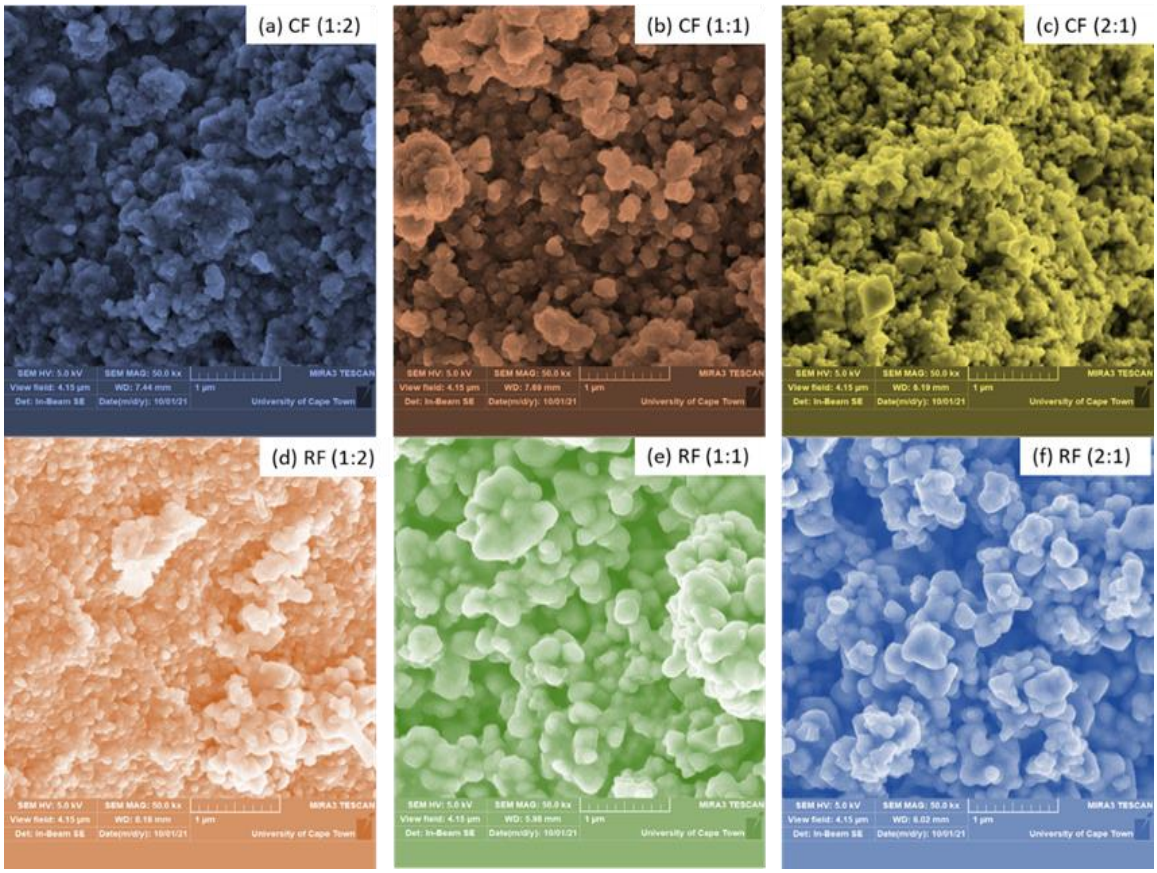

Figure 4-3 SEM images (a-f) of the magnetized coagulants

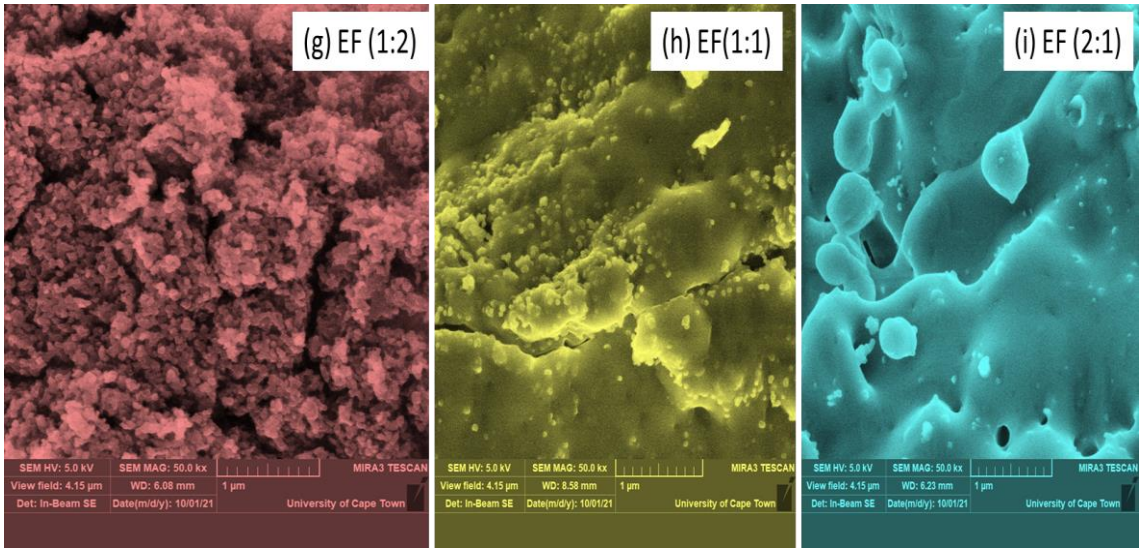

Figure 4-4 SEM images (g-i) of the magnetized coagulants

Figure 4-5 and 4-6 depicts the EDX spectrum with the tabulated elemental distribution of all magnetized coagulants, with observation of Fe binding energies at 0.6, 6.4, and 7 keV. Also, carbon (15 to 64.31% C), oxygen (24 to 43% O), sulphur (0.82 to 13.1% S), chlorine (0.8 to 15.70% Cl) and iron (7.0 to 26.4% Fe) were found to be the most dominating constituents in all MCs. This affirms with Equation 3.1, which revealed that the magnetite is made up primarily of Fe and O (Petcharoen *et al.* 2012; Talekar *et al.* 2017; Amo-Duodu *et al.* 2021; Samrot *et al.* 2021).While additional components (S and Cl) may increased their surface area, allowing for better biosorption and reusability (Amo-Duodu *et al.* 2021). In addition to the foregoing elemental compositions of the magnetized, RF, EF, and CF included potassium (0.3 to 2.2% K), calcium (4.7 to 17.50% C), and sodium (1.5 to 6.80% Na), respectively.

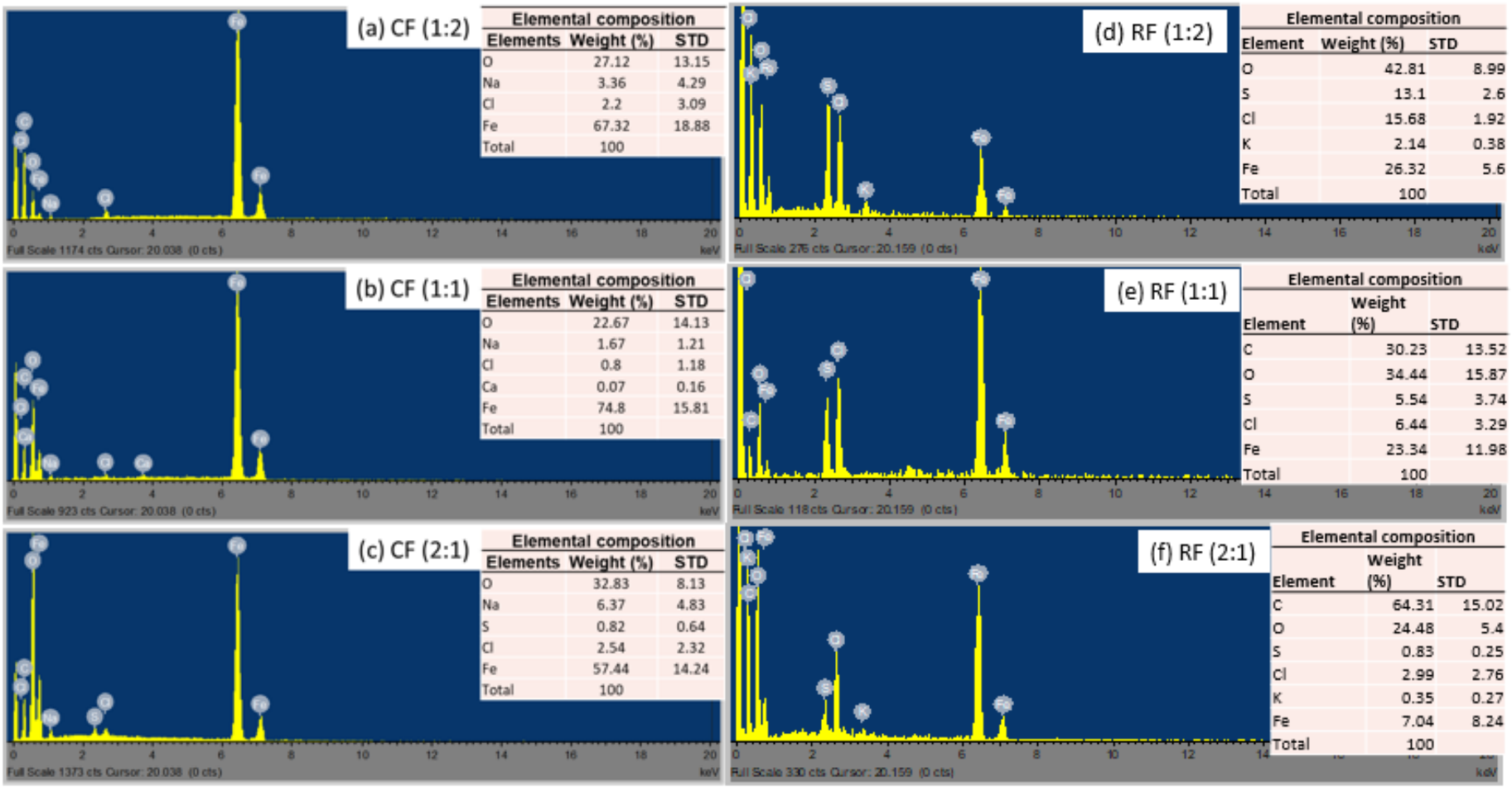

Figure 4-5 EDX images (a-f) of magnetized coagulants

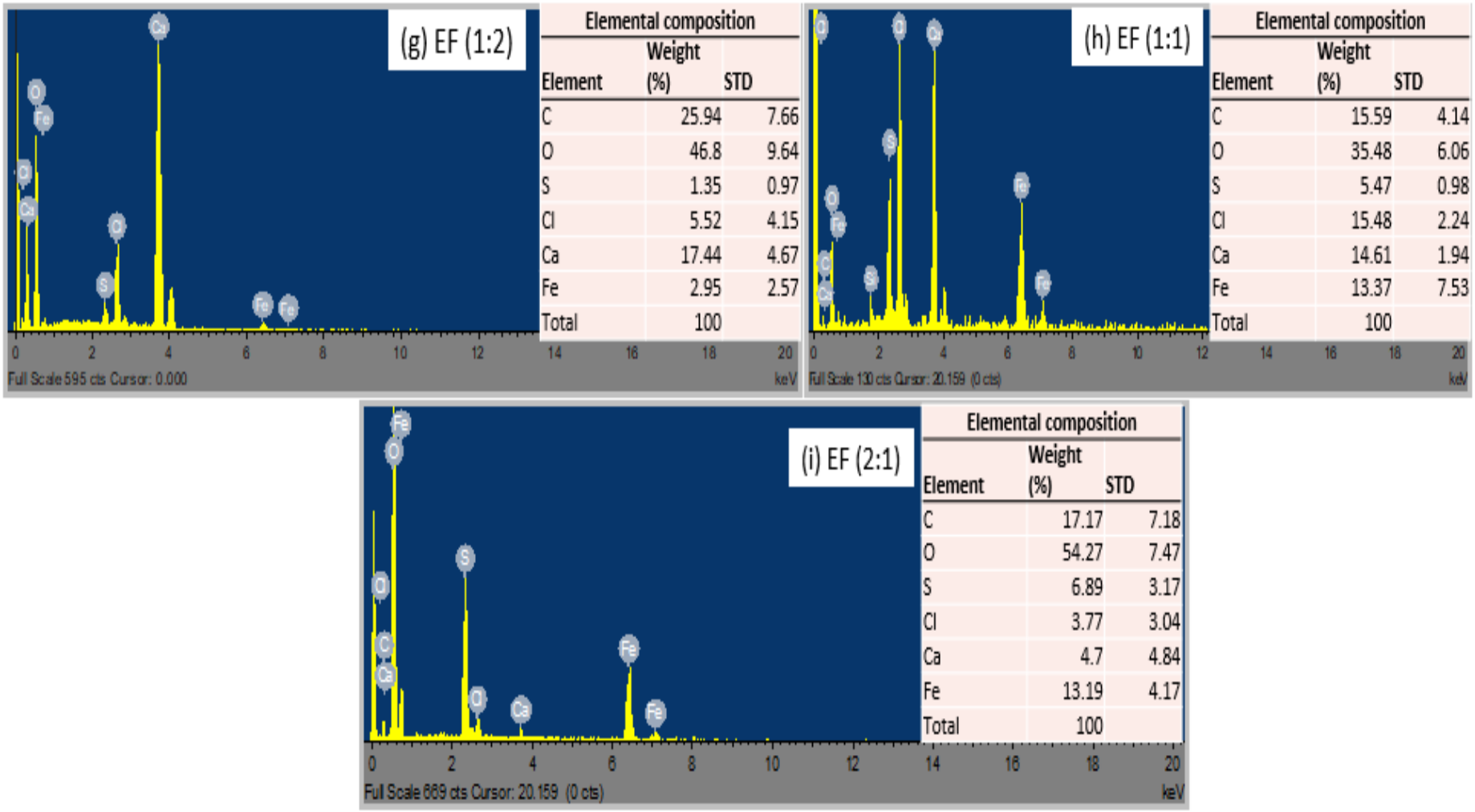

Figure 4-6 EDX images (g-i) of magnetized coagulants

4.2.2. Crystal structure examination (XRD)

X-ray diffraction (XRD) analysis were performed in equipment seen in figure A-2 to determine the structure, crystallinity, and formation of a metal oxide (Wong *et al.* 2015; Helwani *et al.* 2020). The Debye-Scherrer equation 3.2, which demonstrates a link between X-ray diffraction peak broadening and crystallite size, may be used to estimate the crystallite size of produced Fe_3O_4-NPs (Yuvakkumar *et al.* 2014; Ouyang *et al.* 2015). The XRD pattern of iron oxide nanoparticles generated is remarkably similar to the JCPDS pattern (Table 4-1) for magnetite, natural coagulants, and MCs studied in this research. The reflection at 2θ values of 21.398°, 35.423° and 46.8° correspond to lattice planes of (14), (227) and (148), respectively, for magnetite as shown in figure 4-7. In addition, the Scherer's equations with a pseudo-Voigt Function were applied to the peak at 2θ of 35.423° to determine the size of magnetite crystallites of magnetite obtained at various periods (Baumgartner *et al.* 2013; Rashid *et al.* 2020). The investigated diffraction peaks corresponded closely to the conventional magnetite XRD patterns, indicating a cubic crystallographic system (Yew *et al.* 2016). Furthermore, by contrasting the XRD patterns to the maghemite JCPDS pattern number 00-039-1346, the nanoparticles were confirmed to be magnetite rather than maghemite. Figure 4-7a, shows the XRD patterns of CS and its magnetized coagulants (CF ratios). Chitosan pattern revealed one distinctive wide diffraction peak at $2\theta = 20.15°$, which is typical of semi-crystalline chitosan (Bourtoom *et al.* 2008; Jana *et al.* 2015; Dey *et al.* 2016; Billah *et al.* 2020). This peak is associated with crystal I and crystal II in the chitosan structure, and it indicates that the chitosan has a high degree of crystallinity (Kumar *et al.* 2012; Mohanasrinivasan *et al.* 2013). The (225) plane corresponds to the peak at about 30.1°. Its magnetized coagulants exhibit similar behaviour with notable peak at about 35.423° which correspond to the (227) plane.

The XRD patterns of ES and its magnetized coagulants is shown in figure 4-7b. The pattern of ES revealed the presence of a thermodynamically stable calcite ($CaCO_3$) phase defined by its indices (167) in 2θ of 29.406° as a major component (Tsai *et al.* 2006a; Zaman *et al.* 2018). which is comparable to a calcium carbonate mineral (Mosaddegh *et al.* 2013). Also, peak 37.381° represent calcite while those occurring at 2θ = 36.0°, 39.323°, 43.144°, 47.104°, and 48.463° belong to the calcium oxide (CaO) phase defined by plane indices (167) which is also found by Pradhan *et al.* (2017) and Haddad *et al.* (2021). These findings support the existence of calcite and calcium oxide as the primary elements of ES (Verziu *et al.* 2011; Eswararao *et al.* 2016). Therefore, this resulted in the occurrence of more than 90% $CaCO_3$ with a rhombohedra structure (Guatame-Garcia *et al.* 2018; Zaman *et al.* 2018; de la Torre *et al.* 2019). Lastly , the EFs show calcium oxide peaks at 2θ = 57.381° and 64.304° (Haddad *et al.* 2021).

Figure 4-7c shows the XRD image of RS and its magnetized coagulants. RS displayed a typical A-type XRD pattern with strong peaks at 2θ = 17.374° (160), 24.482° (225) and 25.432° (63) which was widely accepted as the typical cereal starch and legume crystal form (Bule´on *et al.* 1998; Shih *et al.* 2007; Matmin *et al.* 2018; Yang *et al.* 2021). The presence of very small crystallite sizes was suggested by the broad and difficult-to-distinguish diffraction peaks (Matmin *et al.* 2018). Starches with an A-type diffraction pattern are described as having a helical arrangement in the unit cells with monoclinic symmetry (Rao *et al.* 2014). RF (2:1), RF (1:1) and RF (1:2) exhibit a similar pattern with major peaks at 33.153°, 35.423°, 54.5° and 63.5° which correspond to lattice plane of (104), (227), (116) and (214), respectively which similar to the study by Matmin *et al.* (2018). However, RF (1:1) have higher values of intensity compared to other RF ratios in figure 4-7c.

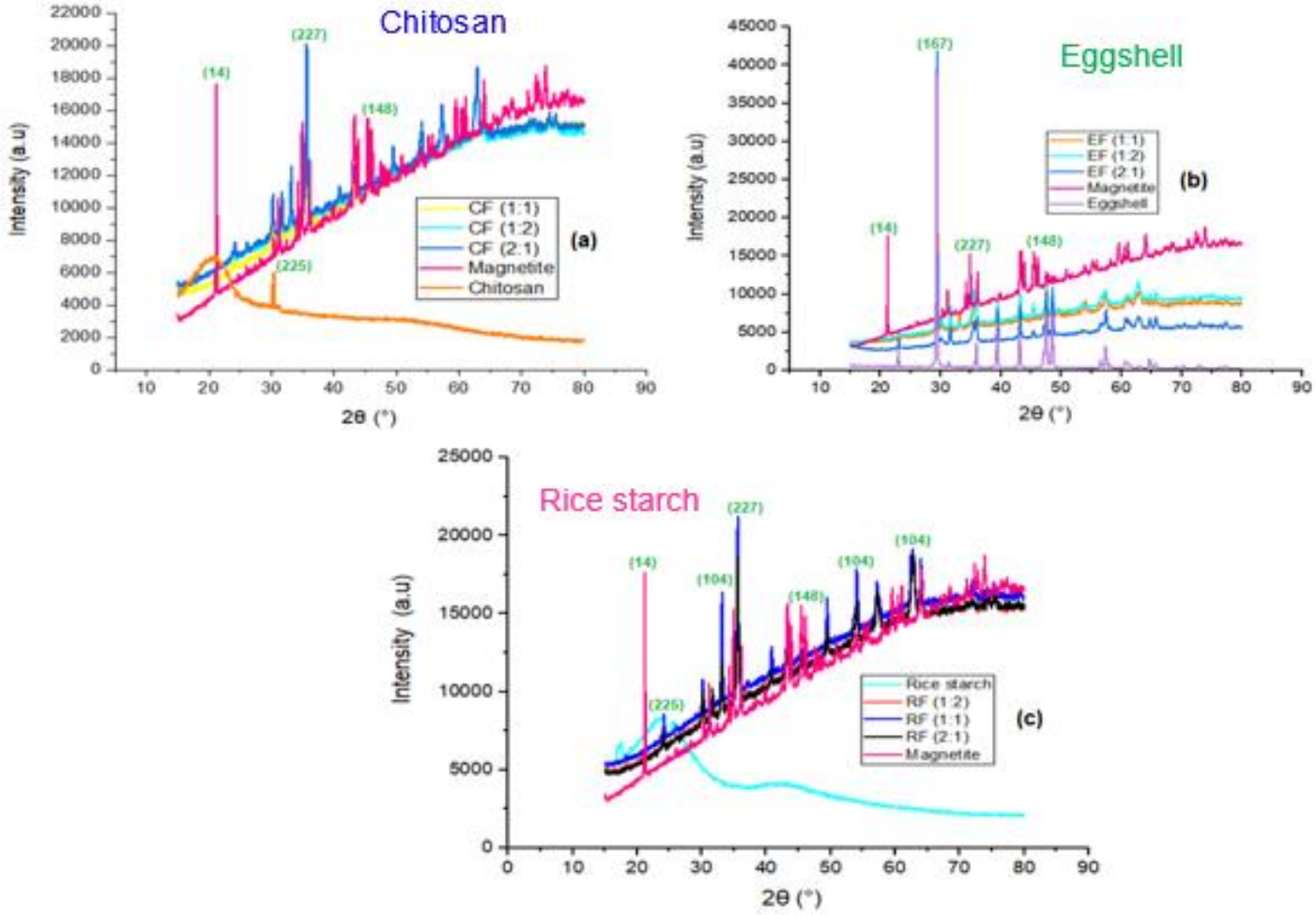

Figure 4-7 XRD spectra (a-c) of the magnetized coagulants (MCs) with their compositions defined in Table 3-3

Table 4-1 Physical and chemical properties of the MCs characterised obtained from the XRD

2θ (degree)	Miller indices plane (hkl)	dhkl (nm)	Crystal structure	Nanostructure	JCPDS pattern
24.865	(62)	3.549	Orthohombic	β-$FeSO_4$	00-033-0682
28.294	(0)	2.297	Monoclinic	Calcium sulphite	00-038-0701
24.482	(225)	1.988	Face-centered cubic	Sylvite	00-41-1476
46.8	(148)	3.157	Rhombohedral	Mikasaite	00-047-1774
21.398	(14)	3.202	Monoclinic	Ferrimagnetite	00-070-2091
25.432	(63)	2.961	Base-centered orthohombic	Calcium sulfate ($CaSO_4$)	01-070-0909
48.491	(12)	2.106	Monoclinic	Clinoptilolite	01-071-1425
76.561	(59)	3.606	Orthohombic	Iron oxide chloride	01-072-0619
47.197	(63)	3.654	Base-centered orthohombic	Iron sulfate	01-073-1057
36.989	(15)	3.102	Base-centered monoclinic	Szomolnokite	01-074-1332
51.44	(44)	2.162	Base-centered orthohombic	Sodium nitrate	01-075-2073
22.337	(12)	2.174	Monoclinic	Heulandite	01-082-1228
40.224	(152)	2.635	Hexagonal	Quartz	01-083-0539
27.589	(15)	1.572	Monoclinic	Sodium oxide hydrate	01-083-0597
67.934	(139)	3.232	Body-centered tetragonal	Calcium oxide (CaO)	00-003-0865
29.406	(167)	2.711	Rhombohedral	Calcite ($CaCO_3$)	00-005-0586
27.335	(225)	2.163	Face-centered cubic	Halite (NaCl)	00-005-0628
32.497	(29)	2.263	Orthohombic	Thermonatrite	00-008-0448
20.212	(13)	1.96	Monoclinic	Iron chloride hydrate	00-016-0123
35.525	(227)	4.523	Face-centered cubic	Magnesioferrite	00-017-0464
35.423	(227)	5.197	Face-centered cubic	Magnetite (Fe_3O_4)	00-019-0629
27.335	(53)	3.336	Orthohombic	Iron sulfate	00-021-0428
41.806	(150)	1.712	Hexagonal	Antarctictite	00-026-1053
33.837	(15)	2.124	Monoclinic	Trona	00-029-1447
17.374	(160)	3.065	Rhombohedral	Hydronium jarosite	00-031-0650
33.153	(104)	5.27	Rhombohedral	Hematite (α-Fe_2O_3)	00-033-0664
24.717	(148)	3.06	Rhombohedral	Mikasaite	00-033-0679
35.631	(110)	4.858	Cubic	Maghemite (y-Fe_2O_3)	00-039-1346

4.2.3. Functional and molecular examination (FTIR)

The functional groups of the coagulants examined were determined using FT-IR spectroscopy. For each measurement, 200 scans were collected between 400 – 1200 cm^{-1} with a resolution of 7

cm^{-1} (Figure 4-8).The peaks between 1200 - 900 cm^{-1}, corresponds to the vibrational area in agreement with the surfactant utilized in this investigation, oleic acid was used (Benning *et al.* 2004; Zhang *et al.* 2006). The absorption bands of the Fe_3O_4 were observed at 1055, 936, 846, 548 and 436 cm^{-1} (Figure 4-8). The peak at 1055 cm^{-1} was attributed to the C–O stretching band, which is associated with the C–O–SO_3 group (Barros Gomes Camara *et al.* 2011; Yew *et al.* 2016). The appearance of an aromatic C–H bending band was revealed by the absorption peaks 936 and 846 cm^{-1}. Also, Fe_3O contained two notable peaks at 548 and 436 cm^{-1}, which correspond to the stretched vibration mode of Fe–O (Khoza *et al.* 2012; Demir *et al.* 2013; Beasley *et al.* 2014; Massoumi *et al.* 2018; Mohammadi *et al.* 2021). The metal oxygen band at 548 cm^{-1} corresponded to intrinsic metal stretching vibrations at the tetrahedral site (Yew *et al.* 2016), whereas the metal-oxygen band at 436 cm^{-1} was assigned to octahedral-metal stretching of Fe–O in magnetite (Demir *et al.* 2013). The formation of Fe_3O_4-NPs was confirmed by these characteristic peaks, as the peaks located between 400 and 600 cm^{-1} corresponded to the magnetite phase (Zhang *et al.* 2006; Petcharoen *et al.* 2012; Yuvakkumar *et al.* 2014).

Figure 4-8a shows the absorption bands at 1160 cm^{-1} (asymmetric stretching of the –COOC– bridge), 1086 cm^{-1} and 1030 cm^{-1} (skeletal vibration involving the COO stretching) were typical of CS's saccharine structure (Kumar *et al.* 2012; Jana *et al.* 2015; Dey *et al.* 2016). Also, at 680 cm^{-1}, off plane bending -OH vibrations are found. In general, the FTIR spectra of CS contains distinctive bands corresponding to amide groups between 1305 and 1660 cm^{-1} (El Knidri *et al.* 2016; Wang *et al.* 2021a) and N-H peaks as well as hydrogen-bonded hydroxyl groups between 3270 and 3800 cm^{-1} (El Knidri *et al.* 2016; Ren *et al.* 2017; Danko *et al.* 2021). The FTIR spectra for RS and its magnetized coagulants (Figure 4-8b) showed a distinct strong peak at around 995 cm^{-1} that was assigned to the C-O of C-O-C bonds of starch (Teh 2014; Ferreira-Villadiego *et al.* 2018). It also shows that shoulder peaks at approximately 939 cm^{-1} (skeletal mode vibrations of -1,4 glycosidic linkage) similar to the study by Talekar *et al.* (2013) and Fan *et al.* (2012), 1085 cm^{-1} (C-O-H bending), and 1148 cm^{-1} (C-O , O-H and C -C stretching) were observed (Kizil *et al.* 2002; Yao *et al.* 2002; Fan *et al.* 2012; Kumar *et al.* 2017a; Matmin *et al.* 2018). A distinct peak at 852 cm^{-1} was caused by C -H and CH_2 deformation in the region below 900 cm^{-1} (Teh 2014). The C-C stretching caused a peak at 760 cm^{-1} and lastly peaks obtained between 600 to 400 cm^{-1} are found to be skeletal modes of pyranose (Bourtoom *et al.* 2008; Bashir *et al.* 2017; Kumar *et al.* 2017a; Matmin *et al.* 2018).

If RS was incorporated with Fe_3O_4, changes in the characteristic spectra peaks influenced the physical versus chemical interactions (Bourtoom *et al.* 2008). The RFs show a similar behavior throughout, however the RF (1:2) displays a highest transmittance > RF (2:1) > RF (1:1). The C-

O stretch peak in RFs spectrums shifted from 1148 to 1100 cm^{-1}. Also, the C-C stretch peak shifted from 852 to 689 cm^{-1}. This phenomenon revealed the presence of interactions between the hydroxyl groups of RS and Fe_3O_4 (Bourtoom *et al.* 2008) which may result in the formation of hydrogen bond as the result of interactions (Xu *et al.* 2012; Kumar *et al.* 2017a; Yang *et al.* 2021). The positions of the peaks in the FTIR patterns of the EFs were identical (figure 4-8c). An intensity band at 700 cm^{-1} is ascribed to enhanced vibration of the P–OH group (Tsai *et al.* 2006b; Mosaddegh *et al.* 2013). The involvement of phosphorus as phosphate in eggshell has been mentioned in the literature (Witoon 2011; Waheed *et al.* 2020; Burezq 2021). In the presence of calcium carbonate, there are two detectable peaks at roughly 700 cm^{-1} and 850 cm^{-1}, which should be related with the in-plane deformation and out-of-plane deformation modes, respectively (Donners *et al.* 2002; Tsai *et al.* 2006b; Krithiga *et al.* 2011; Mosaddegh *et al.* 2013; Pradhan *et al.* 2017; Luna Vera *et al.* 2018). Also, the oscillations of the carbonate CO_3^{-2} anions are responsible for the absorption bands at 1080 cm^{-1} (Engin *et al.* 2006; Rohim *et al.* 2014; Eswararao *et al.* 2016; Ni *et al.* 2018). The Ca–O band exists between 670 and 400 cm^{-1} (Rohim *et al.* 2014). CaO is particularly sensitive to moisture and it was easily converted to its hydroxide form during calcination (550℃), which is responsible for dehydration (Luna Vera *et al.* 2018). As a result, the FTIR and XRD spectra of eggshell powder confirms the presence of calcite in the polymer structure and demonstrates that this product is hygroscopic and certainly contains water (Mosaddegh *et al.* 2013; Rohim *et al.* 2014).

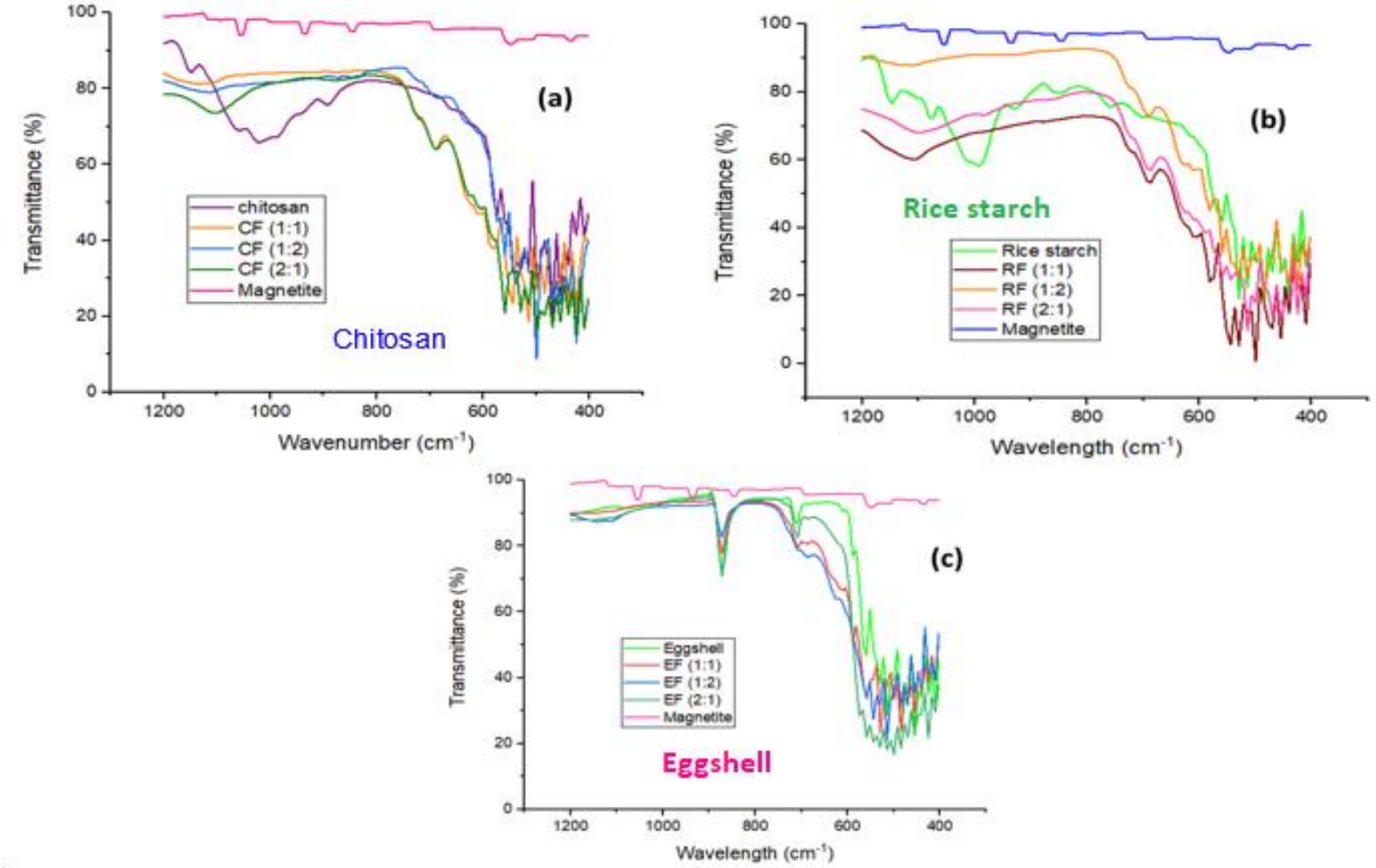

Figure 4-8 FTIR spectra (a-c) of magnetized coagulants (MCs) with their composition defined in table 3-3

4.2.4. Surface area examination (BET)

BET gas sorptometry analysis was used to investigate the porosity nature of magnetite, natural coagulants, and MCs (Table 4-2). The findings revealed that incorporating Fe_3O_4 into polymers (eggshell, chitosan, and rice starch) increased the surface area of the magnetic coagulants, improving their adsorption capacity due to the fact that magnetite has distinct magnetic characteristics and stability (Teh *et al.* 2014a, 2014b; Maksoud *et al.* 2020; Amo-Duodu *et al.* 2021; Sibiya *et al.* 2021). RF (1:1) had the highest surface area of pores and porosity among the coagulants examined. The BET results strongly endorse the concept that the RF (1:1) has a high surface area (S_{BET}), which is consistent with the SEM observations (figure 4-3e). The greater the S_{BET} of coagulant particles, the higher the reaction conversion (Viriya-empikul *et al.* 2010; Mosaddegh *et al.* 2013). The descending order of surface areas was RF (1:1) > RF (2:1) > RF (1:2) > Fe_3O_4 > EF (1:1) > CF (1:1) > EF (2:1) > CF (2:1) > CF (1:2) > EF (1:2) > RS > CS> ES. ES had a slightly larger pore size (21.1610 nm) than the other samples because the grafting reaction caused some pores to collapse, increasing the cumulative pore volume as indicated by Figure 4-1b (Tsai *et al.* 2006b).

Table 4-2 Comparison of the BET surface area of the coagulants

Sample/(s)	**S_{BET} surface area (m^2/g)**	**Pore volume (cm^3/g)**	**Pore size (nm)**
Fe_3O_4	27.597	0.0080	1.4840
RS	1.267	0.0020	6.7600
RF (1:1)	31.438	0.0015	1.6102
RF (2:1)	30.021	0.0012	1.6098
RF (1:2)	29.388	0.0010	1.5418
CS	1.2010	0.0007	5.4180
CF (1:1)	18.773	0.0008	4.5560
CF (2:1)	16.291	0.0008	4.5110
CF (1:2)	13.918	0.0004	3.7361
ES	0.0921	0.0061	21.1610
EF (1:1)	21.112	0.0059	1.3817
EF (2:1)	17.164	0.0048	1.3560
EF (1:2)	11.854	0.0032	1.2424

4.3. Coagulation-sedimentation

4.3.1. Effect of different magnetized coagulants on contaminants removal

The organic content in the sample can be described by both COD and turbidity (Bachmann *et al.* 2015; Abdelsalam *et al.* 2019; Gumbi 2020). TSS and COD measurements were taken utilizing a HACH spectrophotometer (DR3900) at a wavelength of 630 nm (Figure A-3a). Figure 4-9 (a and b) depicts the effect of MCs on turbidity and TSS reduction, respectively. Most coagulants had removal efficiency values for turbidity and TSS in the descending order of RF (1:1): 84.80% and 86.13% > RF (1:2): 82.07% and 82.75% > EF (1:1): 81.89% and 81.74% > RF (2:1): 80.17% and 80.60% had over 80% removal with content in table 3-3. RF (1:1) had the highest turbidity and TSS removal reduction, with 84.80 and 86.13%, respectively. The larger molecular weight chain of amylopectin in the rice starch produced is similar to other starches, leading in higher efficiency destabilization, resulting in the maximum turbidity and TSS removal efficiency, as found in this study, which is consistent with prior studies (Lin *et al.* 2011; Teh 2014; Teh *et al.* 2014a; Sibiya *et al.* 2022b). RS has been discovered as one of the most efficient coagulants for turbidity reduction (Choya *et al.* 2018) and it is ideal for adsorption of negatively charged particles due to the concentration of cationic components (Asharuddin *et al.* 2018; Huzir *et al.* 2019). Figure 4-9c represents that EF (2:1) performed admirably, with a COD reduction rate of 51.73% at an initial COD concentration of 315 ± 0.781 mg/L. Thereafter, comes RF (1:1): 50.02% > RF (2:1): 49.34% > RF (1:2): 47.98% > CF (1:1): 45.77%.

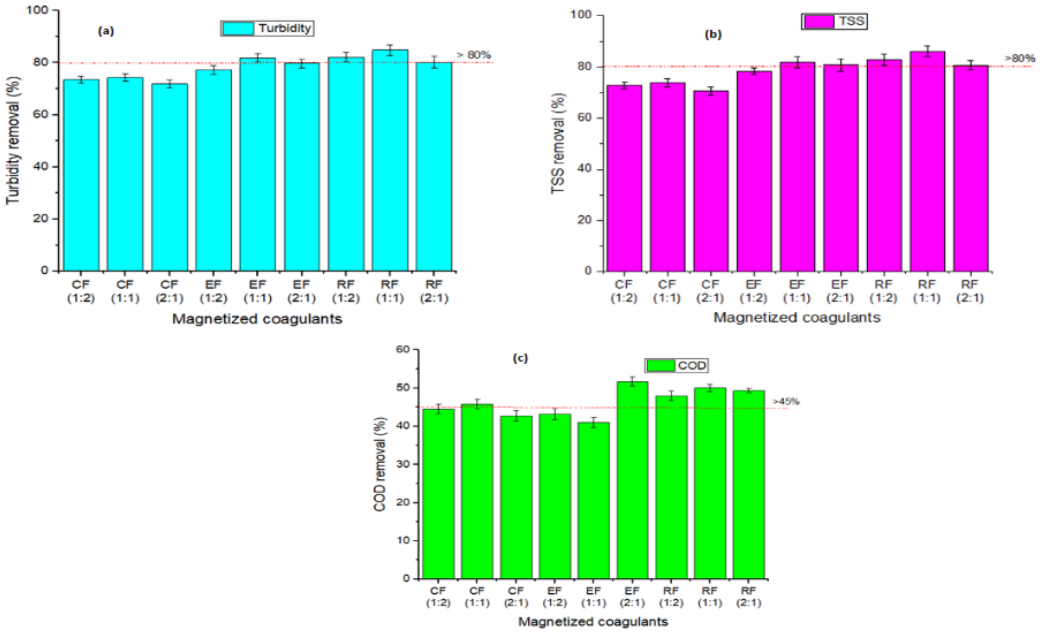

Figure 4-9 Effect of magnetized coagulants on (a) turbidity; (b) TSS and (c) COD removal (%)

4.3.2. Effect of settling time on contaminants removal

Settling time is an essential metric to evaluate for the pre-treatment process since it affects the entire cost and efficiency of the process (Teh *et al.* 2016; Asharuddin *et al.* 2018). This study compared the magnetized coagulants to find cheap coagulant for treating of industrial effluent. The jar test trials for each coagulant (with 3 g dose) were conducted by varying the settling time (10–60 min) to determine the optimum settling time. The supernatants were pipetted ,the contaminant (TSS, turbidity, and COD) levels were measured according to APHA (2012) and their efficiencies calculated by equation 3.3. The results for turbidity and TSS removal are presented in figure 4-10, and COD removal in figure 4-11 using different magnetized coagulants at different settling time. It was discovered that there is an intermolecular link between turbidity and TSS removal (Figure 4-10), since both exhibit a similar pattern (Mateus *et al.* 2018a; Sibiya *et al.* 2021). Findings (Figure 4-10) show that increasing the settling time enhances the efficacy of removal for CF (1:2,1:1), EF (1:2 and 2:1) and RF (1:2,1:1 and 2:1) until 40 min is reached, at which point the effectiveness begins to decrease until 60 min. The residual contaminants diminish between 10 and 40 minutes due to the formation of large-size flocs with a higher settling velocity (Asharuddin *et al.* 2018; Momeni *et al.* 2018) while from 50 to 60 minutes the trend is almost reversed which might be due to the occurrence of colloidal entrapment and high attractive force dominants (Zhao *et al.* 2011; Zahrim *et al.* 2017; Sibiya *et al.* 2021; Zhang *et al.* 2021a). In figure 4-10, EF (1:1) shows an increase from 10 until 30 min, followed by a sharp drop at 40 min and thereafter it increases until the 60^{th} min.

Also, CF (2:1) had highest contaminant removal at 30 min. Even though most coagulants performed better after 40 minutes, owing to the economic implications, 30 minutes was chosen as the most appropriate. Consequently, the lesser the period of settling, the greater the technique in terms of sludge reduction or handling (Sibiya *et al.* 2021). At 30 min, the removal efficiency values for turbidity and TSS were respectively recorded in descending order for each coagulant as RF (1:1): 86.25% and 87.11% > RF (1:2): 83.46% and 84.22% > RF (2:1): 82.96% and 81.13%> EF (1:1): 82.04% and 83.40% > EF (2:1): 79.10% and 81.12% > EF (1:2): 77.46% and 78.33% > CF (1:1): 74.91% and 74.02% > CF (2:1): 74.57% and 73.97% > CF (1:2): 74.50% and 72.96%. RF (1:1) which provides the turbidity removal above 80% at all the settling times.

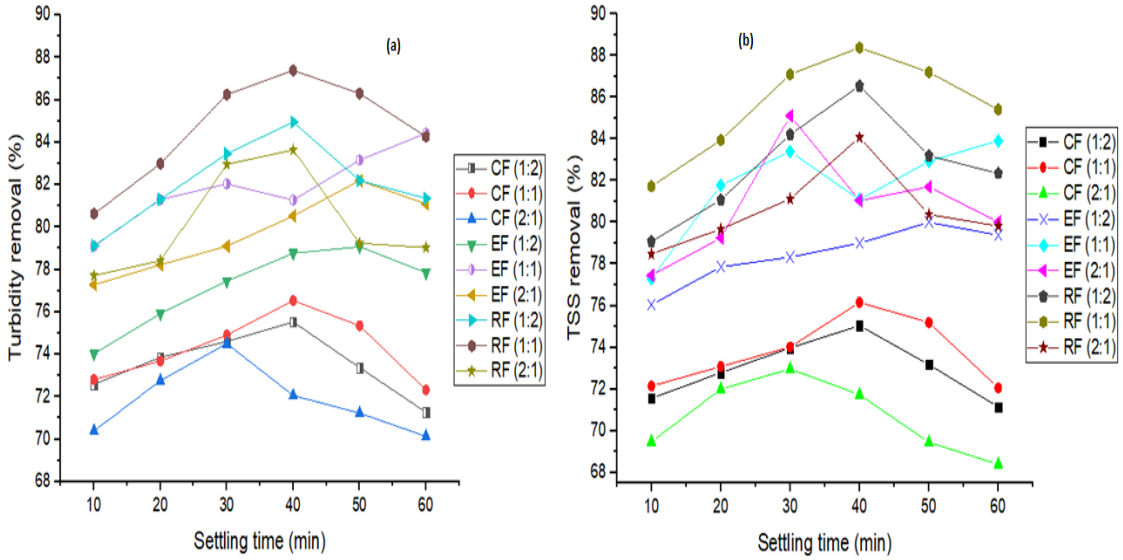

Figure 4-10 Effect of settling time on the removal of turbidity (a) and TSS (b) by magnetized coagulants with their content in table 3-3

Figure 4-11 shows the COD removal for all coagulants over 60 min settling time. Findings show the efficiency of CF (2:1) decreases from 10 to 30 min while the rest of the coagulants have an increasing trend from 10 to 20 min. After 20 minutes, coagulants exhibit an uneven pattern, which might be due to sampling during the settling phase, which caused the contained pollutant to break apart and increase the quantity of COD. This also validates the disadvantages of the coagulation process's settling time. Other research has suggested that low efficacy may be due to pH, because at low pH, the surface of the coagulant is massively protonated by cations (H^+), which tends to result in an electrostatic strength between the contaminated molecules and the surface, causing strong adsorption (Freitas *et al.* 2017). At 20 min, the top performing coagulant is EF (2:1) with an efficiency of 53.34%. This confirms that there was an increase in hydrolyte, which created additional cationic charged species for the pollutants to coalesce (Teh *et al.* 2014a; Jagaba *et al.* 2016; Jagaba *et al.* 2020; Sibiya *et al.* 2021). Natural coagulants like ES, CS, RS, bentonite, and others include carbonyl, hydroxyl, and aliphatic amine functional groups (Vishakha *et al.* 2012; Nnaji *et al.* 2014; Nharingo *et al.* 2015; Siddique *et al.* 2016; Usefi *et al.* 2019; Gautam *et al.* 2020; Nath *et al.* 2020; El-Gaayda *et al.* 2021; Noor *et al.* 2021). At 20 min, each coagulant shown distinct responded differently in terms of COD removal, as follows: EF (2:1) > RF (1:1) > RF (1:2) > RF (2:1) > CF (1:1) > CF (1:2) > CF (2:1) > EF (1:2) > EF (1:1).

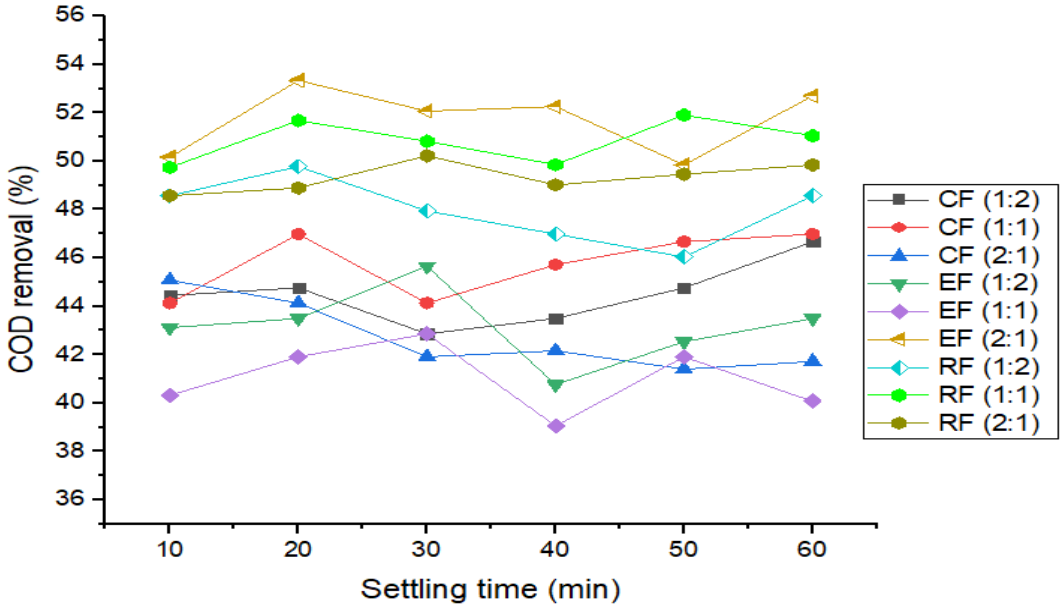

Figure 4-11 Effect of settling time on the removal of COD by magnetized coagulants with their content in table 3-3.

4.3.3. Effect of magnetic field vs settling time on decontamination using RF (1:1)

The influence of MF on removing contaminants (Figure 4-12) was examined by comparing alum and RF (1:1) treaments with and without an external magnetic field. The results show that exposing RF (1:1) to a magnetic field greatly improved contaminant removal (TSS, turbidity, and COD). When alum was used, colloidal aggregation and destabilizing (as seen in the treatment of organic material and hydrophilic organic matter) were detected to have improved with settling times ranging from 10 to 30 min. Colloidal stability and destabilization can be caused by an increase in ionic strength with a little decrease in zeta potential and a drop in the thickness of the diffuse half of the electrical double layer (Duan *et al.* 2003a; Maiga *et al.* 2020; Matusiak *et al.* 2021; Rakshit *et al.* 2021; Sibiya *et al.* 2021). Thereafter, both contaminants treatability became unstable. This was caused by the flocs' poor settling capacity as a result of colloidal breakdown in suspension (Daud *et al.* 2015; Tetteh *et al.* 2020) since more contaminants had been adsorbed. This may have rendered the surfaces more hydrophilic (less hydrophobic) due to the interaction between groups contained by oxygen (hydroxyl and carboxyl) and negatively charged colloidal particles (Zhao *et al.* 2011; Siddique *et al.* 2016; Arulmathi *et al.* 2019; Sibiya *et al.* 2021; Xue *et al.* 2021). Figure 4-12c, shows that has alum (>30 min), the efficiiency dropped at 40 min and then increased until the 60th min. In comparison, RF(1:1) and RF(1:1)_MF removed considerably greater COD, TSS, and turbidity (50 to 88%) than alum (40 to 75%). According to Baek et al.

(2015) and Xiang et al. (2019), any use of iron-oxide NPs in treating wastewater seems to be more beneficial because magnetite contains several adsorption sites that may take a variety of pollutants.

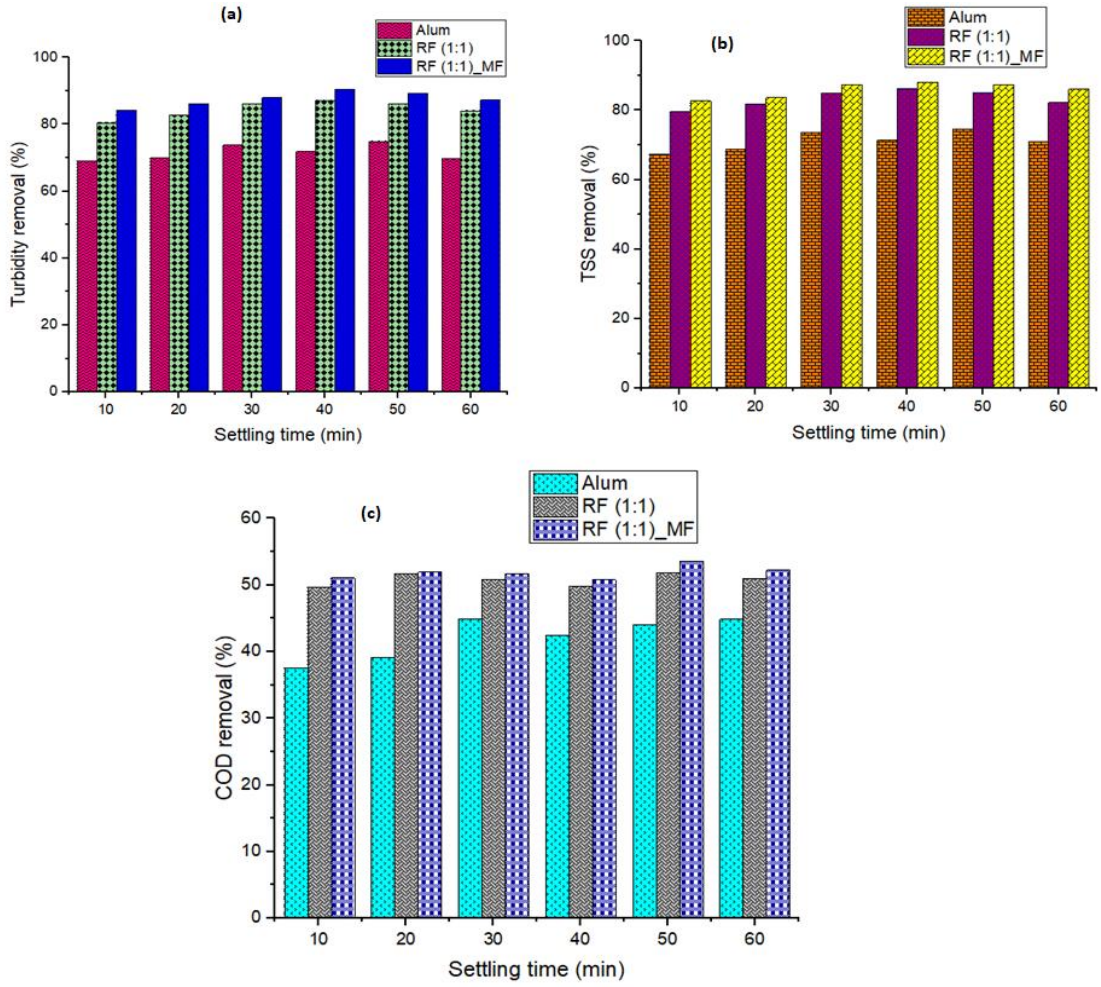

Figure 4-12 Comaprative results on (a) turbidity, (b) TSS and (c) COD removal (%) with the effect off settling time

4.3.4. Comparative study of magnetic effect using RF and Alum

Figure 4-13 depicts the turbidity efficiency of alum and the best performing coagulant (RF (1:1)) with and without exposure of a magnetic field (20 mT), as shown if figure A-9. According to the findings, the RF reduced turbidity by more than 80% in both samples, whereas alum reduced turbidity by more than 70%. When a magnetic field was supplied during the settling phase (60 min), the turbidity efficiency of the coagulation process employing RF (1:1) improved from 84.78% to 87.57% (figure 4-13). According to Alabdraba *et al.* (2013), MF has a significant impact on sedimentation but a minor impact on slow and quick mixing stage of coagulation.

Therefore, it is preferable to remove the magnetic field during the two phases namely slow and quick mixing to achieve high efficiency. Also, the positively charged magnetite aided the adsorption of negatively charged pollutants in the wastewater sample (Saifuddin *et al.* 2011), while the cationic exchange mechanism (electrostatic, van der Waals, and chemical bonding) and the generation of hydroxide on the surface of magnetized rice starch coagulant were used to remove turbidity by magnetic measures (Hatamie *et al.* 2016; Tetteh *et al.* 2020; Sibiya *et al.* 2022a). Lastly, rice starch contains amylase and amylopectin which destabilize the colloidal particles by bridging and aggregation (Teh 2014; Bratby 2016; Sibiya *et al.* 2022a). Table 4-3 shows the other pollutants (COD and TSS) that had been reported for all coagulants. The maximal COD and TSS for RF (1:1) exposed in a magnetic field were 56.22 and 86.53%, respectively. The current study shows that the magnetic field had no effect on contaminants removal using alum which proves that alum does not contain any ferromagnetic materials. Hence, the results obtained with and without MF were the same. The presence of magnetite in rice starch and MF resulted in improved efficiencies which can enhance greater controlling ability, simpler manipulation, and comparably reduced energy usage (Ambashta *et al.* 2010; Zhang *et al.* 2016).

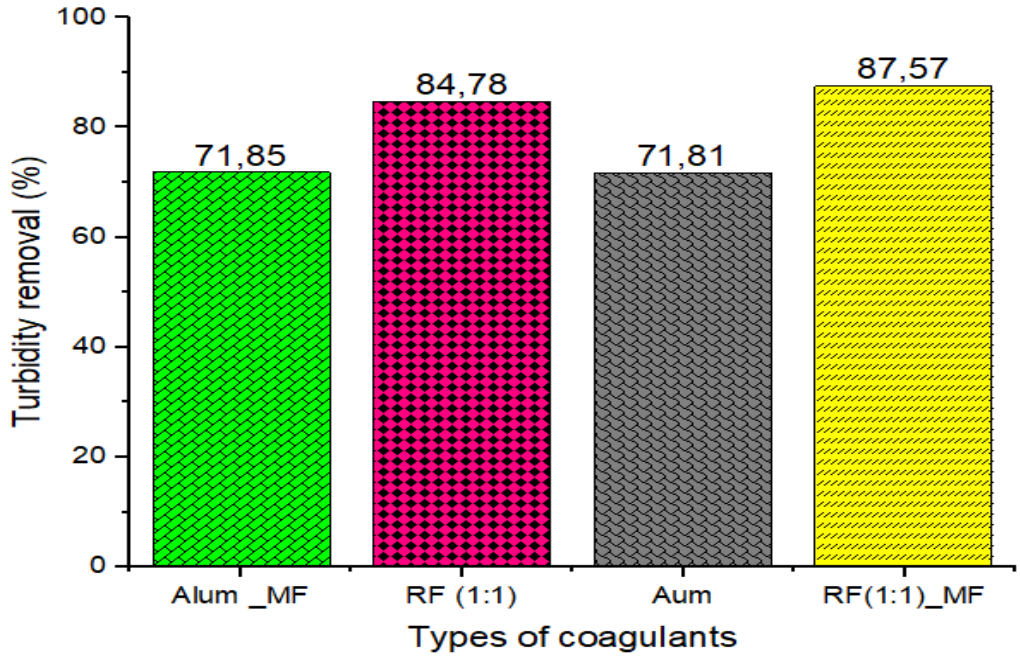

Figure 4-13 The effect of magnetic field using alum and RF (1:1) on turbidity removal (%)

*MF-Exposed in magnetic field

Table 4-3 Comparison results of alum and RF (1:1)

Contaminant removal (%)	**Alum_ MF**	**RF (1:1)**	**Alum**	**RF (1:1) _MF**
TSS	70.45	83.55	70.52	86.73
COD	42.92	50.94	42.96	56.22

4.3.5. Coagulation kinetics

The amount of aggregation was measured to better understand the coagulation–flocculation dynamics. This was accomplished by examining the influence of sedimentation (time 10–60 min) with and without a magnetic field at a constant dose of 3g for the best performing coagulant (RF (1:1). Figure 4-12 shows that a short time (10 – 30 min) of the lag phase is preferable owing to energy and time savings. The raw acquired data (resultants is RF (1:1) turbidity efficiency in figure 4-12a) was fitted to kinetics in equations 3.4 and 3.11 to assess the performance of the pollutants' treatment. The rate of contaminant reduction in a reaction-based system is affected by a variety of internal and external parameters, including temperature, dose, and the properties of the wastewater itself (Adelodun *et al.* 2020; Sibiya *et al.* 2021). Pollutant particles connect to both chemical and physical binding sites as the process progresses. The reaction continues until the free sites are completely saturated, followed by quick settling. The incorporation of Fe_3O_4 into natural coagulants increased agglomeration efficacy (Hashem 2013; Svobodova *et al.* 2020; Tetteh *et al.* 2020; Sibiya *et al.* 2021; Sibiya *et al.* 2022b) compared to coagulants such as rice starch, eggshell, chitosan, alum, bentonite, moringa oleifera, etc. (Pritchard *et al.* 2010; Choy *et al.* 2014; Siddique *et al.* 2016; Freitas *et al.* 2017; Gaikwad *et al.* 2019; Adelodun *et al.* 2020; Muniza *et al.* 2020). As a result, the acquired data was well fitted and significant enough for the model to be used for turbidity reduction (Figure 4-14).

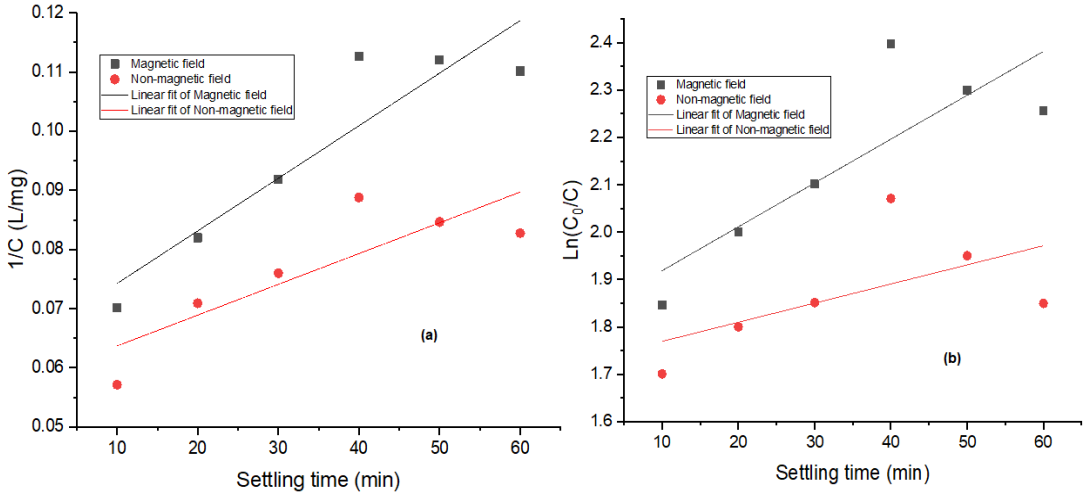

Figure 4-14 Kinetics of (a) second order and (b) first order models for the removal of turbidity

The coefficient of determination ($0.85 < R^2 < 0.95$) for the magnetic field (MF) was clearly preferred in both kinetic models (Table 4-4). Furthermore, the highest contaminant removal matched to realistic kinetic constants (Tan *et al.* 2017; Sibiya *et al.* 2021). The plateau of R-values demonstrated the degree of particle aggregation in relation to the time required for floc breakdown. The existence of flocculation, as well as the findings obtained, demonstrate that the integration of magnetite enhanced the molecular weight (Gaikwad *et al.* 2019; Adelodun *et al.* 2020) and BET surface area of the coagulant components (Table 4-2).

Table 4-4 Comparative kinetic study

First-order kinetics		
Kinetics parameters	**MF exposure**	**Non-MF exposure**
R^2	0.9248	0.8457
K_1	0.0008896	0.0005207
SSE	0.0002344	0.0001889
y-intercept	0.06539	0.05849
Second-order kinetics		
R^2	0.8874	0.8424
K_1	0.009270	0.004491
SSE	0.06146	0.05648
y-intercept	1.82599	1.72186

4.4. Coagulation –Flotation (DAF)

Edzwald (2010) and (Tetteh 2018a) found above 50% reduction of the contaminants with the saturation pressure range of 300 to 500 kPa. Hence, the mean saturated pressure (400 ± 50 kPa) was used in this study. This was done with a jar tester (Figure 3-3) under coagulation conditions of costant dose (3 g for RF (1:1), quick stirring (150 rpm) for 2 minutes, slow stirring (30 rpm) for 15 min, a 10% air-water ratio, an air saturator pressure of 400 ± 50 kPa and flotation time (10-60 min). The wastewater had an initial concentration of 39.20 ± 0.419 NTU turbidity, 43.20 ± 0.216 mg/L TSS, and 351.80 ± 0.718 mg/L COD. Extending the flotation period from 10 to 60 min enhanced the removal of contaminants, as a result of which there has been a massive rise in reduction of TSS and turbidity from 86 to 95%, and COD from 50 to 65% (Figure 4-15). This was owing to a strong charge layer around the flocs, which resulted in good contaminant aggregation and floatability, as well as clarity of the treated water (Santana *et al.* 2012; Karhu *et al.* 2014; eSilva *et al.* 2018; Tian *et al.* 2018; Soares *et al.* 2021). By prolonging the floating phase, the surface area of the contact zone between the air bubble and contaminants was increased, strengthening the flocs' bonds and preventing them from breaking (Al Ansari *et al.* 2021; Kyzas *et al.* 2021; Levitsky *et al.* 2022).

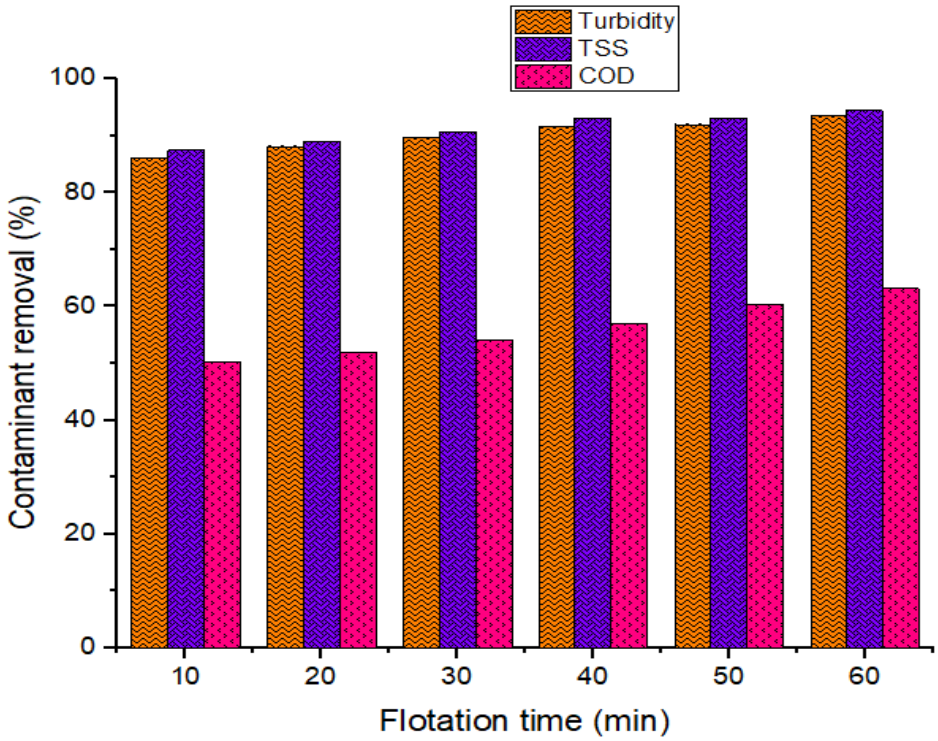

Figure 4-15 Effects of flotation time on pollutant removal (%); employing RF (1:1) at 3 g dosage

4.5. Optimization of coagulation and DAF using RSM

The main purpose of optimazation was to establish the optimal operating conditions for industrial wastewater (Table 3-1) treatment. The OFAT technique was used to generate ranges for the operational parameters (coagulant dosage, mixing rate and settling or flotation time). Tables 4-5 and 4-6 present the results of 14 runs using the BBD design matrix for coagulation and DAF, respectively. The findings consist of the investigated factors in coded form, the experimentalresults, and the model-predicted response factor results. The experimental values are the calculated COD and turbidity (using equation 3.3) and measured TSS (using DR 3900 HACH spectrophotometer) response data from a particular run, whereas the predicted values are computed from the model (Tables 4-5 and 4-6). These results were subjected to four step processes of the RSM analysis: (i) the statistical significance of the model developed was tested using ANOVA, (ii) the diagnostic and response plots were used to establish the optimum region and interactive conditions, (iii) a numerical optimization technique was used to optimize the desired goals fixed for maximum TSS (mg/L), turbidity and COD removal (%), and (iv) validation was conducted (Sibiya *et al.* 2022a). The coefficient of determination (R^2), adjusted R^2, standard deviation (SD) and coefficient of variance (CV), and adequate precision (AP) demonstrated the model's fit. In addition, Fisher's F-values and associated p-values with 95% confidence level were utilized to determine the relevance of the model equations for each output parameter (Tables 4-7 to 4-9 and Tables 4-11 to 4-13).

4.5.1. Coagulation-sedimentation process

The acquired findings were then examined using ANOVA to determine the "goodness of fit" (Ghafari *et al.* 2009; Singh *et al.* 2020a). ANOVA is used to assess the interactions between variables and their corresponding responses (Galan *et al.* 2021; Pandit *et al.* 2021; Usman *et al.* 2021; Rifi *et al.* 2022). Equations 4.1 to 4.3 represent the software-generated models for the COD, turbidity and TSS, respectively in coded form for the coagulation process. The predicted results had been defined as the sum of a constant and three first-order effects (terms in A , B and C), and three interaction effects (AB, BC, and AC) as a result of mixing rate (A), settling time (B), and coagulant dosage (C). The linear model was found to be the most acceptable in terms of turbidity and COD removal while turbidity reduction was acceptable for a 2FI (two factor interaction) model.

$$\text{COD removal} = 42.281 + 2.7094\,A + 0.6839\,B + 8.1764\,C \qquad \text{Equation 4.1}$$

$$\text{Turbidity removal} = 64.9662 - 0.2224\ A + 0.2711\ B + 0.0543\ C - 0.4351\ AB + 0.3856\ AC + 0.4386\ BC \quad \text{Equation 4.2}$$

$$\text{TSS removal} = 44.8056 - 1.3081\ A + 1.6259\ B - 0.4051\ C \quad \text{Equation 4.3}$$

Table 4-5 BBD design matrix for coagulation technique, displaying the experimental and predicted results

Std.	Run	FACTORS			Experimental Responses			RSM Predicted Responses		
					Resp. 1	Resp. 2	Resp. 3	Resp. 1	Resp. 2	Resp. 3
		A: Mixing rate (rpm)	B: Settling time (min)	C: Coagulant dosage (g)	COD removal (%)	Turbidity removal (%)	TSS reduction (mg/L)	COD removal (%)	Turbidity removal (%)	TSS removal (mg/L)
14	1	100	22.5	3	41.95	64.96	43.42	42.22	64.97	44.81
4	2	150	30	3	45.34	64.51	43.96	45.61	64.58	45.12
12	3	100	30	4	50.81	65.66	46.84	51.08	65.73	46.03
7	4	50	22.5	4	47.41	64.99	45.25	47.69	64.86	45.71
9	5	100	15	2	33.08	65.14	43.32	33.36	65.08	43.58
10	6	100	30	2	34.45	64.81	47.50	34.73	64.74	46.84
1	7	50	15	3	38.55	64.55	43.42	38.82	64.48	44.49
8	8	150	22.5	4	52.83	65.45	43.37	53.10	65.18	43.09
13	9	100	22.5	3	45.77	64.45	44.18	42.22	64.97	44.81
3	10	50	30	3	39.92	65.96	48.13	40.19	65.89	47.74
6	11	150	22.5	2	36.48	64.44	43.45	36.75	64.30	43.90
11	12	100	15	4	49.44	64.24	43.35	49.71	64.31	42.77
2	13	150	15	3	43.97	64.84	43.32	44.24	64.91	41.87
5	14	50	22.5	2	31.06	65.52	47.78	31.33	65.52	46.52

***Resp. – Response**

Table 4-6 BBD design matrix for DAF technique, displaying the experimental and predicted results

Std	Run	FACTORS			Experimental Responses			RSM Predicted Responses		
					Resp. 1	**Resp. 2**	**Resp. 3**	**Resp. 1**	**Resp. 2**	**Resp. 3**
		A: Mixing rate (rpm)	B: Flotation time (min)	C: Coagulant dosage (g)	COD removal (%)	Turbidity removal (%)	TSS reduction (mg/L)	COD removal (%)	Turbidity removal (%)	TSS removal (mg/L)
14	1	100	22.5	3	50	78.31	4.45	48.20	79.15	3.98
4	2	150	30	3	45.15	83.51	5	45.76	83.51	4.93
12	3	100	30	4	50.38	77.12	5.09	50.41	77.12	5.30
7	4	50	22.5	4	53.12	80.03	4.79	52.85	80.03	4.72
9	5	100	15	2	45.39	82.27	2.45	46	82.27	2.66
10	6	100	30	2	48.19	84.06	2.56	48.80	84.06	2.66
1	7	50	15	3	50.62	84.46	3.85	50.65	84.46	2.76
8	8	150	22.5	4	44.85	85.13	5.83	45.17	85.13	3.78
13	9	100	22.5	3	47.89	80	3.77	48.20	79.15	5.76
3	10	50	30	3	53.42	82.23	3.20	53.45	82.23	3.98
6	11	150	22.5	2	45	84.23	3.30	43.56	84.23	3.13
11	12	100	15	4	47.58	83.14	4.99	47.61	83.14	3.23
2	13	150	15	3	42.35	85.52	4.14	42.96	85.52	5.19
5	14	50	22.5	2	50.93	86.99	2.26	51.24	86.99	4.07

***Resp. – Response**

4.5.1.1. Model fitting and statistical analysis

Using Design-Expert software, regression analysis and ANOVA were used to investigate the statistical fitness of the created model at the 95% confidence level (Singh *et al.* 2020a; Pandit *et al.* 2021; Rifi *et al.* 2022; Sibiya *et al.* 2022a). F-value describes the variation in responses, which can be verified by the regression equation whereas, p-value ascertains the statistical fitness of the developed model. For a model to be significant, the p-value cannot be greater than 0.05, whereas the p-value for the lack of fit (LOF) test must be more than 0.05 (Singh *et al.* 2020a; Khui *et al.* 2021; Sada 2021; Wu *et al.* 2022; Zubair *et al.* 2022). The R^2 values for COD, turbidity, and TSS reduction were 0.9778, 0.9446, and 0.8724, respectively, indicating a solid relationship between dependent and independent variables. This also revealed that the total variance explained by the developed model was 97.78%, 94.46%, and 87.24%, respectively, and that 2.22, 5.54, and 12.76 % of the overall variance was not addressed by the produced model. The adjusted R^2 for COD, turbidity, and TSS reduction was determined to be 0.97109, 0.9256, and 0.8691, respectively, which were extremely close to the R^2 values presented in Tables 4-7 to 4-9. As a result, the prediction of experimental data is very good, with a difference of less than 13%. The models were well verified since all of the LOF were not significant, indicating the model's incapacity to adequately capture the functional agreements between the experimental components and the response variables (Tetteh 2018a; Chen *et al.* 2022; Nocera *et al.* 2022).

Furthermore, the appropriate precision values were larger than 4, indicating that the model is adequate and may be securely utilized to explore the whole design space (Ghafari *et al.* 2009; Baytar *et al.* 2020; Chen *et al.* 2022). The coefficient of variance (CV), described as the ratio of the standard deviation of estimation to the mean value of the observable response, determines the repeatability and reliability of the model (Jalilibal *et al.* 2021; Wang *et al.* 2021b; Arachchige *et al.* 2022). In this situation, the CV for COD, turbidity, and TSS reduction were determined to be 2.7608, 0.3718, and 2.3034%, respectively, indicating that the models are replicable since their CV was less than 10% (Singh *et al.* 2020a; Jalilibal *et al.* 2021; Khui *et al.* 2021; Pandit *et al.* 2021; Arachchige *et al.* 2022; Chen *et al.* 2022; Rifi *et al.* 2022).

Table 4-7 ANOVA of linear regression model for COD removal

Source	**Sum of Squares**	**Df**	**Mean**	**F-value**	**p-value**	
Model	597.2990	3	199.0997	146.5542	<0.0001	significant
A-Mixing rate	58.7280	1	58.7280	43.2288	<0.0001	
B-Settling time	3.7417	1	3.7417	2.7542	0,1280	
C-Coagulant dosage	534.8292	1	534.8292	393.6797	<0.0001	
Residual	13.5854	10	1.35854			
Lack of Fit	6.2702	9	0.6967	0.0952	0,9898	not significant
Pure Error	7.3152	1	7.152			
Cor Total	610.8843	13				
R^2 (0,9778)	Adjusted R^2 **(0.97109)**	Predicted R^2 **(0.97272)**	Adeq Precision **(34.9454)**	Std. Dev. **(1.1656)**	Mean **(42.2182)**	C.V. % **(2.7608)**

Table 4-8 ANOVA of 2FI regression model for turbidity removal

Source	**Sum of squares**	**df**	**Mean**	**F-value**	**p-value**	
Model	3.1289	6	0.5215	8.9400	0.0054	significant
A-Mixing rate	0.3957	1	0.3957	6.7835	0.0352	
B-Settling time	0.5880	1	0.5880	10.0810	0.0156	
C-Coagulant dosage	0.0236	1	0.0236	0.4043	0.5451	
AB	0.7574	1	0.7574	12.9837	0.0087	
AC	0.5948	1	0.5948	10.1961	0.0152	
BC	0.7695	1	0.7695	13.1917	0.0084	

Residual	0.4083	7	0.0583			
Lack of Fit	0.2759	6	0.0460	0.3471	0.8594	not significant
Pure Error	0.1324	1	0.1324			
Cor Total	3.5372	13				

R^2 (0,9446)	Adjusted R^2 **(0.9256)**	Predicted R^2 **(0.9243)**	Adeq Precision **(9.3158)**	Std. Dev. **(0.2415)**	Mean **(64.9662)**	C.V. % **(0.3718)**

Table 4-9 ANOVA of linear regression model for TSS removal

Source	**Sum of squares**	**Df**	**Mean**	**F-value**	**p-value**	
Model	36.1494	3	12.0498	11.3129	0.0015	significant
A-Mixing rate	13.6885	1	13.6885	12.8515	0.0050	
B-Settling time	21.1481	1	21.1481	19.8549	0.0012	
C-Coagulant dosage	1.3128	1	1.3128	1.2325	0.2929	
Residual	10.6513	10	1.0651			
Lack of Fit	10.3628	9	1.1514	3.9905	0.3713	not significant
Pure Error	0.2885	1	0.2885			
Cor Total	46.8007	13				

R^2 (0,8724)	Adjusted R^2 **(0.8691)**	Predicted R^2 **(0.8661)**	Adeq Precision **(10.6369)**	Std. Dev. **(1.0321)**	Mean **(44.8056)**	C.V. % **(2.3034)**

Figure 4-16 depicts the relationship between predicted and experimental COD, turbidity, and TSS removal values. These diagnostic plots aided in determining the model's suitability. They showed a good agreement between the experimental data and the predicted results of the models, implying that the models are well-matched to form a relationship between independent and dependent variables during the coagulation process (Baytar *et al.* 2020; Singh *et al.* 2020a; Galan *et al.* 2021; Pandit *et al.* 2021; Wu *et al.* 2022). Furthermore, all replies with AP values greater than four (Tables 4-7 to 4-9) show that all anticipated models may be employed to explore the design space (Ghafari *et al.* 2009; Baytar *et al.* 2020; Jalilibal *et al.* 2021; Wu *et al.* 2022).

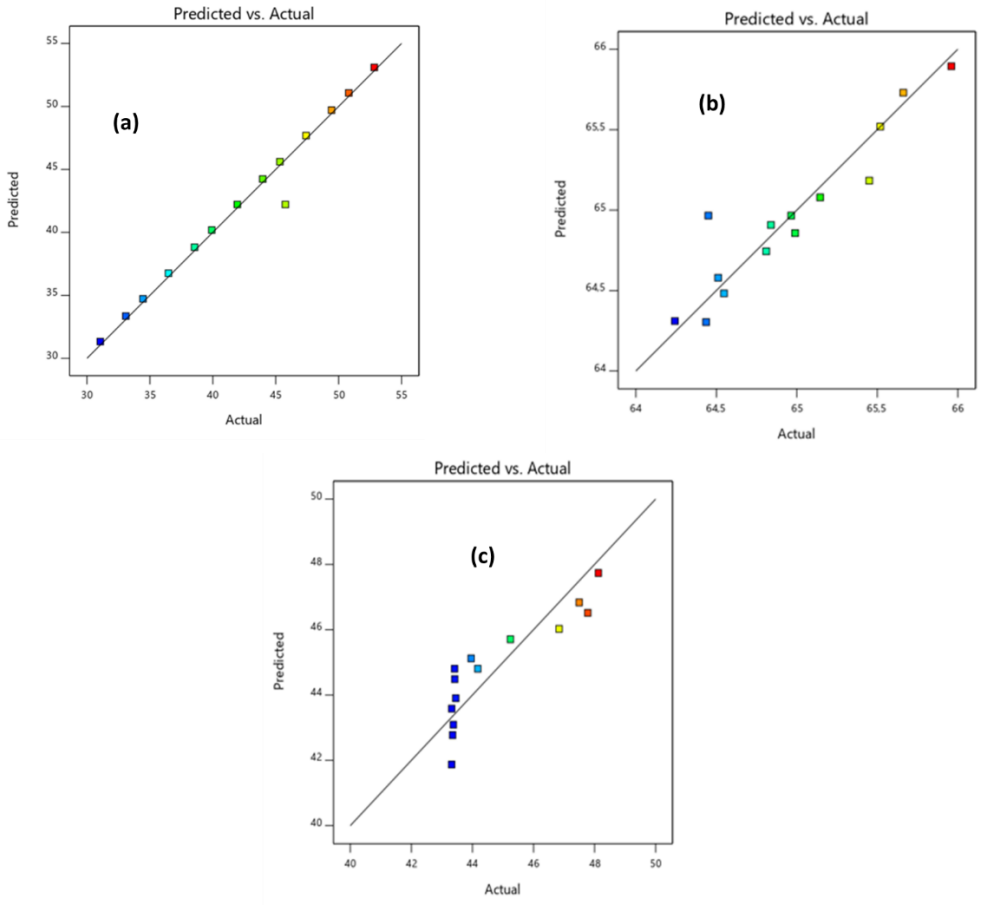

Figure 4-16 Design expert plot, predicted vs. actual plots (a) COD (b) turbidity and (c) TSS removal

4.5.1.2. Three dimensional (3D) and contour plots

The graphical depiction of the effects of settling time and mixing rate on COD, turbidity and TSS removal is shown in 3D and contour plots in Figures 4-17 to 4-19, with regards to each response regression model. The fixed variables were chosen based on the variables' sensitivity to the

responses as shown in perturbation plots (Adlan *et al.* 2011) of figures C-15 to C-20. All the 3D graphs exhibit distinct peaks, showing that the optimal circumstances for maximal response values in the design space are attributable to mixing rate and coagulant which were established to be within the design space's range. Figure 4-17 shows that the influence of settling time on COD efficiency is constant. COD reduction did not change from 15 to 30 minutes. This leads to a COD reduction effectiveness of 40%. Increasing the mixing rate resulted in a rise in COD removal efficiency, suggesting that a high mixing rate with a short settling time can achieve a high COD efficiency (>40%).

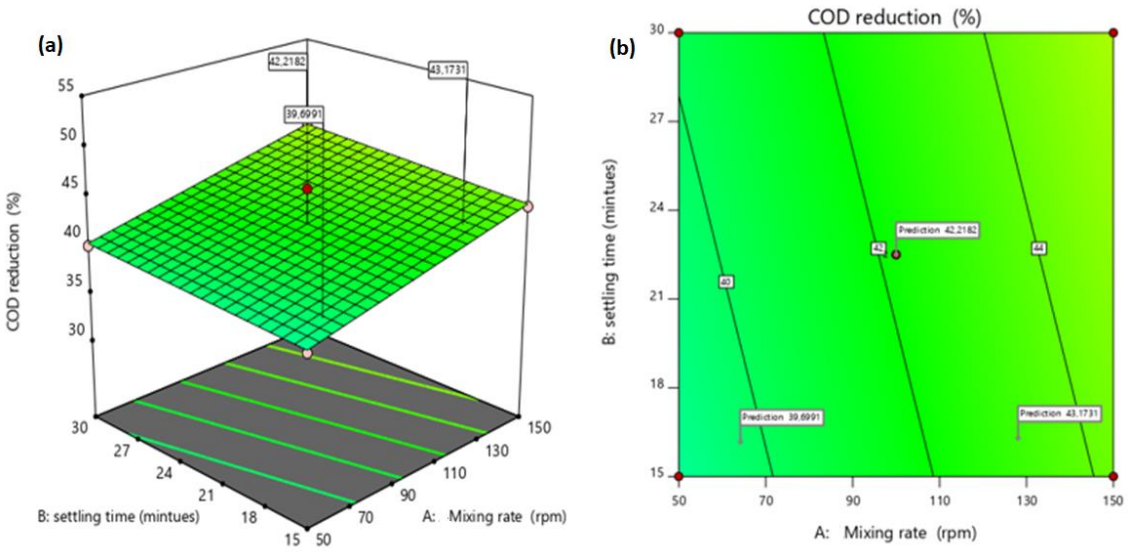

Figure 4-17 Response surface plots showing cross factor interactions for COD removal (%); (a) 3D plot (b) contour plot

In Figure 4-18, the mixing rate and settling time interaction indicated that turbidity removal decreased for settling times ranging from 30 to 15 min and increased at mixing rates ranging from 50 to 150 rpm. The settling time and mixing rate were adjusted according to the relevance of the perturbation plot (Figure C-16). Similar trends are also attained in figure 4-19, the efficiency of TSS shows an increasing trend between 15 and 30 min and drecreasing trend when the mixing rate increases to 150 rpm.

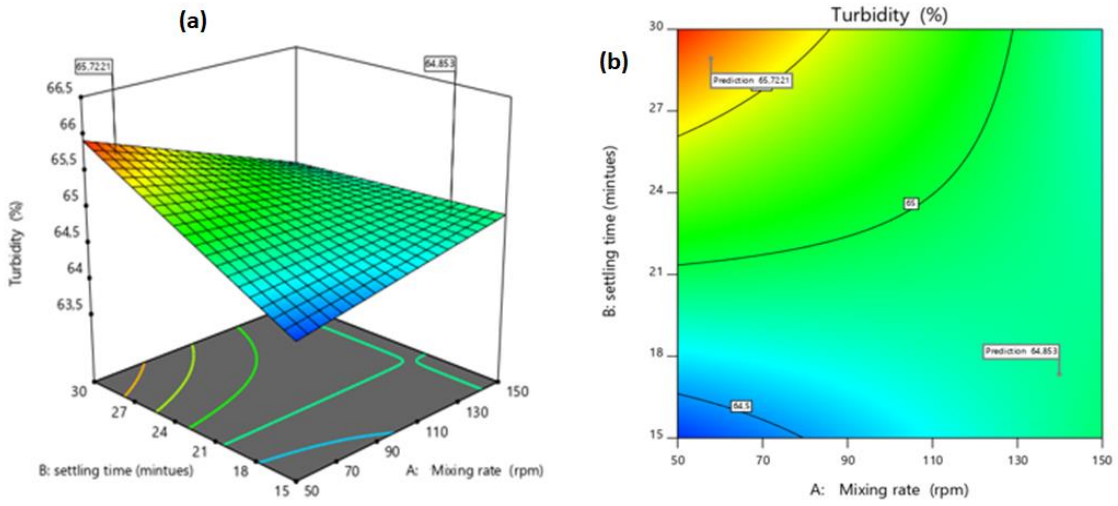

Figure 4-18 Response surface plots showing cross factor interactions for turbidity removal (%); (a) 3D plot (b) contour plot

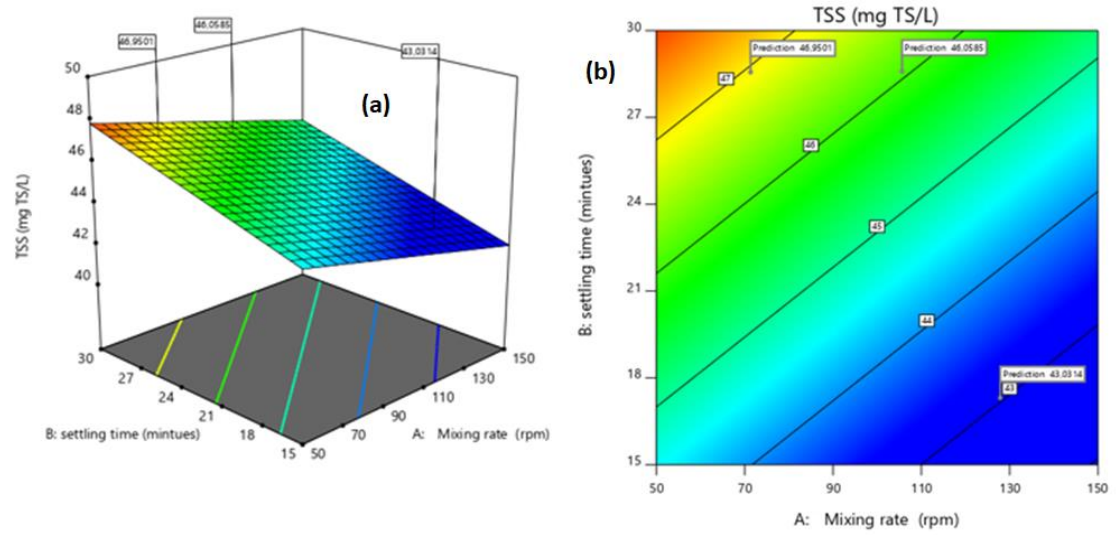

Figure 4-19 Response surface plots showing cross factor interactions for TSS removal (mg/L); (a) 3D plot (b) contour plot

4.5.1.3. Optimazation of the coagulation technique

To optimize the three coagulation operational variables, the numerical optimization tool in RSM was used. Table 4-10 demonstrates that all process responses were maximized whereas the input variables (mixing rate, settling time and coagulant dosage) remained within the range. Figure 4-

20 shows the ramp graphs that indicate the optimal operating parameters and the desirability gained. It was discovered that with a coagulant dose of 4 g, a settling period of 30 minutes, and a mixing rate of 50 rpm, at a desirability performance of 87.20%, 48.631% COD removal, 66.0021% turbidity removal and 47.3345 mg/L TSS removal was achieved. The models' validity and forecasting effectiveness under the optimal circumstances (Figure 4-20) were evaluated using triplicated experimental runs, as detailed in section 4.6.

Table 4-10 Conditions for optimization of coagulation process variables

Variables	**Low limit**	**High limit**	**Goal**
Mixing rate (rpm)	50	150	is in range
Settling time (min)	15	30	is in range
Coagulant dosage (g)	2	4	is in range
COD removal (%)	31.0592	52.8309	Maximize
Turbidity removal (%)	64.2423	65.9603	Maximize
TSS removal (mg/L)	43.3198	48.1262	Maximize

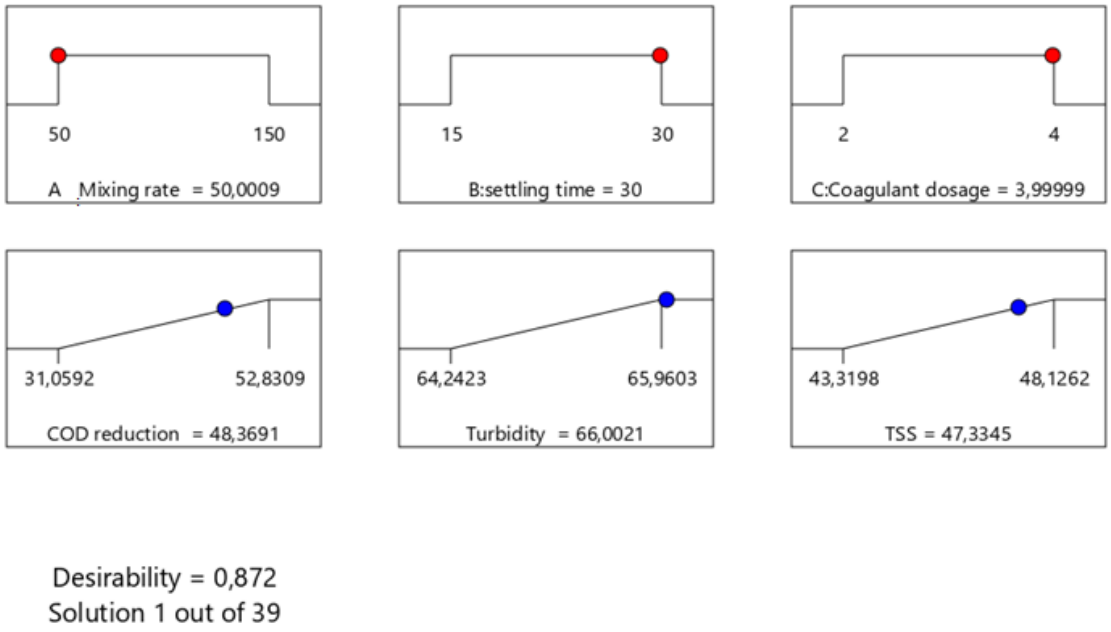

Figure 4-20 Ramp plot displaying the optimized conditions of coagulation process variables at a desirability of 87.20%

4.5.2. Coagulation-Flotation (DAF) process

These equations (4.4 to 4.6) were also computed as the sum of a constant, two first-order effects (terms in A, B, and C), three interaction effects (AB, AC, and BC), and three second-order effects (A^2, B^2, and C^2). Equation 4.5 depicts the reduced quadratic model, and equations 4.4 and 4.6 depict the linear and 2FI models, respectively. Positive terms in the equations imply a positive influence, whilst negative signs suggest an antagonistic effect of each factor (Bala *et al.* 2020; Singh *et al.* 2020a; Kassem *et al.* 2022).

$$\text{COD removal} = 48.2046 - 3.8421\,\text{A} + 1.3990\,\text{B} + 0.8028\,\text{C} \qquad \text{Equation 4.4}$$

$$\text{Turbidity removal} = 79.1528 + 0.5861\,\text{A} - 1.0608\,\text{B} - 1.5169\,\text{C} + 0.0543\,\text{AB} + 1.9640\,\text{AC} - 1.9523\,\text{BC} + 3.6120\,A^2 + 1.1642\,B^2 + 1.3305\,C^2 \qquad \text{Equation 4.5}$$

$$\text{TSS removal} = 3.9773 + 0.5205\,\text{A} + 0.0523\,\text{B} + 1.2669\,\text{C} + 0.3757\,\text{AB} \qquad \text{Equation 4.6}$$

4.5.2.1. Model fitting and statistical analysis

The ANOVA results for the created models are shown in the tables below (Tables 4-11 to 4-13). The significant p-values for LOF was greater than 0.05 and for COD, turbidity, and TSS were determined to be 0.9256, 1 and 0,9747, respectively, which were insignificant, as shown in these tables. P-values are between 0.05 and 0.1 suggests that the models are marginally significant (Tetteh 2018a; Galan *et al.* 2021; Sada 2021; Rifi *et al.* 2022). The R^2 values obtained for COD (linear regression), turbidity (quadratic regression), and TSS (2FI regression) were 0.9509, 0.9864, and 0.9704, which are very close to 1 (Ghafari *et al.* 2009; Baytar *et al.* 2020; Sada 2021; Rifi *et al.* 2022). These models are suitable since their R^2 were within limit with adjusted R^2 values as (0.9362, 0.9457, and 0.9485), predicted R^2 (0.9164, 0.9457 and 0.9485), AP (23.1550, 19.5001 and 26.0273) and CV (1.7569, 0.7249 and 5.7783%).

Table 4-11 ANOVA of linear regression model for COD removal

Source	**Sum of squares**	**Df**	**Mean**	**F-value**	**p-value**	
Model	138.9083	3	46.3028	64.5534	7.566E-07	significant
A-Mixing rate	118.0945	1	118.0945	164.6424	1.552E-07	
B-Flotation time	15.6582	1	15.6582	21.8300	0.00088	
C-Coagulant dosage	5.1556	1	5.1556	7.1877	0.0022305	
Residual	7.1728	10	0.7173			
Lack of Fit	4.9385	9	0.5487	0.2456	0.9256	not significant
Pure Error	2.2343	1	2.2343			
Cor Total	146.0810	13				
R^2 (0.9509)	Adjusted R^2 **(0.9362)**	Predicted R^2 **(0.9164)**	Adeq Precision **(23.1550)**	Std. Dev. **(0.8469)**	Mean **(48.2046**	C.V. % **(1.7569)**

Table 4-12 ANOVA of quadratic regression model for turbidity removal

Source	**Sum of squares**	**df**	**Mean**	**F-value**	**p-value**	
Model	104.2251	9	11.5806	32.2702	0.0022	significant
A-Mixing rate	27481	1	2.7481	7.6579	0.0505	
B-Flotation time	9.0032	1	9.0032	25.0881	0.0074	
C-Coagulant dosage	18.4089	1	18.4089	51.2980	0.0020	
AB	0.0118	1	0.0118	0.0329	0.8648	
AC	15.4289	1	15.4289	42.9939	0.0028	
BC	15.2453	1	15.2453	42.4822	0.0029	
A^2	41.7489	1	41.7489	116.3368	0.0004	
B^2	4.3373	1	4.3373	12.0862	0.0254	
C^2	5.6644	1	5.6644	15.7842	0.0165	
Residual	1.4355	4	0,3589			
Lack of Fit	0	3	0	0	1	not significant
Pure Error	1.4355	1	1.4355			
Cor Total	105.6605	13				

R^2 (0,9864)	Adjusted R^2 **(0.9558)**	Predicted R^2 **(0.9457)**	Adeq Precision **(19.5001)**	Std. Dev. **(0.5991)**	Mean **(82.6423)**	C.V. % **(0.7249)**

Table 4-13 ANOVA of 2FI regression model for TSS removal

Source	**Sum of squares**	**df**	**Mean**	**F-value**	**p-value**	
Model	15.5946	4	3.8986	73.8078	7.0696E-07	significant
A-Mixing rate	2.1672	1	2.1672	41.0286	1.2449E-04	
B-Settling time	0.0218	1	0.0218	0.4136	0.5362	
C-Coagulant dosage	12.8410	1	12.8410	243.1019	8.0579E-08	
AB	0.5645	1	0.5645	10.6871	0.0097	
Residual	0.4754	9	0.0528			
Lack of Fit	0.2448	8	0.0306	0,1327	0.9747	not significant
Pure Error	0.2306	1	0.2306			
Cor Total	16.0701	13				
R^2 (0,9704)	Adjusted R^2 **(0.9573)**	Predicted R^2 **(0.9485)**	Adeq Precision **(26.0273)**	Std. Dev. **(0.2298)**	Mean **(3.9773)**	C.V. % **(5.7786)**

Figure 4-21 depicts plots of predicted vs actual values for a better understanding of the proposed model's suitability. In this case, all of the points for the replies were scattered pretty near to the line of equality; the distribution of the points observed shows that the models' fitting precision is good, and the experimental results agree with each other. Appendix C depicts further diagnostic analyses (effect of process variables on contaminants removal and response surface plot of 3-factors) of the produced models.

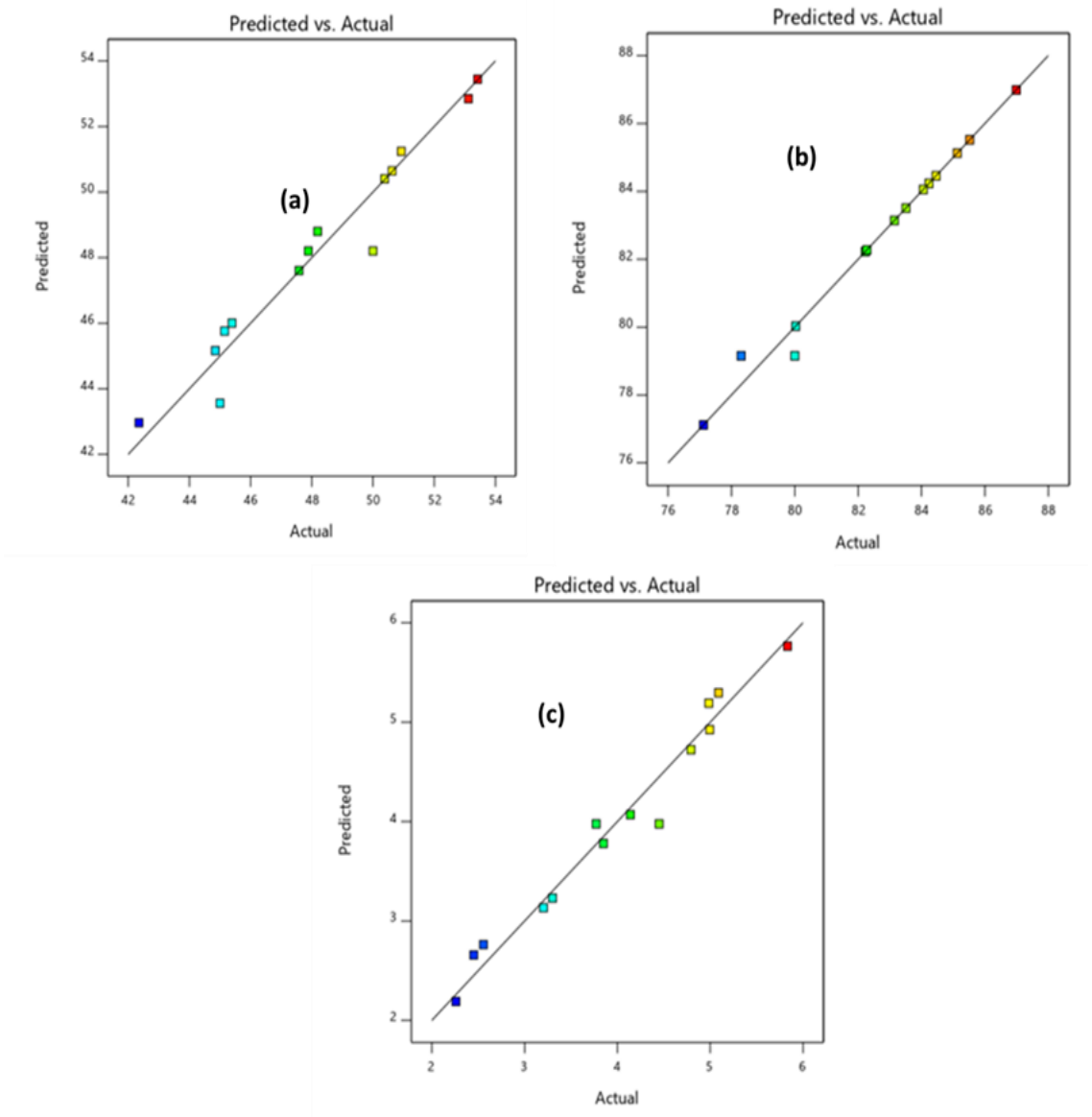

Figure 4-21 Design expert plot, predicted vs.actual plots (a) COD, (b) turbidity, and (c) TSS removal

4.5.2.2. Three dimensional (3D) and contour plots for DAF

COD removal shows and increasing trend when the flotation time increases to 30 minutes (Figure 4-22). This proves that the flocs were unstable and soon disintegrated. Higher COD efficacy was achieved at low mixing rates due to the fact that efficiency diminishes as mixing rate increases.

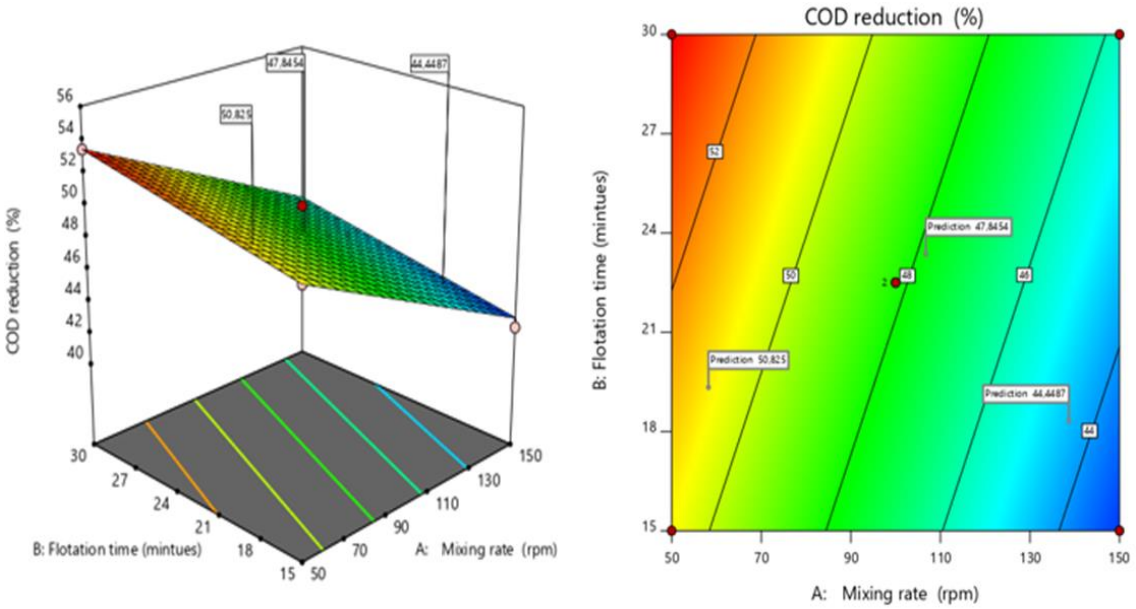

Figure 4-22 Response surface plots showing cross factor interactions for COD removal (%); (a) 3D plot (b) contour plot

The lowest turbidity efficiency is found in figure 4-23 towards the middle values of both flotation time and mixng rate. The turbidity efficiency steadily increases when the mixing rate is increased from 50 to 150 rpm. Lower values of flotation time suggest basically steady turbidity removal effectiveness. In figure 4-24, TSS efficiency declines as flotation time rises, whereas it increases when the mixing rate is increased to 150 rpm.

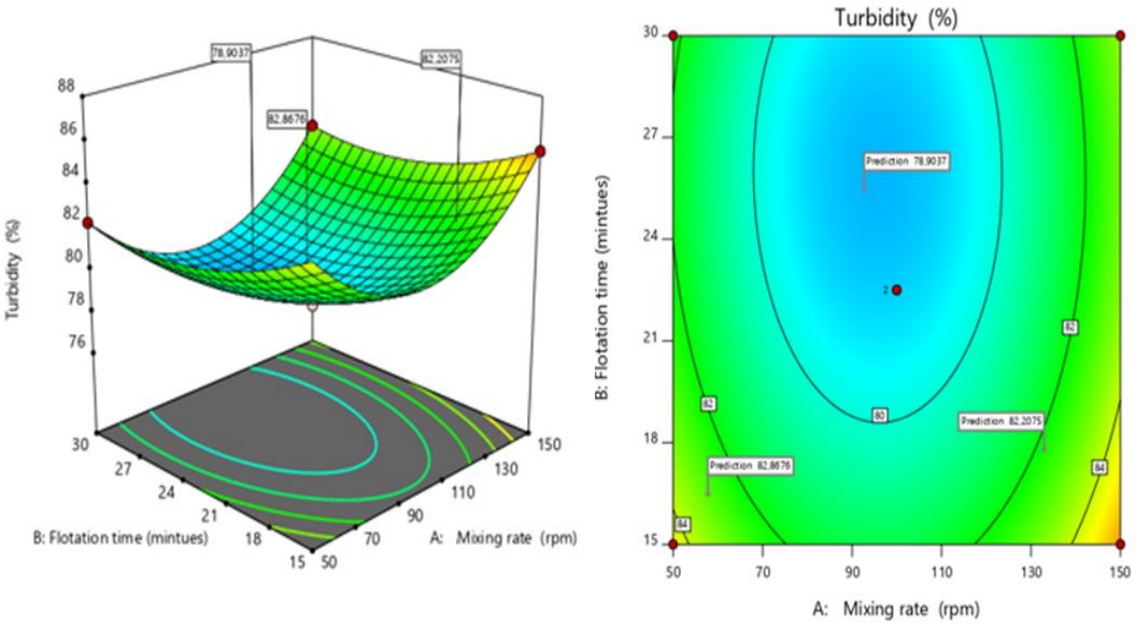

Figure 4-23 Response surface plots showing cross factor interactions for turbidity removal (%); (a) 3D plot (b) contour plot

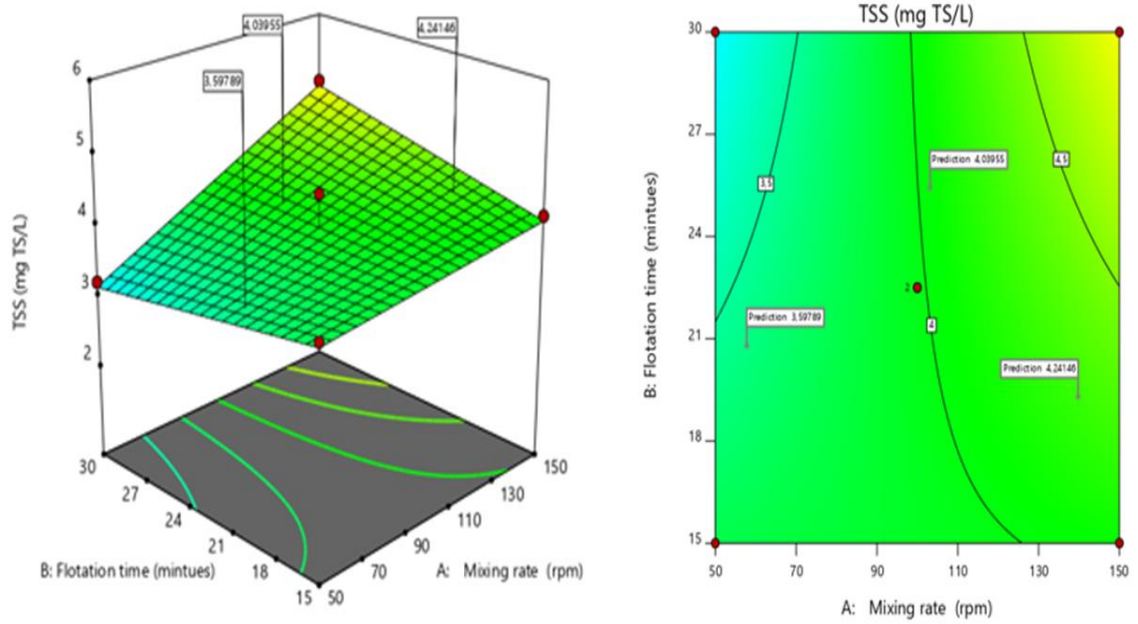

Figure 4-24 Response surface plots showing cross factor interactions for TSS removal (mg/L); (a) 3D plot (b) contour plot

4.5.2.3. Optimization of the DAF process

Figure 4-25 shows the results of another optimization study. The ramp plots indicate the ideal operating conditions as well as the desirability that was achieved. This was accomplished by keeping the input variables (coagulant dose, mixing rate, and flotation time) within their respective ranges and the responses maximized to target 95% confidence predicted levels (Table 4-14). Following the achievement of 100 conditional solutions, the ideal condition with 77.4% desirability was obtained at 4 g coagulant dose, 15 min of flotation time, and mixing rate of 50 rpm. This corresponded to removal efficiency of COD, turbidity, and TSS of 51.45%, 84.26%, and 5.05 mg/L, respectively. Three confirmation runs were used to validate these findings (Table 4-15).

Table 4-14 Conditions for optimization of DAF process variables

Variables	Low limit	High limit	Goal
Mixing rate (rpm)	50	150	is in range
Settling time (min)	15	30	is in range
Coagulant dosage (g)	2	4	is in range
COD removal (%)	42.3518	53.4204	Maximize
Turbidity removal (%)	77.1174	86.9901	Maximize
TSS removal (mg/L)	2.2597	5.8346	Maximize

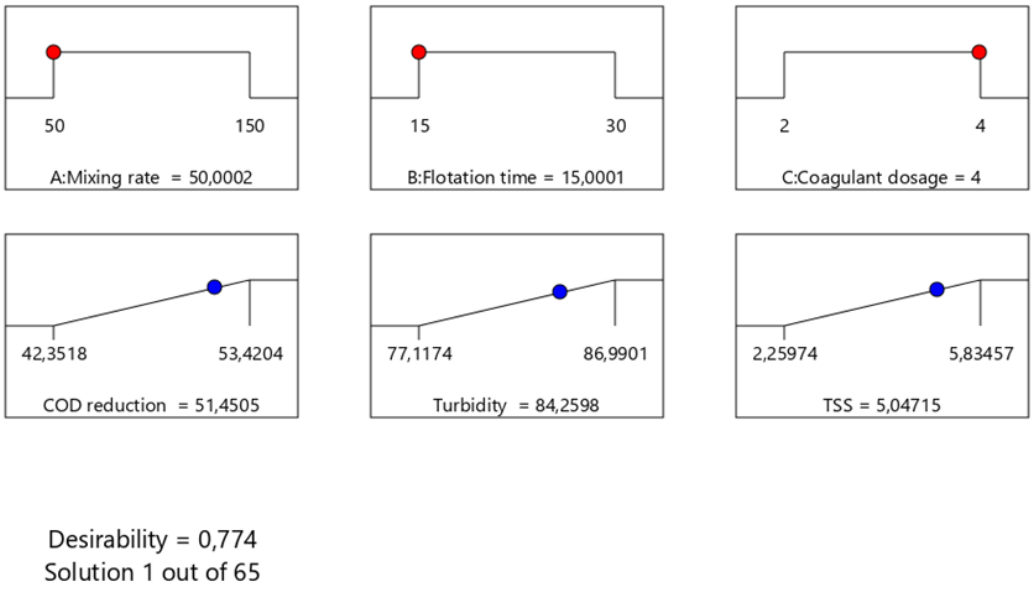

Figure 4-25 Ramp plot displaying the optimized conditions of DAF process variables at desirability of 77.40%

4.6. Comparative study of coagulation and DAF based on optimization

Table 4-15 presents the three experimental runs for each process that were performed under ideal operating circumstances to test the appropriateness and validity of the suggested models (figures 4-20 and 4-25). The coagulation method yielded mean COD, turbidity, and TSS removal values of 46.43%, 68.42%, and 46.69 mg/L, respectively at a settling time of 30 min. DAF achieved levels of 50.545, 85.50%, and 6.06 mg/L, for COD, turbidity and TSS, respectively at 15 min flotation time. These observed values were close to the predicted values and their difference was found to be less than 5%. This is indicating that the models can appropriately capture the link between experimental and numerical results. Hence, the models showed acceptable for predicting and improving coagulation-sedimentation and coagulation-flotation performance. DAF was more successful and had a major benefit (like time saving) (15 min flotation time) over the sedimentation-coagulation process with 30 min settling time. According to Tetteh (2018a), DAF requires less costs in downstream treatment and produces less sludge.

Table 4-15 Results attained for confirmatory runs in each process, using 4 g dosage and 50 rpm mixing rate

Variables	Run 1	Run 2	Run 3	Average (Run) values	RSM Pred. Values
COAGULATION PROCESS: 30 min settling time					
COD removal (%)	45.94	46.86	46.48	46.43	48.37
Turbidity removal (%)	69.45	67.13	68.68	68.42	66.00
TSS removal (mg/L)	45.94	46.86	46.10	46.69	47.33
DAF PROCESS: 15 min Flotation time					
COD removal (%)	50.03	50.60	50.99	50.54	51.45
Turbidity removal (%)	85.75	84.65	86.10	85.50	84.26
TSS removal (mg/L)	6.21	6.32	5.91	6.15	5.05

4.7. Summary

The study synthesized nine magnetic coagulants, and the best coagulants were chosen based on their ability to remove contaminants (COD, turbidity and TSS). At a settling period of 30 min, RF (1:1) was shown to be more effective at removing turbidity and TSS with above 80% efficiency. EF (2:1) was superior for COD removal at the optimum time of 20 min, with 53.34% effectiveness, followed by RF (1:1) with 51.58%, showing a 1.76% difference between the coagulants. The best efficient coagulant was subsequently determined to be RF (1:1). RF (1:1) was then evaluated in the DAF process which provided a glimpse at how powerful the coagulant would be if used on a pilot-scale. With 4 experimental runs, which had resulted in fewer coagulants utilized, the optimization of coagulation and DAF processes using RSM was proven to be economically feasible. The optimum parameters for the coagulation process were discovered to be 4 g for the coagulant dosage, 30 min of settling time, and mixing rate of 50 rpm, with desirability of 87.20% obtained. Whilst the DAF process achieved 77.4% desirability at 15 min flotation time and the same mixing rate (50 rpm) and coagulant dosage (4 g) as the coagulation process. Three tests were carried out under the above optimal circumstances to demonstrate the

consistency in findings obtained from models for both processes. The results show that the RSM in conjunction with the DoE approach is an effective tool for optimizing the operational conditions of industrial wastewater treatment with magnetized rice starch.

CHAPTER 5-CONCLUSIONS AND RECOMMENDATIONS

The study focused on the development and the use of three magnetized coagulants (chitosan magnetite (CF), eggshell magnetite (EF), and rice starch magnetite (RF)) as a substitute for alum in the pre-treatment of industrial effluents. This chapter summarizes the key results and makes recommendations for future research and decision-making.

The specific objectives were:

1. To synthesize and characterize an iron oxide nanoparticle (Ferro-magnetite) and functionalize it with natural coagulants viz. chitosan, egg shell, and rice starch in different ratios (1:1; 1:2 and 2:1).
2. To apply and evaluate the synthesized coagulants treatability efficiency using coagulation with settling and dissolved air flotation (DAF) techniques.
3. To apply the best-synthesized coagulant and optimize the coagulation with settling and DAF process using response surface methodology (RSM).
4. To compare and validate the coagulation and DAF treatability efficiency under the optimum conditions.

5.1. Conclusion

Three magnetized coagulants (MCs) such as chitosan magnetite (CF), eggshell magnetite (EF), and rice starch magnetite (RF) were synthesized via co-precipitation technique by using chitosan, eggshell, or rice starch with Fe_3O_4 in three distinct ratios (1:2, 1:1, and 2:1). The analytical results via the Fourier-transform infrared (FTIR) spectroscopy, Brunauer–Emmett–Teller (BET) analyzer, X-ray diffraction (XRD) analyzer, and scanning electron microscopy (SEM) combined with energy-dispersive X-ray (EDX) spectroscopy respectively affirmed the success of the MCs functional and molecular properties, surface area, crystal structure, surface morphology, and elemental compositions. SEM/EDX confirmed the existence of multivalent ions (Fe, Ca) and their related carbonates, confirming a successful synthesis. Furthermore, the BET findings revealed that adding magnetite to natural coagulant greatly changed the pore size of the MCs.

Subsequently, a series of investigations were carried out using coagulation and dissolved air flotation (DAF) techniques, whereby application and treatability performance of the MCs were explored. Amongst the coagulants investigated, RF (1:1) demonstrated a treatability efficacy of

more than 80% reduction of turbidity and TSS), and above 50% in COD reduction from local industrial effluent. Therefore, RF (1:1) was shown to have special physiochemical features, including the capacity to be isolated from suspension via MF, altering the pollutants removal. The BBD adopted from RSM was used to experimentally develop, optimize, and evaluate the influences of the input variables (coagulation dose, mixing rate, and settling/flotation duration) on the responses like turbidity, TSS, and COD removal. The acquired findings were analyzed and modeled as a function of the input parameters using ANOVA with a significant regression coefficient ($R^2 > 0.85$ for coagulation and 0.95 for DAF) at a 95% confidence level. Furthermore, the optimization and comparison of coagulation and DAF techniques was employed. At numerical optimal circumstances of coagulant dose (4 g), settling and flotation time (30 and 15 min, respectively), and mixing rate (50 rpm), the DAF and coagulation processes achieved 77.40% and 87.20% desired treatability efficiency, respectively. Herein, by using settling/flotation time and a desirability of 75% at 95% confidence, the DAF process was recommended to be more favorable with a shorter settling/flotation time.

5.2. Recommendations

The milestone of this study has demostrated sythesizing of magnetized natural coagulants is feasibile for water and wastewater treatment with great recoverability potential for reuse. Also exploring magnetic seperation technology together with engineering green coagulants as a niche area of research has great economic potential of adding value to organic waste. Therefore, enforcing these findings on real world wastewater treatment settings warrants future research interest in toxicological analysis, life cycle assessment, cost-benefit analysis and process optimisation using 4IR tools such as artificial neural networks (ANN). The thermodynamic kinetic reaction analysis of these coagulants, as well as their further characterization, were not carried out since the expenditures involved surpassed the budget for this study; nonetheless, it is recommended for the future. Furthermore, because to Covid-19, this trial ran longer than expected, limiting further study.

REFERENCES

Abdallh, M. N., Abdelhalim, W. S. and Abdelhalim, H. S. 2016. Industrial wastewater treatment of food industry using best techniques. *International Journal of Engineering Science Invention*, 5 (8): 15-28.

Abdelaal, A. M. 2004. Using a natural coagulant for treating wastewater. Paper presented at the *Eighth International Water Technology Conference*. Egypt.Alexandria Egypt: Suez Canal University, 781-792.

Abdelsalam, E., Samer, M., Attia, Y., Abdel-Hadi, M., Hassan, H. and Badr, Y. 2017. Influence of zero valent iron nanoparticles and magnetic iron oxide nanoparticles on biogas and methane production from anaerobic digestion of manure. *Energy*, 120: 842-853.

Abdelsalam, E. M. and Samer, M. 2019. Biostimulation of anaerobic digestion using nanomaterials for increasing biogas production. *Reviews in Environmental Science and Bio/Technology*, 18 (3): 525-541.

Abdelwahab, T. A. M., Mohanty, M. K., Sahoo, P. K. and Behera, D. 2020. Application of nanoparticles for biogas production: Current status and perspectives. *Energy sources, part a: recovery, utilization, and environmental Effects*: 1-13.

Abdulhameed, A. S., Jawad, A. H. and Mohammad, A.-T. 2019. Synthesis of chitosan-ethylene glycol diglycidyl ether/TiO2 nanoparticles for adsorption of reactive orange 16 dye using a response surface methodology approach. *Bioresource technology*, 293: 122071.

Aboelfetoh, E. F., Aboubaraka, A. E. and Ebeid, E.-Z. M. 2021. Binary coagulation system (graphene oxide/chitosan) for polluted surface water treatment. *Journal of environmental management*, 288: 112481.

Adelodun, B., Ogunshina, M. S., Ajibade, F. O., Abdulkadir, T. S., Bakare, H. O. and Choi, K. S. 2020. Kinetic and prediction modeling studies of organic pollutants removal from municipal wastewater using Moringa oleifera biomass as a coagulant. *Water*, 12 (7): 2052.

Adeogun, A. I., Bhagawati, P. and Shivayogimath, C. 2021. Pollutants removals and energy consumption in electrochemical cell for pulping processes wastewater treatment: Artificial neural network, response surface methodology and kinetic studies. *Journal of environmental management*, 281: 111897.

Adlan, M. N., Palaniandy, P. and Aziz, H. A. 2011. Optimization of coagulation and dissolved air flotation (DAF) treatment of semi-aerobic landfill leachate using response surface methodology (RSM). *Desalination*, 277 (1-3): 74-82.

Adschiri, T., Hakuta, Y., Sue, K. and Arai, K. 2001. Hydrothermal synthesis of metal oxide nanoparticles at supercritical conditions. *Journal of Nanoparticle Research*, 3 (2-3): 227-235.

Ahmed, D. N., Naji, L. A., Faisal, A. A., Al-Ansari, N. and Naushad, M. 2020a. Waste foundry sand/MgFe-layered double hydroxides composite material for efficient removal of Congo red dye from aqueous solution. *Scientific Reports*, 10 (1): 1-12.

Ahmed, I., Kormin, K., Rajput, R., Albeirutty, M., Rehan, Z. and Zeb, J. 2018. The Importance of Iron oxides in Natural Environment and Significance of its Nanoparticles Application. *Nanomaterials for Environmental Applications and their Fascinating Attributes*, 2: 218.

Ahmed, M. Z., Muteeb, G., Khan, S., Alqahtani, A. S., Somvanshi, P., Alqahtani, M. S., Ameta, K. L. and Haque, S. 2021a. Identifying novel inhibitor of quorum sensing transcriptional regulator (SdiA) of Klebsiella pneumoniae through modelling, docking and molecular dynamics simulation. *Journal of Biomolecular Structure and Dynamics*, 39 (10): 3594-3604.

Ahmed, S. I., Heiba, Z. K., Ibrahim, M. M., Shaltout, A. A., Alzahrani, E., Wahba, H. H. and Alsubaie, M. F. 2021b. Synthesis and Characterization of Eco-Friendly CMC/Maghemite Nanocomposite Films. *Journal of Electronic Materials*, 50 (12): 7098-7109.

Ahmed, S. N., Ali, S. J., Ali, A. H. and Mohammed, A. 2020b. Improvement of organic matter removal in water produced of oilfields using low cost Moringa peels as a new green environmental adsorbent. *Global Nest*, 22: 1-7.

Ahmed, Z., Yusoff, M. S., Kamal, N. H. M. and Aziz, H. A. 2021c. Optimization of the humic acid separation and coagulation with natural starch by RSM for the removal of COD and colour from stabilized leachate. *Waste Management & Research*: 0734242X211012775.

Ahn, J. and Lim, M. 2009. Characteristics of wastewater from the pulp paper industry and its biological treatment technologies. *Journal of Korean Institute of Resources Recycling*, 18 (2): 16-29.

Ain, Q. U., Rasheed, U., Yaseen, M., Zhang, H. and Tong, Z. 2020. Superior dye degradation and adsorption capability of polydopamine modified Fe3O4-pillared bentonite composite. *Journal of hazardous materials*, 397: 122758.

Akbarzadeh, A., Samiei, M. and Davaran, S. 2012. Magnetic nanoparticles: preparation, physical properties, and applications in biomedicine. *Nanoscale research letters*, 7 (1): 144.

Akratos, C. S. 2016. Book Review:“Wetlands for Water Pollution Control”, by Miklas Scholz (2015), Elsevier, Amsterdam, Netherlands. *Environmental Processes*, 3: 105-107.

Al-Abri, O. H., Lakkimsetty, N. R. and Shaik, F. 2020. Pretreatment of oil produces water using low cost adsorbents *International Journal of Mechanical and Production Engineering Research and Development (IJMPERD)*, 10 (3): 2435–2444.

Al-Khalid, T. and El-Naas, M. H. 2018. Organic contaminants in refinery wastewater:Characterization and novel approaches for biotreatment. In: *Recent insights in petroleum science and engineering*. InTech, 372-391.

Al-Shamrani, A. A., James, A. and Xiao, H. 2002. Destabilisation of oil–water emulsions and separation by dissolved air flotation. *Water research (Oxford)*, 36 (6): 1503-1512.

Al Ansari, Z., Ouda, M., Naddeo, V., Al Ali, K. and Hasan, S. W. 2021. Impact of electrodes' configuration in an electrokinetic cell for oil-water separation. *Case Studies in Chemical and Environmental Engineering*, 4: 100135.

Al Kindi, G. Y., Hassan, A. K., Yahya, D. G. and Alhaidri, H. A. 2021. The nanoparticles zero-valent synthesis by black tea extract to remove rb 238 using synthetic and natural wastewater by packed bed reactor. In: Proceedings of *IOP Conference Series: Earth and Environmental Science*. IOP Publishing, 012092.

Alabdraba, W. M. S., Albayati, M. B. A., Radeef, A. Y., Rejab, M. M. and 2013. Influence of Magnetic Field on The Efficiency of The Coagulation Process to Remove Turbidity From Water. *International Review of Chemical Engineering (I.RE.CH.E.)*, 5 (4): 1-8.

Alabresm, A. 2020. The use of polymer-coated magnetic nanoparticles for Amelioration oil toxicity and enhancement microbial remediation. University of South Carolina. Available: https://www.proquest.com/openview/60f89d5ab30ed3674721bb0135a9af4f/1?cbl=18750&diss=y&pq-origsite=gscholar (Accessed 5 December 2021).

Alhajabdalla, M., Mahmoud, H., Nasser, M. S., Hussein, I. A., Ahmed, R. and Karami, H. 2021. Application of Response Surface Methodology and Box–Behnken Design for the optimization of the stability of fibrous dispersion used in drilling and completion operations. *ACS omega*, 6 (4): 2513-2525.

Ali, A., Hira Zafar, M. Z., ul Haq, I., Phull, A. R., Ali, J. S. and Hussain, A. 2016. Synthesis, characterization, applications, and challenges of iron oxide nanoparticles. *Nanotechnology, science and applications*, 9: 49.

Ali, A. M., Abu-Hassan, M. A., Ibrahim, R. R. K., Zaini, M. A. A., Abdulkarim, B. I., Hussein, A. S., Su, S. M. and Halim, M. I. M. 2017. Characterization of petroleum sludge from refinery industry biological wastewater treatment unit. *The International Journal of Engineering and Science*, 6 (9): 61-65.

Ali Dheyab, M., Aziz, A. A. and Jameel, M. S. 2021. Recent advances in inorganic nanomaterials synthesis using sonochemistry: A comprehensive review on iron oxide, gold and iron oxide coated gold nanoparticles. *Molecules*, 26 (9): 2453.

Ali, G., Park, Y. J., Kim, J. W. and Cho, S. O. 2018. A green, general, and ultrafast route for the synthesis of diverse metal oxide nanoparticles with controllable sizes and enhanced catalytic activity. *ACS Applied Nano Materials*, 1 (11): 6112-6122.

Ali, I. 2014. Water treatment by adsorption columns: evaluation at ground level. *Separation & Purification Reviews*, 43 (3): 175-205.

Alwan, H. H., Ali, A. A. and Makki, H. F. 2020. Optimization of oxidative desulfurization reaction with Fe2O3 catalyst supported on graphene using Box-Behnken experimental method. *Bulletin of Chemical Reaction Engineering & Catalysis*, 15 (1): 175-185.

Amaral Filho, J., Azevedo, A., Etchepare, R. and Rubio, J. 2016. Removal of sulfate ions by dissolved air flotation (DAF) following precipitation and flocculation. *International Journal of Mineral Processing*, 149: 1-8.

Amatya, R., Hwang, S., Park, T., Min, K. A. and Shin, M. C. 2021. In Vitro and In Vivo Evaluation of PEGylated Starch-Coated Iron Oxide Nanoparticles for Enhanced Photothermal Cancer Therapy. *Pharmaceutics*, 13 (6): 871.

Ambashta, R. D. and Sillanpaa, M. 2010. Water purification using magnetic assistance: a review. *Journal of Hazardous Materials*, 180: 38-49.

Amo-Duodu, G., Tetteh , E. K., Rathilal, S., Armar, E. K., Adedeji, J., Chollom, M. N. and Chetty, M. 2021. Effect of engineered biomaterials and magnetite on wastewater treatment: Biogas and kinetic evaluation. *Polymers*, 13: 4323.

Amran, A. H., Zaidi, N. S., Muda, K. and Loan, L. W. 2018. Effectiveness of natural coagulant in coagulation process: A review. *International Journal of Environmental Science and Technology*, 7 (3.9): 34-37.

Ang, T.-H., Chua, S.-C., Kiatkittipong , K., Kiatkittipong, W., Lim, J. W., Show, P.-L. S., Bashir, M. J. K. and Ho, Y.-C. 2020a. Insight on extraction and characterisation of biopolymers as the green coagulants for microalgae harvesting. *Water*, 12: 1388.

Ang, W. L. and Mohammad, A. W. 2020b. State of the art and sustainability of natural coagulants in water and wastewater treatment. *Journal of cleaner production*, 262: 121267.

Anju, S. and Mophin-Kani, K. 2016. Exploring the use of orange peel and neem leaf powder as alternative coagulant in treatment of dairy wastewater. 7 (4): 238 - 244.

Aoki, N., Sato, A., Sasaki, H., Litwinowicz, A.-A., Seong, G., Aida, T., Hojo, D., Takami, S. and Adschiri, T. 2016. Kinetics study to identify reaction-controlled conditions for supercritical hydrothermal nanoparticle synthesis with flow-type reactors. *The Journal of Supercritical Fluids*, 110: 161-166.

Aparnadevi, N., Saravana Kumar, K., Manikandan, M., Paul Joseph, D. and Venkateswaran, C. 2016. Room temperature dual ferroic behaviour of ball mill synthesized NdFeO3 orthoferrite. *Journal of Applied Physics*, 120 (3): 034101.

APHA. 2012. *Standard methods for the examination of water and wastewater*. Washington, DC.: APHA. Available: https://www.standardmethods.org/doi/book/10.2105/SMWW.2882?gclid=CjwKCAiA25v_BRBNEiwAZb4-ZRdKz6ceq6 (Accessed 27 December 2020).

Arachchige, C. N., Prendergast, L. A. and Staudte, R. G. 2022. Robust analogs to the coefficient of variation. *Journal of Applied Statistics*, 49 (2): 268-290.

Arasu, M. V., Arokiyaraj, S., Viayaraghavan, P., Kumar, T. S. J., Duraipandiyan, V., Al-Dhabi, N. A. and Kaviyarasu, K. 2019. One step green synthesis of larvicidal, and azo dye degrading antibacterial nanoparticles by response surface methodology. *Journal of Photochemistry and Photobiology B: Biology*, 190: 154-162.

Arulmathi, P., Jeyaprabha, C., Sivasankar, P. and Rajkumar, V. 2019. Treatment of textile wastewater by coagulation–flocculation process using gossypium herbaceum and polyaniline coagulants. *Clean–Soil, Air, Water*, 47 (7): 1800464.

Asgari, G., Faradmal, J., Nasab, H. Z. and Ehsani, H. 2019. Catalytic ozonation of industrial textile wastewater using modified C-doped MgO eggshell membrane powder. *Advanced Powder Technology*, 30 (7): 1297-1311.

Asharuddin, S. M., Othman, N., Altowayti, W. A. H., Bakar, N. A. and Hassan, A. 2021. Recent advancement in starch modification and its application as water treatment agent. *Environmental Technology & Innovation*, 23: 101637.

Asharuddin, S. M., Othman, N., Zin, N. S. M., Tajarudin, H. A., Md. Din, M. F. and Kumar, V. 2018. Performance assessment of cassava peel starch and alum as dual coagulant for turbidity removal in dam water *International Journal of Integrated Engineering*, 10 (4): 185-192.

Asri, N. S., Tetuko, A. P., Esmawan, A., Addin, M., Setiadi, E. A., Putri, W. B., Ginting, M. and Sebayang, P. 2021. Syntheses of ferrofluids using polyethylene glycol (PEG) coated magnetite (Fe3O4), citric acid, and water as the working liquid in a cylindrical heat pipe. *Nano-Structures & Nano-Objects*, 25: 100654.

Asthana, M., Kumar, A. and Sharma, B. 2017. Wastewater treatment. In: *Principles and applications of environmental biotechnology for a sustainable future*. Springer, 173-232.

Azadi, M., Nguyen, A. V. and Yakubov, G. E. 2020. The effect of dissolved gases on the short-range attractive force between hydrophobic surfaces in the absence of nanobubble bridging. *Langmuir*, 36 (34): 9987-9992.

Azanza, M. P. V., Alejandro, C. B. S. and Jim, J. T. 2021. Impact of Processing Stages and Additives on the Structural Quality of Cornstarch Bihon-Type Noodles. *Philippine Journal of Science*, 150 (6A): 1451-1460.

Aziz, M., Abbas, S. S. and Wan Baharom, R. 2013. Size-controlled synthesis of SnO2 nanoparticles by sol–gel method. *Materials Letters*, 91: 31-34.

Aziz, O. A. A., Arafa, K., Dena, A. S. A. and El-Sherbiny, I. M. 2020. Superparamagnetic Iron Oxide Nanoparticles (SPIONs): Preparation and Recent Applications. *J. Nanotechnol. Adv. Mater.*, 8: 21-29.

Babakhani, A. and Sartaj, M. 2020. Removal of Cadmium (II) from aqueous solution using tripolyphosphate cross-linked chitosan. *Journal of Environmental Chemical Engineering*, 8 (4): 103842.

Bachmann, N., la Cour Jansen, J., Bochmann, G. and Montpart, N. 2015. *Sustainable biogas production in municipal wastewater treatment plants*. Switzerland: IEA Bioenergy.

Bala, N., Napiah, M. and Kamaruddin, I. 2020. Nanosilica composite asphalt mixtures performance-based design and optimisation using response surface methodology. *International Journal of Pavement Engineering*, 21 (1): 29-40.

Balls, M. 2014. Relationships between floc properties and NOM removal using a moorland water source. University College London. Available:

https://discovery.ucl.ac.uk/id/eprint/1417138/1/Balls_M_Thesis.pdf (Accessed 14 June 2020).

Bang, J. H. and Suslick, K. S. 2010. Applications of ultrasound to the synthesis of nanostructured materials. *Advanced Materials*, 22 (10): 1039-1059.

Barros Gomes Camara, R., Silva Costa, L., Pereira Fidelis, G., Duarte Barreto Nobre, L. T., Dantas-Santos, N., Lima Cordeiro, S., Santana Santos Pereira Costa, M., Guimaraes Alves, L. and Oliveira Rocha, H. A. 2011. Heterofucans from the brown seaweed Canistrocarpus cervicornis with anticoagulant and antioxidant activities. *Marine Drugs*, 9 (1): 124-138.

Bashir, K., Swer, T. L., Prakash, K. S. and Aggarwal, M. 2017. Physico-chemical and functional properties of gamma irradiated whole wheat flour and starch. *LWT-Food Science and Technology*, 76: 131-139.

Basina, G., Khurshid, H., Tzitzios, N., Hadjipanayis, G. and Tzitzios, V. 2021. Facile organometallic synthesis of Fe-based nanomaterials by hot injection reaction. *Nanomaterials*, 11 (5): 1141.

Basso, A., Hamad, F. and Ganesan, P. 2019. Initial results from the experimental and computational study of microbubble generation. In: Proceedings of *Proceedings of the 4th World Congress on Momentum, Heat and Mass Transfer; Avestia Publishing: Orléans, ON, Canada*.

Batlle, X., Moya, C., Escoda-Torroella, M., Iglesias, Ò., Rodríguez, A. F. and Labarta, A. 2021. Magnetic nanoparticles: From the nanostructure to the physical properties. *Journal of magnetism and magnetic materials*, 543: 168594.

Baumgartner, J., Dey, A., Bomans, P. H., Le Coadou, C., Fratzl, P., Sommerdijk, N. A. and Faivre, D. 2013. Nucleation and growth of magnetite from solution. *Nature materials*, 12 (4): 310-314.

Baytar, O., Şahin, Ö., Horoz, S. and Kutluay, S. 2020. High-performance gas-phase adsorption of benzene and toluene on activated carbon: response surface optimization, reusability, equilibrium, kinetic, and competitive adsorption studies. *Environmental Science and Pollution Research*, 27 (21): 26191-26210.

Beasley, M. M., Bartelink, E. J., Taylor, L. and Miller, R. M. 2014. Comparison of transmission FTIR, ATR, and DRIFT spectra: implications for assessment of bone bioapatite diagenesis. *Journal of Archaeological Science*, 46: 16-22.

Becker, J., Hald, P., Bremholm, M., Pedersen, J. S., Chevallier, J., Iversen, S. B. and Iversen, B. B. 2008. Critical size of crystalline ZrO2 nanoparticles synthesized in near- and supercritical water and supercritical isopropyl alcohol. *ACS nano*, 2 (5): 1058-1068.

Bell, N. L., Kupper, M. and Cronin, L. 2021. Design of experiments for optimization of polyoxometalate syntheses. *Chemistry of Materials*, 33 (18): 7263-7271.

Benning, L. G., Phoenix, V., Yee, N. and Konhauser, K. 2004. The dynamics of cyanobacterial silicification: an infrared micro-spectroscopic investigation. *Geochimica et Cosmochimica Acta*, 68 (4): 743-757.

Beyene, H. D., Hailegebrial, T. D. and Direrssa, W. B. 2016. Investigation of coagulation activity of cactus powder in water treatment. *Journal of Applied Chemistry*, 2016 (1): 1-9.

Bhamidipati, S. H., Vadlamudi, D. P. and Moka, S. 2021. Polymers as coagulants for wastewater treatment In: *Advanced Materials and Technologies for Wastewater Treatment*. CRC Press, 85. Available: https://books.google.co.za/books?hl=en&lr=&id=gIo7EAAAQBAJ&oi=fnd&pg=PA85&dq=Tripathy,+T.+and+De,+B.+R.+2006.+Flocculation+:+A+new+way+to+treat+the+waste+water.+Journal+of+Physical+Sciences,+10:+93-127.&ots=bim-ll_MjY&sig=YSjJHcl2058wqtvjlgHWTzNzLJc#v=onepage&q&f=false (Accessed 18 November 2021).

Bhateria, R. and Singh, R. 2019. A review on nanotechnological application of magnetic iron oxides for heavy metal removal. *Journal of water process engineering*, 31: 100845.

Bhatnagar, A. and Sillanpää, M. 2009. Applications of chitin- and chitosan-derivatives for the detoxification of water and wastewater — A short review. *Advances in colloid and interface science*, 152: 26-38.

Bi, X.-y., Peng, W., Jiang, H., Xu, H.-y., Shi, S.-J. and Huang, J.-l. 2007. Treatment of phenol wastewater by microwave-induced ClO2-CuOx/Al2O3 catalytic oxidation process. *Journal of Environmental Sciences*, 19 (12): 1510-1515.

Billah, R. E. K., Abdellaoui, Y., AnfarZakaria , Giácoman-Vallejos, G., Agunaou, M. and Soufi, A. 2020. ynthesis and Characterization ofChitosan/Fluorapatite Composites for the Removal ofCr (VI) from Aqueous Solutions and Optimized Parameters. *Water Air Soil Pollut*, 231: 163.

Biswas, A., Patra, A. K., Sarkar, S., Das, D., Chattopadhyay, D. and De, S. 2020. Synthesis of highly magnetic iron oxide nanomaterials from waste iron by one-step approach. *Colloids and Surfaces A: Physicochemical and Engineering Aspects*, 589: 124420.

Blake, J. R. and Gibson, D. 1987. Cavitation bubbles near boundaries. *Annual review of fluid mechanics*, 19 (1): 99-123.

Blanco-Gutiérrez, V., Andrada-Chacón, A., Sánchez-Benítez, J., Urones-Garrote, E., Sáez-Puche, R. and Torralvo-Fernández, M. a. J. 2019. Superparamagnetic behavior at room temperature through crystal chemistry modification and particle assembly formation: Zinc and nickel ferrite systems. *The Journal of Physical Chemistry C*, 123 (27): 16973-16981.

Blandin, G., Galizia, A., Monclús, H., Lesage, G., Héran, M. and Martinez-Lladó, X. 2021. Submerged osmotic processes: Design and operation of hollow fiber forward osmosis modules. *Desalination*, 518: 115281.

Bodlund, I. 2013a. Coagulants protein from plant materials:Potential water treatment agent. Msc Biotechnology, Royal Institute of Technology. Available: https://www.diva-portal.org/smash/record.jsf?pid=diva2%3A575557&dswid=-1205 (Accessed 12 February 2020).

Bodlund, I. 2013b. Coagulants protein from plant materials:Potential water treatment agent. Msc Biotechnology, Royal Institute of Technology. Available: https://www.diva-portal.org/smash/record.jsf?pid=diva2%3A575557&dswid=-1205 (Accessed 12 February 2020).

Boskovic, M., Fabián, M., Vranjes-Djuric, S. and Antic, B. 2021. Magnetic nano-and micro-particles based on Gd-substituted magnetite with improved colloidal stability. *Applied Physics A*, 127 (5): 1-10.

Bourtoom, T. and Chinnan, M. S. 2008. Preparation and properties of rice starchechitosan blend biodegradable film. *Science Drirect*, 41: 1633-1641.

Bozhinova, D. P. 2004. Synthesis, modification and characterisation of magnetic micro-matrices for covalent immobilisation of biomolecules. Model investigations with penicillin amidase from E. coli. Available: https://epub.uni-regensburg.de/10208/ (Accessed 30 March 2021).

Braga de Oliveira, F., Álvares da Silva, G. and Graca, L. M. 2020. Defining the hematite topotaxial crystal growth in magnetite–hematite phase transformation. *Journal of Applied Crystallography*, 53 (4): 896-903.

Bratby, J. 2016. *Coagulation and flocculation in water and wastewater treatment*. 3rd ed. London IWA Publishing.

Bule´on, A., Colonna, P., Planchot, V. and Ball, S. 1998. Starch granules: structure and biosynthesis. *International journal of biological macromolecules*, 23: 85-112.

Bumajdad, A., Eastoe, J. and Mathew, A. 2009. Cerium oxide nanoparticles prepared in self-assembled systems. *Advances in colloid and interface science*, 147: 56-66.

Burezq, H. A. 2021. Utilization of Eggshell as Valuable Products for Sustainable Ecosystem and Agriculture. *Poultry Science Journal*, 9 (2): 147-165.

Burns, K. E., Uhrig, R. F., Jewett, M. E., Bourbon, M. F. and Krupa, K. A. 2021. Characterizing the Role of Biologically Relevant Fluid Dynamics on Silver Nanoparticle Dependent Oxidative Stress in Adherent and Suspension In Vitro Models. *Antioxidants*, 10 (6): 832.

Cai, W. and Wan, J. 2007. Facile synthesis of superparamagnetic magnetite nanoparticles in liquid polyols. *Journal of Colloid and Interface Science*, 305 (2): 366-370.

Cai, Y., Long, X., Meng, X., Ji, J., Wang, Y. and Xie, S. 2021. Coordinated and competitive formation of soil magnetic particles driven by contrary climate development. *Geophysical Research Letters*, 48 (16): e2021GL094506.

Calvache-Muñoz, J., Prado, F. A. and Rodriguez-Paez, J. E. 2017. Cerium oxide nanoparticles: Synthesis, characterization and tentative mechanism of particle formation. *Colloids and Surfaces A: Physicochemical and Engineering Aspects*, 529: 146-159.

Calvino-Casilda, V., López-Peinado, A. J., Martín-Aranda, R. M. and Mayoral, E. P. 2019. *Nanocatalysis: applications and technologies*. CRC Press.

Cam, T. S., Omarov, S. O., Chebanenko, M. I., Izotova, S. G. and Popkov, V. I. 2021. Recent progress in CeO2-based nanocatalysts toward efficient oxidation of CO. *Journal of Science: Advanced Materials and Devices*, 7 (1): 100399.

Carmona, M., Khemis, M., Leclere, J.-P. and Lapicque, F. 2006. A simple model to predict the removal of oil suspensions from water using the electrocoagulation technique. *Chemical engineering science*, 61 (4): 1237-1246.

Cartwright, A., Jackson, K., Morgan, C., Anderson, A. and Britt, D. W. 2020. A review of metal and metal-oxide nanoparticle coating technologies to inhibit agglomeration and increase bioactivity for agricultural applications. *Agronomy*, 10 (7): 1018.

Castanha, N., Villar, J., da Matta Junior, M. D., Dos Anjos, C. B. P. and Augusto, P. E. D. 2018. Structure and properties of starches from Arracacha (Arracacia xanthorrhiza) roots. *International journal of biological macromolecules*, 117: 1029-1038.

Chang, P.-H., Chou, T.-H., Sahu, R. S. and Shih, Y.-h. 2019. Chemical reduction-aided zerovalent copper nanoparticles for 2, 4-dichlorophenol removal. *Applied Nanoscience*, 9 (3): 387-395.

Chang, Y.-C., Chang, S.-W. and Chen, D.-H. 2006. Magnetic chitosan nanoparticles: Studies on chitosan binding and adsorption of Co(II) ions. *Reactive & Functional Polymers*, 66: 335-341.

Chastellain, M., Petri, A. and Hofmann, H. 2004. Particle size investigations of a multistep synthesis of PVA coated superparamagnetic nanoparticles. *Journal of Colloid and Interface Science*, 278 (2): 353-360.

Chaudhary, S., Kumar, M., Ahmed, S. and Kaushik, M. 2021. Detection and removal of heavy metals from wastewater using nanomaterials. *Pollutants and Water Management: Resources, Strategies and Scarcity*: 241-272.

Chaves, L., Fernandes, J., Mendes, J., Tito, G., Guerra, H. and Laurentino, L. 2021. Optimization of Cadmium Adsorption Using Poultry Litter Biochar Through Response Surface Methodology. *Chemical Engineering Transactions*, 86: 1507-1512.

Chelliah, R., Chandrashekar, S., Saravanakumar, K., Ramakrishnan, S. R., Rubab, M., Daliri, E. B.-M., Barathikannan, K., Tyagi, A., Kwame Ofosu, F. and Chen, X. 2019. Effect of rice processing towards lower rapidly available glucose (RAG) favors Idli, a south indian fermented food suitable for diabetic patients. *Nutrients*, 11 (7): 1497.

Chen, C., Yaari, Z., Apfelbaum, E., Grodzinski, P., Shamay, Y. and Heller, D. A. 2022. Merging Data Curation and Machine Learning to Improve Nanomedicines. *Advanced Drug Delivery Reviews*: 114172.

Chen, Q., Zhang, M., Ma, Q. and Wang, Q. 2019. The structure, spectra and properties of Dy2O3 modified diamagentic lead-bismuth-germanium glasses. *Journal of Non-Crystalline Solids*, 507: 46-55.

Chen, X., Zhou, Y., Han, H., Wang, X., Zhou, L., Yi, Z., Fu, Z., Wu, X., Li, G. and Zeng, L. 2021. Optical and magnetic properties of small-size core–shell Fe3O4@ C nanoparticles. *Materials Today Chemistry*, 22: 100556.

Cheng, F.-Y., Su, C.-H., Yang, Y.-S., Yeh, C.-S., Tsai, C.-Y., Wu, C.-L., Wu, M.-T. and Shieh, D.-B. 2005. Characterization of aqueous dispersions of Fe3O4 nanoparticles and their biomedical applications. *Biomaterials*, 26 (7): 729-738.

Cheng, R., Kang, M., Shi, L., Wang, J.-l., Zheng, X. and Wang, J.-l. 2021. Fe-Based Nanomaterials for Removing the Environmental Endocrine Disrupting Chemicals in Water: A Review. *Environmental Nanotechnology Volume 5*: 261-292.

Chinenye Adaobi Igwegbea, Leili Mohmmadib, Shahin Ahmadi, Rahdar, A., Khadkhodaiy, D., Dehghani, R. and Rahdar, S. 2019. Modeling of adsorption of methylene blue dye on Ho-CaWO4 nanoparticles using response surface methodology (RSM) and artificial neural network (ANN) techniques. *MethodsX*, 6: 1779-1797.

Choi, S. and Kim, Y. 2018. Pre-treatment of oily wastewater using a coagulation-DAF process with slit-nozzle. *Journal of Korean Society of Water and Wastewater*, 32 (6): 479-485.

Chollom, M. N., Rathilal, S., Swalaha, F. M., Bakare, B. and Tetteh, E. K. 2019. Anaerobic treatment of slaughterhouse wastewater: Evaluating operating conditions. *WIT Transactions on Ecology and the Environment*, 239: 251-262.

Chollom, M. N., Rathilal, S., Swalaha, F. M., Bakare, B. F. and Tetteh, E. K. 2020. Removal of antibiotics during the anaerobic digestion of slaughterhouse wastewater. *International Journal of Sustainable Development and Planning*, 15 (3): 335-343.

Choy, S., Prasad, K., Wu, T. and Ramanan, R. 2015. A review on common vegetables and legumes as promising plant-based natural coagulants in water clarification. *International Journal of Environmental Science and Technology*, 12 (1): 367-390.

Choy, S. Y., Prasad, K. M. N., Wu, T. Y., Raghunandan, M. E. and Ramanan, R. N. 2014. Utilization of plant-based natural coagulants as future alternatives towards sustainable water clarification. *Journal of Environmental Sciences*, 26 (11): 2178-2189.

Choy, S. Y., Prasad, K. M. N., Wu, T. Y., Raghunandan, M. E., Yang, B., Phang, S.-M. and Ramanan, R. N. 2017. Isolation, characterization and the potential use of starch from jackfruit seed wastes as a coagulant aid for treatment of turbid water. *Environmental science and pollution research international*, 24 (3): 2876-2889.

Choy, S. Y., Prasad, K. N., Wu, T. Y., Raghunandan, M. E. and Ramanan, R. N. 2016. Performance of conventional starches as natural coagulants for turbidity removal. *Ecological engineering*, 94: 352-364.

Choya, S. Y., Prasada, K. M. N., Wua, T. Y., Raghunandan, M. E., Phang, S.-M., Juane, J. C. and Ramanan, R. N. 2018. Separation of Chlorella biomass from culture medium by flocculation with rice starch. *Algal Research*: 162-172.

Chua, S.-C., Chong, F.-K., Yen, C.-H. and Ho, Y.-C. 2019. Valorization of conventional rice starch in drinking water treatment and optimization using response surface methodology (RSM). *Chemical Engineering Communications*, 208 (5): 613-623.

Chua, S.-C., Chong, F.-K., Yen, C.-H. and Ho, Y.-C. 2021a. Valorization of conventional rice starch in drinking water treatment and optimization using response surface methodology (RSM). *Chemical Engineering Communications*, 208 (5): 613-623.

Chua, S.-C., Ho, Y.-C. and Chong, F.-K. 2021b. Synthesis and application of a novel composite coagulant aid from rice starch and sesbania seed gum for water treatment. *Malaysian Journal of Chemistry*, 23 (1): 7-14.

Conde-Cid, M., Paíga, P., Moreira, M., Albergaria, J., Álvarez-Rodríguez, E., Arias-Estévez, M. and Delerue-Matos, C. 2021. Sulfadiazine removal using green zero-valent iron nanoparticles: A low-cost and eco-friendly alternative technology for water remediation. *Environmental Research*, 198: 110451.

Cook, A. M. 2016. Double perovskites with strong spin-orbit coupling. University of Toronto (Canada). Available: https://www.proquest.com/openview/205f88be181441b35f38ecff84fbee17/1?pq-origsite=gscholar&cbl=18750 (Accessed 15 June 2021).

Cornell, R. M. and Schwertmann, U. 2003. *The iron oxides: structure, properties, reactions, occurrences and uses*. John Wiley & Sons.

Crini, G. and Lichtfouse, E. 2018. Advantages and disadvantages of techniques used for wastewater treatment. *Environmental Chemistry Letters*, 17: 145-155.

Cui, H., Huang, X., Yu, Z., Ping Chen, P. and Cao, X. 2020. Application progress of enhanced coagulation in water treatment. *RSC advances*, 10: 20231.

Damager, I., Engelsen, S. B., Blennow, A., Lindberg Møller, B. and Motawia, M. S. 2010. First principles insight into the α-glucan structures of starch: their synthesis, conformation, and hydration. *Chemical reviews*, 110 (4): 2049-2080.

Danko, M., Kronekova, Z., Krupa, I., Tkac, J., Matúš, P. and Kasak, P. 2021. Exchange Counterion in Polycationic Hydrogels: Tunability of Hydrophobicity, Water State, and Floating Capability for a Floating pH Device. *Gels*, 7 (3): 109.

Das, R., Kim, N. P., Attanayake, S. B., Phan, M.-H. and Srikanth, H. 2021. Role of Magnetic Anisotropy on the Hyperthermia Efficiency in Spherical Fe3− xCoxO4 (x= 0–1) Nanoparticles. *Applied Sciences*, 11 (3): 930.

Das, R. C. 2021. The Effect of Stoichiometric Variation on the Magnetocaloric Properties of Selected Mn-Fe-Ni-Si-Al Intermetallic Compounds. Miami University. Available: https://www.proquest.com/openview/8a827460ee3c936ce55cc20572874a87/1?pq-origsite=gscholar&cbl=18750&diss=y (Accessed 15 March 2022).

Dassey, A. and Theegala, C. 2012. Optimizing the air dissolution parameters in an unpacked dissolved air flotation system. *Water*, 4 (1): 1-11.

Daud, Z., Awang, H., Latif, A. A. A. and Nasir, N. 2015. Suspended solid, color, COD and oil and grease removal from biodiesel wastewater by coagulation and flocculation processes. *Procedia, social and behavioral sciences*, 195: 2407-2411.

de la Torre, E. and Gámez, S. 2019. Not reacted core model applied in palm nut shell pyrolysis. *International Journal of Chemical Engineering*, 2019: 1-9.

de Oliveira, F. W. F., dos Reis, S. C., Ribeiro, L. S., Velásquez, L. N. M., Cotta, A. A. C., dos Santos, V. L., Gastelois, P. L., Ardisson, J. D. and Santos, A. 2021. Fluorine adsorption on floating iron nanoparticles confined to gigaporous structure of large adsorbent water spheres. *Environmental Technology & Innovation*, 24: 101995.

de Souza Fermino, L., de Castro Silva Pedrangelo, A., de Matos Silva, P. K., de Azevedo, R. E. C., Yamaguchi, N. U. and Ribeiro, R. M. 2017. Water treatment with conventional and alternative coagulants. *Chemical Engineering Transactions*, 57 (2017): 1189-1194.

Demir, A., Topkaya, R. and Baykal, A. 2013. Green synthesis of superparamagnetic Fe3O4 nanoparticles with maltose: its magnetic investigation. *Polyhedron*, 65: 282-287.

Deravi, L. F. 2009. *Piezoelectric inkjet printing of multicomposite biomaterials*. Vanderbilt University. Available: https://www.proquest.com/openview/bc18535906aab23476d21ec5361bc8b1/1?pq-origsite=gscholar&cbl=18750 (Accessed 30 January 2022).

Deshmukh, R. A., Joshi, K., Bhand, S. and Roy, U. 2016. Recent developments in detection and enumeration of waterborne bacteria: a retrospective minireview. *MicrobiologyOpen*, 5 (6): 901-922.

Devi, M. G., Dumaran, J. J. and Feroz, S. 2012. Dairy wastewater treatment using low molecular weight crab shell chitosan. *Journal of The Institution of Engineers (India): Series E*, 93 (1): 9-14.

Dey, S. C., Al-Amin, M., Rashid, T. U., Sultan, M. Z., Ashaduzzaman, M., Sarker, M. and Shamsuddin, S. M. 2016. PREPARATION, CHARACTERIZATION AND PERFORMANCE EVALUATION OF CHITOSAN AS AN ADSORBENT FOR RE. *International Journal of Latest Research in Engineering and Technology* 2(21): 52-62.

Dheyab, M. A., Aziz, A. A., Jameel, M. S., Khaniabadi, P. M. and Mehrdel, B. 2020. Mechanisms of effective gold shell on Fe3O4 core nanoparticles formation using sonochemistry method. *Ultrasonics sonochemistry*, 64: 104865.

Diya'uddeen, B. H., Daud, W. M. A. W. and Abdul Aziz, A. R. 2011. Treatment technologies for petroleum refinery effluents: A review. *Process Safety and Environmental Protection*, 89 (2): 95-105.

Dlangamandla, C., Ntwampe, S. K. O. and Basitere, M. 2018. A bioflocculant-supported dissolved air flotation system for the removal of suspended solids, lipids and protein matter from poultry slaughterhouse wastewater. *Water Science and Technology*, 78 (2): 452-458.

Doblhoff-Dier, K. and Koper, M. T. 2021. Modeling the Gouy–Chapman diffuse capacitance with attractive ion–surface interaction. *The Journal of Physical Chemistry C*, 125 (30): 16664-16673.

Donners, J. J., Heywood, B. R., Meijer, E., Nolte, R. J. and Sommerdijk, N. A. 2002. Control over calcium carbonate phase formation by dendrimer/surfactant templates. *Chemistry–A European Journal*, 8 (11): 2561-2567.

dos Santos Pereira, M., Borges, A. C., Heleno, F. F., Squillace, L. F. A. and Faroni, L. R. D. A. 2018. Treatment of synthetic milk industry wastewater using batch dissolved air flotation. *Journal of cleaner production*, 189: 729-737.

dos Santos, T. R. T., Mateus, G. A. P., Silva, M. F., Miyashiro, C. S., Nishi, L., de Andrade, M. B., Fagundes-Klen, M. R., Gomes, R. G. and Bergamasco, R. 2018a. Evaluation of Magnetic Coagulant (α-Fe2O3-MO) and its Reuse in Textile Wastewater Treatment. *Water, air, and soil pollution*, 229 (3): 92.

dos Santos, T. R. T., Silva, M. F., dme Andrade, M. B., Vieira, M. F. and Bergamasco, R. 2018b. Magnetic coagulant based on Moringa oleifera seeds extract and super paramagnetic nanoparticles: optimization of operational conditions and reuse evaluation. *Desalination and Water Treatment*, 106: 226-237.

Duan, J. and Gregory, J. 2003a. Coagulation by hydrolysing metal salts. *Advances in colloid and interface science*, 100-102: 475-502.

Duan, J. and Gregory, J. 2003b. Coagulation by hydrolysing metal salts. *Advances in colloid and interface science*, 100-102 (2003): 475-502.

Duan, J., Niu, A., Shi, D., Wilson, F. and Graham, N. 2009. Factors affecting the coagulation of seawater by ferric chloride. *Desalination and Water Treatment*, 11 (1-3): 173-183.

Dung, D. T. K., Hai, T. H., Phuc, L. H., Long, B. D., Vinh, L. K. and Truc, P. N. 2009. Preparation and characterization of magnetic nanoparticles with chitosan coating. *Journal of Physics: Conference Series*, 187: 012036.

Dunne, P. W., Munn, A. S., Starkey, C. L., Huddle, T. A. and Lester, E. H. 2015. Continuous-flow hydrothermal synthesis for the production of inorganic nanomaterials. *Philosophical Transactions of the Royal Society A: Mathematical, Physical and Engineering Sciences*, 373 (2057): 20150015.

Duran-García, E. I., Martínez-Santana, J., Torres-Gómez, N., Vilchis-Nestor, A. R. and García-Orozco, I. 2021. Copper sulfide nanoparticles produced by the reaction of N-alkyldithiocarbamatecopper (II) complexes with sodium borohydride. *Materials chemistry and physics*, 269: 124743.

Ealias, A. M. and Saracanakumar, M. P. 2017. A review on the classification, characterisation, synthesis of nanoparticles and their application. *IOP Conference Series: Materials Science and Engineering*, 263: 032019.

Edzwald, J. K. 2010. Dissolved air flotation and me. *Water Research*, 44 (7): 2077-2106.

El-Gaayda, J., Titchou, F. E., Oukhrib, R., Yap, P.-S., Liu, T., Hamdani, M. and Akbour, R. A. 2021. Natural flocculants for the treatment of wastewaters containing dyes or heavy metals: a state-of-the-art review. *Journal of Environmental Chemical Engineering*, 9 (5): 106060.

El-Gohary, F., Tawfik, A. and Mahmoud, U. 2010. Comparative study between chemical coagulation/precipitation (C/P) versus coagulation/dissolved air flotation (C/DAF) for pre-treatment of personal care products (PCPs) wastewater. *Desalination*, 252 (1-3): 106-112.

El Ghandoor, H., Zidan, H., Khalil, M. M. and Ismail, M. 2012. Synthesis and some physical properties of magnetite (Fe3O4) nanoparticles. *Int. J. Electrochem. Sci*, 7 (6): 5734-5745.

El Knidri, H., El Khalfaouy, R., Laajeb, A., Addaou, A. and Lahsini, A. 2016. Eco-friendly extraction and characterization of chitin and chitosan from the shrimp shell waste via microwave irradiation. *Process Safety and Environmental Protection*, 104: 395–405.

Elhambakhsh, A., Zaeri, M. R., Mehdipour, M. and Keshavarz, P. 2020. Synthesis of different modified magnetic nanoparticles for selective physical/chemical absorption of CO2 in a bubble column reactor. *Journal of Environmental Chemical Engineering*, 8 (5): 104195.

Elumalai, V. 2018. Novel synthetic methodology and total syntheses of highly functionalized carbazoles and benzo [c] cinnolines. Degree of Philosophiae Doctor (PhD), University of Bergen. Available: https://hdl.handle.net/1956/17263 (Accessed 22 November 2021).

Engin, B., Demirtaş, H. and Eken, M. 2006. Temperature effects on egg shells investigated by XRD, IR and ESR techniques. *Radiation Physics and Chemistry*, 75 (2): 268-277.

Epoyan, S., Syrovatsky, O., Haiduchok, O. and Titov, A. 2020. Effect of technological parameters on clarification low-concentration suspension by dissolved air flotation. In: Proceedings of *IOP Conference Series: Materials Science and Engineering*. IOP Publishing, 012084.

Ernest, E., Onyeka, O., David, N. and Blessing, O. 2017. Effects of pH, dosage, temperature and mixing speed on the efficiency of water melon seed in removing the turbidity and colour of atabong river, Awka-Ibom State, Nigeria. *International Journal of Advanced engineering, Management and Science*, 3 (5): 427-434.

Escoda-Torroella, M., Moya, C., Rodríguez, A. F., Batlle, X. and Labarta, A. 2020. Selective control over the morphology and the oxidation state of iron oxide nanoparticles. *Langmuir*, 37 (1): 35-45.

eSilva, F. C. P. R., eSilva, N. M. P. R., Luna, J. M., Rufino, R. D., Santos, V. A. and Sarubbo, L. A. 2018. Dissolved air flotation combined to biosurfactants: a clean and efficient alternative to treat industrial oily water. *Reviews in Environmental Science and Bio/Technology*, 17 (4): 591-602.

Eswararao, Y., Niju, S., Meera Sheriffa Begum, K., Anantharaman, N. and Malik Raj, S. 2016. Transesterification of jatropha oil using a mixture of natural shells as solid catalyst. *Biofuels*, 7 (4): 345-351.

Ewerts, H., Barnard, S., Swanepoel, A., Du Preez, H. and Janse van Vuuren, S. 2014. Strategies of coagulant optimisation to improve the removal of turbidity and Ceratium hirundinella cells during conventional drinking water purification. *Water Science and Technology: Water Supply*, 14 (5): 820-828.

Ezugbe, E. O. and Rathilal, S. 2020. Membrane Technologies in Wastewater Treatment: A review. *Membranes*, 10: 89.

Fan, D., Ma, W., Wang, L.-j., Huang, J.-C. H., Zhao, J., Zhang, H. and Chen, W. 2012. Determination of structural changes in microwaved rice starch using Fourier transform infrared and Raman spectroscopy. *Starch*, 64: 598-606.

Fantechi, E., Ponti, A. and Ferretti, A. M. 2020. Synthesis and design of ferro-and ferrimagnetic NPs: Size and shape control in wet-chemistry synthesis. In: *Advances in Nanostructured Materials and Nanopatterning Technologies*. Elsevier, 333-379.

Fard, M. B., Hamidi, D., Alavi, J., Jamshidian, R., Pendashteh, A. and Mirbagheri, S. A. 2021a. Saline oily wastewater treatment using Lallemantia mucilage as a natural coagulant: Kinetic study, process optimization, and modeling. *Industrial Crops and Products*, 163: 113326.

Fard, M. B., Hamidi, D., Yetilmezsoy, K., Alavi, J. and Hosseinpour, F. 2021b. Utilization of Alyssum mucilage as a natural coagulant in oily-saline wastewater treatment. *Journal of water process engineering*, 40: 101763.

Fath, V., Kockmann, N., Otto, J. and Röder, T. 2020. Self-optimising processes and real-time-optimisation of organic syntheses in a microreactor system using Nelder–Mead and design of experiments. *Reaction Chemistry & Engineering*, 5 (7): 1281-1299.

Fearing, D. A. 2004. *Process options for the treatment of humic rich waters*. UK: Cranfield University. Available: https://core.ac.uk/download/pdf/137903.pdf (Accessed 30 March 2020).

Ferreira-Villadiego, J., Garcia-Echeverri, J., Mejia, M. V., Pasqualino, J., Meza-Catellar, P. and Lambis, H. 2018. Chemical modification and characterization of starch derived from plantain (Musa paradisiaca) Peel waste, as a source of biodegradable material. *Chemical Engineering Transactions*, 65: 763-768.

Ferreira, S. C., Bruns, R., Ferreira, H., Matos, G., David, J., Brandão, G., da Silva, E. P., Portugal, L., Dos Reis, P. and Souza, A. 2007. Box-Behnken design: an alternative for the optimization of analytical methods. *Analytica chimica acta*, 597 (2): 179-186.

Filip, J., Kolařík, J., Petala, E., Petr, M., Šráček, O. and Zbořil, R. 2019. Nanoscale zerovalent iron particles for treatment of metalloids. In: *Nanoscale Zerovalent Iron Particles for Environmental Restoration*. Springer, 157-199.

Filippou, P. C. 2019. Unit cell thick ferrimagnetic Heusler domain wall motion using Chemical Templating Layers. Available: http://dx.doi.org/10.25673/13914 (Accessed 25 March 2021).

Fitzpatrick, C. S. B., Fradin, E. and Gregory, J. 2004. Temperature effects on flocculation, using different coagulants. *Water Science and Technology*, 50 (12): 171-175.

Flannigan, D. J. and Suslick, K. S. 2005. Plasma formation and temperature measurement during single-bubble cavitation. *Nature*, 434 (7029): 52-55.

Foltynowicz, Z., Czajka, B., Maranda, A. and Wachowski, L. 2020. Aspects of nanomaterials for civil and military applications. Part 1. Origins, characteristics and fabrication methods. *Materiały Wysokoenergetyczne*, 12 (1): 5-16.

Fonseca, R. R., Thompson Jr, J. P., Franco, I. C. and da Silva, F. V. 2017. Automation and control of a dissolved air flotation pilot plant. *IFAC-PapersOnLine*, 50 (1): 3911-3916.

Franger, S., Berthet, r. P. and Berthon, J. 2004. Electrochemical synthesis of Fe3O4 nanoparticles in alkaline aqueous solutions containing complexing agents. *Journal of Solid State Electrochemistry*, 8 (4): 218-223.

Frattini, D., Karunakaran, G., Cho, E.-B. and Kwon, Y. 2021. Sustainable syntheses and sources of nanomaterials for microbial fuel/electrolysis cell applications: An overview of recent progress. *Processes*, 9 (7): 1221.

Fredriksson, H., Björck, I., Andersson, R., Liljeberg, H., Silverio, J., Eliasson, A.-C. and Åman, P. 2000. Studies on α-amylase degradation of retrograded starch gels from waxy maize and high-amylopectin potato. *Carbohydrate polymers*, 43 (1): 81-87.

Freitas, T. K. F. S., Almeida, C. A., Manholer, D. D., Geraldino, H. C. L., de Souza, M. T. F. and Garcia, J. C. 2017. Review of utilization plant-based coagulants as alternatives to textile wastewater treatment. In: *Detox Fashion*. Springer, 27-79. Available: https://link.springer.com/chapter/10.1007/978-981-10-4780-0_2#Sec11 (Accessed 23 August 2021).

Frick, J. M., Ambrosi, A., Pollo, L. D. and Tessaro, I. C. 2018. Influence of glutaraldehyde crosslinking and alkaline post-treatment on the properties of chitosan-based films. *Journal of Polymers and the Environment*, 26 (7): 2748-2757.

Fu, C. and Ravindra, N. M. 2012. Magnetic iron oxide nanoparticles: synthesis and applications. *Bioinspired, Biomimetic and Nanobiomaterials*, 1 (4): 229-244.

Fuad, N., Omar, R., Kamarudin, S., Harun, R., Idris, A. and WAKG, W. A. 2021. Harvesting marine microalgae Nannochloropsis sp. using Dissolved Air Flotation (DAF) technique. *Sains Malaysiana*, 50 (1): 73-83.

Fufaeva, V. and Nikiforova, T. 2020. Preparation of Zif/Chitosan composite beads for highly efficient removal of Copper (ii). *International Journal of Advanced Studies in Medicine and Biomedical Sciences*, (2): 3-6.

Gadkari, R. R., Ali, S. W., Alagirusamy, R. and Das, A. 2018. Silver nanoparticles in water purification: opportunities and challenges. *Modern age environmental problems and their remediation*: 229-237.

Gaikwad, V. and Munavalli, G. 2019. Turbidity removal by conventional and ballasted coagulation with natural coagulants. *Applied Water Science*, 9 (5): 1-9.

Galan, J., Trilleras, J., Zapata, P. A., Arana, V. A. and Grande-Tovar, C. D. 2021. Optimization of chitosan glutaraldehyde-crosslinked beads for reactive blue 4 anionic dye removal using a surface response methodology. *Life*, 11 (2): 85.

Galluzzia, A., Murariuc, M., Raquezc, J.-M., Dubois, P. and Polichettia, M. 2021. Effect of magnetite nanoparticles content on the magnetic properties of polylactide and polystyrene composites. *Chemical Engineering Transactions*, 84: 1-6.

Ganea, I.-V., Nan, A., Baciu, C. and Turcu, R. 2021. Effective removal of crystal violet dye using neoteric magnetic nanostructures based on functionalized Poly (Benzofuran-co-Arylacetic Acid): Investigation of the adsorption behaviour and reusability. *Nanomaterials*, 11 (3): 679.

Gautam, S. and Saini, G. 2020. Use of natural coagulants for industrial wastewater treatment. *Global Journal of Environmental Science and Management*, 6 (4): 553-578.

Gautron, J., Stapane, L., Le Roy, N., Nys, Y., Rodriguez-Navarro, A. and Hincke, M. 2021. Avian eggshell biomineralization: an update on its structure, mineralogy and protein tool kit. *BMC molecular and cell biology*, 22 (1): 1-17.

Gedanken, A. 2004. Using sonochemistry for the fabrication of nanomaterials. *Ultrasonics sonochemistry*, 11 (2): 47-55.

Gerçekaslan, K. E. 2020. Hydration level significantly impacts the freezable-and unfreezable-water contents of native and modified starches. *Food Science and Technology*, 41: 426-431.

Ghaedi, M., Hajjati, S., Mahmudi, Z., Tyagi, I., Agarwal, S., Maity, A. and Gupta, V. 2015. Modeling of competitive ultrasonic assisted removal of the dyes–Methylene blue and Safranin-O using Fe3O4 nanoparticles. *Chemical Engineering Journal*, 268: 28-37.

Ghafari, S., Aziz, H. A., Isa, M. H. and Zinatizadeh, A. A. 2009. Application of response surface methodology (RSM) to optimize coagulation–flocculation treatment of leachate using poly-aluminum chloride (PAC) and alum. *Journal of hazardous materials*, 163: 650-656.

Ghernaout, D. 2020. Enhanced Coagulation: Promising Findings and Challenges. *Open Access Library Journal*, 7 (7): 1-19.

Ghorbani, M., Chen, H., Villanueva, L. G., Grishenkov, D. and Koşar, A. 2018. Intensifying cavitating flows in microfluidic devices with poly (vinyl alcohol)(PVA) microbubbles. *Physics of Fluids*, 30 (10): 102001.

Ghorpade, A. and Ahammed, M. M. 2018. Water treatment sludge for removal of heavy metals from electroplating wastewater. *Environmental Engineering Research*, 23 (1): 92-98.

Goel, C., Semwal, A. D., Khan, A., Kumar, S. and Sharma, G. K. 2020. Physical modification of starch: changes in glycemic index, starch fractions, physicochemical and functional properties of heat-moisture treated buckwheat starch. *Journal of Food Science and Technology*, 57 (8): 2941-2948.

Goli, J. and Sahu, O. 2018. Development of heterogeneous alkali catalyst from waste chicken eggshell for biodiesel production. *Renewable Energy*, 128: 142-154.

Gonzales-Weimuller, M., Zeisberger, M. and Krishnan, K. M. 2009. Size-dependant heating rates of iron oxide nanoparticles for magnetic fluid hyperthermia. *Journal of magnetism and magnetic materials*, 321 (13): 1947-1950.

Gonzalez-Perez, A., Hägg, K. and Duteil, F. 2021. Optimizing NOM Removal: Impact of Calcium Chloride. *Sustainability*, 13 (11): 6338.

Gopi, D., Ansari, M. T. and Kavitha, L. 2016. Electrochemical synthesis and characterization of cubic magnetite nanoparticle in aqueous ferrous perchlorate medium. *Arabian Journal of Chemistry*, 9: S829-S834.

Gottesman, R., Shukla, S., Perkas, N., Solovyov, L. A., Nitzan, Y. and Gedanken, A. 2011. Sonochemical coating of paper by microbiocidal silver nanoparticles. *Langmuir*, 27 (2): 720-726.

Gregory, J. 2009. Monitoring particle aggregation processes. *Advances in colloid and interface science*, 147: 109-123.

Guatame-Garcia, A. and Buxton, M. 2018. The use of infrared spectroscopy to determine the quality of carbonate-rich diatomite ores. *Minerals*, 8 (3): 120.

Guha, S., Majumder, K. and Mine, Y. 2019. Egg proteins. *Encyclopedia of Food Chemistry; Melton, L., Shahidi, F., Varelis, P., Eds*: 74-84.

Guillou, F., Paudyal, D., Mudryk, Y., Pathak, A. K., Smetana, V., Mudring, A.-V. and Pecharsky, V. K. 2020. Metamagnetic transition, magnetocaloric effect and electronic structure of the rare-earth anti-perovskite SnOEu3. *Journal of magnetism and magnetic materials*, 501: 166405.

Gulbagca, F., Yildiz, B., Elmusa, F., Ahamed, M. I. and Sen, F. 2020. State of the art, challenges and future prospects in magnetochemistry. *Magnetochemistry: Materials and Applications*, 66: 130.

Gumbi, N. 2020. The effectiveness of domestic water treatment processes, North West Province, South Africa. North-West University (South Africa). Available: http://repository.nwu.ac.za/bitstream/handle/10394/35536/Gumbi_N.pdf?sequence=1 (Accessed 14 October 2021).

Gupta, V. K., Ali, I., Saleh, T. A., Nayak, A. and Agarwal, S. 2012. Chemical treatment technologies for waste-water recycling—an overview. *RSC advances*, 2 (16): 6380.

Guru, P. S. and Dash, S. 2014. Sorption on eggshell waste—A review on ultrastructure, biomineralization and other applications. *Advances in colloid and interface science*, 209: 49-67.

Gutierrez, A. M., Dziubla, T. D. and Hilt, J. Z. 2017. Recent advances on iron oxide magnetic nanoparticles as sorbents of organic pollutants in water and wastewater treatment. *Rev Environ Health*, 32 (1-2): 111-117.

Haddad, B., Mittal, A., Mittal, J., Paolone , A., Villemin, D., Debdab , M., Mimanne , G., Habibi , A., Hamidi, Z., Boumediene, M. and Belarbi, E.-h. 2021. Synthesis and characterization of Egg shell (ES) and Egg shell with membrane (ESM) modified by ionic liquids. *Chemical Data Collections*, 33: 100717.

Hajalilou, A., Ferreira, L., Jorge, M. M., Reis, C. and Cruz, M. 2021. Superparamagnetic Ag-Fe3O4 composites nanoparticles for magnetic fluid hyperthermia. *Journal of magnetism and magnetic materials*, 537: 168242.

Hamidi, D., Fard, M. B., Yetilmezsoy, K., Alavi, J. and Zarei, H. 2021. Application of Orchis mascula tuber starch as a natural coagulant for oily-saline wastewater treatment:

Modeling and optimization by multivariate adaptive regression splines method and response surface methodology. *Journal of Environmental Chemical Engineering*, 9 (1): 104745.

Han, X., Zhang, M., Zhang, R., Huang, L., Jia, X., Huang, F. and Liu, L. 2020. Physicochemical interactions between rice starch and different polyphenols and structural characterization of their complexes. *LWT - Food Science and Technology*, 125: 109227.

Hanafy, M. and Nabih, H. 2007. Treatment of oily wastewater using dissolved air flotation technique. *Energy Sources, Part A*, 29 (2): 143-159.

Handojo, L., Nursanto, E. B. and Indarto, A. 2019. Progress of Nanomaterials Application in Environmental Concerns. In: *Nanohybrids in Environmental & Biomedical Applications*. CRC Press, 189-205.

Haritwal, A., Mohan, D., Chaudhary, M., Asopa, P. P. and Modi, G. 2015. Study on the improved biogas generation through magnetic field modified anaerobic digestion. *International Journal of Engineering Research & Technology*, 4 (5): 1175-1179.

Hasan, S. 2015. A review on nanoparticles: their synthesis and types. *Research Journal of Recent Sciences*, 2277: 2502.

Hasany, S. F., Abdurahman, N. H., Sunarti, A. R. and Jose, R. 2013. Magnetic iron oxide nanoparticles: Chemical synthesis and applications review. *Current Nanoscience*, 9: 561-575.

Hashem, F. 2013. Removal of methylene blue by magnetitecovered bentonite nano-composite. *European Chemical Bulletin*, 2 (8): 524-529.

Hassan, A. M., Ibrahim, W. A. W., Bakar, M. B., Sanagi, M. M., Sutirman, Z. A., Nodeh, H. R. and Mokhter, M. A. 2020. New effective 3-aminopropyltrimethoxysilane functionalized magnetic sporopollenin-based silica coated graphene oxide adsorbent for removal of Pb (II) from aqueous environment. *Journal of environmental management*, 253: 109658.

Hatamie, A., Parham, H., Zargar, B. and Heidari, Z. 2016. Evaluating magnetic nano-ferrofluid as a novel coagulant for surface water treatment. *Journal of Molecular Liquids*, 219: 694-702.

He, Y., Miao, Y., Li, C., Wang, S., Cao, L., Xie, S., Yang, G., Zou, B. and Burda, C. 2005. Size and structure effect on optical transitions of iron oxide nanocrystals. *Physical Review B*, 71 (12): 125411.

Helwani, Z., Ramli, M., Saputra, E., Bahruddin, B., Yolanda, D., Fatra, W., Idroes, G. M., Muslem, M., Mahlia, T. M. I. and Idroes, R. 2020. Impregnation of CaO from Eggshell Waste with Magnetite as a Solid Catalyst (Fe3O4/CaO) for Transesterification of Palm Oil Off-Grade. *Catalysts*, 10: 164.

Hoang Tran, V., Lam Dai, T., Thinh Nguyen, N., Nguyet Tran Thi, M., Long Bui, D., Nguyen Van, B., Ha Le Thi, T. and Thuy Tran Thi, P. 2009. Preparation of chitosan/magnetite composite beads and their application for removal of Pb(II) and Ni(II) from aqueous solution. *Materials Science and Engineering: C*, 30 (2): 304-310.

Hollanda, L. R., Santos, S. B. F., Faustino, J. G. A. A., Dotto, G. L., Foletto, E. L. and Chiavone-Filho, O. 2021. Oil field–produced water treatment: characterization, photochemical systems, and combined processes. *Environmental Science and Pollution Research*: 1-20.

Hong, C. W. and Chan, N. W. 2016. *Chapter 21: Wastewater*. Malaysia: Chan Ngai Weng. Available: https://www.researchgate.net/profile/Ngai-Weng-Chan/publication/308984010_CHAPTER_21_WASTE_WATER/links/57fcaaf208ae51472e7ffeb2/CHAPTER-21-WASTE-WATER.pdf (Accessed 20 February 2020).

Hong, E.-M., Rho, S.-J., Kim, U. and Kim, Y.-R. 2021. Physicochemical properties and freeze–thaw stability of rice flour blends among rice cultivars with different amylose contents. *Food Science and Biotechnology*, 30 (10): 1347-1356.

Hoslett, J., Massara, T. M., Malamis, S., Ahmad, D., van den Boogaert, I., Katsou, E., Ahmad, B., Ghazal, H., Simons, S. and Wrobel, L. 2018. Surface water filtration using granular media and membranes: A review. *Science of the Total Environment*, 639: 1268-1282.

Hossain, M., Omar, F., Asis, A. J., Bachmann, R. T., Sarker, M. I. and Ab Kadir, M. O. 2019. Effective treatment of palm oil mill effluent using FeSO4.7H2O waste from titanium oxide industry: Coagulation adsorption isotherm and kinetics studies. *Journal of Clear Production*, 29: 86-98.

Hribernik, S., Sfiligoj-Smole, M., Bele, M., Gyergyek, S., Jamnik, J. and Stana-Kleinschek, K. 2012. Synthesis of magnetic iron oxide particles: development of an in situ coating procedure for fibrous materials. *Colloids and Surfaces A: Physicochemical and Engineering Aspects*, 400: 58-66.

Huang, J., Wang, H., Sun, X., Zhang, X. and Wang, H. 2018. Multifunctional La0. 67Sr0. 33MnO3 (LSMO) thin films integrated on mica substrates toward flexible spintronics and electronics. *ACS applied materials & interfaces*, 10 (49): 42698-42705.

Hubbe, M. A., Metts, J. R., Hermosilla, D., Blanco, M. A., Yerushalmi, L., Haghighat, F., Lindholm-Lehto, P., Khodaparast, Z., Kamali, M. and Elliott, A. 2016. Wastewater treatment and reclamation: A review of pulp and paper industry practices and opportunities. *BioResources*, 11 (3): 7953-8091.

Hufschmid, R., Arami, H., Ferguson, R. M., Gonzales, M., Teeman, E., Brush, L. N., Browning, N. D. and Krishnan, K. M. 2015. Synthesis of phase-pure and monodisperse iron oxide nanoparticles by thermal decomposition. *Nanoscale*, 7 (25): 11142-11154.

Huzir, N. M., Aziz, M. M. A., Ismail, S. B., Mahmood, N. A. N., Umor, N. A. and Muhammad, S. A. F. S. 2019. Optimization of coagulation-flocculationprocess for the palm oil milleffluent treatment by using rice husk ash. *Industrial Crops & Products*, 139: 111482.

Hyeon, T., Lee, S. S., Park, J., Chung, Y. and Na, H. B. 2001. Synthesis of highly crystalline and monodisperse maghemite nanocrystallites without a size-selection process. *Journal of the American Chemical Society*, 123 (51): 12798-12801.

Igunnu, E. T. 2014. Produced water treatment technologies. *International journal of low carbon technologies*, 9 (3): 157-177.

Iloms, E. C. 2018. *Investigating industrial effluent impacts on municipal wastewater treatment plant*. South Africa: University of South Africa. Available: https://core.ac.uk/download/pdf/231923024.pdf (Accessed 16 June 2020).

Ince, M. and Ince, O. K. 2019. Heavy metal removal techniques using response surface methodology: Water/wastewater treatment. In: *Biochemical Toxicology-Heavy Metals and Nanomaterials*. IntechOpen. Available: https://www.intechopen.com/chapters/68822 (Accessed 1 January 2022).

Inozemtseva, O. A., German, S. V., Navolokin, N. A., Bucharskaya, A. B., Maslyakova, G. N. and Gorin, D. A. 2018. Encapsulated magnetite nanoparticles: preparation and application as multifunctional tool for drug delivery systems. In: *Nanotechnology and Biosensors*. Elsevier, 175-192.

Iqbal, M., Iqbal, N., Bhatti, I. A., Ahmad, N. and Zahid, M. 2016. Response surface methodology application in optimization of cadmium adsorption by shoe waste: a good option of waste mitigation by waste. *Ecological engineering*, 88: 265-275.

Irinislimane, H. and Belhaneche-Bensemra, N. 2017. Extraction and characterization of starch from oak acorn, sorghum, and potato and adsorption application for removal of maxilon red GRL from wastewater. *Chemical Engineering Communications*, 204 (8): 897-906.

Islama, J., Gangulia, P., Mondala, S. and Chaudhuria, S. 2020. Green synthesis of iron oxide magnetic nanoparticles for the adsorption of lead (II) from aqueous medium. *Journal of the Indian Chemical Society*, 97 (10b): 1854-1860.

Jagaba, A. H., Kutty, S. R. M., Hayder, G., Latiff, A. A. A., Aziz, N. A. A., Umaru , I., Ghaleb, A. A. S., Abubakar, S., Lawal, I. M. and Nasara, M. A. 2020. Sustainable use of natural and chemical coagulants for contaminants removal from palm oil mill effluent: A comparative analysis. *Ain Shams Engineering Journal*, 11951-960

Jagaba, A. H., Latiff, A. A., Umaru, I., Abubakar, S. and Lawal, I. M. 2016. Treatment of palm oil mill effluent (POME) by coagulation-flocculation using different natural and chemical coagulants: A review. *IOSR Journal of Mechanical and Civil Engineering*, 13 (6): 67-75.

Jahangirian, H., Rafiee-Moghaddam, R., Jahangirian, N., Nikpey, B., Jahangirian, S., Bassous, N., Saleh, B., Kalantari, K. and Webster, T. J. 2020. Green synthesis of zeolite/Fe2O3 nanocomposites: toxicity & cell proliferation assays and application as a smart iron nanofertilizer. *International Journal of Nanomedicine*, 15: 1005.

Jalilibal, Z., Amiri, A., Castagliola, P. and Khoo, M. B. 2021. Monitoring the coefficient of variation: A literature review. *Computers & Industrial Engineering*, 161: 107600.

Jana, S., Gandhi, A. and Sen, K. K. 2019. Chitosan-Based Interpenetrating Polymer Networks: Drug Delivery Application. *Functional Chitosan*: 269-295.

Jana, S., Trivedi, M. K., Tallapragada, R. M., Branton, A., Trivedi, D., Nayak, G. and Mishra, R. K. 2015. Characterization of Physicochemical and Thermal Properties of Chitosan and Sodium Alginate after Biofield Treatment. *Pharmaceutica Analytica Acta*, 6: 10.

Jayan, V. and Anitha, K. 2015. Heavy metal removal (Pb & Cu) from waste water using pumpkin and egg shell along with chitosan as filter media. *Small (Weinheim an der Bergstrasse, Germany)*, 2: 2.

Jelodar, A. H., Rad, H. A., Borghei, S. M., Vossoughi, M. and Rouhollahi, R. 2021. Particle removal optimization in rotating dissolved air flotation used in paper‐recycling wastewater treatment. *Water and Environment Journal*: 1-15.

Jiang, C., Wang, R. and Ma, W. 2010. The effect of magnetic nanoparticles on Microcystis aeruginosa removal by a composite coagulant. *Colloids and Surfaces A: Physicochemical and Engineering Aspects*, 369: 260-267.

Jiang, J.-Q. 2015. The role of coagulation in water treatment. *Current Opinion in Chemical Engineering*, 8: 36-44.

Jiao, D., Lesage, K., Yardimci, M. Y., El Cheikh, K., Shi, C. and De Schutter, G. 2021. Rheological behavior of cement paste with nano-Fe3O4 under magnetic field: Magneto-rheological responses and conceptual calculations. *Cement and Concrete Composites*, 120: 104035.

Jo, S. H., Choi, C. and Choi, S.-K. 2019. Depolymerization of α-& β-Chitosan by e-Beam Irradiation. *Journal of Biosciences and Medicines*, 7 (10): 72.

Johnson, A. L. 2015. Reproduction in the female. In: *Sturkie's avian physiology*. Elsevier, 635-665.

Jung, H. and Schimpf, A. M. 2021. Photochemical reduction of nanocrystalline maghemite to magnetite. *Nanoscale*, 13 (41): 17465-17472.

Kalifah, S. B. 2019. Determination of Organic and Inorganic Components of Commercial Chicken Eggshell Obtained From Sebha Local Market-Libya. *Journal of Pure & Applied Sciences*, 18 (1): 2019.

Kalita, D. and Bellare, J. R. 2017. Chemical synthesis of nanoparticles for diverse applications. In: *Nanotoxicology*. 17-38.

Kamaruddin, M., Abdullah, M., Yusoff, M., Alrozi, R. and Neculai, O. 2017. Coagulation-flocculation process in landfill leachate treatment: focus on coagulants and coagulants aid. In: Proceedings of *IOP Conference Series: Materials Science and Engineering*. IOP Publishing, 012083.

Kango, S., Kalia, S., Celli, A., Njuguna, J., Habibi, Y. and Kumar, R. 2013. Surface modification of inorganic nanoparticles for development of organic–inorganic nanocomposites—A review. *Progress in Polymer Science*, 38 (8): 1232-1261.

Kanwal, Z., Raza, M. A., Manzoor, F., Riaz, S., Jabeen, G., Fatima, S. and Naseem, S. 2019. A comparative assessment of nanotoxicity induced by metal (silver, nickel) and metal oxide (cobalt, chromium) nanoparticles in Labeo rohita. *Nanomaterials*, 9 (2): 309.

Karami, S., Rostamizadeh, K., Shademani, N. and Parsa, M. 2020. Synthesis and investigation of the curcumin-loaded magnetic lipid nanoparticles and their cytotoxicity assessment on human breast carcinoma cell line. *Jundishapur Journal of Natural Pharmaceutical Products*, 15 (2): 1-10.

Karapinar, N. 2003. Magnetic separation: An alernative method to the treatment of wastewater. *The European Journal of Mineral Processing and Environment Protection*, 3 (2): 215-223.

Karhu, M., Leiviskä, T. and Tanskanen, J. 2014. Enhanced DAF in breaking up oil-in-water emulsions. *Separation and purification technology*, 122: 231-241.

Karimifard, S. and Moghaddam, M. R. A. 2018. Application of response surface methodology in physicochemical removal of dyes from wastewater: a critical review. *Science of the Total Environment*, 640: 772-797.

Karp, S. G., Pagnoncelli, M. G. B., Prado, F., de Oliveira Penha, R., Junior, A. I. M., Kumlehn, G. S. and Soccol, C. R. 2021. Chapter5-Starch. *Biomass, Biofuels, Biochemicals*: 75-100.

Kassem, A. A., Salama, A. and Mohsen, A. M. 2022. Formulation and optimization of cationic nanoemulsions for enhanced ocular delivery of dorzolamide hydrochloride using Box-Behnken design: In vitro and in vivo assessments. *Journal of Drug Delivery Science and Technology*, 68: 103047.

Katz, E. 2019. Synthesis, properties and applications of magnetic nanoparticles and nanowires—A brief introduction. *Magnetochemistry*, 5 (4): 61.

Kaur, R. 2010. *Relationship of organic precursors of uterine fluid with eggshell quality and its crystalline structure*. Dalhousie University. Available: https://www.collectionscanada.gc.ca/obj/thesescanada/vol2/002/MR69820.PDF?is_thesis=1&oclc_number=814658537 (Accessed 15 September 2021).

Kausar, A. 2020. Polymeric materials filled with hematite nanoparticle: current state and prospective application. *Polymer-Plastics Technology and Materials*, 59 (3): 323-338.

Keçili, R., Ghorbani-Bidkorbeh, F., Dolak, I., Canpolat, G., Karabörk, M. and Hussain, C. M. 2021. Functionalized magnetic nanoparticles as powerful sorbents and stationary phases for the extraction and chromatographic applications. *TrAC Trends in Analytical Chemistry*, 143: 116380.

Kekalo, K., Koo, K., Zeitchick, E. and Baker, I. 2012. Microemulsion synthesis of iron core/iron oxide shell magnetic nanoparticles and their physicochemical properties. *MRS Online Proceedings Library (OPL)*, 1416. Available: https://www.ncbi.nlm.nih.gov/pmc/articles/PMC4633094/ (Accessed 15 December 2021).

Khan, A. U., Chen, L. and Ge, G. 2021a. Recent development for biomedical applications of magnetic nanoparticles. *Inorganic Chemistry Communications*: 108995.

Khan, S., Naushad, M., Al-Gheethi, A. and Iqbal, J. 2021b. Engineered nanoparticles for removal of pollutants from wastewater: Current status and future prospects of nanotechnology for remediation strategies. *Journal of Environmental Chemical Engineering*, 9: 106160.

Khan, S., Naushad, M., Lima, E. C., Zhang, S., Shaheen, S. M. and Rinklebe, J. 2021c. Global soil pollution by toxic elements: Current status and future perspectives on the risk

assessment and remediation strategies–A review. *Journal of hazardous materials*, 417: 126039.

Khan, S., Sengul, H. and Dan, Z. 2018. Transport of TiO2 nanoparticles and their effects on the mobility of Cu in soil media. *salination and Water Treatment*, 131: 230-237.

Khannous, L., Abid, D., Gharsallah, N., Kechaou, N. and Mihoub, N. B. 2011. Optimization of coagulation-flocculation process for pastas industry effluent using response surface methodology. *African Journal of Biotechnology*, 10 (63): 13823-13834.

Khettaf, S., Khounı, I., Louhichi, G., Ghrabi, A., Bousselmi, L., Bouhidel, K.-E. and Bouhelassa, M. 2021. Optimization of coagulation-flocculation process in the treatment of surface water for a maximum dissolved organic matter removal using RSM approach. *Water Supply*, 21 (6): 3042–3056.

Khiadani, M., Kolivand, R., Ahooghalandari, M. and Mohajer, M. 2014. Removal of turbidity from water by dissolved air flotation and conventional sedimentation systems using poly aluminum chloride as coagulant. *Desalination and Water Treatment*, 52 (4-6): 985-989.

Khouni, I., Louhichi, G., Ghrabi, A. and Moulin, P. 2020. Efficiency of a coagulation/flocculation–membrane filtration hybrid process for the treatment of vegetable oil refinery wastewater for safe reuse and recovery. *Process Safety and Environmental Protection*, 135: 323-341.

Khoza, P. B., Moloto, M. J. and Sikhwivhilu, L. M. 2012. The effect of solvents, acetone, water, and ethanol, on the morphological and optical properties of ZnO nanoparticles prepared by microwave. *Journal of Nanotechnology*, 2012

Khui, P. N., Rahman, M. R., Kuok, K. K., Bakri, M. B., Adamu, M., Tazeddinova, D., Kazhmukanbetkyzy, Z. A. and Torebek, B. 2021. Small-size jatropha seed biochar extracted from microwave pyrolysis: Optimization of its biocomposites mechanical properties by mixture design. *BioResources*, 16 (3): 4716.

Khuntia, S., Majumder, S. K. and Ghosh, P. 2012. Microbubble-aided water and wastewater purification: a review. *Reviews in Chemical Engineering*, 28 (4-6): 191-221.

Kildeeva, N., Chalykh, A., Belokon, M., Petrova, T., Matveev, V., Svidchenko, E., Surin, N. and Sazhnev, N. 2020. Influence of genipin crosslinking on the properties of chitosan-based films. *Polymers*, 12 (5): 1086.

Kim, D. K., Mikhaylova, M., Zhang, Y. and Muhammed, M. 2003. Protective coating of superparamagnetic iron oxide nanoparticles. *Chemistry of Materials*, 15 (8): 1617-1627.

King, J. and Pienaar, H. 2011. Sustainable use of South Africa's inland waters: a situation assessment of Resource Directed Measures 12 years after the 1998 National Water Act. Available: http://researchspace.csir.co.za/dspace/handle/10204/12429 (Accessed 25 Junue 2020).

Kitimasak, W., Thirakhupt, K. and Moll, D. L. 2003. Eggshell structure of the siamese narrow-headed softshell turtle Chitra chitra Nutphand, 1986 (Testudines: Trionychidae). *Science Asia*, 29: 95-98.

Kizil, R., Irudayaraj, J. and Seetharaman, K. 2002. Characterization of irradiated starches by using FT-Raman and FTIR spectroscopy. *Journal of agricultural and food chemistry*, 50 (14): 3912-3918.

Kocabas, B. B. and Satir, I. T. 2019. Investigation of the chitosan immobilized eggshell for the biosorption of brillant blue R dye. *Hittite Journal of Science and Engineering*, 6 (4): 287-295.

Kolasinski, K. 2021. Photochemical and nonthermal chemical modification of porous silicon. In: *Porous Silicon for Biomedical Applications*. Elsevier, 51-112.

Kombaya-Touckia-Linin, E.-M., Gaucel, S., Sougrati, M. T., Khederlou, K., Pen, N., Stievano, L., Gontard, N. and Guillard, V. 2019. Hybrid iron montmorillonite nano-particles as an oxygen scavenger. *Chemical Engineering Journal*, 357: 750-760.

Kristanda, J., Sintiago, K. S., Kristianto, H., Prasetyo, S. and Sugih, A. K. 2021. Optimization study of Leucaena leucocephala seed extract as natural coagulant on decolorization of aqueous Congo red solutions. *Arabian Journal for Science & Engineering (Springer Science & Business Media BV)*, 46 (7): 6275–6286.

Kristianto, H., Tanuarto, M. Y., Prasetyo, S. and Sugih, A. K. 2020. Magnetically assisted coagulation using iron oxide nanoparticles-Leucaena leucocephala seeds' extract to treat synthetic Congo red wastewater. *International Journal of Environmental Science and Technology*, 17: 3561-3570.

Krithiga, G. and Sastry, T. P. 2011. Preparation and characterization of a novel bone graft composite containing bone ash and egg shell powder. *Bulletin of Materials Science*, 34 (1): 177-181.

Kulpa, O., Marwizi, T. S. and Kulpa, P. K. 2018. Optimisation of biodiesel production from dairy efuent scum using calcined egg shell as a transesterifcation catalyst. *SN Applied Sciences*, 3: 247.

Kumar, M. M., Karthikeyan, R., Anbalagan, K. and Bhanushali, M. N. 2016. Coagulation process for tannery industry effluent treatment using Moringa oleifera seeds protein: Kinetic study, pH effect on floc characteristics and design of a thickener unit. *Separation Science and Technology*, 51 (12): 2028-2037.

Kumar, P., Prakash, K. S., Jan, K., Swer, T. L., Jan, S., Verma, R., Deepika, K., Dar, M. Z., Verma, K. and Bashir, K. 2017a. Effects of gamma irradiation on starch granule structure and physicochemical properties of brown rice starch. *Journal of cereal science*, 77: 194-200.

Kumar, P. R., Chaudhari, S., Khilar, K. C. and Mahajan, S. P. 2004. Removal of arsenic from water by electrocoagulation. *Chemosphere*, 55 (9): 1245-1252.

Kumar, S. and Koh, J. 2012. Physiochemical, Optical and Biological Activity of Chitosan-Chromone Derivative for Biomedical Applications. *International Journal of Molecular Sciences*, 13: 6102-6116.

Kumar, S., Singh, R., Singh, T. and Batish, A. 2021a. Investigations for magnetic properties of PLA-PVC-Fe3O4-wood dust blend for self-assembly applications. *Journal of Thermoplastic Composite Materials*, 34 (7): 929-951.

Kumar, V., Al-Gheethi, A., Asharuddin, S. M. and Othman, N. 2021b. Potential of cassava peels as a sustainable coagulant aid for institutional wastewater treatment: Characterisation, optimisation and techno-economic analysis. *Chemical Engineering Journal*, 420: 127642.

Kumar, V., Othman, N. and Asharuddin, S. 2017b. Applications of natural coagulants to treat wastewater− a review. In: Proceedings of *MATEC Web of Conferences*. EDP Sciences, 06016.

Kurnia, K., Kaseside, M. and Iwamony, S. 2021. Study Microstructure of Fe3O4 Modification Using PEG 4000 form Iron Sand at Wari Ino Beach As A Biosensor Application. *Indo. J. Chem. Res.*, 8 (3): 168-171.

Kurniawan, S. B., Abdullah, S. R. S., Imron, M. F., Said, N. S. M., Ismail, N. I., Hasan, H. A., Othman, A. R. and Purwanti, I. F. 2020. Challenges and opportunities of biocoagulant/bioflocculant application for drinking water and wastewater treatment and its potential for sludge recovery. *International journal of environmental research and public health*, 17 (24): 9312.

Kyzas, G. Z., Mitropoulos, A. C. and Matis, K. A. 2021. From microbubbles to nanobubbles: Effect on flotation. *Processes*, 9 (8): 1287.

Lakshmanan, R., Okoli, C., Boutonnet , M., Järås , S. and Rajarao, G. K. 2013. Effect of magnetic iron oxide nanoparticles in surface water treatment: Trace minerals and microbes. *Bioresource technology*, 129: 612-615.

Lauterborn, W. and Mettin, R. 2015. Acoustic cavitation: Bubble dynamics in high-power ultrasonic fields. In: *Power Ultrasonics*. Elsevier, 37-78.

Lee, C. S., Robinson, J. and Chong, M. F. 2014. A review on application of flocculants in wastewater treatment. *Process Safety and Environmental Protection*, 92 (6): 489-508.

Lester, E., Blood, P., Denyer, J., Giddings, D., Azzopardi, B. and Poliakoff, M. 2006. Reaction engineering: The supercritical water hydrothermal synthesis of nano-particles. *The Journal of Supercritical Fluids*, 37 (2): 209-214.

Levitsky, I., Tavor, D. and Gitis, V. 2022. Micro and nanobubbles in water and wastewater treatment: A state-of-the-art review. *Journal of Water Process Engineering*, 47: 102688.

Li, B.-x., Wang, W.-c., Zhang, X.-p., Zhang, D.-x., Mu, W. and Liu, F. 2017. Integrating uniform design and response surface methodology to optimize thiacloprid suspension. *Scientific Reports*, 7 (1): 1-9.

Li, F., Yang, H., Zhuo, Q., Zhou, D., Wu, X., Zhang, P., Yao, Z. and Sun, L. 2021a. A Cobalt@ Cucurbit [5] uril Complex as a Highly Efficient Supramolecular Catalyst for Electrochemical and Photoelectrochemical Water Splitting. *Angewandte Chemie*, 133 (4): 2004-2013.

Li, J., Lan, X., Lei, S., Ou-Yang, J., Yang, X. and Zhu, B. 2019. Effects of carbon nanotube thermal conductivity on optoacoustic transducer performance. *Carbon*, 145: 112-118.

Li, J., Wang, J., Li, J., Yang, X., Wan, J., Zheng, C., Du, Q., Zhou, G. and Yang, X. 2021b. Fabrication of Fe3O4@ PVA microspheres by one-step electrospray for magnetic resonance imaging during transcatheter arterial embolization. *Acta Biomaterialia*, 131: 532-543.

Li, N., Hu, Y., Lu, Y.-Z., Zeng, R. J. and Sheng, G.-P. 2016. Multiple response optimization of the coagulation process for upgrading the quality of effluent from municipal wastewater treatment plant. *Scientific Reports*, 6 (1): 1-13.

Li, X.-q., Elliott, D. W. and Zhang, W.-x. 2006. Zero-valent iron nanoparticles for abatement of environmental pollutants: materials and engineering aspects. *Critical reviews in solid state and materials sciences*, 31 (4): 111-122.

Li, X., Wang, C., Zhang, J., Liu, J., Liu, B. and Chen, G. 2020. Preparation and application of magnetic biochar in water treatment: A critical review. *Science of the Total Environment*, 711: 134847.

Li, Y., Deng, M., Wang, X., Wang, Y., Li, J., Xia, S. and Zhao, J. 2021c. In-situ remediation of oxytetracycline and Cr (VI) co-contaminated soil and groundwater by using blast furnace slag-supported nanosized Fe0/FeSx. *Chemical Engineering Journal*, 412: 128706.

Lim, I., Lee, E., Park, H.-U., Jang, J., Jung, N., Yang, T.-H., Yim, S.-D. and Park, G.-G. 2021. Sonochemical gram-scale synthesis of core–shell PdCo@ Pt nanoparticle and investigation of post heat-treatment effect for various gas atmospheres. *Journal of alloys and compounds*, 879: 160441.

Lim, J.-M., Swami, A., Gilson, L. M., Chopra, S., Choi, S., Wu, J., Langer, R., Karnik, R. and Farokhzad, O. C. 2014. Ultra-high throughput synthesis of nanoparticles with homogeneous size distribution using a coaxial turbulent jet mixer. *ACS nano*, 8 (6): 6056-6065.

Lin, C.-L., Lee, C.-F. and Chiu, W.-Y. 2005. Preparation and properties of poly (acrylic acid) oligomer stabilized superparamagnetic ferrofluid. *Journal of Colloid and Interface Science*, 291 (2): 411-420.

Lin, Q.-l., Xiao, H.-x., Fu, X.-j., Wei, T., Li, L.-h. and Yu, F.-x. 2011. Physico-chemical properties of flour, starch, and modified starch of two rice varieties. *Agricultural sciences in China*, 10 (6): 960-968.

Liu, A. and Zhang, W.-x. 2014. Fine structural features of nanoscale zero-valent iron characterized by spherical aberration corrected scanning transmission electron microscopy (Cs-STEM). *Analyst*, 139 (18): 4512-4518.

Liu, C., Luan, P., Li, Q., Cheng, Z., Xiang, P., Liu, D., Hou, Y., Yang, Y. and Zhu, H. 2020. Biopolymers derived from trees as sustainable multifunctional materials: a review. *Advanced Materials*: 2001654.

Liu, P., Yao, Z., Ng, V. M. H., Zhou, J., Kong, L. B. and Yue, K. 2018. Facile synthesis of ultrasmall Fe3O4 nanoparticles on MXenes for high microwave absorption performance. *Composites Part A: Applied Science and Manufacturing*, 115: 371-382.

Liu, Z., Huang, M., Li, A. and Yang, H. 2017. Flocculation and antimicrobial properties of a cationized starch. *Water research (Oxford)*, 119: 57-66.

Lombi, E., Donner, E., Tavakkoli, E., Turney, T. W., Naidu, R., Miller, B. W. and Scheckel, K. G. 2012. Fate of zinc oxide nanoparticles during anaerobic digestion of wastewater and post-treatment processing of sewage sludge. *Environmental science & technology*, 46 (16): 9089-9096.

Louhichi, G., Bousselmi, L., Ghrabi, A. and Khouni, I. 2019. Process optimization via response surface methodology in the physico-chemical treatment of vegetable oil refinery wastewater. *Environmental Science and Pollution Research*, 26: 18993–19011.

Lozano-Navarro, J. I., Díaz-Zavala, N. P., Velasco-Santos, C., Melo-Banda, J. A., Páramo-García, U., Paraguay-Delgado, F., García-Alamilla, R., Martínez-Hernández, A. L. and Zapién-Castillo, S. 2018. Chitosan-starch films with natural extracts: Physical, chemical, morphological and thermal properties. *Materials*, 11 (1): 120.

Luna Vera, F., Guancha Chalapud, M., Castillo Viveros, I. and Vásquez Medina, E. A. 2018. From eggshells to quicklime: using carbonate cycle as an integrating concept to introduce students to materials analysis by TGA and FTIR. *Journal of Chemical Education*, 95 (4): 625-630.

Lupi, F. R., Franco, G., Baldino, N. and Gabriele, D. 2020. The effect of operating conditions on the physicochemical characteristics of whey protein–based systems. *Rheologica Acta*, 59 (4): 227-238.

Machado, S., Pacheco, J., Nouws, H., Albergaria, J. and Delerue-Matos, C. 2017. Green zero-valent iron nanoparticles for the degradation of amoxicillin. *International Journal of Environmental Science and Technology*, 14 (5): 1109-1118.

Machala, L., Zboril, R. and Gedanken, A. 2007. Amorphous iron (III) oxide a review. *The Journal of Physical Chemistry B*, 111 (16): 4003-4018.

Madhura, L., Singh, S., Kanchi, S., Sabela, M. and Bisetty, K. 2019. Nanotechnology-based water quality management for wastewater treatment. *Environmental Chemistry Letters*, 17 (1): 65-121.

Mahmoud, E. K. 2009. Chemically enhanced primary treatment of textile industrial effluents. *Polish Journal of Environmental Studies*, 18 (4): 651-655.

Maiga, D. T., Nyoni, H., Nkambule, T. T., Mamba, B. B. and Msagati, T. A. M. 2020. Impact of zinc oxide nanoparticles in aqueous environments: Influence of concentrations, natural organic matter and ionic strength. *Inorganic and Nano-Metal Chemistry*, 50 (8): 680-692.

Majewski, P. and Thierry, B. 2007. Functionalized magnetite nanoparticles—synthesis, properties, and bio-applications. *Critical Reviews in Solid State and Materials Sciences*, 32 (3-4): 203-215.

Majumdar, D. 2019. Ultrasound-Assisted Synthesis, Exfoliation and Functionalisation of Graphene Derivatives. In: *Graphene Functionalization Strategies*. Springer, 63-103.

Makarova, T. 2005. Unconventional magnetism in carbon based materials. In: *Frontiers in magnetic materials*. Springer, 209-246.

Maksoud, M. A., Elgarahy, A. M., Farrell, C., Ala'a, H., Rooney, D. W. and Osman, A. I. 2020. Insight on water remediation application using magnetic nanomaterials and biosorbents. *Coordination Chemistry Reviews*, 403: 213096.

Maneeprakorn, W., Maurizi, L., Siriket, H., Wutikhun, T., Dharakul, T. and Hofmann, H. 2017. Superparamagnetic nanohybrids with cross-linked polymers providing higher in vitro stability. *Journal of Materials Science*, 52 (16): 9249-9261.

Mansoori, S., Davarnejad, R., Matsuura, T. and Ismail, A. F. 2020. Membranes based on non-synthetic (natural) polymers for wastewater treatment *Polymers Testing*, 84: 106381.

Martins, F., Machado, S., Albergaria, T. and Delerue-Matos, C. 2017. LCA applied to nano scale zero valent iron synthesis. *The International Journal of Life Cycle Assessment*, 22 (5): 707-714.

Mascolo, M. C., Pei, Y. and Ring, T. A. 2013. Room temperature co-precipitation synthesis of magnetite nanoparticles in a large pH window with different bases. *Materials*, 6: 5549-5567.

Massart, R. and Cabuil, V. 1987. Synthèse en milieu alcalin de magnétite colloïdale: contrôle du rendement et de la taille des particules. *Journal de chimie physique*, 84: 967-973.

Massoumi, B., Mozaffari, Z. and Jaymand, M. 2018. A starch-based stimuli-responsive magnetite nanohydrogel as de novo drug delivery system. *International journal of biological macromolecules*, 117: 418-426.

Materón, E. M., Miyazaki, C. M., Carr, O., Joshi, N., Picciani, P. H., Dalmaschio, C. J., Davis, F. and Shimizu, F. M. 2021. Magnetic nanoparticles in biomedical applications: A review. *Applied Surface Science Advances*, 6: 100163.

Mateus, G. A. P., dos Santos, T. R. T., Sanches, I. S., Silva, M. F., de Andrade, M. B., Paludo, M. P., Gomes, R. G. and Bergamasco, R. 2018a. Evaluation of a magnetic coagulant based on Fe3O4 nanoparticles and Moringa oleifera extract on tartrazine removal: coagulation-adsorption and kinetics studies. *Environmental Technology*, 41 (13): 1-16.

Mateus, G. A. P., Paludo, M. P., dos Santos, T. R. T., Silva, M. F., Nishi, L., Fagundes-Klen, M. R., Gomes, R. G. and Bergamasco, R. 2018b. Obtaining drinking water using a

magnetic coagulant composed of magnetite nanoparticles functionalized with Moringa oleifera seed extract. *Journal of environmental chemical engineering*, 6 (4): 4084-4092.

Matilainen, A., Vepsäläinen, M. and Sillanpää, M. 2010. Natural organic matter removal by coagulation during drinking water treatment: A review. *Advances in colloid and interface science*, 159: 189-197.

Matmin, J., Affendi, I., Ibrahim, S. I. and Endud, S. 2018. Additive-free rice starch-assisted synthesis of spherical nanostructured hematite for degradation of dye contaminant. *Nanomaterials*, 8 (9): 702.

Matusiak, J., Grządka, E. and Bastrzyk, A. 2021. Removal of hazardous oxide nanoparticles by the biopolymer flocculation in the presence of divalent salt. *Chemical Engineering Journal*, 423: 130264.

McCloy, J. S. 2019. Spin and Ferroic Glasses. In: *Springer Handbook of Glass*. Springer, 687-718.

McKenzie, T. G., Karimi, F., Ashokkumar, M. and Qiao, G. G. 2019. Ultrasound and sonochemistry for radical polymerization: sound synthesis. *Chemistry–A European Journal*, 25 (21): 5372-5388.

Mecha, A. C., Onyango, M. S., Ochieng, A., Fourie, C. J. S. and Momba, M. N. B. 2016. Synergistic effect of UV–vis and solar photocatalytic ozonation on the degradation of phenol in municipal wastewater: A comparative study. *Journal of Catalysis*, 341: 116-125.

Meyer, E. E., Lin, Q. and Israelachvili, J. N. 2005. Effects of dissolved gas on the hydrophobic attraction between surfactant-coated surfaces. *Langmuir*, 21 (1): 256-259.

Mine, Y. 2007. Egg proteins and peptides in human health-chemistry, bioactivity and production. *Current Pharmaceutical Design*, 13 (9): 875-884.

Miyashiro, C. S., Mateus, G. A. P., da Santos, T. R. T., Paludo, M. P., Bergamasco, R. and Fagundes-Klena, M. T. 2021. Synthesis and performance evaluation of a magnetic biocoagulant in the removal of reactive black 5 dye in aqueous medium. *Materials Science & Engineering C*, 119: 111523.

Moerland, C., Van IJzendoorn, L. and Prins, M. 2019. Rotating magnetic particles for lab-on-chip applications–a comprehensive review. *Lab on a Chip*, 19 (6): 919-933.

Mohammad, A.-T., Abdulhameed, A. S. and Jawad, A. H. 2019. Box-Behnken design to optimize the synthesis of new crosslinked chitosan-glyoxal/TiO2 nanocomposite: methyl orange adsorption and mechanism studies. *International journal of biological macromolecules*, 129: 98-109.

Mohammadi, M.-R., Ansari, S., Bahmaninia, H., Ostadhassan, M., Norouzi-Apourvari, S., Hemmati-Sarapardeh, A., Schaffie, M. and Ranjbar, M. 2021. Experimental Measurement and Equilibrium Modeling of Adsorption of Asphaltenes from Various Origins onto the Magnetite Surface under Static and Dynamic Conditions. *ACS omega*, 6 (37): 24256-24268.

Mohanasrinivasan, V., Paliwal, J. S., Selvarajan, E., Mishra, M., Singh, S. K., Suganthi, V. and Devi, C. S. 2013. Studies on heavy metal removal efficiency and antibacterial activity of chitosan prepared from shrimp shell waste. *Biotechnology*, 4 (2): 167 - 175.

Mohd-Salleh, S. N. A., Mohd-Zin, N. S. and Othman, N. 2019. A review of wastewater treatment using natural material and its potential as aid and composite coagulant. *Sains Malays*, 48 (1): 155-164.

Mokonyama, S., Schalkwyk, M. and Rajagopaul, R. 2017. *Guidelines and good practices for water treatment residues handling, disposal and reuse in South Africa*. Available: http://www.wrc.org.za/wp-content/uploads/mdocs/TT738.pdf (Accessed 15 November 2021).

Momba, M., Obi, C. L. and Thompson, P. 2009. Survey of disinfection efficiency of small drinking water treatment plants: Challenges facing small water treatment plants in South Africa. *Water SA*, 35 (4): 485-494.

Momeni, M. M., Kahforoushan, D., Abbasi, F. and Ghanbarian, S. 2018. Using chitosan/CHPATC as coagulant to remove color and turbidity of industrial wastewater: optimization through RSM design. *Journal of environmental management*, 211: 347-355.

Morales, M. d. P., Veintemillas-Verdaguer, S., Montero, M., Serna, C., Roig, A., Casas, L., Martinez, B. and Sandiumenge, F. 1999. Surface and internal spin canting in γ-Fe2O3 nanoparticles. *Chemistry of Materials*, 11 (11): 3058-3064.

Moreno-Azanza, M., Bauluz, B., Canudo, J. I., Gasca, J. M. and Fernández-Baldor, F. T. 2016. Combined use of electron and light microscopy techniques reveals false secondary shell units in Megaloolithidae eggshells. *PLoS ONE*, 11 (5): e0153026.

Morozova, A. and Eskin, A. 2017. Centrifugal pump effect on average particle diameter of oil-water emulsion. In: Proceedings of *IOP Conference Series: Materials Science and Engineering*. IOP Publishing, 012215.

Morsi, R. E., Al-Sabagh, A. M., Moustafa, Y. M., ElKholy, S. G. and Sayed, M. S. 2018. Polythiophene modified chitosan/magnetite nanocomposites for heavy metals and selective mercury removal. *Egyptian journal of petroleum*, 27 (4): 1077-1085.

Moruzzi, R., de Oliveira, A. and Almeida, T. d. 2018. Fractal aggregates evolution during flocculation. *Brazilian Journal of Chemical Engineering*, 35: 1203-1210.

Mosaddegh, E. and Hassankhani, A. 2013. Application and characterization of eggshell as a new biodegradable and heterogeneous catalyst in green synthesis of 7,8-dihydro-4H-chromen-5(6H)-ones. *Catalysis Communications*, 33: 70-75.

Mosaddeghi, M. R., Pajoum Shariati, F., Vaziri Yazdi, S. A. and Nabi Bidhendi, G. 2020. Application of response surface methodology (RSM) for optimizing coagulation process of paper recycling wastewater using Ocimum basilicum. *Environmental Technology*, 41 (1): 100-108.

Mosisa, B., Belete, A. and Gebre‐Mariam, T. 2021. Isolation and Physico‐chemical Characterization of Triticum Decocum Starch. *Starch‐Stärke*: 2000226.

Mu, H., Chen, Y. and Xiao, N. 2011. Effects of metal oxide nanoparticles (TiO2, Al2O3, SiO2 and ZnO) on waste activated sludge anaerobic digestion. *Bioresource technology*, 102 (22): 10305-10311.

Muhammad, S. S. S. B. I. 2014. *Treatment of food processing industrial wastewater using two stages anaerobic system*. Malaysia: Universiti Tun Hussein Onn Malaysia, Faculty of Civil and Environmental Engineering. Available: https://ozhen.co/wp-content/uploads/2019/11/%D8%AA%D8%B5%D9%81%DB%8C%D9%87-%D9%81%D8%A7%D8%B6%D9%84%D8%A7%D8%A8-%D8%B5%D9%86%D8%B9%D8%AA%DB%8C-%D9%81%D8%B1%D8%A2%D9%88%D8%B1%DB%8C-%D9%85%D9%88%D8%A7%D8%AF-%D8%BA%D8%B0%D8%A7%DB%8C%DB%8C-%D8%A8%D8%A7-%D8%A7%D8%B3%D8%AA%D9%81%D8%A7%D8%AF%D9%87-%D8%A7%D8%B2-%D8%B3%DB%8C%D8%B3%D8%AA%D9%85-%D8%A8%DB%8C-%D9%87%D9%88%D8%A7%D8%B2%DB%8C-%D8%AF%D9%88-%D9%85%D8%B1%D8%AD%D9%84%D9%87-%D8%A7%DB%8C.pdf (Accessed 14 June 2020).

Mukandi, M., Basitere, M., Okeleye, B., Chidi, B., Ntwampe, S. and Thole, A. 2021. Influence of diffuser design on selected operating variables for wastewater flotation systems: a review. *Water Practice & Technology*, 16 (4): 1049-1066.

Mukherjee, S. 2011. Special Mineral Properties And Related Structures. In: *Applied Mineralogy*. Springer, 136-154.

Muniz, G. L., Borges, A. C. and da Silva, T. C. F. 2020. Performance of natural coagulants obtained from agro-industrial wastes in dairy wastewater treatment using dissolved air flotation. *Journal of water process engineering*, 37: 101453.

Muniza, G. L., Borges, A. C., da Silva, T. C. F., Batista, R. O. and de Castro, S. R. 2020. Chemically enhanced primary treatment of dairy wastewater using chitosan obtained from shrimp wastes: optimization using a Doehlert matrix design. *Environmental Technology*: 1-18.

Muro Cruces, J. 2020. *Improved synthesis routes and coating approaches of anisotropic magnetite nanoparticles for theranostics*. Universitat Autònoma de Barcelona. Available: https://www.tdx.cat/handle/10803/669374 (Accessed 16 July 2021).

Muscas, G., Yaacoub, N. and Peddis, D. 2018. Magnetic disorder in nanostructured materials. In: *Novel Magnetic Nanostructures*. Elsevier, 127-163.

Nadejde, C., Neamtu, M. and Creanga, D. 2015. Environment-friendly magnetic fluids for wastewater remediation-Synthesis and characterization. *Acta Physica Polonica A*, 127 (2): 647-649.

Naghizadeh , M., Mohammadi, P., Sheibani, H. and Taher, M. A. 2017. Synthesis of Fe3O4/Eggshell nanocomposite and application for preparation of tetrahydrobenzo[b]pyran derivatives. *Iranian Journal of Energy & Environment*, 8 (2): 136-141.

Namgung, S. and Lee, G. 2021. Rhodochrosite oxidation by dissolved oxygen and the formation of Mn Oxide product: The impact of Goethite as a foreign solid substrate. *Environmental science & technology*, 55: 14436–14444.

Nanda, T., Rathore, A. and Sharma, D. 2020. Biomineralized and chemically synthesized magnetic nanoparticles: A contrast. *Frontiers of Materials Science*: 1-15.

Nath, A., Mishra, A. and Pande, P. P. 2020. A review natural polymeric coagulants in wastewater treatment. *Materials Today: Proceedings*, (46): 6113-6117.

Nechita, P. 2017. Applications of chitosan in wastewater treatment. *Biological activities and application of marine polysaccharides*, 1: 209-228.

Nelson, N. R., Port, J. D. and Pandey, M. K. 2020. Use of Superparamagnetic Iron Oxide Nanoparticles (SPIONs) via Multiple Imaging Modalities and Modifications to Reduce Cytotoxicity: An Educational Review. *Journal of Nanotheranostics*, 1 (1): 105-135.

Neuberger, T., Schöpf, B., Hofmann, H., Hofmann, M. and Von Rechenberg, B. 2005. Superparamagnetic nanoparticles for biomedical applications: possibilities and limitations of a new drug delivery system. *Journal of magnetism and magnetic materials*, 293 (1): 483-496.

Ng, M. H. and Elshikh, M. S. 2021. Utilization of Moringa oleifera as Natural Coagulant for Water Purification. *Industrial and Domestic Waste Management*, 1 (1): 1-11.

Ngah, W. S., Endud, C. S. and Mayanar, R. 2002. Removal of copper(II) ions from aqueous solution onto chitosan and cross-linked chitosan beads. *Reactive & Functional Polymers*, 50: 181-190.

Ngwena, C. 2003. Equity and the development of the South African health care system: from the Public Health Act of 1919 to the present day. *Fundamina: A Journal of Legal History*, 2003 (9): 124-133.

Nharingo, T., Zivurawa, M. T. and Guyo, U. 2015. Exploring the use of cactus opuntia ficus indica in the biocoagulation–flocculation of Pb(II) ions from wastewaters. *International Journal of Environmental Science and Technology*, 12 (12): 3791-3802.

Ni, J., Yang, B., Jia, F., She, Y., Song, S. and Quintana, M. 2018. Theoretical investigation of the sensing mechanism of the pure graphene and AL, B, N, P doped mono-vacancy graphene-based methane. *Chemical Physics Letters*, 710: 221-225.

Ni'am , M. F. 2006. Combined magnetic field and electrocoagulation process for suspended solid removal from wastewater. In: Othman, F., Sohaili, J. and Fauzia, Z. eds. Proceedings of *1st International Conference on Natural Resources Engineering & Technology*. Putrajaya, Malaysia, July 2006. Universitas Islam Sultan Agung, 384-393.

Nikfar, M. H., Parsaeian, H., Amani Tehrani, A., Kouhestani, A., Masoumi Isfahani, H. and Bazargan, A. 2021. A two-stage dissolved air flotation saturator configuration for significant microbubble improvement. *Environmental Technology*, : 1-25.

Nimesha, S., Hewawasam, C., Jayasanka, D., Murakami, Y., Araki, N. and Maharjan, N. 2021. Effectiveness of natural coagulants in water and wastewater treatment. *Global Journal of Environmental Science and Management*, 8 (1): 1-16.

Nizamuddin, S., Siddiqui, M., Mubarak, N., Baloch, H. A., Abdullah, E., Mazari, S. A., Griffin, G., Srinivasan, M. and Tanksale, A. 2019. Iron oxide nanomaterials for the removal of heavy metals and dyes from wastewater. *Nanoscale materials in water purification*: 447-472.

Nnaji, N. J. N., Ani, J. U., Aneke, L. E., Onukwuli, O. D., Okoro, U. C. and Ume, J. I. 2014. Modelling the coag-flocculation kinetics of cashew nut testa tannins in an industrial effluent. *Journal of Industrial and Engineering Chemistry*, 20 (4): 1930-1935.

Nocera, F. and Gardoni, P. 2022. Selection of the modeling resolution of infrastructure. *Computer‐Aided Civil and Infrastructure Engineering*,. Available: https://onlinelibrary.wiley.com/doi/full/10.1111/mice.12807?casa_token=6Xp-o-K6VTAAAAAA%3AwMKOlo5zVW2sGK0hgngKaSR1S-k7kjkcFYXu18v57lLkDgcXJjJng5JyVGpzYlrgSIFa-sscGHwYN_w (Accessed 15 May 2022).

Noor, M. H. M., Lee, W. J., Azli, M. F. Z. i. M., Ngadi, N. and Mohamed, M. 2021. Moringa oleifera extract as green coagulant for POME Treatment: Preliminary studies and sludge evaluation. *Materials Today: Proceedings*, 46: 1940-1947.

Nys, Y. and Le Roy, N. 2018. Calcium homeostasis and eggshell biomineralization in female chicken. In: *Vitamin D*. Elsevier, 361-382. Available: https://www.sciencedirect.com/science/article/pii/B9780128099650000227 (Accessed 4 January 2022).

Ødegaard, H., Østerhus, Melin, S. E. and Eikebrokk, B. 2010. NOM removal technologies – Norwegian experiences. *Drinking water engineering and science*, 3 (1): 1-9.

Oke, E. O., Araromi, D. O., Jimoda, L. A. and Adetayo Adeniran, J. 2019. Kinetics and neuro-fuzzy soft computing modelling of river turbid water coag-flocculation using mango (Mangifera indica) kernel coagulant. *Chemical Engineering Communications*, 206 (2): 254-267.

Okoli, C., Boutonnet, M., Järås, S. and Rajarao-Kuttuva, G. 2012. Protein-functionalized magnetic iron oxide nanoparticles: time efficient potential-water treatment. *Nanotechnology for Sustainable Development*: 127-135.

Okoli, C., Fornara, A., Qin, J., Toprak, M. S., Dalhammar, G., Muhammed, M. and Rajarao, G. K. 2011. Characterization of Superparamagnetic Iron Oxide Nanoparticles and Its Application in Protein Purification. *Journal of Nanoscience and Nanotechnology*, 11 (11): 10201-10206.

Okpaegbe, U. and Maitera, O. 2021. Removal of Cd (Ii) And Mn (Ii) Ions from Aqueous Solution using Chitosan and Its Derivatives from Fish Scale 'Giwan Ruwa'(Lates Niloticus). *International Journal of Progressive Research in Science and Engineering*, 2 (8): 116-121.

Okubo, T., Akachi, S. and Hatta, H. 2018. Structure of hen eggs and physiology of egg laying. In: *Hen eggs*. CRC Press, 1-12.

Oladoja, N. A. 2015. Headway on natural polymeric coagulants in water and wastewater treatment operations. *Journal of water process engineering*, 6: 174-192.

Oladoja, N. A. 2016. Advances in the quest for substitute for synthetic organic polyelectrolytes as coagulant aid in water and wastewater treatment operations. *Sustainable Chemistry and Pharmacy*, 3: 47-58.

Oliveira, C., Rodrigues, R. T. and Rubio, J. 2014. Operating parameters affecting the formation of kaolin aerated flocs in water and wastewater treatment. *CLEAN–Soil, Air, Water*, 42 (7): 909-916.

Oliveira, P., Bini, R., Dias, G., Alcouffe, P., Santos, I., David, L. and Cótica, L. 2018. Magnetite nanoparticles with controlled sizes via thermal degradation of optimized PVA/Fe (III) complexes. *Journal of magnetism and magnetic materials*, 460: 381-390.

Omara, A. E.-D., Elsakhawy, T., Alshaal, T., El-Ramady, H., Kovács, Z. and Fári, M. 2019. Nanoparticles: a novel approach for sustainable agro-productivity. *Environment, Biodiversity and Soil Security*, 3 (2019): 29-62.

Ortiz-Oliveros, H. and Flores-Espinosa, R. 2019. Simultaneous removal of oil, total Co and 60 Co from radioactive liquid waste by dissolved air flotation. *International Journal of Environmental Science and Technology*, 16 (7): 3679-3686.

Othman, Z., Bhatia, S. and Ahmad, A. L. 2008. Influence of the settleability parameters for palm oil mill effluent pretreatment by using MoringaOleifera seeds as an environmental friendly coagulant. Paper presented at the *Interference conference on Environment*. Malaysia, 1-9.

Ouyang, Z.-W., Chen, E.-C. and Wu, T.-M. 2015. Thermal Stability and Magnetic Properties of Polyvinylidene Fluoride/Magnetite Nanocomposites. *Materials*, 8: 4553-4564.

Owens, F. J. and Poole Jr, C. P. 2008. *The physics and chemistry of nanosolids*. John Wiley & Sons.

Pal, S., Mal, D. and Singh, R. 2005. Cationic starch: an effective flocculating agent. *Carbohydrate polymers*, 59 (4): 417-423.

Palansooriya, K. N., Yang, Y., Tsang, Y. F., Sarkar, B., Hou, D., Cao, X., Meers, E., Rinklebe, J., Kim, K.-H. and Ok, Y. S. 2020. Occurrence of contaminants in drinking water sources and the potential of biochar for water quality improvement: A review. *Critical Reviews in Environmental Science and Technology*, 50 (6): 549-611.

Pambi, R. and Musonge, P. 2016. Application of response surface methodology (RSM) in the treatment of final effluent from the sugar industry using Chitosan. *WIT Transactions on Ecology and the Environment*, 209: 209-219.

Pandit, M., Sood, S., Mishra, P. and Khanna, P. 2021. Mathematical analysis of the effect of process parameters on angular distortion of MIG welded stainless steel 202 plates by using the technique of response surface Methodology. *Materials Today: Proceedings*, 41: 1045-1054.

Park, J.-I., Hong, Y., Jang, Y., Ha, M.-G., An, H.-R., Son, B., Choi, Y., Kim, H., Jeong, Y. and Lee, H. U. 2021. Efficient iron oxide/expanded graphite nanocomposites prepared by underwater plasma discharge for removing heavy metals. *Journal of Materials Research and Technology*, 14: 1884-1892.

Park, J., Lee, E., Hwang, N. M., Kang, M., Kim, S. C., Hwang, Y., Park, J. G., Noh, H. J., Kim, J. Y. and Park, J. H. 2005. One‐nanometer‐scale size‐controlled synthesis of monodisperse magnetic Iron oxide nanoparticles. *Angewandte Chemie*, 117 (19): 2932-2937.

Pascal, C., Pascal, J., Favier, F., Elidrissi Moubtassim, M. and Payen, C. 1999. Electrochemical synthesis for the control of γ-Fe2O3 nanoparticle size. Morphology, microstructure, and magnetic behavior. *Chemistry of Materials*, 11 (1): 141-147.

Pathak, S. 2020. Optimization of magneto-viscoelasticity of magnetic fluids and development of its applications in thermal and mechanical systems. RMIT University.

Patil-Sen, Y. and Chhabria, V. 2018. Superparamagnetic iron oxide nanoparticles for magnetic hyperthermia applications. In: *NanoBioMaterials*. CRC Press, 247-262.

Paudel, B. 2021. Epitaxial Strain, Electric Field, and Domains Controlled Functionality Modulations in Complex Oxide Heterostructures. New Mexico State University.

Pavon, C. 2019. Water Scarce Countries, Present and Future. Available: https://www.worlddata.io/blog/water-stressed-countries-present-and-future (Accessed 24 September 2021).

Peeters, K., Lespes, G., Zuliani, T., Ščančar, J. and Milačič, R. 2016. The fate of iron nanoparticles in environmental waters treated with nanoscale zero-valent iron, FeONPs and Fe3O4NPs. *Water research*, 94: 315-327.

Petcharoen, K. and Sirivat, A. 2012. Synthesis and characterization of magnetite nanoparticles via the chemical co-precipitation method. *Materials Science and Engineering: B*, 177 (5): 421-427.

Phenrat, T. and Lowry, G. V. 2019a. Electromagnetic induction of nanoscale zerovalent iron for enhanced thermal dissolution/desorption and dechlorination of chlorinated volatile organic compounds. In: *Nanoscale Zerovalent Iron Particles for Environmental Restoration*. Springer, 415-434.

Phenrat, T., Lowry, G. V. and Babakhani, P. 2019b. Nanoscale zerovalent iron (NZVI) for environmental decontamination: a brief history of 20 years of research and field-scale application. *Nanoscale Zerovalent Iron Particles for Environmental Restoration*: 1-43.

Plachy, T., Rohrer, P. and Holcapkova, P. 2021. Gelatine-Coated Carbonyl Iron Particles and Their Utilization in Magnetorheological Suspensions. *Materials*, 14 (10): 2503.

Počuča-Nešić, M., Marinković-Stanojević, Z., Cotič-Smole, P., Dapčević, A., Tasić, N., Branković, G. and Branković, Z. 2019. Processing and properties of pure antiferromagnetic h-YMnO3. *Processing and Application of Ceramics*, 13 (4): 427-434.

Pokhrel, D. and Viraraghavan, T. 2004. Treatment of pulp and paper mill wastewater—a review. *The Science of the total environment*, 333 (1-3): 37-58.

Pokhrel, N., Vabbina, P. K. and Pala, N. 2016. Sonochemistry: Science and Engineering. *Ultrasonics sonochemistry*, 29: 104-128.

Polichetti, M., Modestino, M., Galluzzi, A., Pace, S., Iuliano, M., Ciambelli, P. and Sarno, M. 2020. Influence of citric acid and oleic acid coating on the dc magnetic properties of Fe3O4 magnetic nanoparticles. *Materials Today: Proceedings*, 20: 21-24.

Pradeep, N., Raju, A. U. and Venkataraman, U. 2021. Influence of probe amplitude on the preparation of graphene scroll by probe ultrasonicator technique. *Materials Today: Proceedings*, 45: 4012-4019.

Pradhan, A. K. and Sahoo, P. K. 2017. Synthesis and study of thermal, mechanical and biodegradation properties of chitosan-g-PMMA with chicken egg shell (nano-CaO) as a novel bio-filler. *Materials Science and Engineering: C*, 80: 149-155.

Prasetiyo, K. W., Hermawan, D., Hadi, Y. S., Amanda, P. and Kusumah, S. S. 2021. Utilization of water-soluble chitosan as a sizing agent incorporated in a paper composite: effects of pulp weight and water-soluble chitosan concentration. *Biomass Conversion and Biorefinery*: 1-12.

Pritchard, M., Craven, T., Mkandawire, T., Edmondson, A. S. and O'Neill, J. G. 2010. A comparison between Moringa oleifera and chemical coagulants in the purification of drinking water – An alternative sustainable solution for developing countries. *Physics and Chemistry of the Earth*, 35 (13-14): 798-805.

Prosper, O. E., Ugonabo, V. I., Okpala, L. C. and Nwokocha, G. F. 2021. Efficacy study of eggshell (ESC) and alum base coagulant (ABC) for the removal of total suspended solids (TSS) from cosmetics wastewater by coag-flocculation. Available: https://assets.researchsquare.com/files/rs-206327/v1_covered.pdf?c=1631855183 (Accessed 30 November 2021).

Pugazhendhi, A., Vasantharaj, S., Sathiyavimal, S., Raja, R. K., Karuppusamy, I., Narayanan, M., Kandasamy, S. and Brindhadevi, K. 2021. Organic and inorganic nanomaterial coatings for the prevention of microbial growth and infections on biotic and abiotic surfaces. *Surface and Coatings Technology*, 425: 127739.

Pujar, M. S., Hunagund, S. M., Barretto, D. A., Desai, V. R., Patil, S., Vootla, S. K. and Sidarai, A. H. 2020. Synthesis of cerium-oxide NPs and their surface morphology effect on biological activities. *Bulletin of Materials Science*, 43 (1): 1-10.

Pundir, C., Bhambi, M. and Chauhan, N. S. 2009. Chemical activation of egg shell membrane for covalent immobilization of enzymes and its evaluation as inert support in urinary oxalate determination. *Talanta*, 77 (5): 1688-1693.

Qiu, F., Lv, H., Zhao, X. and Zhao, D. 2019. Impact of an extreme winter storm event on the coagulation/flocculation processes in a prototype surface water treatment plant: causes and mitigating measures. *International journal of environmental research and public health*, 16 (15): 2808.

Qrenawi, L. I. and Rabah, F. K. 2021. Sludge management in water treatment plants: literature review. *International Journal of Environment and Waste Management*, 27 (1): 93-125.

Qu, X., Alvarez, P. J. and Li, Q. 2013. Applications of nanotechnology in water and wastewater treatment. *Water Research*, 47 (12): 3931-3946.

Raksha, E., Davydova, A., Oskolkova, O., Glazunova, V., Volkova, G., Burchovetskij, V., Sukhov, P., Gnatovskaya, V., Berestneva, Y. and Verbenko, I. 2021. Carbon Nanoparticles from Graphite Nitrate Cointercalation Compounds with Carboxylic Acids. In: Proceedings of *International Conference on Physics and Mechanics of New Materials and Their Applications*. Springer, 37-45.

Rakshit, A. K., Naskar, B. and Moulik, S. P. 2021. Stability of hydrophobic colloids: Perspectives and current opinion. *Journal of Dispersion Science and Technology*, 42 (4): 503-513.

Ramadan, M., Amin, M. and Sayed, M. A. 2020. Superior physico-mechanical, fire resistivity, morphological characteristics and gamma radiation shielding of hardened OPC pastes incorporating ZnFe2O4 spinel nanoparticles. *Construction and Building Materials*, 234: 117807.

Ramesh, T., Amuthavalli, A. and Kannan, T. R. 2021. Decolorization of textile effluent using plant-based natural coagulants-A review. *Current Perspectives in Bioscience Research*, 1: 142.

Ramimoghadam, D., Bagheri, S. and Abd Hamid, S. B. 2014. Progress in electrochemical synthesis of magnetic iron oxide nanoparticles. *Journal of magnetism and magnetic materials*, 368: 207-229.

Rao, C. N. R. and Nath, M. 2003. Inorganic nanotubes. In: *Advances In Chemistry: A Selection of CNR Rao's Publications (1994–2003)*. World Scientific, 310-333.

Rao, J. S., Parimalavalli, R. and Jagannadham, K. 2014. Impact of Cross-Linking on Physico-Chemical and Functional Properties of Cassava Starch.". *International Journal of Advanced Research*, 2 (5): 284-289.

Rashid, H., Mansoor, M. A., Haider, B., Nasir, R., Hamid, S. B. A. and Abdulrahman, A. 2020. Synthesis and characterization of magnetite nano particles with high selectivity using in-situ precipitation method. *Separation Science and Technology*, 55 (6): 207-1215.

Ratnayake, W. S. and Jackson, D. S. 2006. Gelatinization and solubility of corn starch during heating in excess water: new insights. *Journal of agricultural and food chemistry*, 54 (10): 3712-3716.

Reed, R. B., Faust, J. J., Yang, Y., Doudrick, K., Capco, D. G., Hristovski, K. and Westerhoff, P. 2014. Characterization of nanomaterials in metal colloid-containing dietary supplement drinks and assessment of their potential interactions after ingestion. *ACS Sustainable Chemistry & Engineering*, 2 (7): 1616-1624.

Ren, L., Yan, X., Zhou, J., Tong, J. and Su, X. 2017. Influence of chitosan concentration on mechanical and barrier properties of corn starch/chitosan films. *International Journal of Biological Macromolecules*, 105: 1636-1643.

Rezaeiana, R., Peydaa, M., MohammadianFazlia, M. and Yarahmadi, T. 2016. Optimization of extraction method of the natural coagulant from descurainia sophia seed: Minimization of color generation. *Journal of Human, Environment, and Health Promotion*, 1 (13): 166-171.

Rifi, S. K., Souabi, S., El Fels, L., Driouich, A., Nassri, I., Haddaji, C. and Hafidi, M. 2022. Optimization of coagulation process for treatment of olive oil mill wastewater using Moringa Oleifera as a natural coagulant, CCD combined with RSM for treatment optimization. *Process Safety and Environmental Protection*,

Rodriguez-Granrose, D., Jones, A., Loftus, H., Tandeski, T., Heaton, W., Foley, K. T. and Silverman, L. 2021. Design of experiment (DOE) applied to artificial neural network architecture enables rapid bioprocess improvement. *Bioprocess and biosystems engineering*, 44 (6): 1301-1308.

Rohim, R., Ahmad, R., Ibrahim, N., Hamidin, N. and Abidin, C. Z. A. 2014. Characterization of calcium oxide catalyst from eggshell waste. *Advances in Environmental Biology*, 88 (22): 35-38.

Roostaee, M. and Sheikhshoaie, I. 2020. Magnetic nanoparticles; synthesis, properties and electrochemical application: A review. *Current Biochemical Engineering*, 6 (2): 91-102.

Rossi, L. M., Costa, N. J. S., Silva, F. P. and Gonçalves, R. V. 2013. Magnetic nanocatalysts: supported metal nanoparticles for catalytic applications. *Nanotechnology Reviews*, 2 (5): 597-614.

Roy, S. D., Das, K. C. and Dhar, S. S. 2021. Conventional to green synthesis of magnetic iron oxide nanoparticles; its application as catalyst, photocatalyst and toxicity: A short review. *Inorganic Chemistry Communications*, 134: 109050.

Sada, S. O. 2021. Improving the predictive accuracy of artificial neural network (ANN) approach in a mild steel turning operation. *The International Journal of Advanced Manufacturing Technology volume* 112 (49): 2389–2398.

Sahu, O. P. and Chaudhari, P. K. 2013. Review on chemical treatment of industrial waste water. *Journal of Applied Science and Environmental Management*, 17 (2): 241-257.

Saifuddin, N. and Dinara, S. 2011. Pretreatment of palm oil mill effluent (POME) using magnetic chitosan. *E-Journal of Chemistry*, 8 (S1): S67-S78.

Salazar Alvarez, G. 2004. Synthesis, characterisation and applications of iron oxide nanoparticles. Materialvetenskap. Available: https://www.diva-portal.org/smash/record.jsf?pid=diva2%3A14857&dswid=6523 (Accessed 11 September 2020).

Saleem, M. and Bachmann, R. T. 2019. A contemporary review on plant-based coagulants for applications in water treatment. *Journal of Industrial and Engineering Chemistry*, 72: 281-297.

Samanta, H., Da, R. and Bhattachajee, C. 2016. Influence of nanoparticles for wastewater treatment: a short review, Austin Chem. *Eng*, 3: 1-6.

Samrot, A. V., Sahithya, C. S., Selvarani, J., Purayil, S. K. and Ponnaiah, P. 2021. A review on synthesis, characterization and potential biological applications of superparamagnetic iron oxide nanoparticles. *Current Research in Green and Sustainable Chemistry*, 4: 100042.

Sanchez, O., Labelle, M.-A., Gadbois, A., Laflamme, E., Dold, P. L., Laporte, A. and Comeau, Y. 2018. Recovery of particulate matter from a high-rate moving bed biofilm reactor by high-rate dissolved air flotation. *Water Quality Research Journal*, 53 (4): 181-190.

Sánchez Ortega, C. 2019. Solids and sulfate ions removal from mine water by dissolved air flotation. Available: https://lutpub.lut.fi/handle/10024/160085 (Accessed 16 February 2021).

Santana, R. C., Ribeiro, J. A., Santos, M. A., Reis, A. S., Ataíde, C. H. and Barrozo, M. A. S. 2012. Flotation of fine apatitic ore using microbubbles. *Separation and Purification Technology*, 98: 402-409.

Santiago, A. A., Macedo, E. M., Oliveira, F. K., Tranquilin, R. L., Teodoro, M. D., Longo, E., Motta, F. V. and Bomio, M. R. 2022. Enhanced photocatalytic activity of CaMoO4/g-C3N4 composites obtained via sonochemistry synthesis. *Materials Research Bulletin*, 146: 111621.

Santos, M. A., Capponi, F., Ataíde, C. H. and Barrozo, M. A. 2021. Wastewater treatment using DAF for process water reuse in apatite flotation. *Journal of cleaner production*, 308: 127285.

Santos, T. R., Silva, M. F., Nishi, L., Vieira, A. M., Fagundes-Klen, M. R., Andrade, M. B., Vieira, M. F. and Bergamasco, R. 2016. Development of a magnetic coagulant based on Moringa oleifera seed extract for water treatment. *Environmental Science and Pollution Research*, 23 (8): 7692-7700.

Saratale, R. G., Saratale, G. D., Shin, H. S., Jacob, J. M., Pugazhendhi, A., Bhaisare, M. and Kumar, G. 2018. New insights on the green synthesis of metallic nanoparticles using plant and waste biomaterials: current knowledge, their agricultural and environmental applications. *Environmental Science and Pollution Research*, 25 (11): 10164-10183.

Sargazi, S., Hajinezhad, M. R., Rahdar, A., Mukhtar, M., Karamzadeh-Jahromi, M., Almasi-Kashi, M., Alikhanzadeh-Arani, S., Barani, M. and Baino, F. 2021. CoNi alloy nanoparticles for cancer theranostics: synthesis, physical characterization, in vitro and in vivo studies. *Applied Physics A*, 127 (10): 1-12.

Sarkar, M., Santra, D., Denrah, S., Sarkar, S. and Sarkar, P. 2021. Study on the Efficiency of Metal Modified Bio–Nanocomposite Bead for Removal via Retention of Some Anthraquinone Dye. *Challenges and Advances in Chemical Science Vol. 3*: 60-78.

Satheeshkumar, M., Kumar, E. R., Indhumathi, P., Srinivas, C., Deepty, M., Sathiyaraj, S., Suriyanarayanan, N. and Sastry, D. 2020. Structural, morphological and magnetic properties of algae/CoFe2O4 and algae/Ag-Fe-O nanocomposites and their biomedical applications. *Inorganic Chemistry Communications*, 111: 107578.

Satpathy, K., Rehman, U., Cools, B., Verdickt, L., Peleman, G. and Nopens, I. 2020. CFD-based process optimization of a dissolved air flotation system for drinking water production. *Water Science and Technology*, 81 (8): 1668-1681.

Saxena, K., Brighu, U. and Choudhary, A. 2018. Parameters affecting enhanced coagulation: a review. *Environmental Technology Reviews*, 7 (1): 156-176.

Sekoai, P. T., Ouma, C. N. M., Du Preez, S. P., Modisha, P., Engelbrecht, N., Bessarabov, D. G. and Ghimire, A. 2019. Application of nanoparticles in biofuels: an overview. *Fuel*, 237: 380-397.

Sepúlveda, P., Salazar, R., Espinoza, L. and García, A. G. 2021. Characterization and Application of Fe-Magnetic Materials and Nanomaterials for Application in the Aqueous Matrices Decontamination. In: *Advanced Magnetic Adsorbents for Water Treatment*. Springer, 347-383.

Serrani, D., Ajmone-Marsan, F., Corti, G., Cocco, S., Cardelli, V. and Adamo, P. 2021. Heavy metal load and effects on biochemical properties in urban soils of a medium-sized city, Ancona, Italy. *Environmental Geochemistry and Health*: 1-25.

Šesták, J., Liška, M. and Hubík, P. 2011. Oxide glass structure, non-bridging oxygen and feasible magnetic properties due to the addition of Fe/Mn oxides. In: *Glassy, Amorphous and Nano-Crystalline Materials*. Springer, 199-216.

Setyawan, H. and Widiyastuti, W. 2019. Progress in the preparation of magnetite nanoparticles through the electrochemical method. *KONA Powder and Particle Journal*: 2019011.

Shai, A. 2012. Integration of the electronics and batteries inside the hollow core of a search coil. BEN-GURION UNIVERSITY OF THE NEGEV. Available: http://aranne5.bgu.ac.il/others/AmrusiShai.pdf (Accessed 11 December 2021).

Shamaila, S., Bano, T. and Sajjad, A. K. L. 2017. Efficient visible light magnetic modified iron oxide photocatalysts. *Ceramics International*, 43 (17): 14672-14677.

Shamshad, K., Dan, Z. and He, H. 2019. Adsorption mechanism of Pb (II) and Ni (II) from aqueous solution by TiO2 nanoparticles: kinetics, isotherms and thermodynamic studies. *Desalination and Water Treatment*, 155: 237-249.

Shanmuganathan, S., Loganathan, P., Kazner, C., Johir, M. and Vigneswaran, S. 2017. Submerged membrane filtration adsorption hybrid system for the removal of organic micropollutants from a water reclamation plant reverse osmosis concentrate. *Desalination*, 401: 134-141.

Shen, Y. F., Tanga, J., Nie , Z. H., Wanga, Y. D., Rend, Y. and Zuoa, L. 2009. Tailoring size and structural distortion of Fe3O4 nanoparticles for the purification of contaminated water. *Bioresource technology*, 100 (18): 4139-4146.

Sher, F., Malik, A. and Liu, H. 2013. Industrial polymer effluent treatment by chemical coagulation and flocculation. *Journal of Environmental Chemical Engineering*, 1 (4): 684-689.

Shi, Y.-L., Ma, J. and Yang, J.-X. 2017. Improved dissolved air flotation performances using chitosan under different dosing schemes. *Polish Journal of Environmental Studies*, 26 (6)

Shih, F., King, J., Daigle, K., An, H.-J. and Ali, R. 2007. Physicochemical Properties of Rice Starch Modified by Hydrothermal Treatments. *Cereal Chemistry*, 84 (5): 527-531.

Shuang, C., Li, P., Li, A., Zhou, Q., Zhang, M. and Zhou, Y. 2012. Quaternized magnetic microspheres for the efficient removal of reactive dyes. *Water Research*, 46 (14): 4417-4426.

Sibiya, N., Amo-Duodu, G., Tetteh, E. K. and Rathilal, S. 2022a. Response surface optimisation of a magnetic coagulation process for wastewater treatment via Box-Behnken. *Materials Today: Proceedings*, 62 (Supplement 1): S122-S126.

Sibiya, N. P., Amo-Duodu, G., Tetteh, E. K. and Rathilal, S. 2022b. Model prediction of coagulation by magnetised rice starch for wastewater treatment using response surface methodology (RSM) with artificial neural network (ANN). *Scientific African*,. Available: https://www.sciencedirect.com/science/article/pii/S2468227622001892 (Accessed 14 July 2022).

Sibiya, N. P., Rathilal, S. and Tetteh, E. K. 2021. Coagulation Treatment of Wastewater: Kinetics and Natural Coagulant Evaluation. *Molecules*, 26 (3): 698.

Siddique, M., Soomro, S. A., Aziz, S., Jatoi, A. S., Mengal, A. and Mahar , H. 2016. Removal of turbidty from turbid water by bio-cogulant prepared from walnut shell. *Journal of Applied and Emerging Science*, 6 (2): 66-68.

Sierra-Pallares, J., Huddle, T., García-Serna, J., Alonso, E., Mato, F., Shvets, I., Luebben, O., Cocero, M. J. and Lester, E. 2016. Understanding bottom-up continuous hydrothermal synthesis of nanoparticles using empirical measurement and computational simulation. *Nano Research*, 9 (11): 3377-3387.

Singh, B. and Kumar, P. 2020a. Pre-treatment of petroleum refinery wastewater by coagulation and flocculation using mixed coagulant: Optimization of process parameters using response surface methodology (RSM). *Journal of Water Process Engineering*, 36: 101317.

Singh, G. and Patidar, S. K. 2020b. Water quality restoration by harvesting mixed culture microalgae using Moringa oleifera. *Water Environment Research*, 92 (9): 1268-1282.

Singh, S., Barick, K. C. and Bahadur, D. 2011. Surface engineered magnetic nanoparticles for removal of toxic metal ions and bacterial pathogens. *Journal of hazardous materials*, 192 (3): 1539-1547.

Singh, V., Kumar, P. and Sanghi, R. 2012. Use of microwave irradiation in the grafting modification of the polysaccharides–A review. *Progress in polymer science*, 37 (2): 340-364.

Singh, V., Naka, T., Takami, S., Sahraneshin, A., Togashi, T., Aoki, N., Hojo, D., Arita, T. and Adschiri, T. 2013. Hydrothermal synthesis of inorganic–organic hybrid gadolinium hydroxide nanoclusters with controlled size and morphology. *Dalton transactions*, 42 (45): 16176-16184.

Singh, V., Takami, S., Aoki, N., Hojo, D., Arita, T. and Adschiri, T. 2014. Hydrothermal synthesis of luminescent GdVO 4: Eu nanoparticles with dispersibility in organic solvents. *Journal of Nanoparticle Research*, 16 (5): 1-11.

Sirivisoot, S. and Harrison, B. S. 2015. Magnetically stimulated ciprofloxacin release from polymeric microspheres entrapping iron oxide nanoparticles. *International journal of nanomedicine*, 10: 4447.

Soares, F. A., Dos Santos, B. M., Rosa, S. L., Loiola, S. H. N., Suzuki, C. T. N., Sabadini, E., Bresciani, K. D. S., Falcão, A. X. and Gomes, J. F. 2021. Dissolved air flotation as potential new mechanism for intestinal parasite diagnosis in feces. *Acta Tropica*, 224: 106137.

Sobieszuk, P., Ulatowski, K. and Jeżak, R. 2021. Impact of Process Parameters on the Diameter of Nanobubbles Generated by Electrolysis on Platinum-Coated Titanium Electrodes Using Box–Behnken Experimental Design. Energies, 14 (9): 2542.

Song, Y., Liu, Y., Zhan, B., Kaya, C., Stegmaier, T., Han, Z. and Ren, L. 2017. Fabrication of bioinspired structured superhydrophobic and superoleophilic copper mesh for efficient oil-water separation. *Journal of Bionic Engineering*, 14 (3): 497-505.

Souza, A. C. O. e., Ferreira, N. L. and da Silva, F. V. 2021. Empirical modeling of turbidity removal in a dissolved air flotation system: application of artificial neural networks. *Water Supply*, 21 (7): 3946-3959.

Starowicz, M., Starowicz, P., Przewoz´nik, J. Z. J., Leman´ski, A., Kapusta, C. and Banas´, J. 2011. Electrochemical synthesis of magnetic iron oxide nanoparticles with controlled size. *J Nanopart Res* 13: 7167-7176.

Stojanovic, B. D., Dzunuzovic, A. S. and Ilic, N. I. 2018. Review of methods for the preparation of magnetic metal oxides. In: *Magnetic, Ferroelectric, and Multiferroic Metal Oxides*. Elsevier, 333-359.

Sule, K., Umbsaar, J. and Prenner, E. J. 2020. Mechanisms of Co, Ni, and Mn toxicity: From exposure and homeostasis to their interactions with and impact on lipids and biomembranes. *Biochimica et Biophysica Acta (BBA)-Biomembranes*, 1862 (8): 183250.

Sultan, M. Z., Jamil, Y., Javed, Y., Sharma, S. and Tahir, M. S. 2020. Thermal response of iron oxide and metal-based iron oxide. *Magnetic Nanoheterostructures: Diagnostic, Imaging and Treatment*: 333-356.

Sun, S. and Zeng, H. 2002. Size-controlled synthesis of magnetite nanoparticles. *Journal of the American Chemical Society*, 124 (28): 8204-8205.

Sun, Y., Zhou, S., Chiang, P.-C. and Shah, K. J. 2019. Evaluation and optimization of enhanced coagulation process: Water and energy nexus. *Water-Energy Nexus*, 2: 25-36.

Suslick, K. S., Eddingsaas, N. C., Flannigan, D. J., Hopkins, S. D. and Xu, H. 2011. Extreme conditions during multibubble cavitation: Sonoluminescence as a spectroscopic probe. *Ultrasonics sonochemistry*, 18 (4): 842-846.

Suslick, K. S. and Flannigan, D. J. 2008. Inside a collapsing bubble: sonoluminescence and the conditions during cavitation. *Annu. Rev. Phys. Chem.*, 59: 659-683.

Svobodova, H., Kosnáč, D., Tanila, H., Wagner, A., Trnka, M., Vitovič, P., Hlinkova, J., Vavrinsky, E., Ehrlich, H. and Polák, Š. 2020. Iron–oxide minerals in the human tissues. *Biometals*, 33 (1): 1-13.

Tadic, M., Kusigerski, V., Markovic, D., Milosevic, I. and Spasojevic, V. 2009. High concentration of hematite nanoparticles in a silica matrix: structural and magnetic properties. *Journal of magnetism and magnetic materials*, 321 (1): 12-16.

Talekar, S., Joshi, A., Kambale, S., Jadhav, S., Nadar, S. and Ladole, M. 2017. A tri-enzyme magnetic nanobiocatalyst with one pot starch hydrolytic activity. *Chemical Engineering Journal*, 325: 80-90.

Talekar, S., Pandharbale, A., Ladole, M., Nadar, S., Mulla, M., Japhalekar, K., Pattankude, K. and Arage, D. 2013. Carrier free co-immobilization of alpha amylase, glucoamylase and pullulanase as combined cross-linked enzyme aggregates (combi-CLEAs): a tri-enzyme biocatalyst with one pot starch hydrolytic activity. *Bioresource technology*, 147: 269-275.

Taleyarkhan, R. P., West, C., Cho, J., Lahey, R., Nigmatulin, R. I. and Block, R. 2002. Evidence for nuclear emissions during acoustic cavitation. *science*, 295 (5561): 1868-1873.

Tan, G., Mao, Y., Wang, H. and Xu, N. 2020a. A comparative study of arsenic (V), tetracycline and nitrate ions adsorption onto magnetic biochars and activated carbon. *Chemical Engineering Research and Design*, 159: 582-591.

Tan, K. and Hameed, B. 2017. Insight into the adsorption kinetics models for the removal of contaminants from aqueous solutions. *Journal of the Taiwan Institute of Chemical Engineers*, 74: 25-48.

Tan, K. and Yeo, S. 2020b. Velocity estimation of micro-particles driven by cavitation bubble collapses through controlled erosion experiments. *International Journal of Multiphase Flow*, 127: 103271.

Tanboonchuy, V., Hsu, J.-C., Grisdanurak, N. and Liao, C.-H. 2011. Gas-bubbled nano zero-valent iron process for high concentration arsenate removal. *Journal of hazardous materials*, 186 (2-3): 2123-2128.

Tang, J., Myers, M., Bosnick, K. A. and Brus, L. E. 2003. Magnetite Fe3O4 nanocrystals: spectroscopic observation of aqueous oxidation kinetics. *The Journal of Physical Chemistry B*, 107 (30): 7501-7506.

Tartaj, P., Morales, M., Gonzalez-Carreno, T., Veintemillas-Verdaguer, S. and Serna, C. 2005. Advances in magnetic nanoparticles for biotechnology applications. *Journal of magnetism and magnetic materials*, 290: 28-34.

Taspika, M., Desiati, R. D., Mahardika, M., Sugiarti, E. and Abral, H. 2020. Influence of TiO 2 /Ag particles on the properties of chitosan film. *Advances in Natural Sciences: Nanoscience and Nanotechnology*, 11: 015017.

Tee, P. F., Abdullah, M. O., Tan, I. A. W., Rashid, N. K. A., Amin, M. A. M., Nolasco-Hipolito, C. and Bujang, K. 2016. Review on hybrid energy systems for wastewater treatment and bio-energy production. *Renewable and Sustainable Energy Reviews*, 54: 235-246.

Teh, C. Y. 2014. Potential use of rice starch in coagulation–flocculation process of agro-industrial wastewater: Treatment performance and flocs characterization. *Ecological engineering*, 71: 509-519.

Teh, C. Y., Budiman, P. M., Shak, K. P. Y. and Wu, T. Y. 2016. Recent advancement of coagulation–flocculation and its application in wastewater treatment. *Industrial & Engineering Chemistry Research*, 55 (16): 4363-4389.

Teh, C. Y., Wu, T. Y. and Juan, J. C. 2014a. Optimization of agro-industrial wastewater treatment using unmodified rice starch as a natural coagulant. *Industrial Crops and Products*, 56: 17-26.

Teh, C. Y., Wu, T. Y. and Juan, J. C. 2014b. Potential use of rice starch in coagulation–flocculation process of agro-industrial wastewater: treatment performance and flocs characterization. *Ecological engineering*, 71: 509-519.

Tempelhoff, J. 2017. The Water Act, No. 54 of 1956 and the first phase of apartheid in South Africa (1948–1960). *Water History*, 9 (2): 189-213.

Tetteh, E. K. 2018a. Optimisation of dissolved air flotation (DAF) for separating industrial mineral oil from water. Department of Chemical Engineering,. Available: https://openscholar.dut.ac.za/bitstream/10321/3182/1/TETTECHEK_2018.pdf (Accessed 13 March 2020).

Tetteh, E. K. 2018b. Optimisation of dissolved air flotation (DAF) for separating industrial mineral oil from water. Durban University of Technology Durban: Department of Chemical Engineering,. Available: https://openscholar.dut.ac.za/bitstream/10321/3182/1/TETTECHEK_2018.pdf (Accessed 13 March 2020).

Tetteh , E. K., Amo-Duodu, G. and Rathilal, S. 2022. Biogas production from wastewater: Comparing biostimulation impact of magnetised-chitosan and -titania chitosan. *Materials Today: Proceedings*, 62 (Supplement 1): S85-S90.

Tetteh, E. K. and Rathilal, S. 2018a. Effects of a polymeric organic coagulant for industrial mineral oil wastewater treatment using response surface methodology (RSM). *Water SA*, 44 (2): 155-161.

Tetteh, E. K. and Rathilal, S. 2018b. Evaluation of the coagulation floatation process for industrial mineral oil wastewater treatment using response surface methodology (RSM). *International Journal of Environmental Impacts*, 1 (4): 491-502.

Tetteh, E. K. and Rathilal, S. 2018c. Investigating dissolved air flotation factors for oil refinery wastewater treatment. In: Proceedings of *CBU International Conference Proceedings*. 1173-1177.

Tetteh, E. K. and Rathilal, S. 2019. Application of organic coagulants in water and wastewater treatment. In. IntechOpen. Available: http://openscholar.dut.ac.za/bitstream/10321/3390/2/TETTEH_OP_19Pages_2019.pdf (Accessed 13 March 2020).

Tetteh, E. K. and Rathilal, S. 2020. Application of magnetized nanomaterial for textile effluent remediation using response surface methodology. *Materials Today: Proceedings*, 38 (Part 2): 700-711.

Tetteh , E. K. and Rathilal, S. 2020a. Evaluating pre- and post-coagulation configuration of dissolved air flotation using response surface methodology. *Process*, 8: 383.

Tetteh , E. K. and Rathilal, S. 2020b. Kinetics and nanoparticle catalytic enhancement of biogas production from wastewater using a Magnetized Biochemical Methane Potential (MBMP) system. *Catalysts*, 10: 1200.

Tetteh , E. K., Rathilal, S., Chetty, M., Kwaku Armah, E. and Asante-Sackey, D. 2019. Treatment of Water and Wastewater for Reuse and Energy Generation-Emerging Technologies. In: *Water and Wastewater Treatment*. Available: https://books.google.co.za/books?hl=en&lr=&id=Ukr9DwAAQBAJ&oi=fnd&pg=PA1&dq=Tetteh+,+E.+K.,+Rathilal,+S.,+Chetty,+M.,+Kwaku+Armah,+E.+and+Asante-Sackey,+D.+2019.+Treatment+of+Water+and+Wastewater+for+Reuse+and+Energy+Generation-Emerging+Technologies.+In:+Water+and+Wastewater+Treatment.&ots=aiIrY6_UrG&sig=wkhoCOc7Oyx6RBXzONmgyMlknTM#v=onepage&q&f=false (Accessed 20 May 2020).

Tetteh, E. K., Rathilal, S. and Chollom, M. N. 2017. Pre-treatment of industrial mineral oil wastewater using response surface methodology. *Water and Society IV*, 216: 181-191.

Teyssier, J., Saenko, S. V., Van Der Marel, D. and Milinkovitch, M. C. 2015. Photonic crystals cause active colour change in chameleons. *Nature communications*, 6 (1): 1-7.

Thenuwara, A. C., Shetty, P. P. and McDowell, M. T. 2019. Distinct nanoscale interphases and morphology of lithium metal electrodes operating at low temperatures. *Nano letters*, 19 (12): 8664-8672.

Tian, Z., Wang, C. and Ji, M. 2018. Full-scale dissolved air flotation (DAF) equipment for emergency treatment of eutrophic water. *Water Science and Technology*, 77 (7): 1802-1809.

Tiwari, B., Sellamuthu, B., Ouarda, Y., Drogui, P., Tyagi, R. D. and Buelna, G. 2017. Review on fate and mechanism of removal of pharmaceutical pollutants from wastewater using biological approach. *Bioresour Technol*, 224: 1-12.

Tran, M., Rasmussen, E., Shevchenko, E. and Li, J. 2021. High-throughput Screening of Vanadium (IV) Oxide via Continuous Hydrothermal Flow Synthesis Reactor. Available: https://chemrxiv.org/engage/api-gateway/chemrxiv/assets/orp/resource/item/60f8a8e80b093e26e8e2b751/original/high-throughput-screening-of-vanadium-iv-oxide-via-continuous-hydrothermal-flow-synthesis-reactor.pdf (Accessed 21 January 2022).

Tripathy, T. and De, B. R. 2006. Flocculation : A new way to treat the waste water. *Journal of Physical Sciences*, 10: 93-127.

Tsai, W. T., Yang, J. M., Lai, C. W., Cheng, Y. H., Lin , C. C. and Yeh, C. W. 2006a. Characterization and adsorption properties of eggshells and eggshell membrane. *Bioresource Technology*, 97 (3): 488-493.

Tsai, W. T., Yang, J. M., Lai, C. W., Cheng, Y. H., Lin , C. C. and Yeh, C. W. 2006b. Characterization and adsorption properties of eggshells and eggshell membrane. *Bioresource technology*, 97 (3): 488-493

Tshehla, C. and Wright, C. Y. 2019. 15 years after the National Environmental Management Air Quality Act: Is legislation failing to reduce air pollution in South Africa? *South African Journal of Science*, 115 (9-10): 1-4.

Tuttolomondo, M. V., Villanueva, M. E., Alvarez, G. S., Desimone, M. F. and Díaz, L. E. 2013. Preparation of submicrometer monodispersed magnetic silica particles using a novel water in oil microemulsion: properties and application for enzyme immobilization. *Biotechnology letters*, 35 (10): 1571-1577.

Tyagi, S., Sharma, B., Singh, P. and Dobhal, R. 2013. Water quality assessment in terms of water quality index. *American Journal of Water Resource*, 1 (3): 34-38.

Ugya, A. Y. and Imam, T. 2016. The role of green coagulants in wastewater treatment: A review. In: Ugya, A. Y., Imam, T. S. and Aliyu, M. A. eds. *Wastewater remediation using plant techniques*. Nigeria: Bayero University Kano, 1-16.

Ullah, A., Hussain, S., Wasim, A. and Jahanzaib, M. 2020. Development of a decision support system for the selection of wastewater treatment technologies. *Science of the Total Environment*, 731: 139158.

Ummalyma, S. B., Mathew, A. K., Pandey, A. and Sukumaran, R. K. 2016. Harvesting of microalgal biomass: Efficient method for flocculation through pH modulation. *Bioresource technology*, 213: 216-221.

Usefi, S. and Asadi-Ghalhari, M. 2019. Modeling and optimization of the coagulation–flocculation process in turbidity removal from aqueous solutions using rice starch. *Pollution*, 5 (3): 623-636.

Usman, A., Sutanto, M. H., Napiah, M., Zoorob, S. E., Abdulrahman, S. and Saeed, S. M. 2021. Irradiated polyethylene terephthalate fiber and binder contents optimization for

fiber-reinforced asphalt mix using response surface methodology. *Ain Shams Engineering Journal*, 12 (1): 271-282.

Vabbina, P. K., Karabiyik, M., Al‐Amin, C., Pala, N., Das, S., Choi, W., Saxena, T. and Shur, M. 2014. Controlled synthesis of single‐crystalline ZnO nanoflakes on arbitrary substrates at ambient conditions. *Particle & Particle Systems Characterization*, 31 (2): 190-194.

Vaiano, V., Sacco, O., Sannino, D., Stoller, M., Ciambelli, P. and Chianese, A. 2016. Photocatalytic removal of phenol by ferromagnetic N-TiO 2/SiO 2/Fe 3 O 4 nanoparticles in presence of visible light irradiation. *Chemical Engineering Transactions*, 47: 235-240.

Vainshtein, Y., Werner, N., Kirstahler, P., Glanz, K., Grumaz, C., Hahn, T., Zibek, S. and Sohn, K. 2020. Draft Genome Sequence of Andreprevotia sp. Strain IGB-42, a Chitinolytic Bacterium Isolated from a Soil Sample of an Anthill in Stuttgart, Germany. *Microbiology resource announcements*, 9 (10): e01454-01419.

Valtchev, V., Gao, F. and Tosheva, L. 2008. Porous materials via egg-constituents templating. *New Journal of Chemistry*, 32 (8): 1331-1337.

van Wilgen, B. W. and Wannenburgh, A. 2016. Co-facilitating invasive species control, water conservation and poverty relief: achievements and challenges in South Africa's Working for Water programme. *Current Opinion in Environmental Sustainability*, 19: 7-17.

Varjani, S., Joshi, R., Srivastava, V. K., Ngo, H. H. and Guo, W. 2020. Treatment of wastewater from petroleum industry: current practices and perspectives. *Environmental Science and Pollution Research*, 27 (22): 27172-27180.

Varjani, S. J. and Upasani, V. N. 2017. A new look on factors affecting microbial degradation of petroleum hydrocarbon pollutants. *International Biodeterioration & Biodegradation*, 120: 71-83.

Varshney, S., Nigam, A., Pawar, S. J. and Mishra, N. 2021. An overview on biomedical applications of versatile silica nanoparticles, synthesized via several chemical and biological routes: A review. *Phosphorus, Sulfur, and Silicon and the Related Elements*: 1-17.

Vepsäläinen, M. and Sillanpää, M. 2020. Chapter 1 - Electrocoagulation in the treatment of industrial waters and wastewaters. *Advanced Water Treatment*: 1-78.

Verma, A. K. 2017. Treatment of textile wastewaters by electrocoagulation employing Fe-Al composite electrode. *Journal of water process engineering*, 20: 168-172.

Verziu, M., Coman, S. M., Richards, R. and Parvulescu, V. I. 2011. Transesterification of vegetable oils over CaO catalysts. *Catalysis today*, 167 (1): 64-70.

Viculis, L. M., Mack, J. J. and Kaner, R. B. 2003. A chemical route to carbon nanoscrolls.(Brevia). *science*, 299 (5611): 1361-1362.

Vidal, R. R. L. and Moraes, J. S. 2018. Removal of organic pollutants from wastewater using chitosan: a A literature review. *International Journal of Environmental Science and Technology*, 16: 1741-1754.

Vilardi, G., Mpouras, T., Dermatas, D., Verdone, N., Polydera, A. and Di Palma, L. 2018. Nanomaterials application for heavy metals recovery from polluted water: The combination of nano zero-valent iron and carbon nanotubes. Competitive adsorption non-linear modeling. *Chemosphere*, 201: 716-729.

Villacorta, V., Barrero, C. A., Turrión, M.-B., Lafuente, F., Greneche, J.-M. and García, K. E. 2020. Removal of As 3+, As 5+, Sb 3+, and Hg 2+ ions from aqueous solutions by pure and co-precipitated akaganeite nanoparticles: adsorption kinetics studies. *RSC advances*, 10 (70): 42688-42698.

Viriya-empikul, N., Krasae, P., Puttasawat, B., Yoosuk, B., Chollacoop, N. and Faungnawakij, K. 2010. Waste shells of mollusk and egg as biodiesel production catalysts. *Bioresource technology*, 101 (10): 3765-3767.

Vishakha, K. S., Kishor, B. D. and Sudha, R. S. 2012. Natural Polymers – A Comprehensive Review. *International Journal of Research in Pharmaceutical and Biomedical Sciences*, 3 (4): 1597-1613.

Voltairas, P., Fotiadis, D. and Michalis, L. 2002. Hydrodynamics of magnetic drug targeting. *Journal of Biomechanics*, 35 (6): 813-821.

Vukovic, M., Dinic, I., Jardim, P., Marković, S., Veselinović, L., Nikolić, M. and Mancic, L. 2021. The low-temperature sonochemical synthesis of up-converting β NaYF4: Yb, Er mesocrystals. *Advanced Powder Technology*: 103403.

Wahaab, R. A. and Alseroury, F. 2019. Wastewater treatment: a case study of electronics manufacturing industry. *International Journal of Environmental Science and Technology*, 16 (1): 47-58.

Waheed, M., Yousaf, M., Shehzad, A., Inam-Ur-Raheem, M., Khan, M. K. I., Khan, M. R., Ahmad, N. and Aadil, R. M. 2020. Channelling eggshell waste to valuable and utilizable products: a comprehensive review. *Trends in Food Science & Technology*, 106: 78-90.

Wang, F., Li, Y., Gough, C. R., Liu, Q. and Hu, X. 2021a. Dual-Crystallizable Silk Fibroin/Poly (L-lactic Acid) Biocomposite Films: Effect of Polymer Phases on Protein Structures in Protein-Polymer Blends. *International Journal of Molecular Sciences*, 22 (4): 1871.

Wang, J.-P., Chen, Y.-Z., Ge, X.-W. and Yu, H.-Q. 2007. Optimization of coagulation–flocculation process for a paper-recycling wastewater treatment using response surface methodology. *Colloids and surfaces. A, Physicochemical and engineering aspects*, 302 (1-3): 204-210.

Wang, J.-P., Chen, Y.-Z., Yuan, S.-J., Sheng, G.-P. and Yu, H.-Q. 2009. Synthesis and characterization of a novel cationic chitosan-based flocculant with a high water-solubility for pulp mill wastewater treatment. *Water Research*, 43: 5267–5275.

Wang, Y., Li, B., Zhou, Y. and Jia, D. 2008. Chitosan-induced synthesis of magnetite nanoparticles via iron ions assembly. *Polymers for Advanced Technologies*, 19: 1256-1261.

Wang, Y., Tadimalla, S., Rai, R., Goodwin, J., Foster, S., Liney, G., Holloway, L. and Haworth, A. 2021b. Quantitative MRI: Defining repeatability, reproducibility and accuracy for prostate cancer imaging biomarker development. *Magnetic resonance imaging*, 77: 169-179.

Wang, Y., Zhou, C., Wang, W. and Zhao, Y. 2013. Preparation of two dimensional atomic crystals BN, WS2, and MoS2 by supercritical CO2 assisted with ultrasound. *Industrial & Engineering Chemistry Research*, 52 (11): 4379-4382.

Wani, A. A., Singh, P., Shah, M. A., Schweiggert-Weisz, U., Gul, K. and Wani, I. A. 2012. Rice Starch Diversity: Effects on Structural, Morphological, Thermal, and Physicochemical Properties—A Review. *Comprehensive Reviews in Food Science and Food Safety*, 11: 417-436.

Wei, B., Zhou, J., Yao, Z., Haidry, A. A., Guo, X., Lin, H., Qian, K. and Chen, W. 2020. The effect of Ag nanoparticles content on dielectric and microwave absorption properties of β-SiC. *Ceramics International*, 46 (5): 5788-5798.

Wei, H., Gao, B., Ren, J., Li, A. and Yang, H. 2018. Coagulation/flocculation in dewatering of sludge: a review. *Water Research*, 143: 608-631.

Whistler, R. L. 2009. Starch. In: *Chapter 19 - Starch in Polymer Compositions*. 3rd edn. London, UK: Academic Press. Available: https://books.google.co.za/books?hl=en&lr=&id=Anbz_whRM2YC&oi=fnd&pg=PP1&dq=Willett,+J.L.,+2009.+Chapter+19+%E2%88%92+starch+in+polymer+compositions.+In:+BeMiller,+J.,+Whistler,+R.+(Eds.),+Starch.+,+third+edition.+Academic+Press,+San+Diego,+pp.+715%E2%80%93743.&ots=dZK-rP9A1M&sig=5g_fCPm2qQUHbYCaRQVvOc6dvhI#v=onepage&q&f=false (Accessed 6 Jauary 2022).

Willard, M., Kurihara, L., Carpenter, E., Calvin, S. and Harris, V. 2004. Chemically prepared magnetic nanoparticles. *International materials reviews*, 49 (3-4): 125-170.

William, W. Y., Falkner, J. C., Yavuz, C. T. and Colvin, V. L. 2004. Synthesis of monodisperse iron oxide nanocrystals by thermal decomposition of iron carboxylate salts. *Chemical Communications*, (20): 2306-2307.

Witoon, T. 2011. Characterization of calcium oxide derived from waste eggshell and its application as CO2 sorbent. *Ceramics International*, 37 (8): 3291-3298.

Wolff, S., Weber, F., Kerpen, J., Winklhofer, M., Engelhart, M. and Barkmann, L. 2021. Elimination of microplastics by downstream sand filters in wastewater treatment. *Water*, 13 (1): 33.

Wong, Y. C., Tan, Y. P., Taufiq-Yap, Y. H., Ramli, I. and Tee, H. S. 2015. Biodiesel production via transesterification of palm oil by using CaO–CeO2 mixed oxide catalysts. *Fuel*, 162: 288-293.

Woo, K., Hong, J., Choi, S., Lee, H.-W., Ahn, J.-P., Kim, C. S. and Lee, S. W. 2004. Easy synthesis and magnetic properties of iron oxide nanoparticles. *Chemistry of Materials*, 16 (14): 2814-2818.

World Health Organization. 2011. *Guidelines for drinking-water quality*, 4. Switzerland: World Health Organization. Available: https://www.joinforwater.ngo/sites/default/files/library_assets/351_WHO_E13_guidelines_drinking-water.pdf (Accessed 16 June 2020).

Wright, J. P., Attfield, J. P. and Radaelli, P. G. 2002. Charge ordered structure of magnetite Fe 3 O 4 below the Verwey transition. *Physical Review B*, 66 (21): 214422.

Wu, G., Dong, H., Li, J., Guo, L., Cheng, Y., Geng, Y. and Wang, X. 2022. Extraction of parishin B and parishin C from Gastrodiae Rhizoma by subcritical water technology. *Journal of Industrial and Engineering Chemistry*, 108: 280-287.

Wu, W. 2017. Evaluation of a chemical dissolved air flotation system for the treatment of restaurant dishwasher effluents. The University of Regina (Canada). Available: https://www.proquest.com/openview/5e02e4708ad312a82e6f7070af86af16/1?pq-origsite=gscholar&cbl=51922&diss=y (Accessed 15 November 2021).

Wu, W., He, Q. and Jiang, C. 2008. Magnetic iron oxide nanoparticles: synthesis and surface functionalization strategies. *Nanoscale research letters*, 3 (11): 397-415.

Wu, W., Wu, Z., Yu, T., Jiang, C. and Kim, W.-S. 2015. Recent progress on magnetic iron oxide nanoparticles: synthesis, surface functional strategies and biomedical applications. *Science and technology of advanced materials*, 16: 023501.

Xia, K., Liu, X., Wang, W., Yang, X. and Zhang, X. 2020. Synthesis of modified starch/polyvinyl alcohol composite for treating textile wastewater. *Polymers*, 12 (2): 289.

Xiao, F., Huang, J.-C. H., Zhang, B. and Cui, C. 2009. Effects of low temperature on coagulation kinetics and floc surface morphology using alum. *Desalination*, 237 (1-3): 201-213.

Xiao, L., Wen, Z., Ci, S., Chen, J. and He, Z. 2012. Carbon/iron-based nanorod catalysts for hydrogen production in microbial electrolysis cells. *Nano Energy*, 1 (5): 751-756.

Xiao, W., Jones, A. M., Li, X., Collins, R. N. and Waite, T. D. 2018. Effect of Shewanella oneidensis on the kinetics of Fe (II)-catalyzed transformation of ferrihydrite to crystalline iron oxides. *Environmental science & technology*, 52 (1): 114-123.

Xing, J.-j., Li, D., Wang, L.-j. and Adhikari, B. 2018. Temperature thresholds and time-temperature dependence of gelatinization for heat-moisture treated corn starch. *Journal of Food Engineering*, 217: 43-49.

Xu, C., Nasrollahzadeh, M., Selva, M., ssaabadi, Z. I. and Luque, R. 2019. Waste-to-wealth: biowaste valorization into valuable bio(nano)materials. *Royal Society of Chemistry*, 48 (18): 4791-4822.

Xu, H. and Suslick, K. S. 2011. Sonochemical preparation of functionalized graphenes. *Journal of the American Chemical Society*, 133 (24): 9148-9151.

Xu, H., Zeiger, B. W. and Suslick, K. S. 2013. Sonochemical synthesis of nanomaterials. *Chemical Society Reviews*, 42 (7): 2555-2567.

Xu, J., Zhang, H., Guo, X. and Qian, H. 2012. The impact of germination on the characteristics of brown rice flour and starch. *Journal of the Science of Food and Agriculture*, 92 (2): 380-387.

Xu, Z., Shen, C., Tian, Y., Shi, X. and Gao, H.-J. 2010. Organic phase synthesis of monodisperse iron oxide nanocrystals using iron chloride as precursor. *Nanoscale*, 2 (6): 1027-1032.

Xue, J., Peldszus, S., Dyke, M. I. V. and Huck, P. M. 2021. Removal of polystyrene microplastic spheres by alum-based coagulation-flocculation-sedimentation (CFS) treatment of surface waters. *Chemical Engineering Journal*, 422: 130023.

Xue, X.-y., Cheng, R., Shi, L., Ma, Z. and Zheng, X. 2017. Nanomaterials for water pollution monitoring and remediation. *Environmental Chemistry Letters*, 15 (1): 23-27.

Yadollahpour, A. 2020. Cellular and Molecular Targeted Drug Delivery: Nanochemistry in Medical Theranostics. *Current Topics in Medicinal Chemistry*, 20 (27): 2425-2426.

Yang, B., Peng, Y. D., Xie, G. and Qu, C. T. 2019. Study on Performance of Coagulated Particles in Heavy Oil Sewage Treatment by Air Flotation. In: Proceedings of *Materials Science Forum*. Trans Tech Publ, 121-126.

Yang, D., Qi, L. and Ma, J. 2002. Eggshell membrane templating of hierarchically ordered macroporous networks composed of TiO2 tubes. *Advanced Materials*, 14 (21): 1543-1546.

Yang, H. 2021. Size limit of superparamagnetic inclusions in dust grains and difficulty of magnetic grain alignment in protoplanetary disks. *The Astrophysical Journal*, 911 (2): 125.

Yang, H., Tang, M., Wu, W., Ding, W., Ding, B. and Wang, X. 2021. Study on inhibition effects and mechanism of wheat starch retrogradation by polyols. *Food Hydrocolloids*, 121: 106996.

Yang, Z. L., Gao, B. Y., Yue, Q. Y. and Wang, Y. 2010. Effect of pH on the coagulation performance of Al-based coagulants and residual aluminum speciation during the treatment of humic acid–kaolin synthetic water. *Journal of hazardous materials*, 178 (1-3): 596-603.

Yao, H., Fan, M., Wang, Y., Luo, G. and Fei, W. 2015. Magnetic titanium dioxide based nanomaterials: synthesis, characteristics, and photocatalytic application in pollutant degradation. *Journal of Materials Chemistry A*, 3 (34): 17511-17524.

Yao, Y., Zhang, J. and Ding, X. 2002. Structure− Retrogradation Relationship of Rice Starch in Purified Starches and Cooked Rice Grains: A Statistical Investigation. *Journal of agricultural and food chemistry*, 50 (25): 7420-7425.

Yarima, A., Ali, R., Abdullahi, A. and Idris, Z. 2020. Nanotechnology: review on emerging techniques in remediating water and soil pollutions. *Journal of Applied Sciences and Environmental Management*, 24 (5): 933-941.

Yaseen, D. and Scholz, M. 2019. Textile dye wastewater characteristics and constituents of synthetic effluents: a critical review. *International Journal of Environmental Science and Technology*, 16 (2): 1193-1226.

Yasui, K. 2021. Multibubble sonoluminescence from a theoretical perspective. *Molecules*, 26 (15): 4624.

Yew, Y. P., Shameli, K., Miyake, M., Kuwano, N., Khairudin, N. B. B. A., Mohamad, S. E. B. and Lee, K. X. 2016. reen Synthesis of Magnetite (Fe3O4) Nanoparticles Using Seaweed (Kappaphycus alvarezii) Extract. *Nanoscale research letters*, 11: 276.

Younker, J. M. and Walsh, M. E. 2014. Bench-scale investigation of an integrated adsorption–coagulation–dissolved air flotation process for produced water treatment. *Journal of Environmental Chemical Engineering*, 2 (1): 692-697.

Yu, L., Han, M. and He, F. 2013. A review of treating oily wastewater. *Arabian Journal of Chemistry*, 10: S1913-S1922.

Yusri, I. M., Maajeed, A. P. P. A., Mamat, R., Ghazli, M. F., Awad, O. I. and Azmi, W. H. 2018. A review on the application of response surface method and artificial neural network in engine performance and exhaust emissions characteristics in alternative fuel. *Renewable and Sustainable Energy Reviews*, 90: 665-686.

Yuvakkumar, R. and Hong, S. 2014. Green synthesis of spinel magnetite iron oxide nanoparticles. In: Proceedings of *Advanced Materials Research*. Trans Tech Publ, 39-42.

Zahoor, A., Iqbal, T., Majid, A. and Ijaz, M. 2021. Green synthesis of magnetic iron oxide nanoparticle for antibacterial activity: A review. *Biological Sciences-PJSIR*, 64 (2): 202-210.

Zahrim, A. and Hilal, N. 2013. Treatment of highly concentrated dye solution by coagulation/flocculation–sand filtration and nanofiltration. *Water Resources and Industry*, 3: 23-34.

Zahrim, A. Y., Dexter, Z. D., Joseph, C. G. and Hilal, N. 2017. Effective coagulation-flocculation treatment of highly polluted palm oil mill biogas plant wastewater using dual coagulants: decolourisation, kinetics and phytotoxicity studies. *Journal of Water Process Engineering*, 16: 258-269.

Zaidi, A. A., RuiZhe, F., Shi, Y., Khan, S. Z. and Mushtaq, K. 2018. Nanoparticles augmentation on biogas yield from microalgal biomass anaerobic digestion. *International Journal of Hydrogen Energy*, 43 (31): 14202-14213.

Zaidi, N. S., Sohaili, J., Muda, K. and Sillanpää, M. 2014. Magnetic field application and its potential in water and wastewater treatment systems. *Separation & Purification Reviews*, 43 (3): 206-240.

Zaman, T., Mostari, M. S., Mahmood, M. A. A. and Rahman, M. S. 2018. Evolution and characterization of eggshell as a potential candidate of raw material. *Cerâmica* 64: 236-241.

Zanacic, E., Stavrinides, J. and McMartin, D. W. 2016. Field-analysis of potable water quality and ozone efficiency in ozone-assisted biological filtration systems for surface water treatment. *Water Research*, 104: 397-407.

Zeidler, G. 2002. Shell eggs and their nutritional value. In: *Commercial chicken meat and egg production*. Springer, 1109-1128.

Zeiger, B. W. and Suslick, K. S. 2011. Sonofragmentation of molecular crystals. *Journal of the American Chemical Society*, 133 (37): 14530-14533.

Zeng, M., Chen, M., Huang, D., Lei, S., Zhang, X., Wang, L. and Cheng, Z. 2020. Engineered two-dimensional nanomaterials: an emerging paradigm for water purification and monitoring. *Materials Horizons*, 8: 758-802.

Zeng, X. and Ruckenstein, E. 1998. Cross-linked macroporous chitosan anion-exchange membranes for protein separations. *Journal of Membrane Science*, 148 (2): 195-205.

Zhang, H., Lin, H., Li, Q., Cheng, C., Shen, H., Zhang, Z., Zhang, Z. and Wang, H. 2021a. Removal of refractory organics in wastewater by coagulation/flocculation with green chlorine-free coagulants. *Science of the Total Environment*, 787: 147654.

Zhang, H., Lin, H., Li, Q., Cheng, C., Shen, H., Zhang, Z., Zhang, Z. and Wang, H. 2021b. Removal of refractory organics inwastewater by coagulation/flocculation with green chlorine-free coagulants. *Science of the Total Environment*, 787: 147654.

Zhang, L. 2020. Advanced treatment of oilfield wastewater by a combination of DAF, yeast bioreactor, UASB, and BAF processes. *Separation Science and Technology*, 56 (4): 779 - 788.

Zhang, L., He, R. and Gu, H.-C. 2006. Oleic acid coating on the monodisperse magnetite nanoparticles. *Applied Surface Science*, 253 (5): 2611-2617.

Zhang, W., He, W. and Jing, X. 2010. Preparation of a stable graphene dispersion with high concentration by ultrasound. *The Journal of Physical Chemistry B*, 114 (32): 10368-10373.

Zhang, Y., Wu, B., Xu, H., Liu, H., Wang, M., He, Y. and Pan, B. 2016. Nanomaterials-enabled water and wastewater treatment. *NanoImpact*, 3-4: 22-399.

Zhang, Y. and Zhang, J. 2005. Surface modification of monodisperse magnetite nanoparticles for improved intracellular uptake to breast cancer cells. *Journal of Colloid and Interface Science*, 283 (2): 352-357.

Zhang, Z. and Lucia, L. A. 2021c. Chitin–clay composite gels with enhanced thermal stability prepared in a green and facile approach. *Journal of Materials Science*, 56 (4): 3600-3611.

Zhao, B., Ren, L., Du, Y. and Wang, J. 2020. Eco-friendly separation layers based on waste peanut shell for gravity-driven water-in-oil emulsion separation. *Journal of cleaner production*, 255: 120184.

Zhao, C., Zhou, J., Yan, Y., Yang, L., Xing, G., Li, H., Wu, P., Wang, M. and Zheng, H. 2021a. Application of coagulation/flocculation in oily wastewater treatment: A review. *Science of the Total Environment*, 765: 142795.

Zhao, J., Gao, T., Li, Y., He, Y. and Shi, Y. 2021b. Two-dimensional (2D) graphene nanosheets as advanced lubricant additives: A critical review and prospect. *Materials Today Communications*, 29: 102755.

Zhao, L., Liang, L., Guo, M., Li, M., Yu, X., Wang, Y. and Wang, Y. 2021c. Hepatocellular carcinoma targeting and pharmacodynamics of paclitaxel nanoliposomes modified by glycyrrhetinic acid and ferric tetroxide. *Current Topics in Medicinal Chemistry*, 41 (14): 1268-1284(17).

Zhao, Q., Zhang, C., Tong, X., Zou, Y., Li, Y. and Wei, F. 2021d. Fe3O4-NPs/Orange-Peel composite as magnetic heterogeneous Fenton-like catalyst towards high-efficiency degradation of methyl orange. *Water Science and Technology*, 84 (1): 159–171.

Zhao, W. and Ci, S. 2019. Nanomaterials As electrode materials of microbial electrolysis cells for hydrogen generation. In: *Nanomaterials for the Removal of Pollutants and Resource Reutilization*. Elsevier, 213-242.

Zhao, W., Li, M., Qi, Y., Tao, Y., Shi, Z., Liu, Y. and Cheng, J. 2021e. Ultrasound sonochemical synthesis of amorphous Sb2S3-graphene composites for sodium-ion batteries. *Journal of Colloid and Interface Science*, 586: 404-411.

Zhao, Y., Gao, B., Shon, H., Cao, B. and Kim, J.-H. 2011. Coagulation characteristics of titanium (Ti) salt coagulant compared with aluminum (Al) and iron (Fe) salts. *Journal of hazardous materials*, 185 (2-3): 1536-1542.

Zhou, R., Wang, Y., Zhang, M., Yu, P. X. and Li, J. 2019. Adsorptive removal of phosphate from aqueous solutions by thermally modified copper tailings. *Environmental monitoring and assessment*, 191 (4): 1-13.

Zhu, Y., Jiang, F., Chen, K., Kang, F. and Tang, Z. 2013. Modified reverse microemulsion synthesis for iron oxide/silica core–shell colloidal particles. *Journal of sol-gel science and technology*, 66 (1): 180-186.

Zouboulis, A. I. and Avranas, A. 2000. Treatment of oil-in-water emulsions by coagulation and dissolved-air flotation. *Colloids and surfaces. A, Physicochemical and engineering aspects*, 172 (1-3): 153-161.

Zubair, M., Mu'azu, N. D., Nasir, M., Manzar, M. S., Aziz, M. A., Saleem, M. and Al-Harthi, M. A. 2022. Cellulose nanocrystals from office paper waste for green mortar: process optimization modeling, characterization, and mechanical properties. *Arabian Journal for Science and Engineering*: 1-17.

APPENDIX A: GENERAL PROTOCOLS

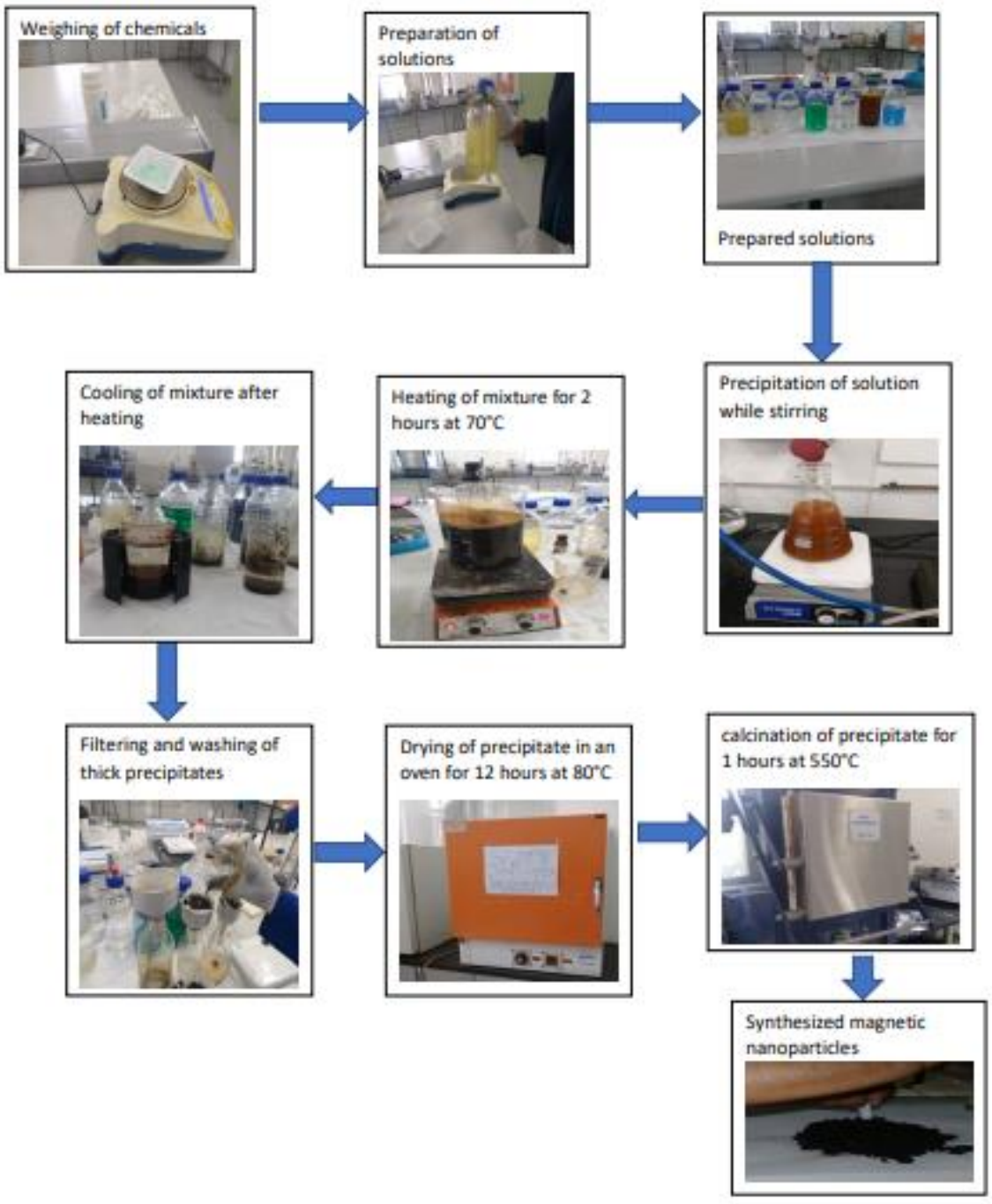

Figure A-1 The flow diagram for co-precipitation method used to synthesize magnetite

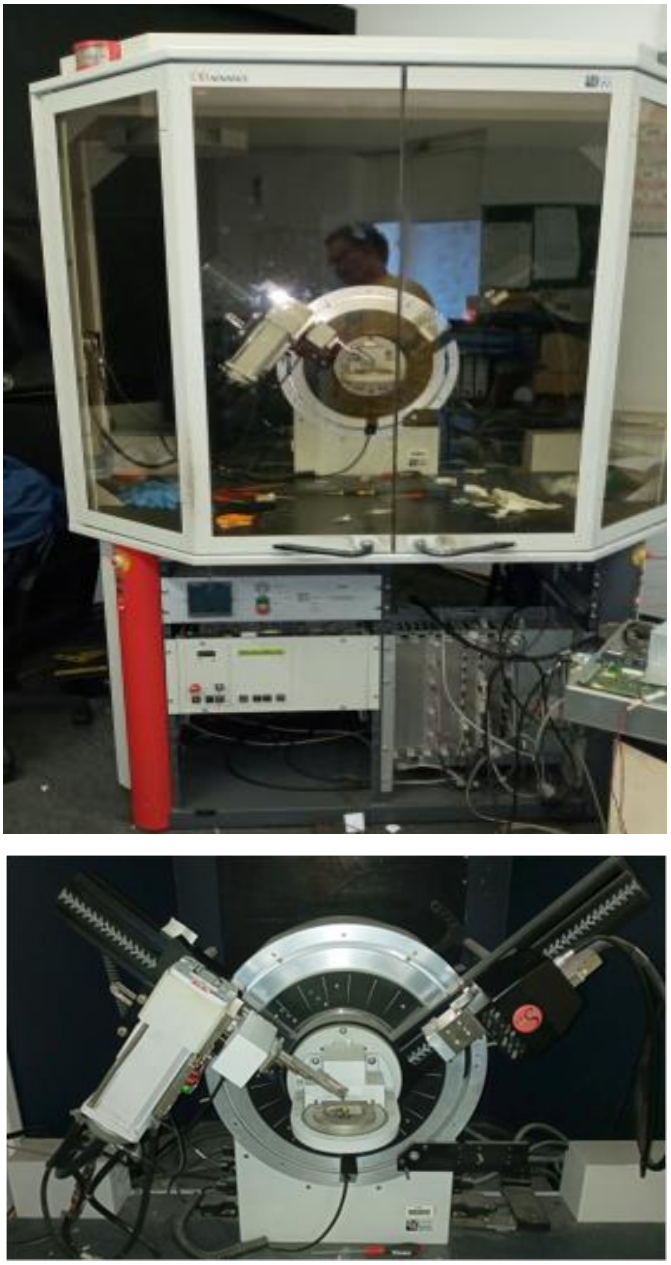

Figure A-2 Diffractometer used for XRD analysis

Figure A-3 Instruments used for COD and TSS ; (a) HACH spectrophotometer (DR3900), and (b) HACH reactor (DRB 200)

Figure A-4 Hach 2100N turbidimeter

Figure A-5 ELGA PURELAB Option-Q water deionizer

Figure A-6 Chemicals used to synthesize wastewater

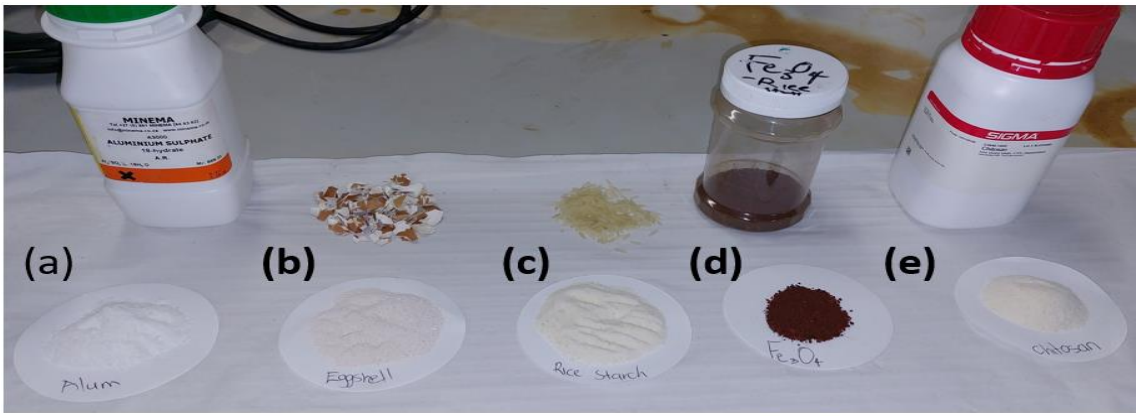

Figure A-7 Coagulants used in the study includes ,(a)-Alum, (b)-Eggshell, (c)-Rice starch , (d)-Magnetite, and (e)- Choitosan

Figure A-8 Sampling the industrial effluent

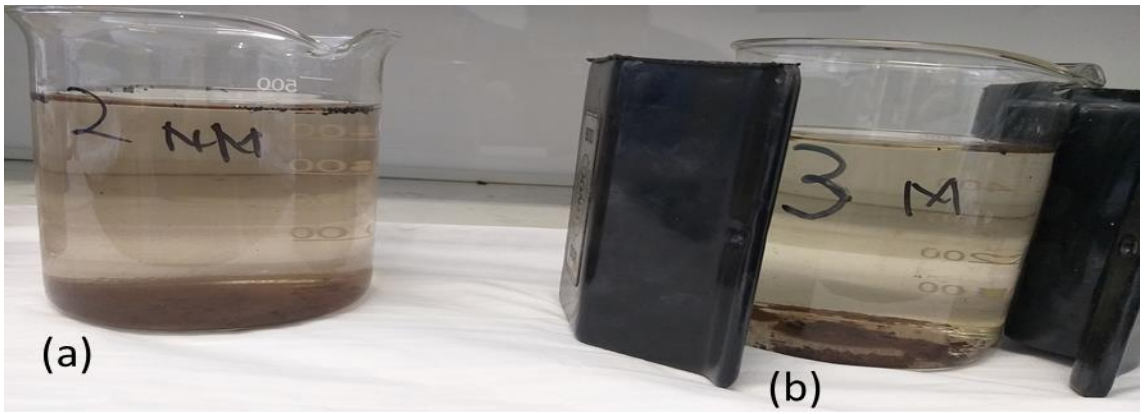

Figure A-9 Different settling configuration ,(a) normal settling , and (b) with magnetic field

APPENDIX B: DAF JAR TESTER

B1: Preparation of the DAF Saturator

1. The saturator was visually inspected for any visible damage or detached hoses, and any hoses that were displaced were reconnected.
2. Jars tubing was attached to the saturator's outlet and manifold. It was made certain that all manifold valves were closed.
3. The water fill valve was opened, and the saturator was filled to the 0mL point on the level indicator with clean water.
4. The water fill and air bleed valves were then closed.
5. The compressed air line to the compressed air inlet was connected. It was assured that the air pressure did not surpass 700kPa.
6. The pressurized air used to pressurize the saturator was admitted.
7. After the pressure gauge exhibited a static reading, the air bleed valve was opened to begin saturation.

B2: Preparation of the saturator for storage

When all testing is finished, the saturator should be depressurized and kept empty. This was accomplished by doing the following:

1. The compressed air inlet valve was closed, and the compressed air line and jars were disconnected.
2. The water fill funnel cover was removed, and the water fill valve was flipped open to decrease the pressure to 0 kPa.
3. The water fill funnel cap was replaced, and the fill valve was turned off. The Platypus DAF saturator was then ready for storage.

B3: Maintenance

1. Keep the device clean and dry while not in use. When not in use, be certain that all equipment is drained.
2. Perform routine visual inspections.
3. The flow controller fitted to the 2L DAF Jar has a very narrow opening. If foreign bodies enter the saturator during filling, they may become trapped in the flow controller. To clean the orifice, remove the elbow from the flow controller on the 2L DAF Jar and rinse

with clean water using a syringe. Before reassembling, be certain that the foreign body has been removed.

APPENDIX C: RSM RAW DATA

C.1. Coagulation process

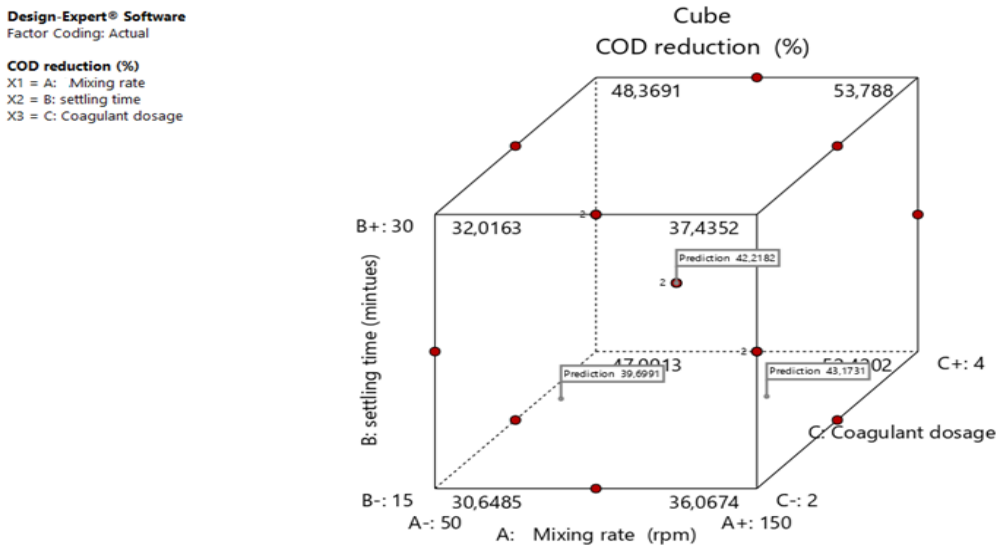

Figure C-1 Response surface plot of 3-factors for COD removal (%) from BBD design for Coagulation 14 experimental runs

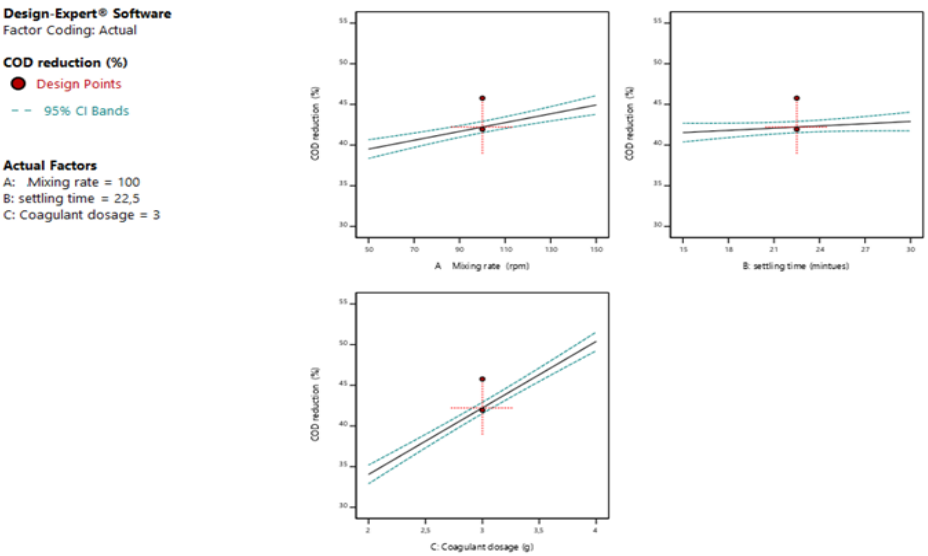

Figure C-2 Effects of coagulation variables on COD removal (%); A: mixing rate; B: settling time ; C: coagulant dosage

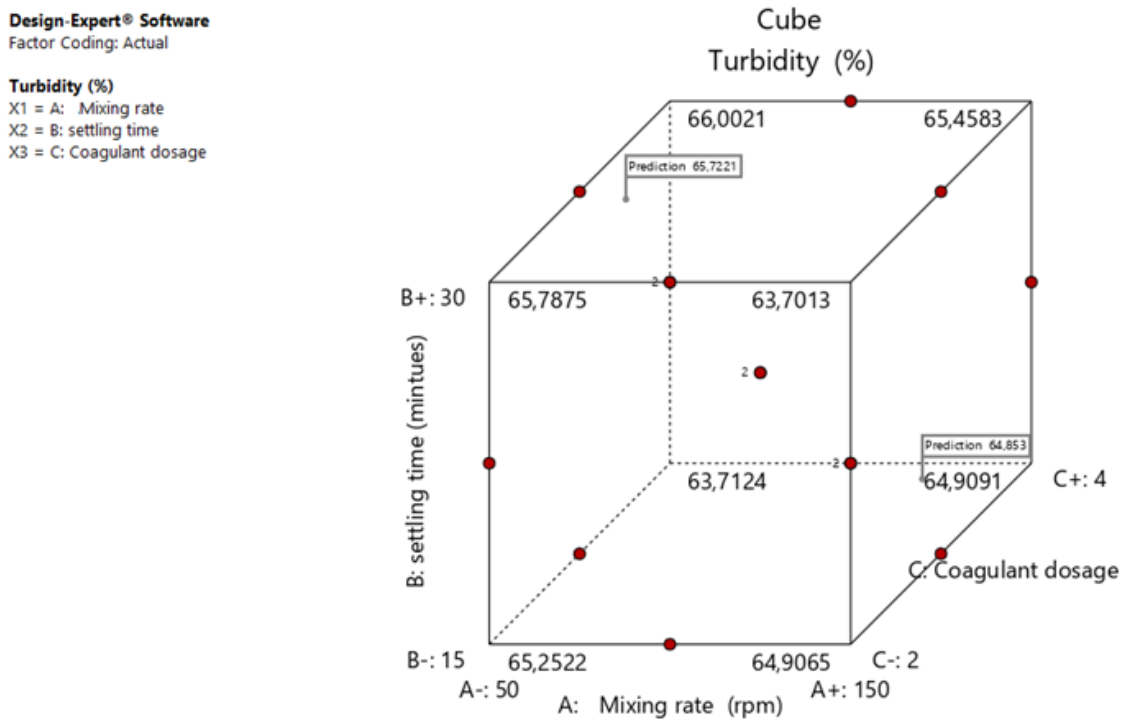

Figure C-3 Response surface plot of 3-factors for turbidity removal (%) from BBD design for Coagulation 14 experimental runs

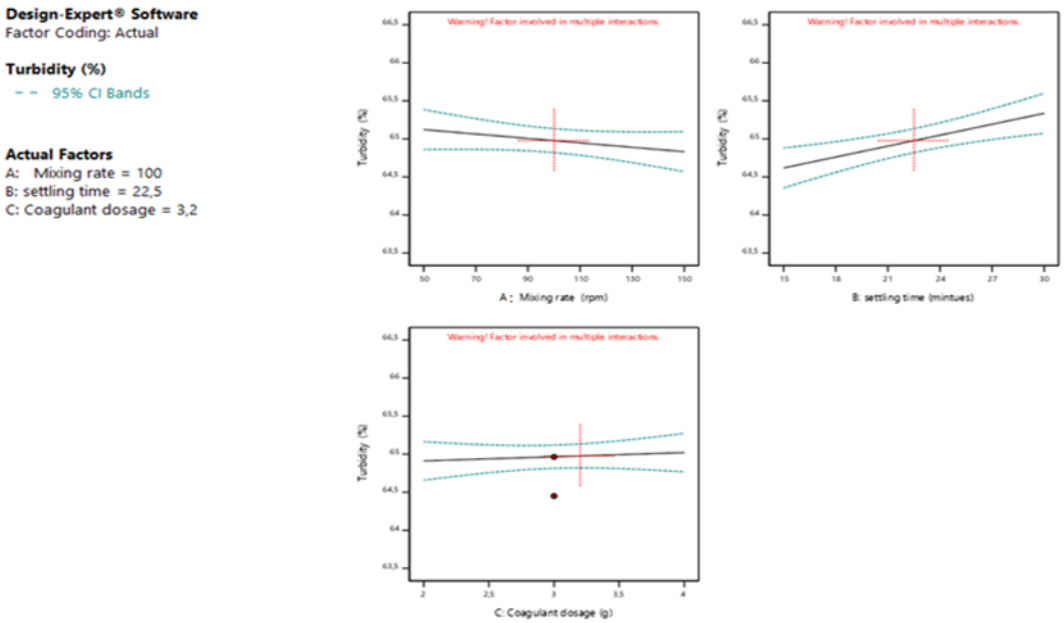

Figure C-4 Effects of coagulation variables on turbidity removal (%); A: mixing rate; B: settling time ; C: coagulant dosage

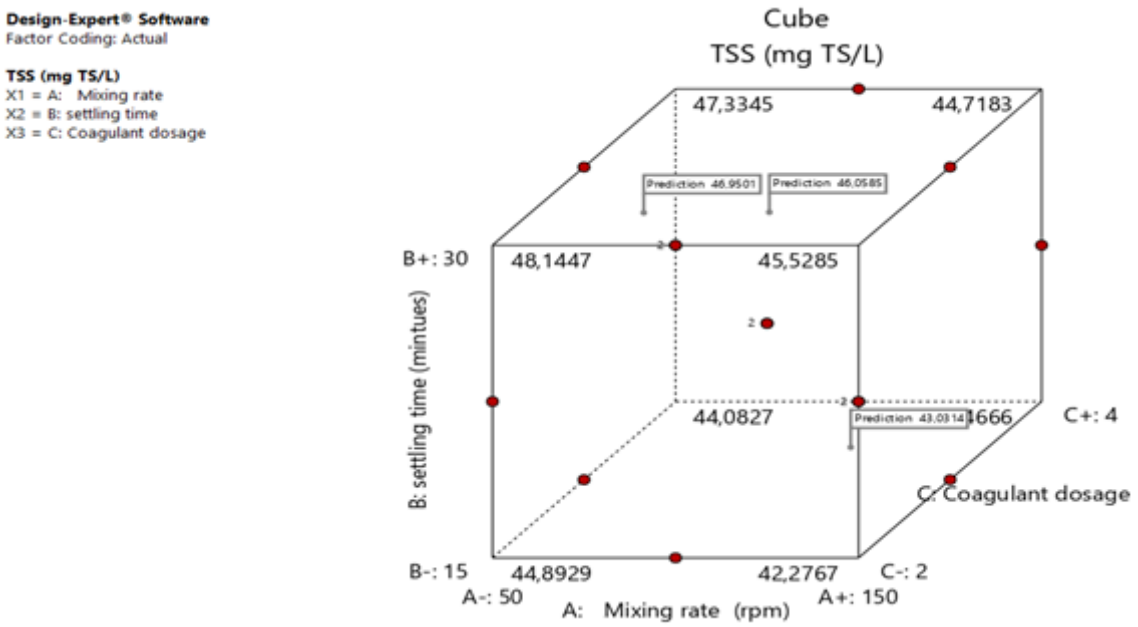

Figure C-5 Response surface plot of 3-factors for TSS removal (mg/L) from BBD design for Coagulation 14 experimental runs

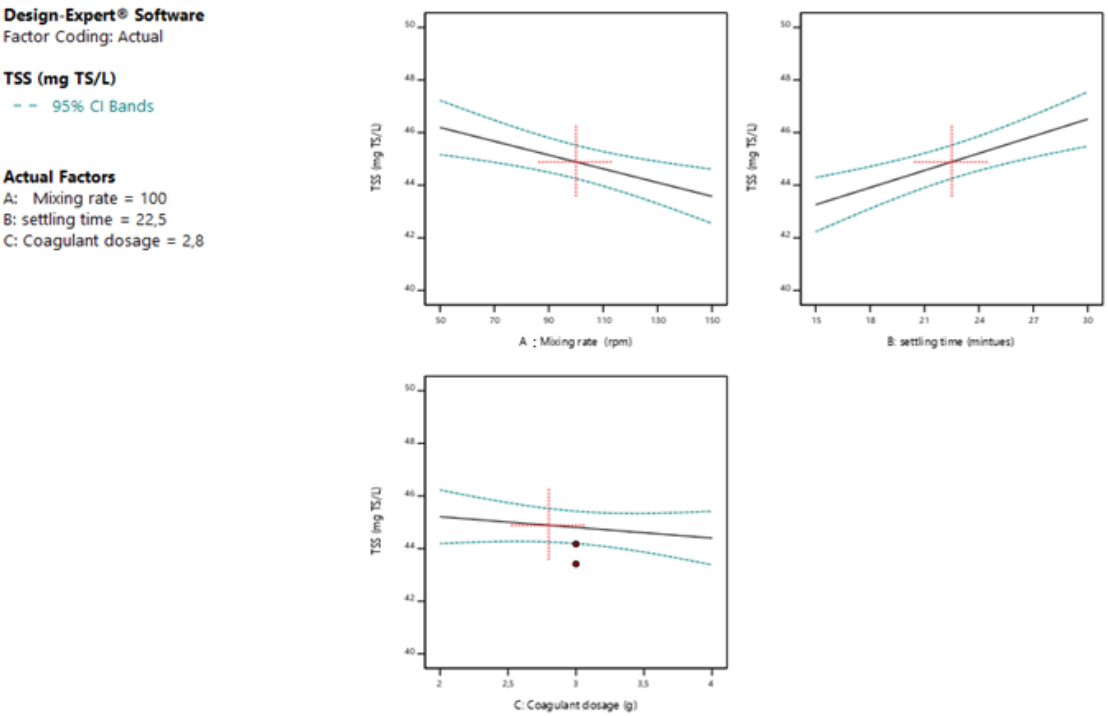

Figure C-6 Effects of coagulation variables on TSS removal (mg/L); A: mixing rate; B: settling time ; C: coagulant dosage

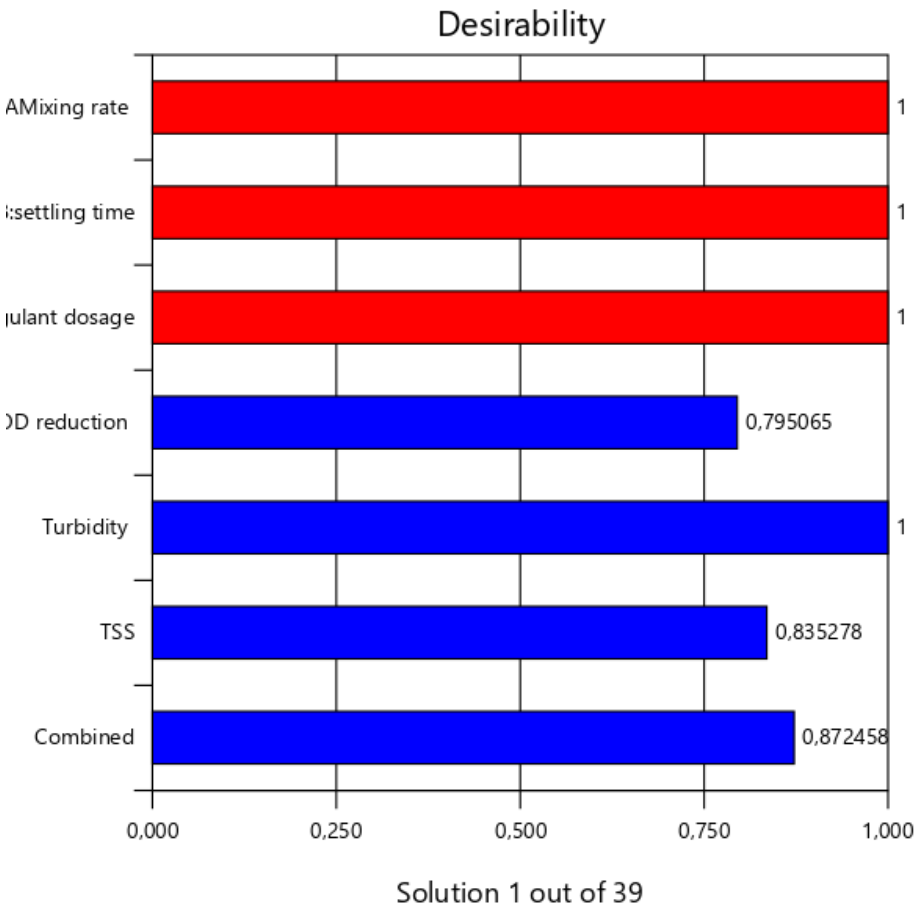

Figure C-7 Optimization solution results for the Coagulation process

C.2. DAF process

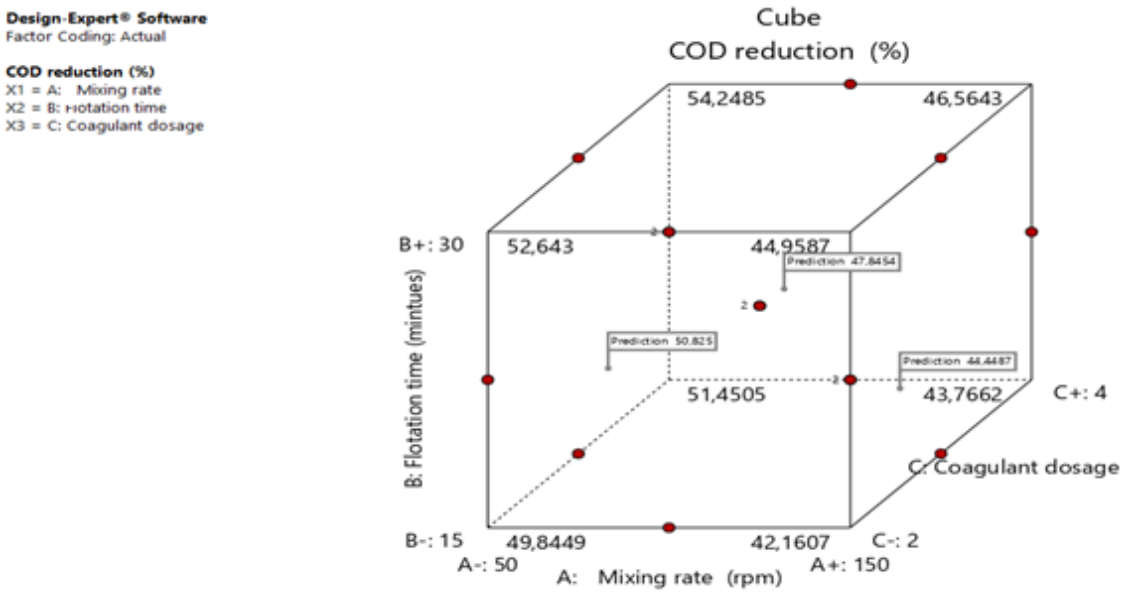

Figure C-8 Response surface plot of 3-factors for COD removal (%) from BBD design for DAF 14 experimental runs

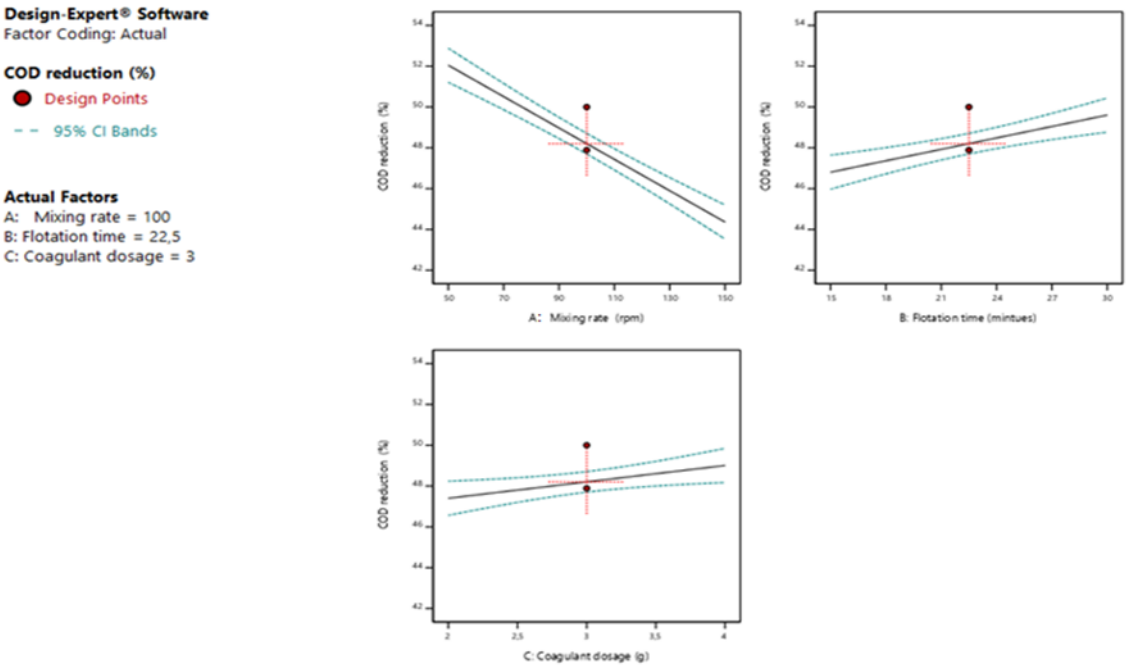

Figure C-9 Effects of DAF variables on COD removal (%); A: mixing rate; B: flotation time ; C: coagulant dosage

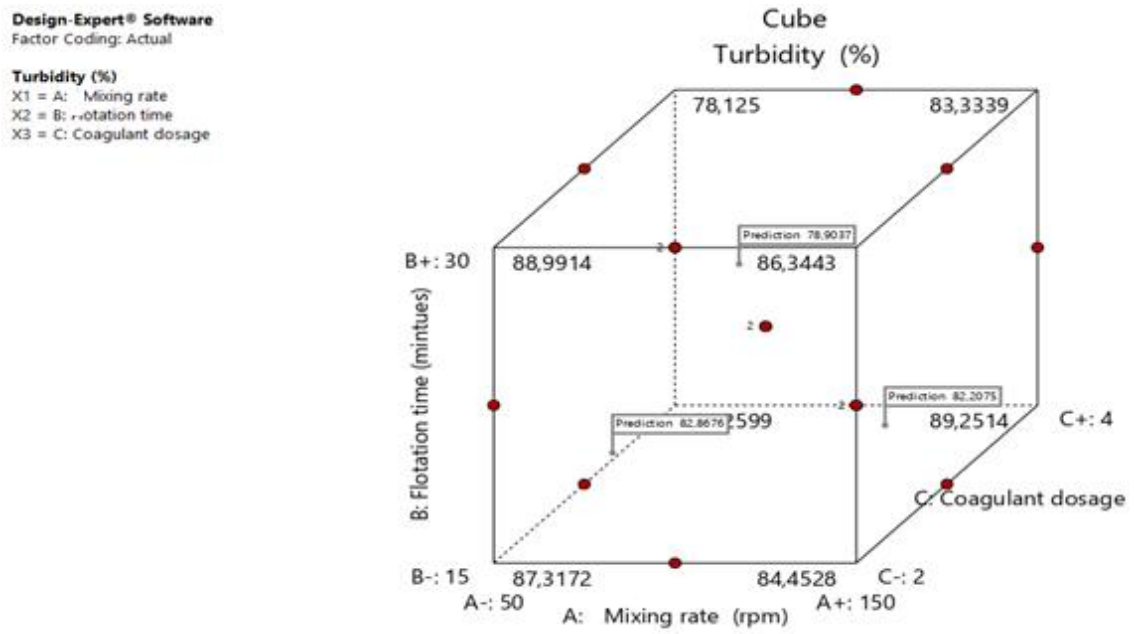

Figure C-10 Response surface plot of 3-factors for turbdity removal (%) from BBD design for DAF 14 experimental runs

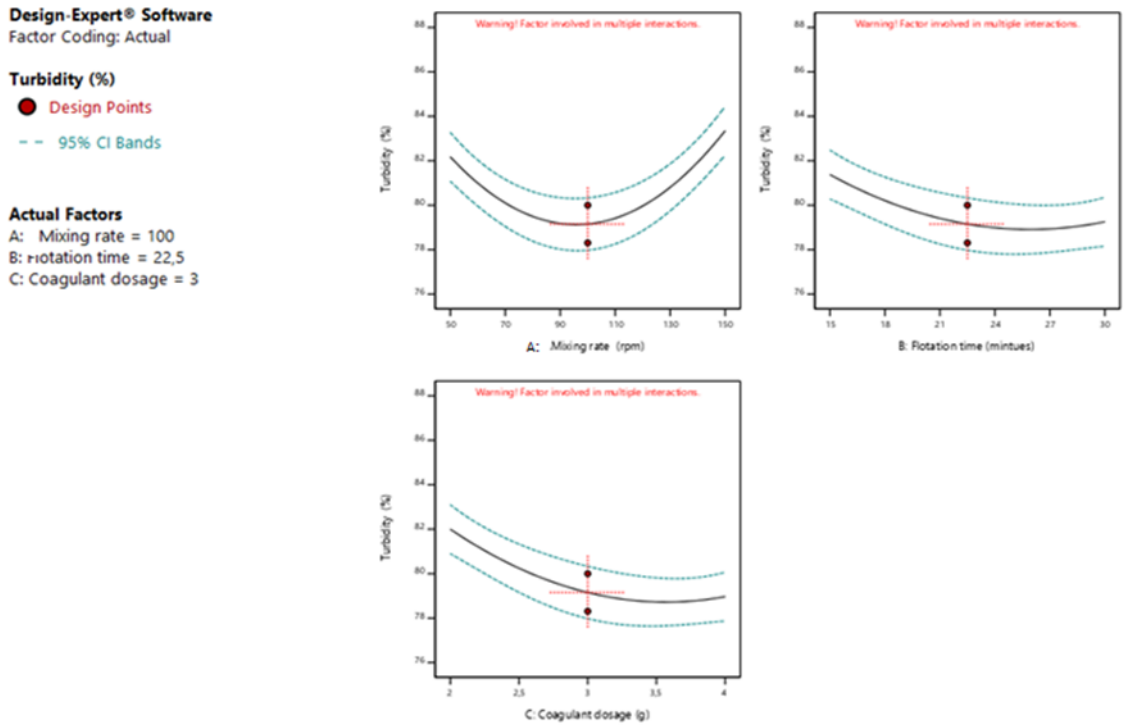

Figure C-11 Effects of DAF variables on turbidty removal (%); A: mixing rate; B: flotation time ; C: coagulant dosage

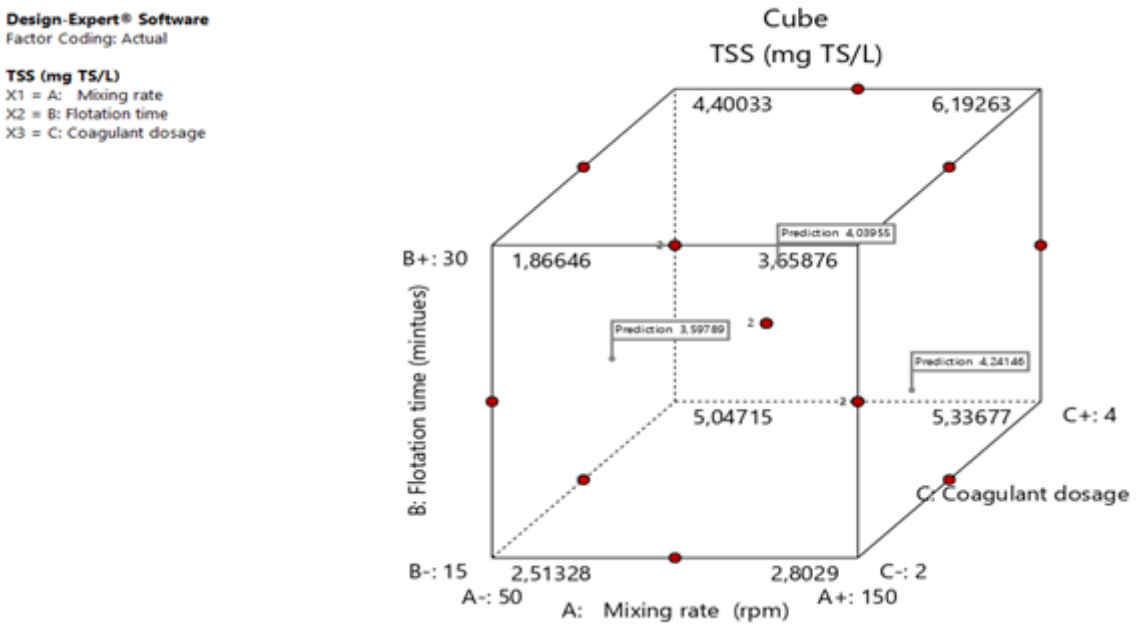

Figure C-12 Response surface plot of 3-factors for TSS removal (mg/L) from BBD design for DAF 14 experimental runs

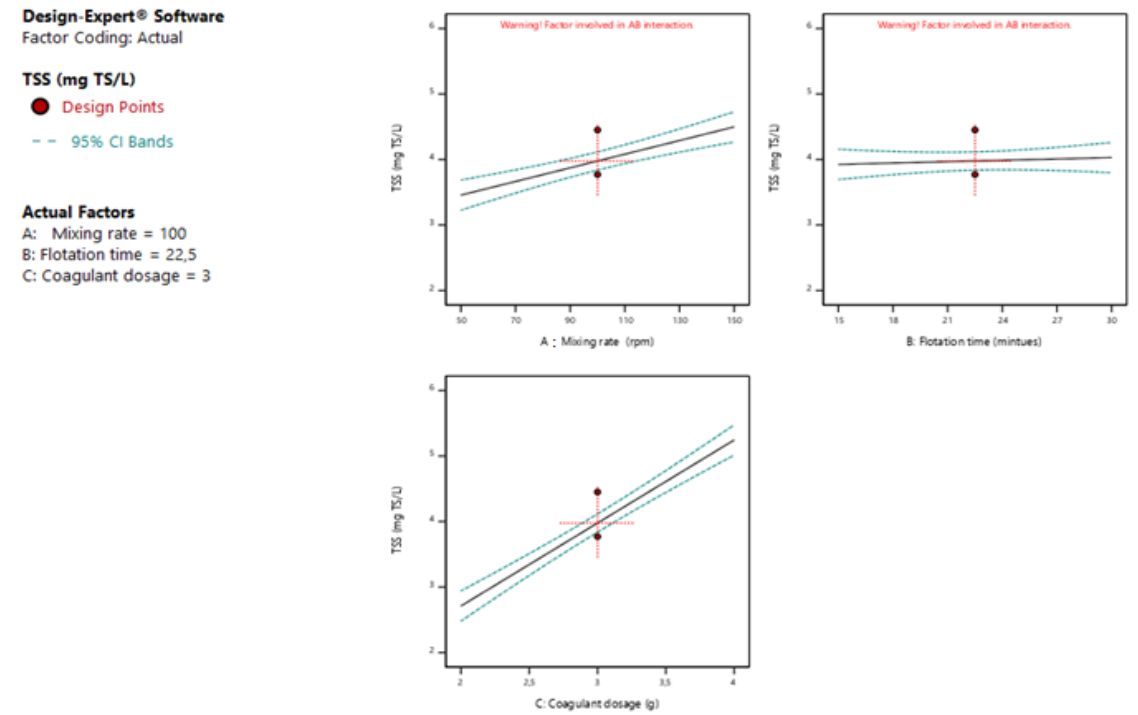

Figure C-13 Effects of DAF variables on TSS removal (mg/L); A: mixing rate; B: flotation time ; C: coagulant dosage

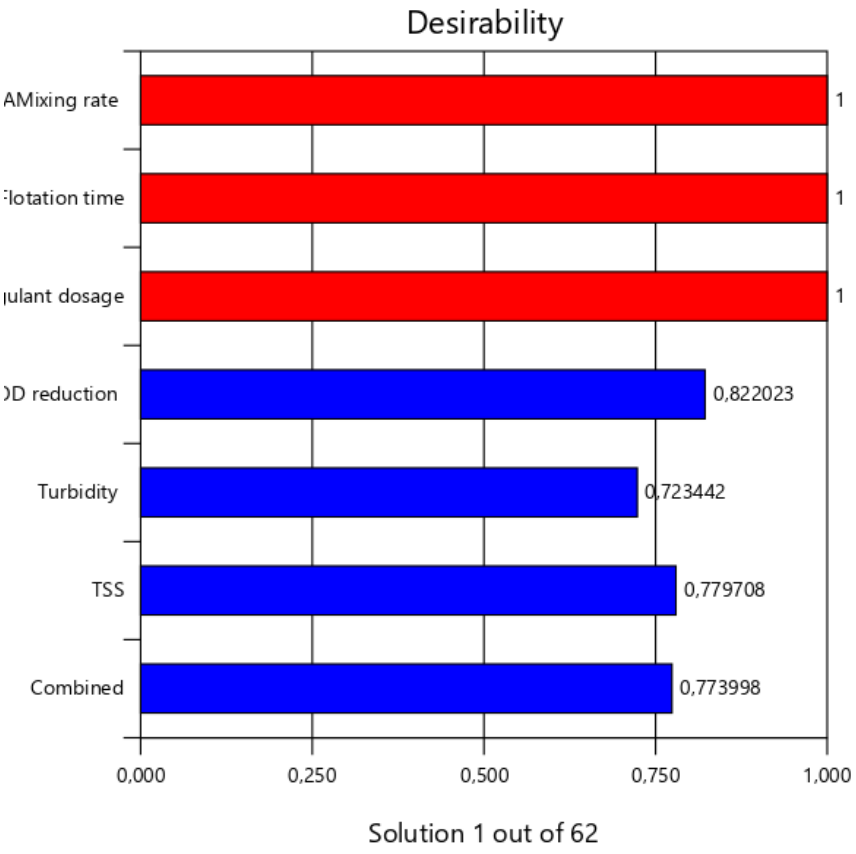

Figure C-14 Optimization solution results for the DAF proces

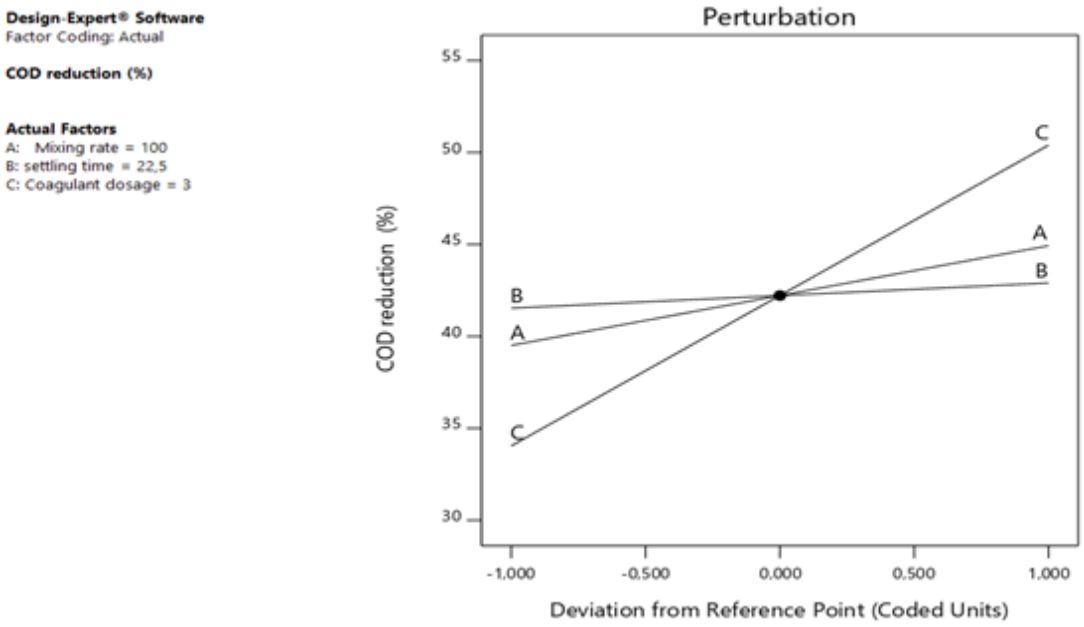

Figure C-15 Perturbation plot for COD removal (%) in coagulation process

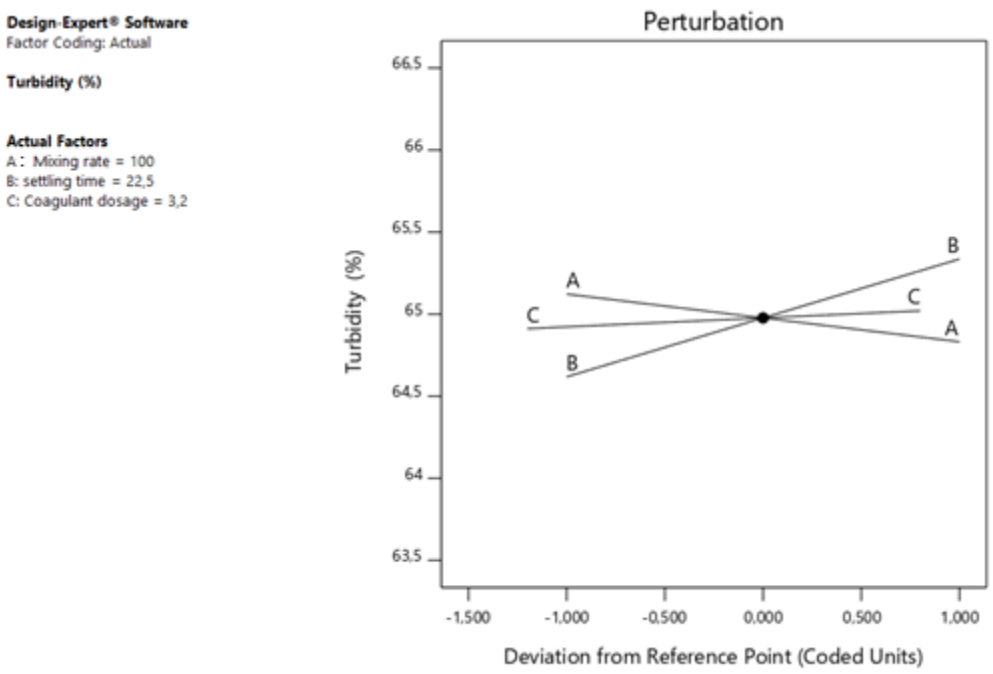

Figure C-16 Perturbation plot for turbidity removal (%) in coaglation process

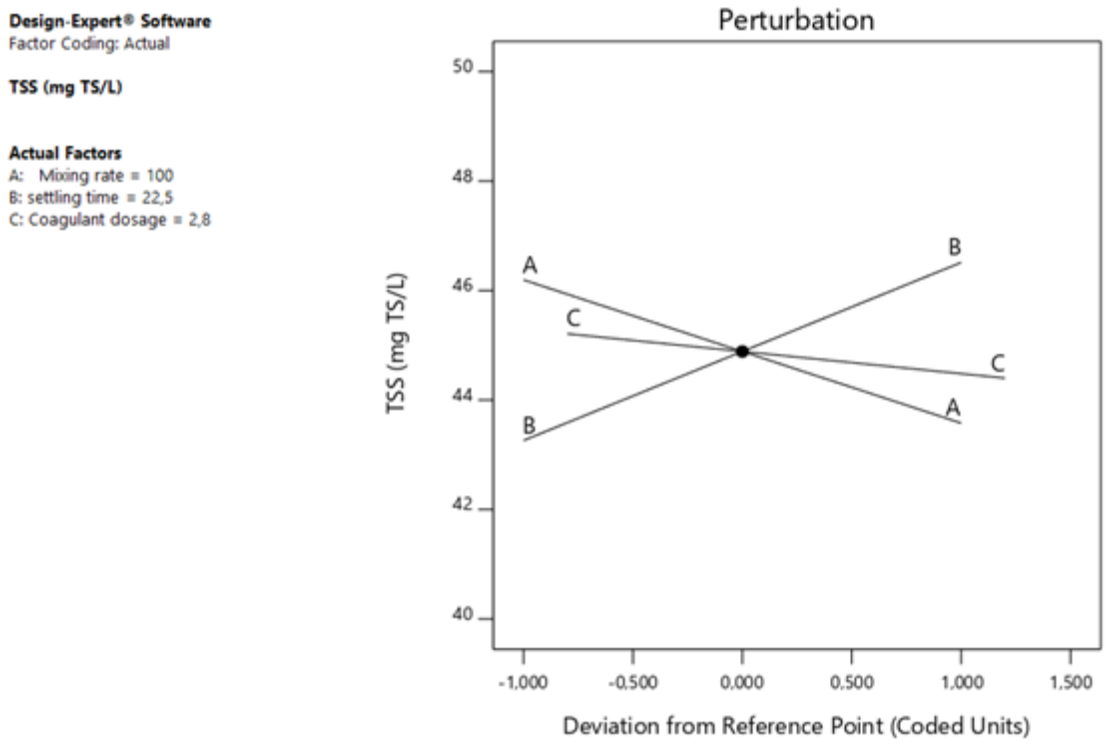

Figure C-17 Perturbation plot for TSS removal (mg/L) in coagulation process

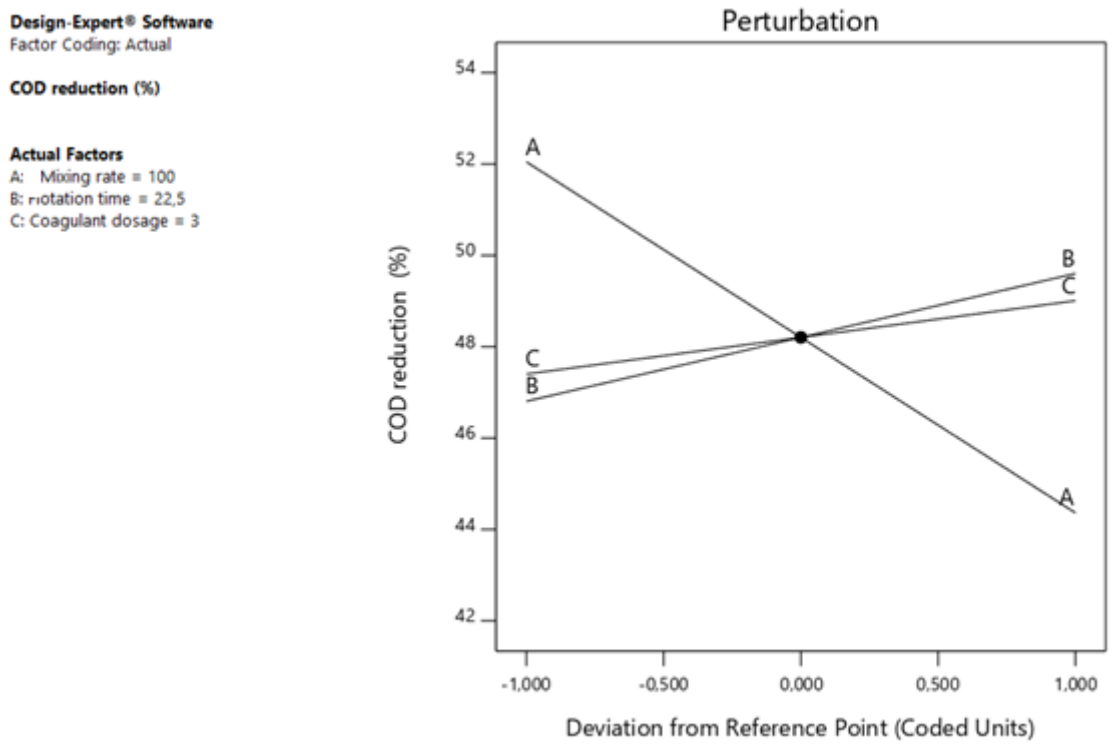

Figure C-18 Perturbation plot for COD removal (%) in DAF process

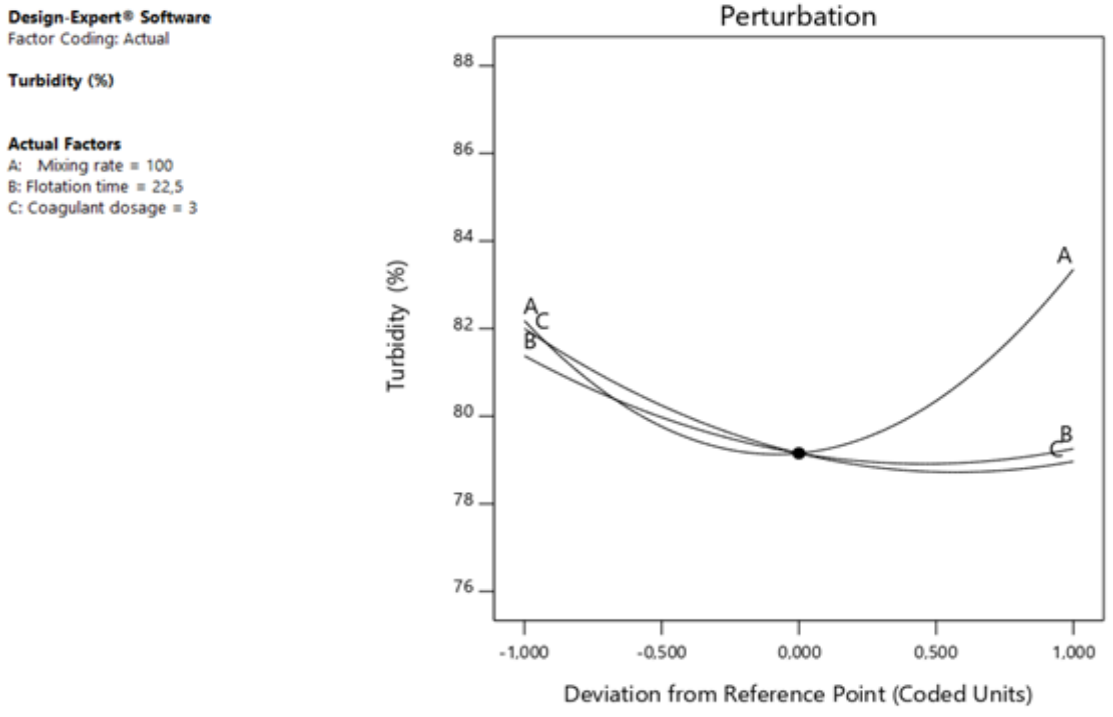

Figure C-19 Perturbation plot for turbidity removal (%) in DAF process

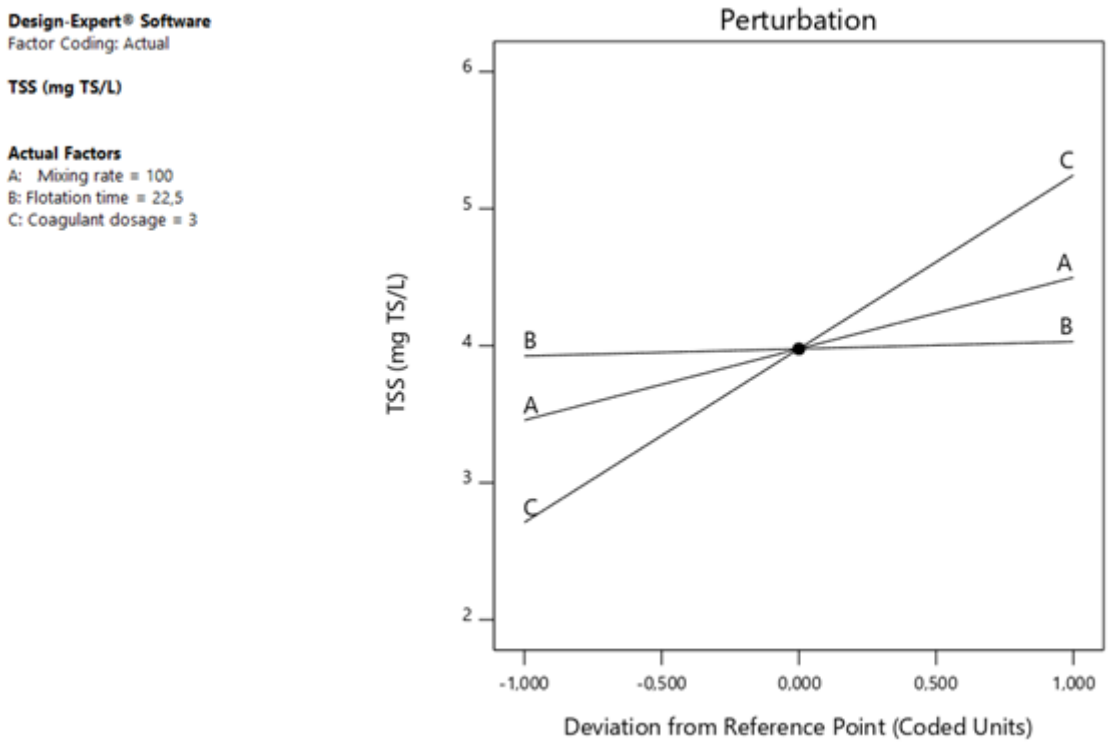

Figure C-20 Perturbation plot for TSS removal (mg/L) in DAF process

APPENDIX D-PUBLICATIONS

18th JOHANNESBURG Int'l Conference on Science, Engineering, Technology & Waste Management (SETWM-20) Nov. 16-17, 2020 Johannesburg (SA)

Application of Natural Coagulants as an Alternative to Alum for Wastewater Treatment

N. P., Sibiya, S, Rathilal, P., Govender and E. Kweinor Tetteh*

***Abstract*—** Coagulation is one of the most widely used pre-treatment technology for water and wastewater treatment. Conventionally, metal-based coagulants (aluminum and iron) poses environmental challenges due to their complexity in biodegradation. Therefore, in this study, three natural-based coagulants (Egg shells, Rice starch and Bentonite) and Alum were evaluated for the removal of turbidity from simulated slaughterhouse wastewater. This was carried out at room temperature at a constant pH of 6.97. Each coagulant was then investigated within the dosage of 10-60 mg/L by using a Jar-test (JTL6). At the end of each run, the supernatant sample was analyzed in triplicate for turbidity (Hach DR3900). With the initial turbidity of 64.08 NTU, the order of maximum turbidity removal efficiencies by the coagulants were Bentonite (98%) > Alum (96%) > Rice starch (85%) > Egg shell (73%) at the optimum dosage of 30 mg/L. Notwithstanding, all the natural coagulants showed great potential for the agglomeration and neutralization of the charges on the pollutants in the water, which might be due to their carboxylic and hydroxyl functional group constituents. In addition, there existed strong linear regression between the coagulant dosage and the turbidity removal, which makes the prospects of the natural coagulants economically viable for wastewater treatment.

***Keywords*—**Alum, bentonite, coagulation, egg shells, natural coagulant, rice starch, wastewater

I. Introduction

Currently fresh water is depleting, the sources are running out and as a result 78 million people live without safe drinking water [1]. Also, fresh water demand increases exponentially with human population and industrial activities [2]. Therefore, treatment of wastewater for reuse comes in handy.

The numerous methods being used in treating wastewater is based on its toxicity in order to protect the aquatic systems [3], such as coagulation, adsorption, dissolved air flotation, membrane technology, biological systems, filtration and so on [3, 4, 5]. Coagulation has been a vital mechanism in physio-chemical wastewater treatment processes, which involves the addition of chemicals. Most of these chemicals are commonly known as coagulants (polymeric, natural, organic and inorganic) responsible for destabilizing and agglomerating the contaminants [6, 7, 8]. Generally, aluminum and iron-based coagulants (cheap) are employed in pre-treatment processes in water and wastewater treatment facilities to efficiently reduce the organic load prior to subsequent treatment processes [3,7, 8]

However, these types of coagulants are associated with the formation of large volumes of sludge associated with complex metals. As a result, this poses great threat to agriculture, human health (memory loss, intestinal constipation, abdomen colic, spasms) and aquatic life if not treated before being disposed into the environment [6, 7, 8]. Therefore, the improvement of the coagulation process by the use of cost-effective or biodegradable or natural coagulants is worth investigating, since there is limited information and studies on natural coagulants used for wastewater treatment. This study investigated three natural-based coagulants (egg shells, rice starch and bentonite) and compared it with alum treatability performance for the removal of turbidity.

Manuscript (EAP1120255) received September 22, 2020. This work was supported in part by Water Research Commission (WRC), South Africa and the for their support on the project identification WRC Project: C2019/2020-00212.

Faculty of Engineering and the Built Environment, Green Engineering and Sustainability Research Group, Department of Chemical Engineering, Durban University of Technology, Steve Biko Campus Block S4 Level 1, Box 1334, Durban 4000, South Africa (EKT)

II. Methodology

A. Chemicals and wastewater sample

The 3 natural-based coagulant powders (egg shells, rice starch and bentonite) were laboratory prepared according to reported method by Jagaba et al [9]. Aluminum sulphate (alum) was supplied by Sigma Aldrich. Municipality based wastewater synthesized to have initial turbidity of 64.08 NTU was used.

B. Jar test procedure

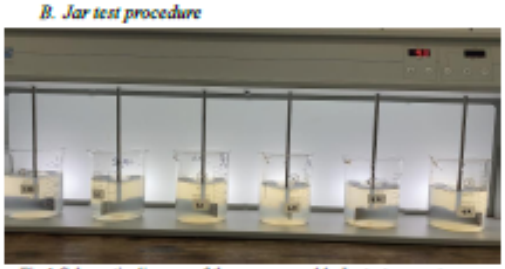

Fig 1 Schematic diagram of the programmable Jar test apparatus (JTL6)

The coagulation experiments were carried out using a jar-test (JT6L) apparatus coupled with six paddles (Fig 1). All the runs were carried out at an ambient temperature (25 ± 2°C). The wastewater samples were mixed thoroughly before being fractionated into beakers containing 500 mL of suspension each. After an addition of desired dosage for each coagulant (10 to 60 mg/l) to the suspension, the beakers were agitated at rapid mixing (90 rpm) for 2 min

molecules

MDPI

Article

Coagulation Treatment of Wastewater: Kinetics and Natural Coagulant Evaluation

Nomthandazo Precious Sibiya, Sudesh Rathilal and Emmanuel Kweinor Tetteh *

Green Engineering and Sustainability Research Group, Department of Chemical Engineering, Faculty of Engineering and the Built Environment, Durban University of Technology, Durban 4001, South Africa; nomtha.presh@gmail.com (N.P.S.); rathilals@dut.ac.za (S.R.)
* Correspondence: emmanuelk@dut.ac.za

Abstract: In this study, three coagulants (ferromagnetite (F), alum (A), and eggshells (E)) and their hybrids (FA, FE, and FEA) were investigated as possible cost-effective coagulants for the treatment of industrial wastewater. Scanning electron microscopy (SEM) coupled with energy-dispersive X-ray (EDX) was used to characterize the morphological and elemental compositions of the coagulants. The effects of coagulant dosage (10–60 mg/L) and settling time were investigated for the removal of turbidity, color, and total suspended solids. A jar tester (JTL6) operating at conditions of 150 rpm for 2 min (rapid mixing) and 30 rpm for 15 min (slow mixing) was employed. Results from the characterized supernatant showed about 80% removal of the contaminants. The prospects of F were proven to be the most effective as compared to the binary (FA > FE) and the ternary hybridized (FEA) coagulants. At an optimum dosage and settling time of 20 mg/L and 30 min, respectively, the treatability performance of F was clearly proven to be viable for wastewater treatment.

Keywords: alum; eggshells; coagulation kinetics; ferromagnetite; magnetic coagulants; nanomaterials; wastewater treatment

check for updates

Citation: Precious Sibiya, N.; Rathilal, S.; Kweinor Tetteh, E. Coagulation Treatment of Wastewater: Kinetics and Natural Coagulant Evaluation. *Molecules* **2021**, *26*, 698. https://doi.org/10.3390/molecules26030698

Academic Editors: Magnus Willander and Ashok Kakkar
Received: 29 October 2020
Accepted: 24 December 2020
Published: 29 January 2021

1. Introduction

Water is a very important resource in agriculture, livestock production, forestry, fisheries, hydropower generation, industrial activities, and other innovation activities [1]. Most industrial effluents undergo some form of treatment and their characteristics depend on the manufacturing processes and types of raw materials used. Generally they contain levels of suspended solids that vary between 300 and 400 mg/L, with pH of 6.5–7.0, chemical oxygen demand (COD) of 2000–3000 mg/L, and total alkalinity of 50–100 mg/L. [2]. The production of huge amounts of heavily polluted wastewater has prompted research in order to develop, improve, and implement appropriate treatment techniques to eliminate

Materials Today: Proceedings xxx (xxxx) xxx

Contents lists available at ScienceDirect

Materials Today: Proceedings

journal homepage: www.elsevier.com/locate/matpr

Response surface optimisation of a magnetic coagulation process for wastewater treatment via Box-Behnken

N.P. Sibiya, G. Amo-Duodu, E. Kweinor Tetteh *, S. Rathilal

Green Engineering and Sustainability Research Group; Department of Chemical Engineering, Faculty of Engineering and The Built Environment, Durban University of Technology, Durban 4001, South Africa

ARTICLE INFO

Article history:
Available online xxxx

Keywords:
Box-Behnken design
Coagulation
Response surface methodology
Rice starch
Magnetite
Wastewater

ABSTRACT

In the wastewater treatment settings, conventional coagulants for wastewater treatment are becoming very complex with environmental concern. This necessitates the investigation for the use of magnetized rice starch as alternate coagulants. Herein, its application in the coagulation operational mechanism for decontamination of wastewater was investigated. The coagulation conditions were optimised via response surface methodology (RSM) based on a Box–Behnken design (BBD). Three operational parameters viz. coagulant dosage (2–4 g), settling time (15–30 min) and mixing rate (50–150 rpm) were investigated with their effects on turbidity and phosphate removal (at a wavelength of 880 nm) with 17 experimental runs by the BBD. Using the analysis of variance (ANOVA), the results obtained were analysed and quadratically modelled as a function of the input parameters with a significant regression coefficient ($R^2 > 0.96$) at a 95% confidence level. At numerical optimum conditions of coagulant dosage (3.4 g), settling time (17.3 min) and mixing rate (103 rpm), 100% desirability treatability efficiency was attained with 100 distinctive conditional solutions. Interestingly, validation of the optimal condition revealed proper adjustment of the coagulant dosage and settling time can maximise the coagulation efficiency. Also, the findings demonstrated that the applicability of the magnetised rice starch in the wastewater settings can be used as a viable coagulant alternative.

© 2022 Published by Elsevier Ltd. This is an open access article under the CC BY-NC-ND license (https://creativecommons.org/licenses/by-nc-nd/4.0) Selection and peer-review under responsibility of the scientific committee of the International Symposium on Nanostructured and Advanced Materials This is an open access article under the CC BY-NC-ND license (http://creativecommons.org/licenses/by-nc-nd/4.0/).